UNIVERSITÀ DEGLI STUDI DI BARI ALDO MORO

DEPARTMENT OF PHARMACY-PHARMACEUTICAL SCIENCES

PhD COURSE IN

PHARMACEUTICAL SCIENCES

XXXVII CYCLE

Medicinal Chemistry (CHIM-07/A)

DRUG DESIGN, SYNTHESIS AND STRUCTURE-ACTIVITY RELATIONSHIPS OF NOVEL MULTIMODAL INDOLE-FUSED TRICYCLIC DERIVATIVES TARGETING CANNABINOID-MODULATED G PROTEIN-COUPLED RECEPTORS AND CHOLINESTERASES

PhD student:
Francesco Samarelli

Coordinator:
Chiar.mo Prof. Nicola Antonio Colabufo

Tutors:
Chiar.mo Prof. Cosimo Damiano Altomare
Prof. Modesto de Candia

FINAL EXAM 2025

ABSTRACT

Due to the multi-factorial nature of most neurological disorders, developing multi-target compounds is still considered among the effective approaches to developing neuroprotective drugs.[1,2] Despite the scientific advances in the areas of neurochemistry, genetics, molecular and cell biology, there is still no effective treatment available that can delay the onset or slow the progression of neurodegenerative diseases, like Alzheimer's disease (AD) and memory impairments. In the context of the challenging multitarget-directed-ligand (MTDL) design strategy of novel therapeutic agents for treating AD and related syndromes, progress has been made in the medicinal chemistry of drugs acting within and beyond the endocannabinoid system. Endogenous lipids, such as palmitoylethanolamide, that act simultaneously at GPCRs, ion channels, and PPARs can be taken as templates.[3]

In this Ph.D. thesis study, starting from the structures of small-molecules inhibiting well-established AD-related targets, such as cholinesterases (AChE and BChE) and N-methyl-D-aspartate (NMDA) receptor, the synthesis has been carried out of novel rationally designed tricyclic indole-fused derivatives which interestingly proved to act as modulators (antagonists and/or inverse agonists) of the cannabinoid-related GPCRs GPR18 and GPR55, in some cases endowed with additional BChE-selective inhibition.[4] The desired outcome is the combination of the anticholinesterase activity with the modulation of these poorly studied receptors, for a synergistic effect against neuroinflammation and neurodegeneration. In particular, tetrahydroazepinol[4,3-*b*]indole (THAI) derivatives exhibited antagonistic activity in the micromolar range at GPR55, with the most potent compounds being **5h** (NB360, IC_{50} = 4.76 μM) and **5e** (RP308, IC_{50} = 4.40 μM); ethyl 1,3,4,5-tetrahydro-2*H*-pyrido[4,3-*b*]indole-2-carboxylate also showed weak antagonistic activity at GPR55 (**21d**, FS962C-1F, IC_{50} = 8.13 μM) confirming the importance of the lactam function for the recognition by the receptor. In contrast, 1,2,3,4,5,6-hexahydroazepino[4,3-*b*]indole (HHAI) and 2,3,4,5-tetrahydro-1H-pyrido[4,3-*b*]indole (THPI) derivatives exhibited antagonist or inverse agonist activity in the very low micromolar range (even < 1 μM) at GPR18, with the most potent compounds being **6a** (NB560, IC_{50} = 0.701 μM), **22a** (NB543-B, IC_{50} = 0.753 μM) and **22e** (NB555-B. IC_{50} = 0.753 μM).

Certain compounds proved to act as multitarget ligands at the cannabinoid-related GPCRs - GPR18 and GPR55 – and BChE. Specifically, compound **22f** acts as dual BChE inhibitor/GPR18 inverse agonist, while compound **5h** acts as dual BChE inhibitor/GPR55 antagonist at low μM level. Design, synthesis, radioligand binding and functional assays, kinetics of enzyme inhibition, and molecular modeling studies, allowed us to infer new structure-activity relationships of these classes of compounds, assess their selectivity for cannabinoid (CB) and CB-like receptors, and choose one candidate for *in vivo* pharmacological testing. Positron emission tomography (PET) imaging studies validated our compounds as CNS-directed agents due to their ability to cross BBB.[5]

As major outcome of this research program, some relevant pharmacological aspects have been highlighted which relate to the modulation of GPR18 and GPR55 relatively to their *β*-arrestin recruitment signaling pathways. The first full inverse agonists of GPR18 documented to date (**22f**, **22g**) are presented, which might allow pharmacologists to gain valuable insight into the physiological role of this receptor and the effects of its constitutive activity. Moreover, dual GPR/CBR derivatives (**20d**, **21d, 22g-i**) could position these compounds as pharmacological tools for exploring biochemical cross-talks in GPR/CBR heteromers.

The results of this work, along with findings from other collaborative projects presented herein, provided us with useful medicinal chemistry information enabling the optimization of MTDLs against neurological disorders, potentially more effective than those currently available.

INDEX

1 INTRODUCTION

1.1 Useful concepts, approaches and tools in medicinal chemistry

Medicinal chemistry concerns the discovery, development, identification, and interpretation of the mode of action of biologically active compounds at a molecular level.[6] This endeavor involves identifying and validating a *hit* compound, followed by its chemical optimization to obtain a *lead* compound with the desired pharmacodynamic profile and suitable pharmacokinetic properties.

Currently, there are several effective methods for identifying hit structures for further development. One of the most widely utilized techniques, particularly within industrial contexts, is high-throughput screening (HTS). This methodology involves the automated testing of extensive molecular libraries in an appropriate testing environment. The primary advantage of high-throughput screening lies in its efficiency, allowing for the rapid evaluation of many compounds. However, this process can be quite costly and requires sophisticated automated testing systems. Moreover, not all pharmacological assays are conducive to automation, especially the cell-based assays that may require media exchanges or filtration and washing steps.

In addition to, or complimentary with HTS, a real advance in the field is represented by computer-based virtual screening, nowadays usefully supported by Artificial Intelligence (AI) algorithms and techniques. This approach uses structural information of the target obtained from crystal structure analysis or, in the absence of such data, from homology modeling, to assess extensive compound libraries effectively.

Another possibility is to identify new hit structures by knowledge-based approaches. Already established ligands and information on the endogenous ligand can be used to identify a suitable lead structure. This methodology is commonly known as the "ligand-based approach". Each approach presents distinct advantages and disadvantages. It is essential for a drug discovery scientist to select methods that align with their specific requirements and the resources at their disposal.

When identifying a hit compound, it becomes essential to assess its suitability as lead structure. This assessment involves chemical modifications to optimize the compound's properties through a process known as “hit-to-lead” optimization (Figure 1). A robust lead structure must fulfill several physicochemical criteria.

These include maintaining an acceptable molecular weight, achieving appropriate logP or logD values, ensuring aqueous solubility, and providing specific positions on the scaffold that allow for further chemical modifications. Furthermore, the compound should exhibit adequate stability and must not be documented as toxic, nor should it contain functional groups associated with known toxic effects. An investigation into the compound's prior uses is also critical, as it may have been employed for alternative purposes or may already be recognized as a drug targeting a different condition. Depending on the target of interest, a high degree of selectivity may also be a requirement in the evaluation process.

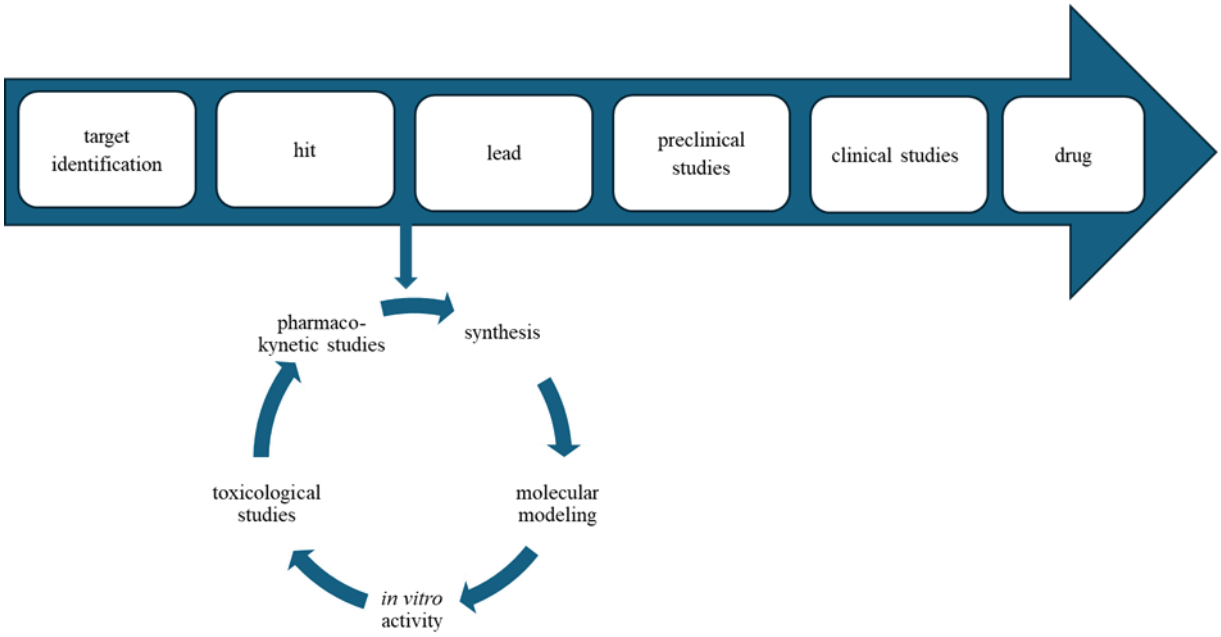

Figure 1. *Hit to lead optimization process is a crucial step in medicinal chemistry and drug development.*

1.2 G protein-coupled receptors

G protein-coupled receptors (GPCRs) represent the largest superfamily of cell surface membrane receptors. They are characterized by a conserved structure of seven transmembrane (7TM) helices, interconnected by three intracellular loops and three extracellular loops. The N-terminus of the protein can be found extracellularly, and the C-terminus intracellularly. GPCRs are dynamic proteins that play essential roles in signal transduction, responding to a diverse range of extracellular signals, including photons, ions, lipids, neurotransmitters, hormones, and peptides. Figure 2 illustrates the main structural features of a GPCR, specifically the cannabinoid receptor type 1 (CB1). Upon activation by these

external stimuli, GPCRs primarily utilize heterotrimeric G-proteins and arrestins as transducers. This activation cascade leads to the generation of second messengers and further initiates downstream signaling pathways within cells.

All GPCRs can be subdivided according to their phylogenetic relationship. The largest group consists of the so-called class A rhodopsin-like receptors. This family can be subdivided based on their phylogenetic relationships into four subfamilies (α-δ). The α-subfamily contains many well-known drug targets such as adenosine, serotonin, cannabinoids, melanocortin receptors, and opsins. The γ-subfamily comprises many peptide receptors, such as opioid and chemokine receptors. The δ-branch receptors are the most diverse class and include the P2Y receptors and the PAR receptors, but they also contain many uncharacterized receptors with unknown functions.

Mutations in GPCRs can impair their functionality by altering key aspects such as constitutive activity, membrane expression, and post-translational modifications. A thorough understanding of the mechanisms in stimuli-GPCR-effector coupling, along with the regulatory processes governing GPCR dysfunction, holds significant therapeutic potential. Insights gained from this research may pave the way for the development of modulators with enhanced potency, selectivity, and biased signaling properties.[7]

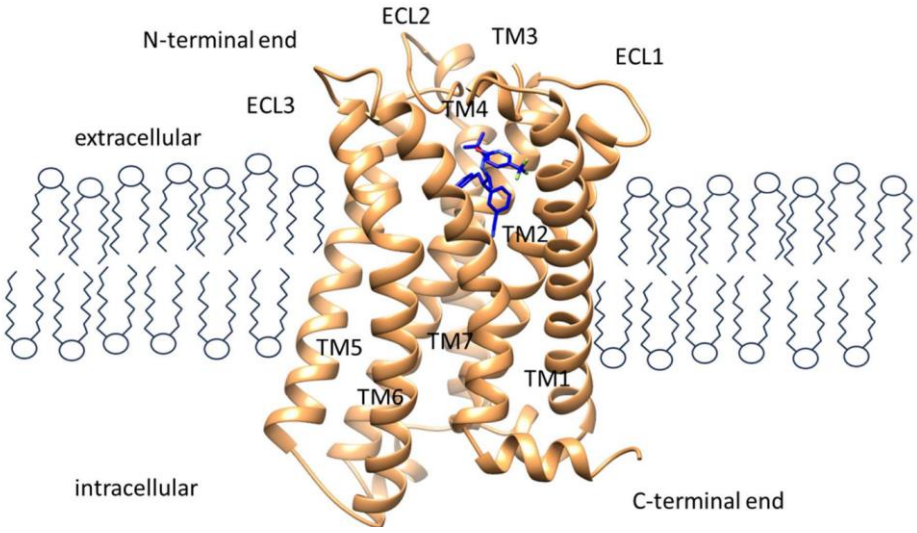

Figure 2. *Representation of the cannabinoid receptor type 1 bound to the inhibitor taranabant (PDB: 5U09). TM = transmembrane domain; ECL = extracellular loops.*

Currently, approximately 34% of drugs approved by the U.S. Food and Drug Administration (FDA) target GPCRs, and the pipeline for modulators in clinical trials or preclinical stages is experiencing substantial growth.[8] The functions and physiological roles of numerous GPCRs are still not fully understood. Targeting these inadequately characterized receptors has the potential to yield effective therapeutic agents for diseases that are currently untreatable.

1.2.1 Mechanism of GPCR activation and signaling

GPCRs are responsible for the transmission of an extracellular signal to the intracellular site, where it causes a response in the cell through two types of transducers: heterotrimeric G proteins and/or β-arrestins.

The binding of an agonist results in a conformational change that leads to the activation of the G proteins. G proteins consist of three subunits (α, β, and γ) and bind guanosine diphosphate (GDP) in their inactive state. Upon activation of the GPCR, GDP is exchanged for guanosine triphosphate (GTP) and the α-subunit dissociates from the G protein complex. Human G proteins comprise four major families depending on the type of G_α subunit (G_s, $G_{i/o}$, $G_{q/11}$, and $G_{12/13}$), which in turn mediate different effects in the cell (Figure 3). A $G_{\alpha s}$ protein stimulates adenylate cyclase resulting in the formation of cyclic adenosine monophosphate (cAMP). The cAMP-dependent protein kinase A can then mediate further effects in the cell. A $G_{\alpha i}$ subunit inhibits adenylate cyclase and, therefore, inhibits the formation of cAMP. $G_{q/11}$ activates phospholipase C, which forms inositol trisphosphate (IP3) and diacylglycerol (DAG) from phosphatidylinositol-4,5-bisphosphate (PIP2). IP3 triggers the release of calcium ions (Ca^{2+}) in the cell. There are also further G proteins, for example, $G_{12/13}$, which activates small GTPases like RhoA, leading to the recruitment of transcription factors such as nuclear factor of activated T-cells (NFAT), nuclear factor 'kappa-light-chain-enhancer' of activated B-cells (NFκB) or serum-response element (SRE). The Gβγ subunit is able to induce a K^+ ion influx into the cell by activating the so-called G protein-coupled inwardly rectifying potassium channels (GIRKs) causing hyperpolarization. The G protein signal is abrogated by the G_α subunit-inherent GTPase activity. Thus, GTP is cleaved to GDP, and the G protein returns to its inactive state.

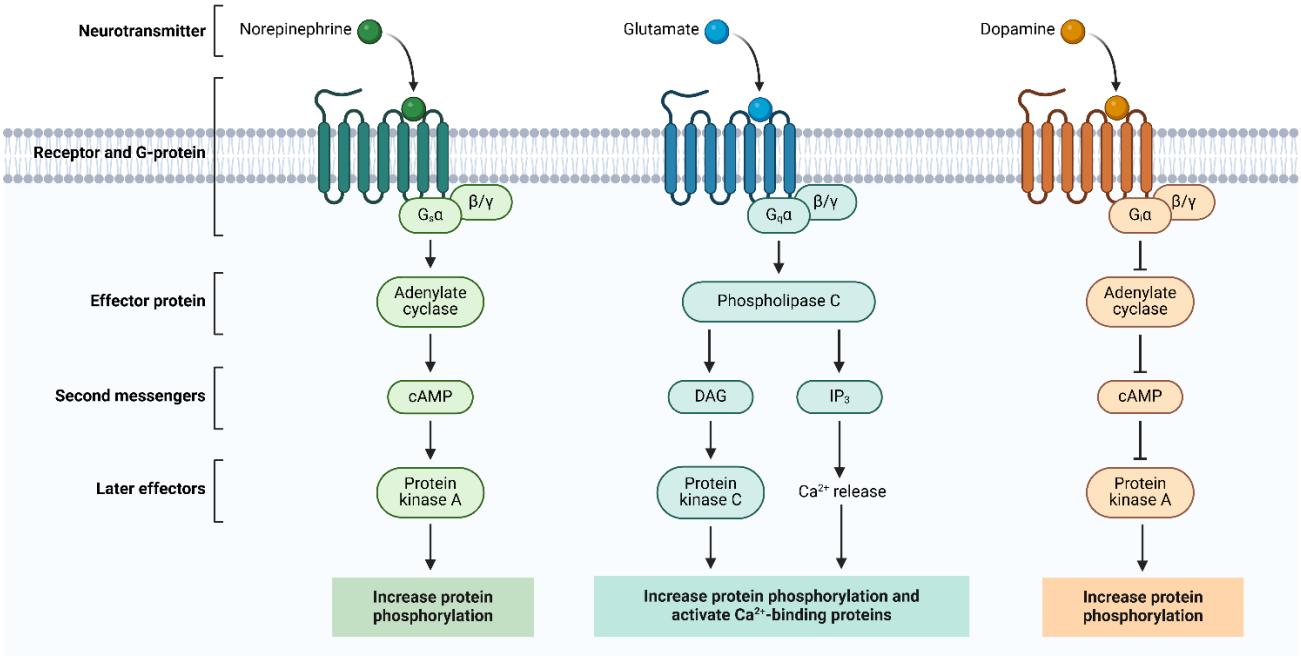

Figure 3. *Schematic representation of GPCR activation process. Upon agonist (colored circles) binding, the receptor couples with the G protein heterotrimer, where the exchange of GDP and GTP in G protein α subunit leads to G protein dissociation and mediate the different G protein signaling pathways.*

To prevent sustained signaling, activated G protein-coupled receptors (GPCRs) can undergo C-terminal phosphorylation, a process facilitated by G protein-coupled receptor kinases (GRKs, Figure 4). This multi-site phosphorylation of GPCRs determines the binding affinity of *β*-arrestin and leads to receptor desensitization. This is followed by clathrin-mediated endocytosis and ubiquitination of the receptor. Additionally, *β*-arrestin can activate signaling pathways independently, such as the mitogen-activated protein kinase (MAPK) pathway, which leads to the phosphorylation of extracellular signal-regulated kinase (ERK). In contrast, when the antagonists bind to the receptor, it stabilizes in an inactive state.

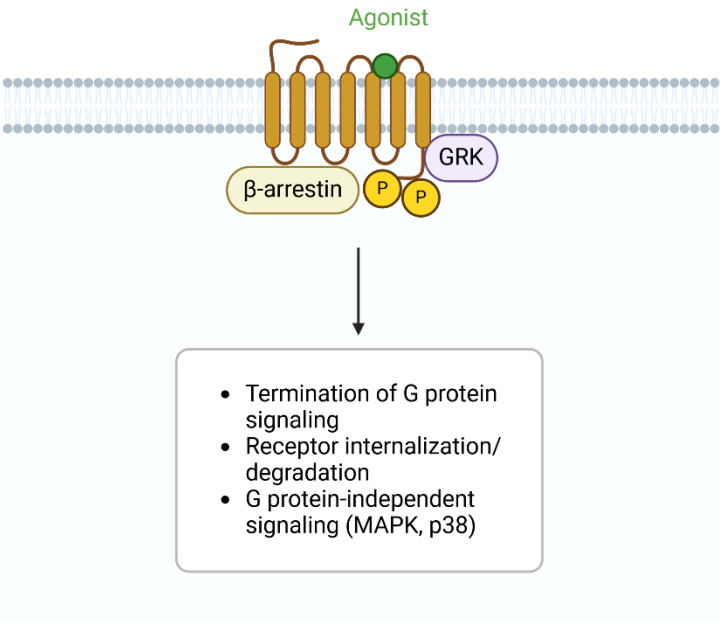

Figure 4. *The phosphorylation of the receptor C-terminal tail by G protein-coupled receptor kinases (GRK) binding promotes β-arrestin recruitment and signaling.*

1.2.2 New trends in GPCR drug discovery

An activated GPCR can have different effects, depending on the conformational state induced by a ligand. Specifically, different agonists can lead to distinct conformational states of the same receptor, which in turn will recruit different transducers (G proteins or β-arrestins), each one activating its own signaling pathway. As a result, this can lead to diverse physiological effects.

This behavior is called "biased agonism" and has become an increasingly active area of research, as it may lead to the identification of compounds with increased efficacy and reduced on-target side effects. [9,10]

GPCR ligands are categorized as (full) agonists, partial agonists, antagonists, and inverse agonists. Compounds inducing a partial activation or inhibition are called partial agonists or antagonists. They can be of interest when a full activation or inhibition causes side effects. Inverse agonists exert the opposite effect of agonists. They bind to the ligand binding site of constitutively activated receptors and stabilize them in an inactive state, effectively exhibiting negative intrinsic activity (Figure 5). Indeed, for many GPCRs, a constitutive activity, which means constant activation without the presence of an agonist, has been reported. Inverse agonists have been described for several families of 7TM receptors. For example, for the ion channels $GABA_A$ several inverse agonists have been reported. The beta carbolines

FG-7142 and DMCM, the heterocyclic annulated 1,4-diazepine Ro19-4603, and the pyrazolo triazine MK-016 are examples of inverse agonists of $GABA_A$ chloride channels.[11] These molecules bind to the benzodiazepine site of $GABA_A$ channels and stabilize them in a resting, closed state. Examples of inverse agonism in GPCR can be found in nearly all antihistamines, which have shown to be inverse agonists at histamine receptors H_1 and/or H_2.[12] Constitutive activity of GPCRs has been discussed to be a target of interest in different pathologies, including cancer.[12,13]

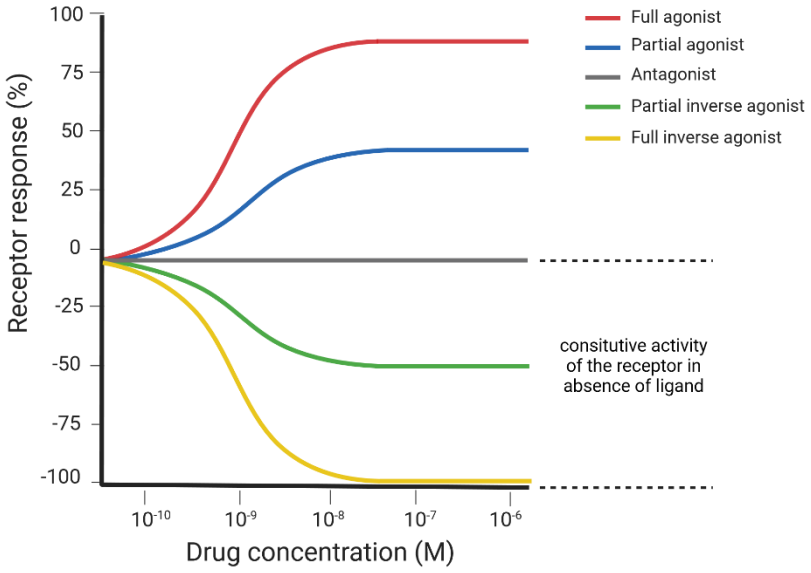

Figure 5. *Modulation of receptor activity by orthosteric ligands with varying efficacies. Original figure modified from Krall, J. et. al., $GABA_A$ Receptor Partial Agonists and Antagonists: Structure, Binding Mode, and Pharmacology, Advances in Pharmacology, 2015, 72, 201–227.*

An area of significant interest is the development of allosteric ligands. The orthosteric binding site is defined by the binding site of the endogenous ligand, whereas allosteric interactions occur at a distinct binding site. Allosteric ligands induce conformational changes in receptor proteins, thereby altering the affinity and/or efficacy of the endogenous ligand. This modulation can lead to beneficial therapeutic outcomes.[14] Moreover, the knowledge of allosteric sites is useful for the design of bitopic ligands, *i.e.* molecules able to bind to both an allosteric and orthosteric site. Bitopic ligands may have several advantages, such as improved affinity and enhanced selectivity over a single allosteric or orthosteric ligand and provide a viable strategy to develop biased ligands.[7]

GPCRs can engage in homo- or hetero-dimerization. They can bind to various transmembrane proteins to regulate their biological functions, such as ligand binding, and intracellular signaling. This promiscuous coupling leads to peculiar biochemical signaling profiles inside the cell called “fingerprints”, which contribute to the complexity of GPCR signaling.[14]

1.3 The endocannabinoidome

The understanding of the cannabinoid system has evolved significantly since its initial discovery. The initial identification of cannabinoid receptors began with the use of ^{3}H-labeled CP-55,940, a synthetic analog of Δ^{9}-tetrahydrocannabinol (THC), which facilitated the identification of high-affinity binding sites for THC within the brain. These binding sites were subsequently characterized as the cannabinoid receptor type 1 (CB_1), a G protein-coupled receptor (GPCR) that is predominantly expressed in cerebral tissues.[15] Following the identification of CB_1, the cannabinoid receptor type 2 (CB_2) was discovered through homology cloning. CB_2 is primarily expressed in the immune system, expanding the understanding of the cannabinoid system beyond the central nervous system.[16,17] The lipids anandamide (the ethanolamide of arachidonic acid) and 2-arachidonoylglycerol (2-AG) were named endocannabinoids after their identification in brain and intestinal samples and the demonstration that they activated CB_1 and CB_2 with high affinity and efficacy (Figure 6).[18]

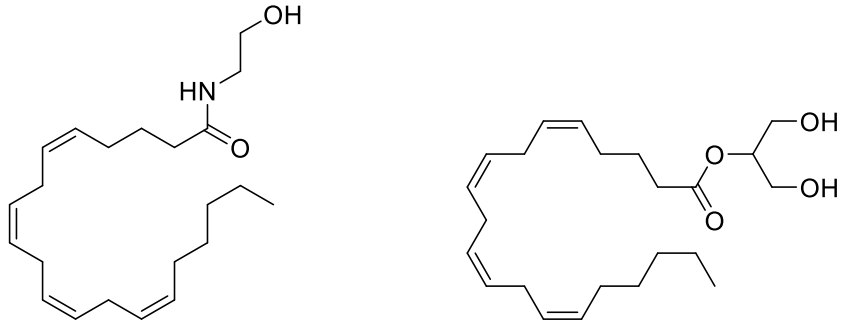

Figure 6. *Chemical structures of the two primary endocannabinoid mediators: anandamide and 2-arachidonoylglycerol.*

This discovery highlighted the role of the endocannabinoid system in physiological processes and their involvement in various signaling pathways that help maintain

homeostasis after pathological insults. Subsequently, a broader array of lipid mediators, receptors, and enzymes like fatty acid amide hydrolase (FAAH), monoacylglycerol lipase (MAGL) and diacylglycerol lipases (DAGL), involved in the degradation and synthesis of endocannabinoids, was identified, which was referred to as the endocannabinoid system. Alterations in the endocannabinoid system are observed in both experimental models and patients with neurological diseases[19–21] and genetic manipulations of this system in mouse models alter susceptibility to neurodegenerative disorders[22,23]. It is now clear that endocannabinoids play a crucial role in maintaining homeostasis after pathological insults through several mechanisms. For example, endocannabinoids, such as anandamide and 2-AG, act as retrograde signaling molecules that help modulate neurotransmitter release. They can inhibit the release of excitatory neurotransmitters like glutamate and γ-aminobutyric acid (GABA), thereby contributing to the regulation of neuronal excitability and maintaining balance in the CNS. These findings suggest that targeting the endocannabinoid system is a possible therapeutic strategy, which in fact ultimately led to the approval of nabiximols — a combination of THC and cannabidiol (CBD) — for the treatment of pain and/or spasticity in multiple sclerosis (MS) in 2005.[24]

Overall, the evolution of cannabinoid system understanding has transitioned from the identification of receptors and ligands to exploring their complex interconnections with other related biomolecules and the resulting physiological effects.

Indeed, the endocannabinoid system is complicated by the promiscuity of mediators and overlap with other pathways and alternative metabolic processes, so modulation of its components affects a wider endocannabinoid-related network known as the endocannabinoidome (Figure 7). The most studied receptors involved in the wider endocannabinoidome are TRPV1, PPARγ, PPARα, GPR55 and GPR18. While this complexity poses novel challenges to the development of selective drugs, it also offers new opportunities for the exploitation of non-THC cannabinoids, which often modulate several endocannabinoidome proteins.[1]

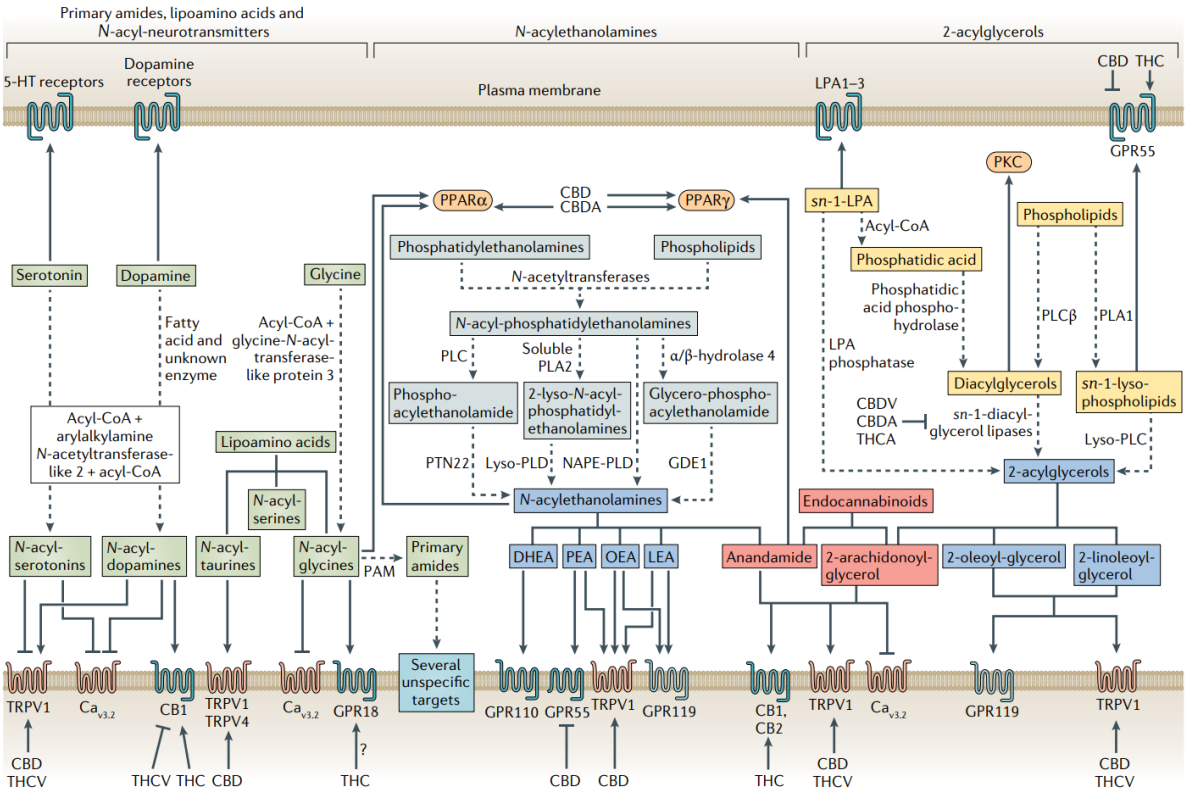

Figure 7. *Schematic representation of the expanded endocannabinoid system (or endocannabinoidome). The endocannabinoids anandamide and 2-arachidonoylglycerol (red boxes) are often accompanied by their congeners, the N-acylethanolamines and the 2-acylglycerols (dark blue boxes). These congeners share biosynthetic pathways and enzymes with the endocannabinoids (pale blue for N-acylethanolamines and yellow for 2-acylglycerols) and modulate targets other than cannabinoid receptor 1 (CB_1) and cannabinoid receptor 2 (CB_2), such as transient receptor potential cation channel subfamily V member 1 (TRPV1), peroxisome proliferator-activated nuclear receptor-α (PPARα) and PPARγ, T-type Ca^{2+} (Cav3.2) channels, and G protein-coupled receptors such as GPR18, GPR55, GPR110 and GPR119. The biosynthetic precursors of 2-acylglycerols also have their own targets, such as protein kinase C (PKC), GPR55 and lysophosphatidic acid receptors 1–3 (LPA1–3). Other long-chain fatty acid amides, such as primary amides, lipoamino acids, and some N-acyl-neurotransmitters, have also been identified as elements of the expanded endocannabinoid system with promiscuous targets, whereas no receptor for N-acyl-serines has been identified. Distinct biosynthetic pathways exist for different lipoamino acids and N-acyl-neurotransmitters (pale green boxes). Intracellular targets are shown as orange rounded boxes. Plant cannabinoids modulate several targets of the expanded endocannabinoid system or endocannabinoidome. 5-HT, 5-hydroxytryptamine; CBD, cannabidiol; CBDA, cannabidiolic acid; CBDV, cannabidivarin; DHEA, N-docosahexaenoyl-ethanolamine; GDE1, glycerophosphodiester phosphodiesterase 1; lyso-PLD, lysophospholipase D; MAGK, monoacylglycerol kinase; NAPE-PLD, N-acyl-phosphatidylethanolamine-specific phospholipase D; PAM, peptidyl-glycine α-amidating monooxygenase; P2Y6, P2Y purinoceptor 6; PG, prostaglandin; PLA, phospholipase A; PLC, phospholipase C; PTN22, tyrosine-protein phosphatase non-receptor type 22; THC, Δ^9 -tetrahydrocannabinol; THCA, Δ^9 -tetrahydrocannabinolic acid; THCV, Δ^9 -tetrahydrocannabivarin. Picture taken from Cristino, L., Bisogno, T. & Di Marzo, V. Cannabinoids and the expanded endocannabinoid system in neurological disorders. Nat Rev Neurol 16, 9–29 (2020).*

1.3.1 Cannabinoid receptors

Cannabinoid receptors (CB receptors) derive their name from the most prominent group of compounds that interact with them, specifically those found in *Cannabis sativa*. The effects and structures of cannabinoids have been understood for an extended period, before the identification of their specific targets. Δ^9-THC, recognized as the primary psychoactive constituent of the plant, was documented as a significant psychoactive agent in the late 1950s. Crystal structures of human cannabinoid receptors are shown in Figure 8.

CB_1 receptors are primarily found in the central nervous system (CNS). Its expression was reported in hippocampus, cortex, basal ganglia and cerebellum, where the receptor can primarily be found presynaptically on both excitatory glutamatergic and inhibitory GABAergic neurons. Activated glutamatergic and GABA-ergic neurons produce endocannabinoids at the postsynaptic end and activate the presynaptically distributed CB receptors. Upon activation, these receptors inhibit voltage-gated calcium (Ca^{2+}) channels and suppress the vesicular release of the neurotransmitters GABA and glutamate. Collectively, these findings suggest that endocannabinoids, especially 2-AG, function as inhibitory retrograde neuromodulators, through processes known as depolarization-induced suppression of excitation (DSE) or depolarization-induced suppression of inhibition (DSI).[25–27]

A major role of CB_2 receptors is immune modulation. In the context of neurological disease, the CB2 receptor is strongly and selectively expressed in microglia in diseases such as Alzheimer's disease (AD), multiple sclerosis (MS), and amyotrophic lateral sclerosis (ALS).[28] Another study has indicated that CB2 activation reduces pro-inflammatory cytokine release from activated microglia in AD.[29]

1.3.2 Medicinal chemistry of cannabinoid receptors

Compounds that exhibit affinity for CB receptors can be categorized into five structurally distinct classes: endogenous ligands (anandamide and 2-AG); phenolic compounds related to Δ^9-THC; *N*-alkyl indoles, originally designed by J. W. Huffman and his colleagues; pyrazoles, such as the CB_1 receptor inverse agonist rimonabant; and other compounds that do not fit into any of these categories (Figure 9).

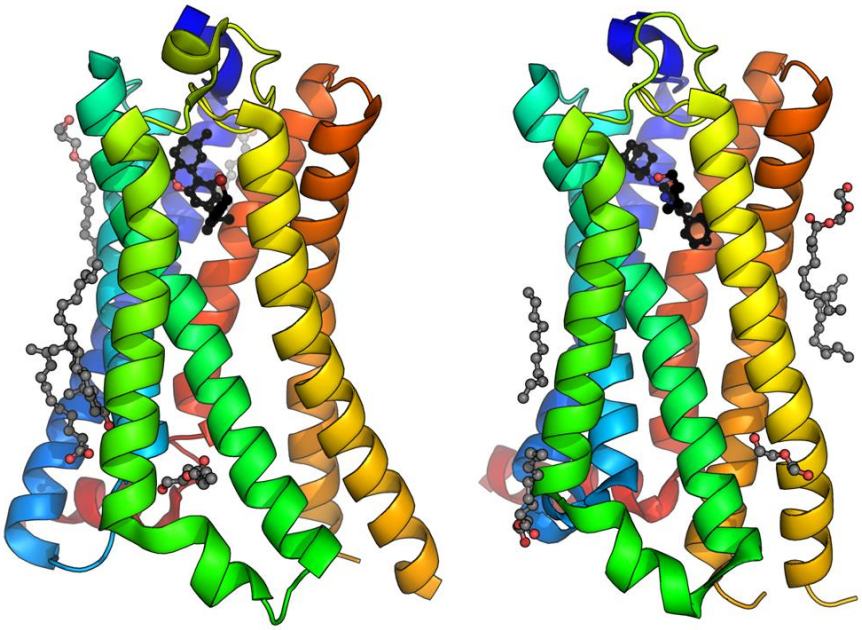

Figure 8. *Crystal structures of human cannabinoid receptors bound to their respective agonists (in black). On the left, cannabinoid receptor 1 (CB_1) bound to agonist AM11542 (PDB: 5XRA); on the right, cannabinoid receptor 2 (CB_2) bound to antagonist AM10257 (PDB: 5ZTY).*

CB_1 receptor agonists are the first group of CB receptors ligands that have been approved for medical use. A combination of THC and CBD in the form of a buccal spray (Sativex®) for the treatment of pain and/or spasticity in MS was approved in 2005 in several European countries. It was further discussed to be beneficial in the treatment of chronic neuropathic pain.[30] A synthetic derivative of Δ^9-THC, nabilone, was developed by Eli Lilly and launched as a treatment against emesis and as a tranquilizer in the 1980s.[31] Due to the psychoactive effects of CB_1 receptor agonists, they are considered controlled drugs in most Western countries.

CB_1 receptor antagonists/inverse agonists have been developed for obesity. Rimonabant (Acomplia®, SR141716A) was approved in Europe in 2006 but was withdrawn in 2008 due to serious psychiatric side effects, such as depression and suicidal behavior.[32,33] This experience emphasizes the complexity of the cannabinoids' actions in the brain. New therapeutic options in the field of CB_1 antagonists and inverse agonists might be the use of allosteric modulators, peripherally acting CB_1 antagonists, or the exploitation of a negative biochemical cross-talk between another receptor (for example GPR55) and CB_1.[34]

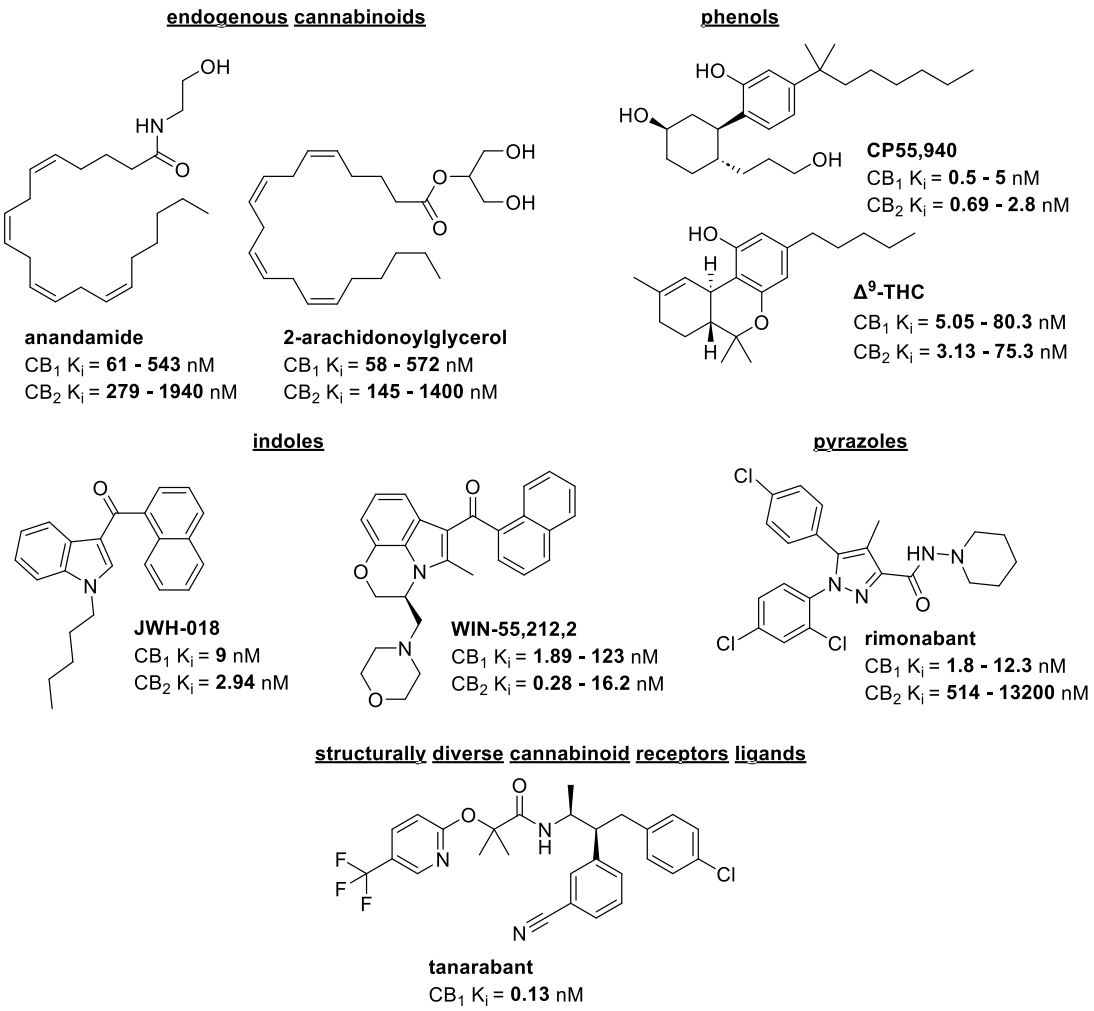

Figure 9. *Chemical structures and affinities of some CB receptor ligands. Affinity data were taken from Pertwee, R. G. et al., International Union of Basic and Clinical Pharmacology. LXXIX. Cannabinoid receptors and their ligands: beyond CB_1 and CB_2. Pharmacol. Rev. 2010, 62, 588–631.*[35]

While undesirable central side effects limit the potential of CB_1 receptor ligands, the interest toward CB_2 receptor ligands is emerging, as there is no evidence of psychoactive side effects. Its distribution in immune system cells has made it an interesting target for neurodegeneration[1], neuropathic pain, immunologic diseases, cancer, and osteoporosis.[36] In the CNS, CB_2 receptors are primarily found in microglia, the cells that participate in neuroinflammatory processes. The activation of these receptors has been shown to produce immunosuppressive and anti-inflammatory effects. As a result, selective CB_2 agonists are being explored as potential therapeutic options for neurological conditions, including multiple sclerosis (MS), Alzheimer's disease (AD), and Huntington's disease (HD).[37] Even if CB_2 receptor agonists show great therapeutic potential, their clinical success has been hindered, with no selective CB_2 receptor agonist making it to market thus far.

Researchers are exploring the therapeutic possibilities of CB_2 receptor antagonists and inverse agonists in clinical applications. For example, a newly identified CB_2 receptor antagonist, TT816 (structure undisclosed, IC_{50} at CB_2 receptor = 26.2 nM) developed by Teon Therapeutics, is currently in phase 2 clinical trials (NCT05525455) for advanced cancers lung, renal cell, and ovarian cancer. Furthermore, the CB_2 receptor inverse agonist SMM-189[38] has shown promise as a potential treatment, proving effective in managing colitis. SMM-189 has been noted to improve colitis symptoms by influencing immune cell populations and anti-inflammatory signaling pathways, indicating its potential as a safe therapeutic option for inflammatory bowel disease (IBD).

The exploration of ligand-biased signaling patterns, the use of allosteric modulators, and the development of pharmacological tools for a better understanding of the biochemical cross-talks in homomers and heteromers of CB receptors represents an opportunity for novel medicinal chemistry approaches as well as clinical advancement in the field of CB receptors modulators.

1.3.3 Cannabinoid-activated G protein-coupled receptors

The G-protein coupled receptors (GPCRs) super-family represents one of the largest groups of proteins found in vertebrate species (Figure 11). These receptors exhibit a wide range of structural and functional diversity, yet they still possess several common structural characteristics. The majority of human GPCRs can be categorized into five primary families known as Glutamate, Rhodopsin, Adhesion, Frizzled/Taste2, and Secretin, which form the GRAFS classification system..[39] The rhodopsin family is the largest and forms four main groups termed alpha, beta, gamma, and delta with 13 sub-branches.

In the rhodopsin-like GPCR subfamily almost one hundred orphan GPCRs can be found. Many of them belong to the δ-branch. Among others, two GPCRs (GPR18 and GPR55) are located in this group of receptors, to which also the purinergic P2Y, peptide-activated and lipid-activated receptors belong. These two receptors, although showing little structural similarity to CB_1 and CB_2 receptors, have been reported to respond to endogenous agents analogous to the endogenous cannabinoid ligands, as well as some natural/synthetic cannabinoid receptor ligands.[35] For this reason, GPR18 and GPR55 are considered cannabinoid-related receptors. Although there are multiple reports to indicate that GPR18 and GPR55 can be activated *in*

vitro by *N*-arachidonoylglycine and lysophosphatidylinositol respectively (Figure 10), there is a lack of evidence for activation by these lipid messengers *in vivo*. For this reason, some authors still refer to them as "orphan receptors".[40]

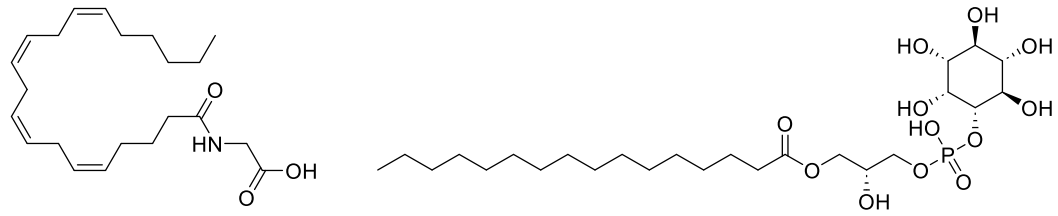

N-arachidonoylglycine (NAGly)
GPR18 agonist, EC_{50} **44.5 – 20** nM

lysophosphatidylinositol (LPI)
GPR55 agonist EC_{50} **1000 – 49** nM

Figure 10. *Proposed endogenous ligands for the G protein-coupled receptors GPR18 and GPR55 and their reported EC_{50} values.*

1.3.4 GPR18

GPR18 was reported to interact with *N*-arachidonoylglycine (NAGly, EC_{50} 44.5 – 20 nM).[41] To identify the endogenous ligand for GPR18, Kohno *et al.* screened a lipid library in Ca^{2+}-mobilization assays on GPR18-transfected cells, and detected a signal induced by NAGly. They confirmed their finding by cAMP accumulation assays in CHO cells stably expressing the receptor and reported an IC_{50} value of 20 ± 8 nM. Their signal was abolished upon pretreatment with PTX, a G_i protein-decoupling agent, thus proving the receptor was G_i-coupled.[42] NAGly was found to be a substrate for FAAH,[43] but not for the cannabinoid receptors, despite its structural similarity with anandamide, the endogenous ligand of the cannabinoid receptors.[44]

Console-Bram *et al*. investigated five cannabinoid ligands – Δ^9-THC, abnormal cannabidiol (Abn-CBD), O-1918, O-1602, and NAGly – in MAPK signaling, Ca^{2+} mobilization, and β-arrestin signaling. Increases in both intracellular calcium and MAPK, two cellular signaling pathways, were observed in HEK/GPR18 cells in the presence of all five cannabinoid ligands. However, the only agonist that exhibited concentration-dependent GPR18-mediated β-arrestin activity was Δ^9-THC. This result reinforces the classification of GPR18 as a cannabinoid receptor. The authors concluded that biased agonism occurs at GPR18.[45]

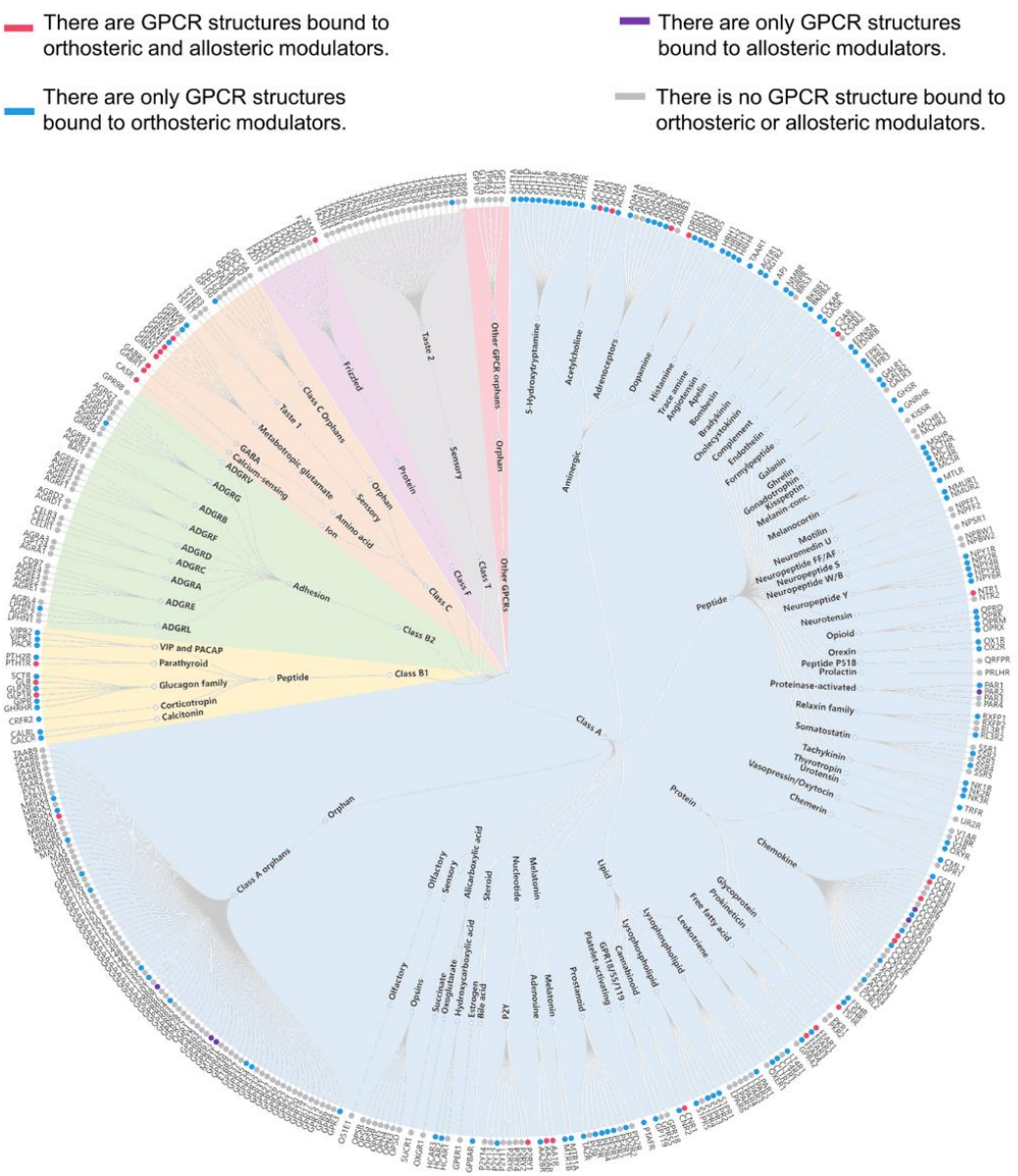

Figure 11. *Phylogenetic tree of GPCRs indicating GPCR structures that have been solved in complex with modulators. Nodes represent GPCRs named according to their UniProt gene name and are organized according to the GPCR database. GPCR structures bound to modulators are highlighted by color. Picture taken from Zhang, M. et al. G protein-coupled receptors (GPCRs): advances in structures, mechanisms and drug discovery. Sig Transduct Target Ther* ***9****, 88 (2024).*[7]

In contrast to the previous studies, Yin et al. did not monitor any activation of GPR18 by NAGly when they were screening a lipid library in an enzyme complementation assay for β-arrestin recruitment.[46] Finlay *et al.* performed a thoroughly controlled study reporting that in several functional assays under various conditions, GPR18-dependent effects on $G\alpha_{i/0}$ or G_s signaling by NAGly were observed in neither Chinese hamster ovary (CHO) nor human embryonic kidney (HEK) cells recombinantly expressing GPR18.[47] These findings are in

agreement with results from Müller C. E. *et al.*[48–52], proving that only THC activates the human GPR18 *via* β-arrestin recruitment and that this receptor retains its orphan status (Figure 12).

However, GPR18 was also reported to be constitutively active.[53] Its constitutive activity remains an interesting facet of receptor function and will have consequences for understanding the role of GPR18 in physiology.[47] Selective inverse agonists are needed to further clarify this aspect.

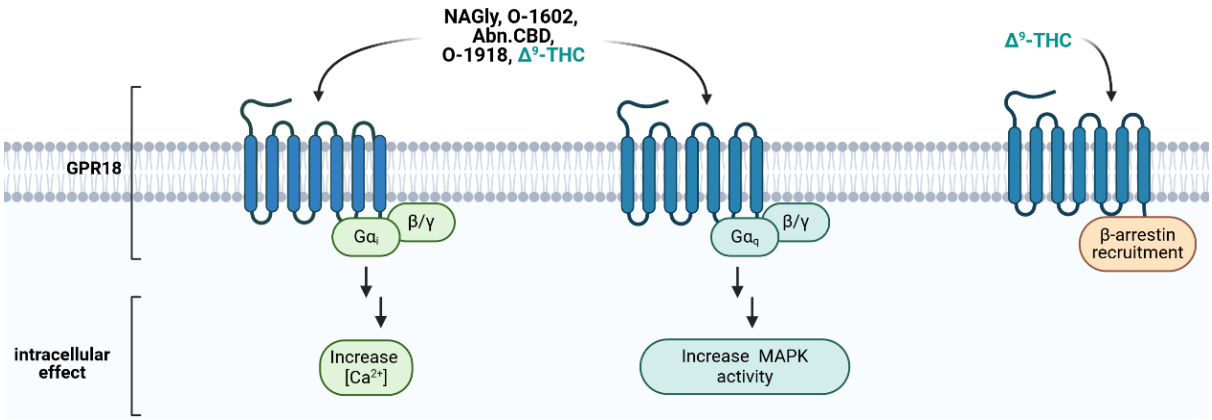

***Figure 12**. Schematic representation of proposed signaling pathways in GPR18 activation. Some groups report GPR18-dependent effects on $G\alpha_{i/0}$ or G_s signaling by NAGly and other cannabinoids (Δ^9-THC, Abn-CBD, O-1918, O-1602) in HEK/GPR18 cells, and β-arrestin recruitment only upon Δ^9-THC activation. Other studies report that only THC activates the human GPR18 via β-arrestin recruitment (see text for references).*

In addition to cannabinoid mimetic compounds, a class of xanthine-derived molecules acts as agonist at the GPR18 receptor. PSB-KK1415 (EC_{50} 19.1 nM) and PSB-KK1445 (EC_{50} 45.4 nM) are the most potent and selective GPR18 agonists reported to date (Figure 13).[52]

GPR18 is expressed in microglia, suggesting a potential role in neuroinflammation.[54] A variety of immune cells express GPR18, which is crucial for the immune response. In addition, GPR18 governs numerous physiological processes, such as neutrophil infiltration, the maturation of CD8αα γδTCR positive lymphocytes, the differentiation and expulsion of macrophages, and the migration and proliferation of BV2 microglial cells, endothelial cells, human sperm, tumor cells, and human endometrial cells. Furthermore, GPR18 may play a role in

reducing the pro-inflammatory M1 phase in macrophages as well as in the migration of microglia and endometrial cells.[55]

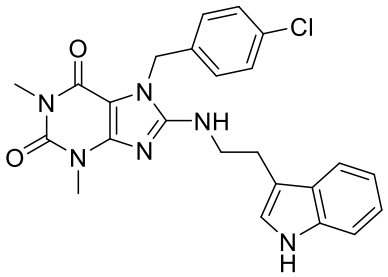

PSB-KK1415
EC_{50} human GPR18: **19.1** nM
(β-arrestin assay)

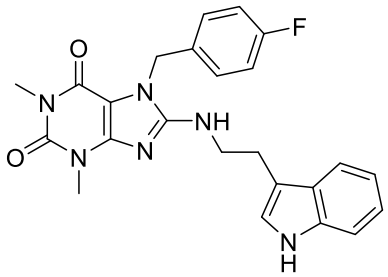

PSB-KK1445
EC_{50} human GPR18: **45.4** nM
(β-arrestin assay)

Figure 13. *The most potent and selective GPR18 agonists reported to date.*

Antagonists for GPR18 have been found among natural products or synthesized molecules. For example, amauromine, an indole-fused diketopiperazine-containing compound, was found in marine sponge extracts. It is not only a potent CB_1 receptor antagonist (K_i value 0.178 μM), but also a GPR18 antagonist with potency in the low micromolar range (IC_{50} = 3.74 μM).[50] Another antagonist, PSB-CB-5, was the first potent and selective antagonist of GPR18, not active at the related GPR55, with no affinity to the CB_1, and a weak affinity to CB_2 (Figure 14).

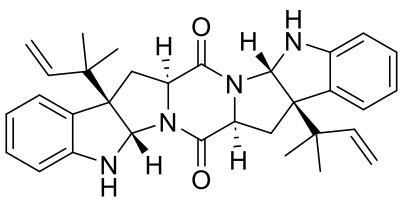

amauromine
GPR18: IC_{50} = **3.74 μM**
GPR55: IC_{50} > 10 μM
CB_1: K_i = **0.178 μM**
CB2: K_i > 10 μM

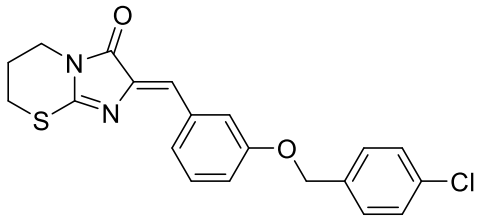

PSB-CB-5
GPR18: IC_{50} = **0.279 μM**
GPR55: IC_{50} > 10 μM
CB_1: K_i > 10 μM
CB_2: K_i = **4.03 μM**

Figure 14. *Examples of antagonists at the GPR18 receptor.*

The therapeutic potential of GPR18 remains largely unvalidated; however, its significant role in inflammatory processes indicates a possible function in the

resolution of inflammation. By stimulating GPR18 in the context of an inflammatory disease, it may be possible to mitigate the progression of the inflammatory response. Various studies have reported the expression of GPR18 in M1 macrophages, which are associated with inflammatory diseases, including neuroinflammatory disorders. Nonetheless, the precise involvement of GPR18 in neuroinflammation and the potential benefits of its activation require further investigation.

Additionally, GPR18 has been examined in relation to cancer and migratory processes, where inhibiting GPR18 activity may yield beneficial therapeutic outcomes. The current ambiguity surrounding GPR18 agonists complicates the reliance on existing published findings.

Contradictory reports and the use of non-selective compounds severely hamper the potential of ongoing GPR18 research. It is imperative that, when investigating GPR18 pharmacology, the pharmacodynamic consequences of the utilized agonists or antagonists are thoroughly characterized. Consequently, there is a pressing need for selective and potent compounds, both agonists and antagonists, to comprehensively elucidate the role of GPR18 in physiological and pathological contexts.

1.3.5 GPR55

In 2007, Oka et al. demonstrated that L-α-lysophosphatidylinositol (LPI) activates GPR55 and that this effect is absent in GPR55 knockdown cells.[56] Following similar discoveries by other groups, LPI has gradually been accepted as the endogenous ligand of GPR55. In the meantime, synthetic CB1 antagonists, such as AM251 and SR141716A, have been shown to activate GPR55 in cell-based reporter assays.[57] As in the case of GPR18, modulation of the receptor occurs upon interaction with endo/phyto and synthetic cannabinoids (Figure 15). Surprisingly, these ligands display opposite effects at the GPR55 compared to CB receptors: usually, CB antagonists activate GPR55, while CB agonists have antagonistic effects at GPR55. Thus, GPR55 has been referred to as an “anti-cannabinoid” receptor (Figure 16).[58] Selective antagonists for this receptor have also been reported (Figure 17). [58–60]

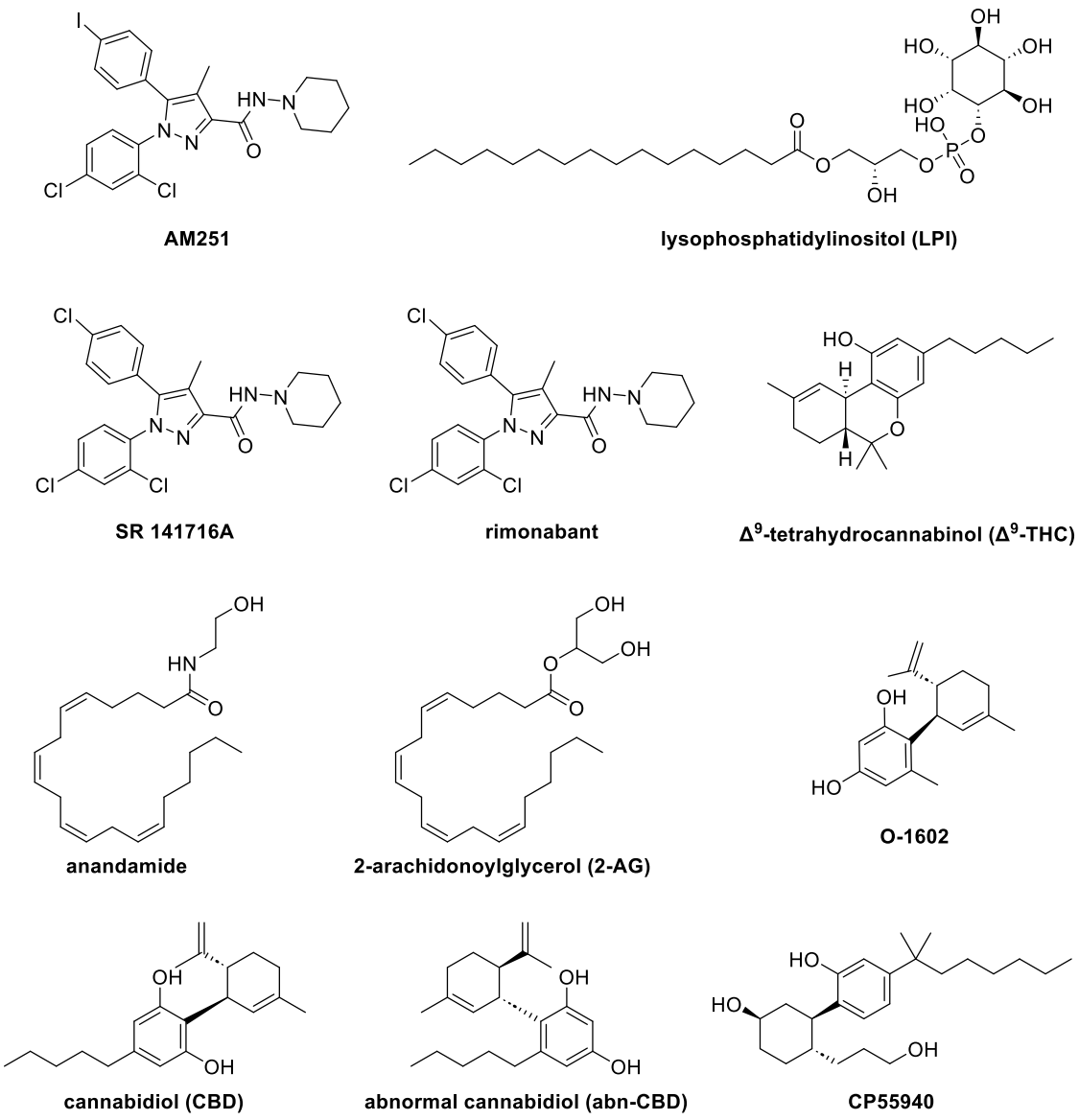

Figure 15. *Chemical structures of some GPR55 ligands. Activities are reported in Table 1.*

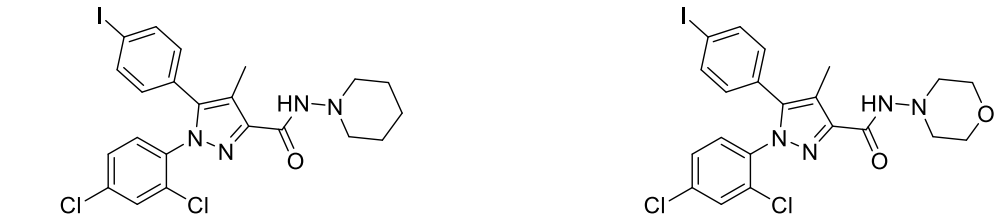

AM251
GPR55 agonist
EC_{50} = **39 nM** ([^{35}S]GTPγS binding assay)
EC_{50} = **612 nM** (Ca^{2+} mobilization assay)
EC_{50} = **3-9.6 μM** (β-arrestin assay)
CB_1 receptor antagonist / inverse agonist
(IC_{50} = **8 nM**, Ki = **7.49 nM**)

AM281
no effect on GPR55
EC_{50} > 30 μM ([^{35}S]GTPγS binding assay)
EC_{50} = N.T. (Ca^{2+} mobilization assay)
EC_{50} = N.E. (β-arrestin assay)
CB_1 receptor antagonist / inverse agonist
(IC_{50} = **9.91 nM**, Ki = **12 nM**)

Figure 16. *Chemical structure of two diarylpyrazole compounds, AM251 and AM281, active as antagonists / inverse agonists at CB_1* receptor. *The aliphatic moiety on the carboxamide group at position 3 of the diarylpyrazole scaffold may be more important for ligand binding to GPR55 than for binding to the CB_1 receptor, within this chemical series of compounds.*[61]

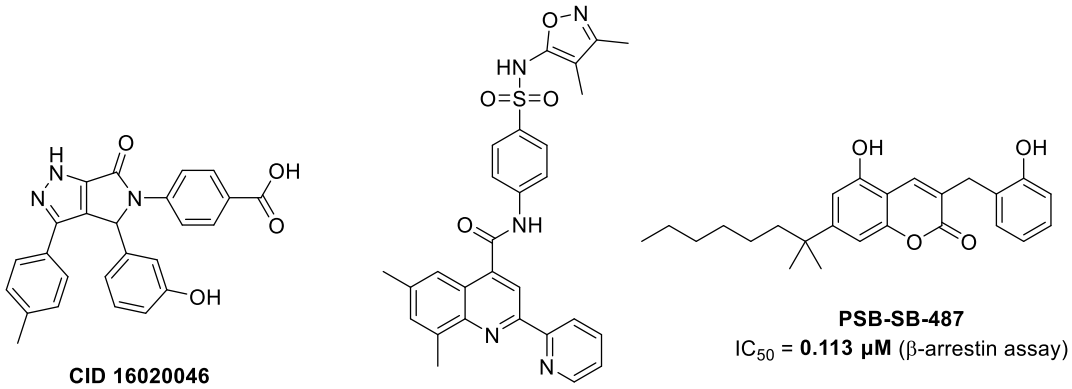

CID 16020046
IC_{50} = **0.21 μM** (Ca^{2+} assay)

ML193
IC_{50} = **0.22 μM** (β-arrestin assay)

PSB-SB-487
IC_{50} = **0.113 μM** (β-arrestin assay)

Figure 17. *Structures of other chemically diverse reported GPR55 antagonists.*

While GPR55 primarily signals through G_{13} pathway, it has been reported to induce G_q signaling under certain circumstances. Ruixue Xia *et al.* showed that LPI most robustly activates GPR55 with an EC_{50} in the micromolar range (~0.34 μM).[62] In contrast, O-1602 and AM251 only weakly activate GPR55 in a BRET dissociation assay of G_{13}. They also proved that LPI and other GPR55 ligands activated G_q signaling, but to a much lesser extent than G_{13} signaling, indicating that GPR55 mainly signals through G_{13} signaling. Similarly, in the NanoBiT recruitment assay of β-arrestin, LPI was able to recruit β-arrestin to GPR5, but not all the other ligands used. β-arrestin recruitment was also proved by other research groups using different compounds (LPI, AM251 and 3-substituted coumarins). [57,58] Collectively,

these data support the conclusion that LPI is a privileged ligand of GPR55 and that different ligands promote receptor coupling to multiple signaling pathways, *i.e.* biased signaling occurs at this receptor.

Very recently, the structures of LPI and AM251-bound GPR55 in complex with G_{13} by single particle analysis of cryo-electron microscopy (cryo-EM) at resolutions of 2.85 Å and 3.19 Å were solved and published (Figure 18). [62]

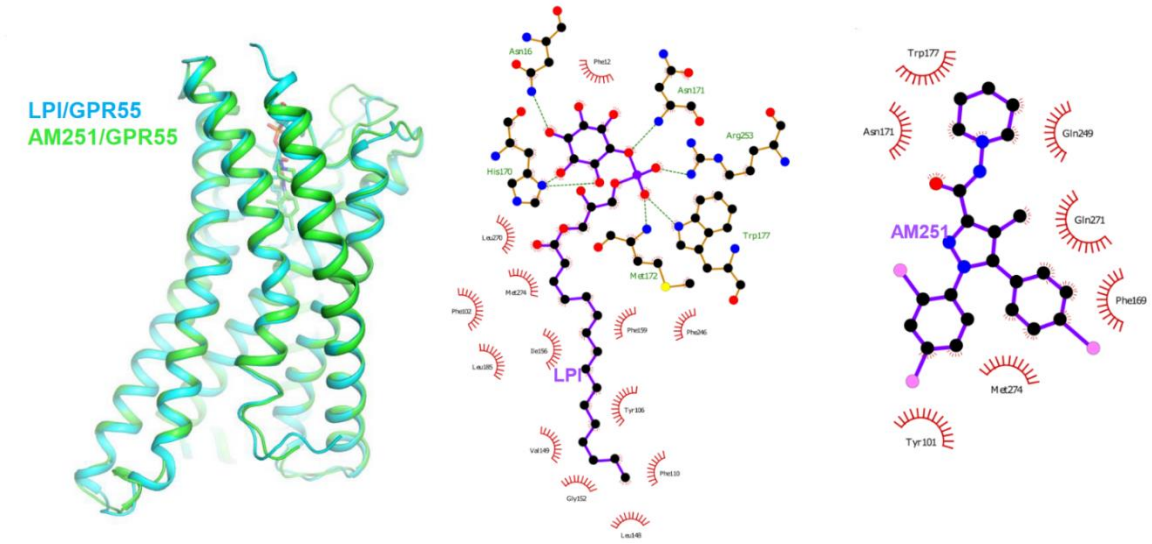

Figure 18. *On the left, the structures of LPI and AM251-bound GPR55. In the middle, a schematic LPI/GPR55 interaction map. On the right, a schematic AM251/GPR55 interaction map.*

The role of GPR55 as an endocannabinoid receptor is described as controversial. It is known to play crucial roles in the nervous and metabolic systems. In the nervous system, GPR55 is highly expressed in hippocampus, brain stem, cerebellum, frontal cortex, hypothalamus, and striatum. GPR55 is intricately linked to sensation, cognition, and pain perception, rendering it a promising target for the treatment of Parkinson's disease. Agonists of GPR55, such as O-1602 and palmitoylethanolamide, have demonstrated efficacy in alleviating pain in animal models. This receptor is abundantly expressed in various tissues within the metabolic system, including adipocytes, pancreatic islets, the gastrointestinal tract, and the adrenal glands. In alignment with its expression profile, GPR55 plays a crucial role in regulating insulin secretion, intestinal inflammatory factors, and

plasma glucose levels, thereby presenting a significant target for addressing metabolic disorders such as diabetes and nonalcoholic steatohepatitis. In the context of neurological disorders, evidence indicates that the activation of GPR55 stimulates excitatory hippocampal neurons, which may be detrimental in conditions characterized by glutamate excitotoxicity, including epilepsy and AD. Furthermore, GPR55 is activated by endocannabinoidome mediators, including anandamide, 2-AG, and palmitoylethanolamide, highlighting its involvement in excitatory neurotransmission. The activation of this receptor may have significant implications for neuroinflammatory conditions; however, specific information regarding its physiological functions remains limited.[1]

Table 1. *Reported activities of cannabinoid receptor ligands at recombinant GPR55 in various assays. The structures of all compounds listed are shown in Figure 15.*

LIGAND	[^{35}S]GTPγS BINDING	ERK1/2 PHOSPHORYLATION	$[Ca^{2+}]_i$ MOBILIZATION	BETA-ARRESTIN	GPR55 INTERNALIZATION	RHOA ACTIVATION
LPI	EC_{50} = 1 μM[a]	EC_{50} = 200 nM[a]	30 nM[a]	EC_{50} = 3.6 μM[b]	3 μM[c]	1 μM[d,e]
		1 μM[d,f]	3 μM[g,h]	EC_{50} = 1.2 μM[c]		
			3 μM[c]	EC_{50} = 49 nM[i]		
			10 μM[i]			
ANANDAMIDE	EC_{50} = 18 nM[k]	10 μM[i]	5 μM[g]	Very weak agonist[b]	N.E.[c]	1 μM[k]
			EC_{50} = 7.3 μM[i]	N.E.[c]		
2-AG	EC_{50} = 3 nM[k]	N.E.[a,c]	N.E.[h,i]	N.E.[c]	N.E.[c]	N.T.
Δ^9-THC	EC_{50} = 8 nM[k]	N.E.[a]	5 μM[g,h]	N.E.[c]	N.E.[c]	5 μM[g]
CANNABIDIOL	IC_{50} = 350 nM[k]	1 μM antagonist[d]	N.E.[g]	N.E.[c]	N.E.[c]	1–10 μM antagonist[d,k]
ABN-CBD	EC_{50} = 2.5 μM[k]	N.E.[a]	N.E.[g]	N.E.[b,c]	N.T.	N.T.
O-1602	EC_{50} = 13 nM[k]	1 μM[d]	10 μM[i]	N.E.[c]	N.T.	1 μM[d,e,f]
	EC_{50} = 2.5 nM[l]					
CP55940	EC_{50} =5 nM[k]	10 μM antagonist[c]	10 μM antagonist[i]	K_i ~200 nM[c]	K_i ~200 nM[c]	N.T.
RIMONABANT	N.T.	N.E.[a]	1–2 μM antagonist[g,h,i]	EC_{50} = 9.3 μM[k]	30 μM[c]	N.T.
				EC_{50} = 3.9 μM[c]		
AM251	EC_{50} =39 nM[k]	N.E.[a]	N.T.	3 μM[b]	30 μM[c]	N.T.
				9.6 μM[c]		
AM281	EC_{50} >30 μM[k]	N.T.	N.T.	N.E.[c]	N.E.[c]	N.T.

N.E., no effect; N.T., not tested. [a] Oka et al. (2007): hGPR55 stably transfected in HEK293 cells with a tetracycline-inducible promoter. [b] Yin et al. (2009): hGPR55 transiently transfected in HEK293 cells. [c] Kapur et al. (2009): hGPR55E stably transfected in HEK293 cells (β-arrestin assay) or U2OS cells (β-arrestin and GPR55 internalization assays). [d] Whyte et al. (2009): human osteoclast primary cultures. [e] Whyte et al.

(2009): mouse osteoclast primary cultures. [f] Pietr et al. (2009): BV-2 (mouse microglial cell line). [g] Lauckner et al. (2008): hGPR55 transiently transfected in HEK293 cells. [h] Lauckner et al. (2008): mouse DRG primary cultures. [i] Henstridge et al. (2009): hGPR55 stably transfected in HEK293 cells. [j] Waldeck-Weiermair et al. (2008): EA.hy926 (human umbilical vein derived endothelial cell line). [k] Ryberg et al. (2007): hGPR55 transiently transfected in HEK293s cells. [l] Johns et al. (2007): hGPR55 transiently transfected in HEK293T cells.

1.4 Targeting AChE and BChE inhibition

The impairment of cholinergic neurotransmission is a consolidated downstream process in the cognitive deficit accompanying neurodegenerative diseases such as AD, and cholinesterases inhibitors (ChEIs) have been reported to interfere with its pathogenesis and progression by recovering cortical cholinergic neurotransmission.[63] The drugs currently available for the symptomatic treatment of mild-to-moderate AD include the competitive (galantamine, donepezil) or pseudo-irreversible carbamate-based (rivastigmine) acetylcholinesterase (AChE) inhibitors (Figure 19).

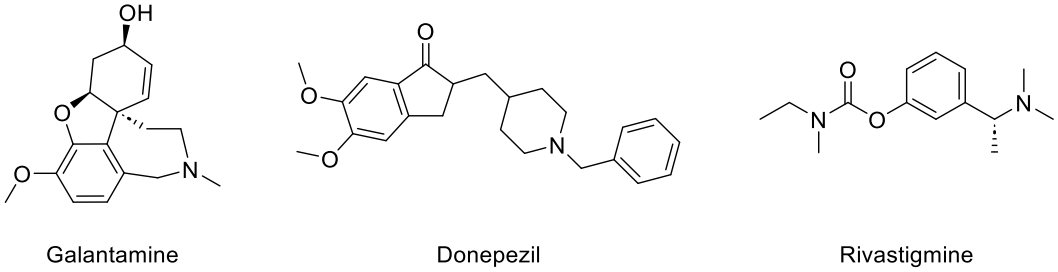

Figure 19. *Approved cholinesterase inhibitors for the treatment of AD.*

The neurotransmitter acetylcholinesterase (ACh) is mainly hydrolyzed by AChE in the synaptic cleft of the cholinergic neurons. At higher concentrations, ACh is also hydrolyzed by butyrylcholinesterase (BChE), the α-glycoprotein produced by liver and primarily distributed in plasma, but also localized in the central and peripheral nervous systems. The exact physiological role and functions of BChE have not yet been completely understood. At present, it is known that plasma BChE is responsible for detoxification metabolism of xenobiotics[64,65], while BChE expressed and secreted in CNS glial cells and neurons likely acts as a co-regulating factor of cholinergic neurotransmission and neuroinflammation.[66] Many studies also suggested a pivotal role of BChE in onset and progression of AD, since the level of AChE, dominant in healthy brain, declines with disease progression, whilst a significative increase (about 30–60%) of BChE expression and activity was found in animal models and in post-mortem brain tissues analysis. Thus, a putative compensating catalytic function of BChE in the synaptic cleft is believed to contribute to behavioral and cognitive dysfunction following the cholinergic

deficit.[67–69] Moreover, the BChE levels resulted in high correlation with the abnormal β-amyloid (Aβ) deposition. Despite limited knowledge on mechanism linking amyloidogenesis and BChE, the selective BChE inhibitor phenethyl cymserine was reported to reduce Aβ fibrils deposition in some cerebral areas (amygdale, hippocampal structures, thalamus and basal ganglia), thus ameliorating cognitive dysfunction induced by Aβ1-40 peptide in animal model, also affecting BChE activity in glia-mediated neuroinflammation.[70] Due to the enzyme distribution, the selective BChE inhibitors can represent an alternative strategy for the treatment of advanced AD, without peripheral side effects (leg cramps and gastrointestinal upset) reported for prolonged treatments with AChEIs.

AChE and BChE share about 70% of sequence homology. The active site of both enzymes is a deep and narrow gorge, and contains the high conserved catalytic triad (Ser203, His447, Glu334), the so-called oxy anion hole stabilizing the transient tetrahedral enzyme-substrate complex, and the acyl binding pocket (ABP). The choline-binding pocket is buried at the bottom of the gorge, in which a residue of Trp is involved in the orientation and stabilization of choline through cation-π interactions. Finally, the peripheral active site (PAS) is located on the rim of the active site gorge. AChE and BChE mainly differ in the ABP and PAS. Two aromatic residues (Phe295 and Phe297) in the ABP of AChE are replaced by aliphatic residues (Leu286 and Val288) in ABP of BChE; six of the aromatic residues lining the AChE gorge rim and PAS are replaced by aliphatic residues in BChE, thus resulting the BChE cavity larger than AChE gorge (Figure 20).[71,72]

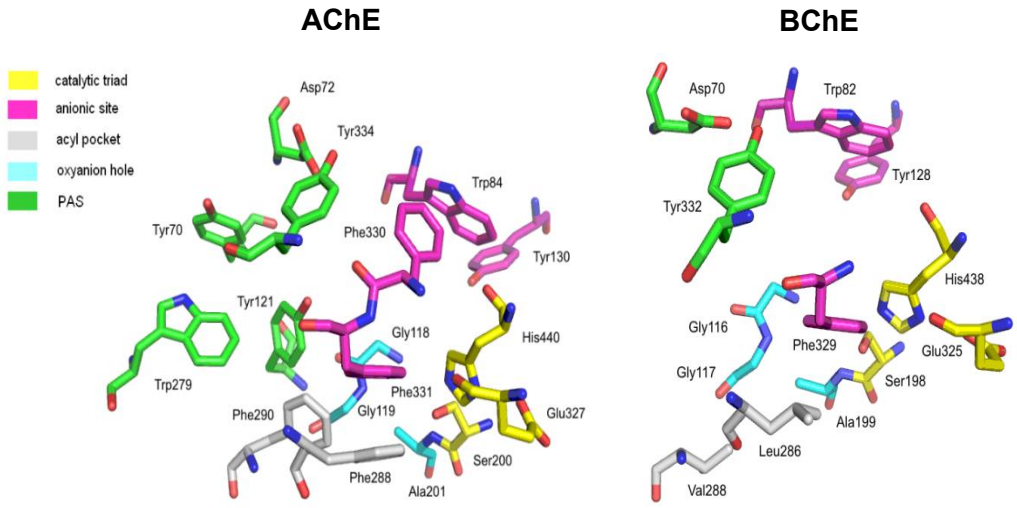

Figure 20. *Active sites of acetylcholinesterase (on the left, PDB: 1EVE) and butyrylcholinesterase (on the right, PDB: 1P0I)*

2 AIM OF THE STUDY

Due to the multi-factorial nature of most neurological disorders, developing novel, rationally designed, multi-target-directed ligands (MTDLs) is considered among the most effective approaches aimed at developing neuroprotective drugs.[1,2] Significant progress has been made in the clinical development of multi-targeted drugs that may act both within and beyond the endocannabinoid system, as shown in Table 2. Endogenous lipids, such as palmitoylethanolamide[73], that act simultaneously at GPCRs, ion channels, and PPARs can be taken as templates.[3] An old cannabinoid derivative named Ajulemic acid (Lenabasum, JBT-101) acting as a peripheral dual CB_1/CB_2 receptor agonist, is recently taken up for fibrotic and inflammatory diseases and being pursued in advanced phases 2 and 3 of clinical trials (NCT03813160, NCT0309340). A recently discovered candidate NTRX-07, a dual CB_1/CB_2 receptor agonist, is being investigated in phase 1 trial as an oral treatment for neuropathic pain and AD (NCT06194552, NCT04375436).[74] Another example of a clinical candidate is dexanabinol (HU-211), which, despite its cannabimimetic structure, is inactive at CB receptors, but exhibits *N*-methyl-D-aspartate (NMDA)-receptor antagonism, antioxidant properties, and inhibition of the synthesis of tumor necrosis factor alpha (TNFα).[75] The promising results, achieved via multiple mechanisms, ultimately led dexanabinol (HU-211) into clinical trials for the treatment of brain cancer (NCT01654497).

Table 2. *Potential future clinical uses of cannabinoid and cannabinoid-related compounds in neurological disorders. PEA, palmitoylethanolamide; PD, Parkinson's disease; MS, multiple sclerosis; ALS, amyotrophic lateral sclerosis.*

Drug	Clinical evidence	Clinicaltrials.gov ID
PEA	Neuropatic pain, PD, MS, ALS, stroke	498 results
JBT-101	Fibrotic and inflammatory diseases	NCT03813160, NCT0309340
NTRX-07	Neuropathic pain and Alzheimer's disease	NCT06194552, NCT04375436
HU-211	Brain cancer	NCT01654497

The aim of this project has been the development of ligands for the cannabinoid-related GPCRs GPR18 and GPR55, starting from the 3,4,5,6-tetrahydroazepino[4,3-*b*]indol-1(2*H*)-one scaffold, with an already proven inhibitory activity against butyrylcholinesterase (BChE).[76] The desired outcome is the combination of the anticholinesterase activity with the modulation of these

poorly studied receptors, for a synergistic effect against neuroinflammation and neurodegeneration.

To achieve this objective, the aforementioned class of indole-fused compounds was firstly identified on the basis of structural similarity with synthetic cannabinoid ligands (Figure 21).[77,78] Once their activity has been established, a wider library of derivatives was synthesized and further tested on CB_1, CB_2, GPR55, GPR18, and both cholinesterase isoenzymes (AChE and BChE).

These findings led to the identification of a new class of tricyclic indole-fused GPR18 and GPR55 modulators (antagonists and/or inverse agonists), often endowed with additional BChE inhibition. Structure-activity relationships have been traced, and structural determinants that enhance or extend activity at these targets have also been investigated.

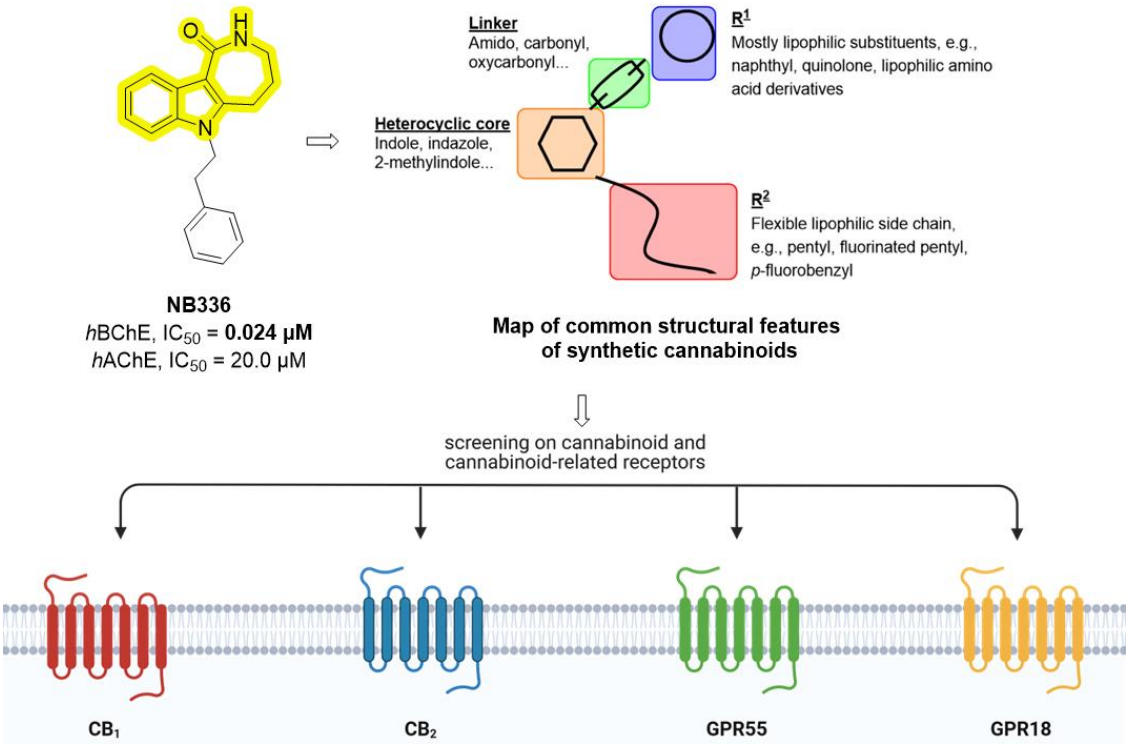

Figure 21. *Schematic representation of the rationale of the present research project. 3,4,5,6-tetrahydroazepino[4,3-b]indol-1(2H)-one derivatives (scaffold highlighted in yellow) have been identified, optimized, and tested at cannabinoid (CB_1, CB_2) and cannabinoid-related receptors (GPR18 and GPR55).*

Chemical synthesis and analysis, computational studies, radioligand binding assays, β-arrestin functional assays, and enzyme kinetics assays have been performed for these purposes.

3 MEDICINAL CHEMISTRY OF INDOLE-FUSED TRICYCLIC DERIVATIVES

3.1 *N*-alkyl indoles are potent cannabinoid receptors ligands

In 1990, Ward et al. reported for the first time that some antinociceptive aminoalkylindoles (AAIs), such as WIN55212-2 and pravadoline, were able to bind the cannabinoid receptors, through displacement of [^{3}H]CP55940 from rat brain cannabinoid receptors.[79] Since then, many other cannabimimetic indoles with a strong affinity for CB receptors have been synthesized, the most extensive series being developed by the Huffman laboratory and known as JHW series (Figure 22).[80]

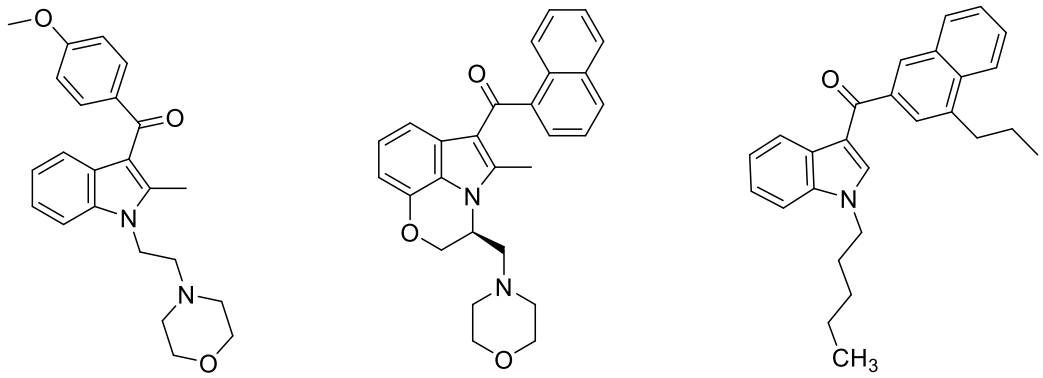

Figure 22. *Chemical structures of aminoalkylindoles (AAIs) with affinity data at cannabinoid receptors.*[35,81,82]

3.2 Discovery of indole-fused tricyclic selective modulators of GPR18 and GPR55

Guided by the structural similarity with cannabimimetic indoles and synthetic cannabinoids, as documented by the European Monitoring Center for Drugs and Drug Addiction[77], we undertook the evaluation of some 3,4,5,6-tetrahydroazepino[4,3-*b*]indol-1(2*H*)-one (THAI, **5a, 5f,** and **5m**) and 1,2,3,4,5,6-hexahydroazepino[4,3-*b*]indole (HHAI, **6c,** Table 3) derivatives at cannabinoid receptors (CB_1, CB_2) and cannabinoid-related receptors (GPR18 and GPR55). The test results are presented in Table 3.

None of the compounds had the ability to replace the binding of the receptor-specific radioligand [^{3}H]CP55,940 at CB_1 and CB_2 receptors. We further

investigated these compounds at other cannabinoid-related receptors, GPR18 and GPR55 using a *β*-arrestin recruitment assay based on enzyme (galactosidase) complementation.[83] GPCRs and *β*-arrestin-2 are tagged with complementary parts of *β*-galactosidase. Upon *β*-arrestin recruitment to the tagged receptor, the enzyme is completed and can hydrolyze an added substrate, resulting in a luminescence signal. This assay thus detects GPCR activation regardless of the G-protein signaling pathway. Artifacts, such as false-positive signals, are rare and can be controlled by performing the same assay using cell lines that express different GPCRs.

None of the compounds were able to activate GPR18 or GPR55 at µM concentrations. On the contrary, 3,4,5,6-tetrahydroazepino[4,3-*b*]indol-1(2*H*)-ones (**5a, 5f, and 5m)** behaved as selective GPR55 antagonists, whereas the corresponding reduced 6-phenethyl-1,2,3,4,5,6-hexahydroazepino[4,3-*b*]indole (**6c**) was a selective GPR18 antagonist. Compounds **5f** and **6c** were also selective human BChE inhibitors (IC_{50} = 24 and 1140 nM respectively).[76]

Table 3. *Affinities of test compounds at human cannabinoid receptors (hCB_1, hCB_2) and activities at cannabinoid-related receptors (hGPR18, hGPR55). THAI derivatives showed selective GPR55 antagonism, whereas the corresponding reduced analog HHAI **6** is a selective GPR18 antagonist.*

cmpd	Azepino [4,3-*b*]indole scaffold	R^1	K_i (µM) or % inhibition (10 µM)[a]		IC_{50} (µM) or % inhibition (10 µM)[b]	
			hCB_1	*h*CB_2	GPR18	GPR55
5a	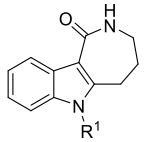	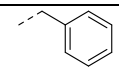	(24%)	(28%)	(11%)	**7.31** ± 0.37
5f		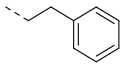	(8%)	(6%)	(1%)	**5.18** ± 1.5
5m		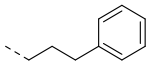	(1%)	(19%)	(11%)	(22%)
6c	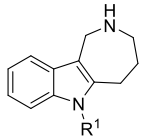	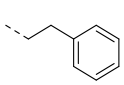	(7%)	(28%)	**8.10** ± 0.56	(-9%)

[a] *radioligand binding assay, % of displacement of [^{3}H]CP55940 binding by test compound at 10 µM;* [b] *β-arrestin assays, data compared to activation of agonist-induced luminescence signal at its corresponding EC_{80} (GPR18: 0.1 µM PSB-KK-1415; GPR55: 4 µM LPI).*

Here we describe the discovery and structure−activity relationships (SARs) of a novel class of GPR18 and GPR55 modulators (antagonists and/or inverse agonists) that are derived from a heterotricyclic azepino[4,3-*b*]indole scaffold (Figure 23).

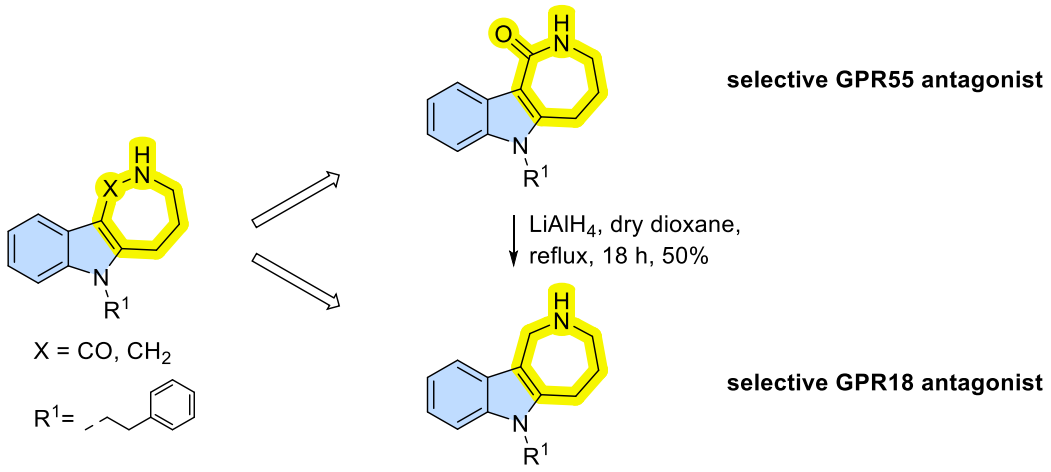

Figure 23. *Identification of new selective GPR55 and GPR18 modulators. Reduction of the lactam group shifts the selectivity of the azepino [4,3-b]indole derivative from GPR55 to GPR18.*

3.3 Experimental design

Encouraged by these findings, we started our investigation to understand the key chemical features responsible for the reported biological activities (Figure 24). We first kept the two reference scaffolds, *i.e.* THAI for GPR55 and HHAI for GPR18, to allow the possibility to easily introduce a variety of substituents into the *N*6-position of the indole. Then, we explored the role of the annulated aliphatic ring, in particular, the fusion isomerism, the diversity of functional groups, the ring size, and the ring opening. Finally, we used differently substituted phenylhydrazines to introduce functional groups on the indole phenyl through Fischer indole synthesis. A library of 55 indole derivatives (**5a-n**, **6a-h**, **7a-c**, **9a-i**, **11a-b**, **14a-b**, **19a-b**, **20 d-e**, **21c-d**, **22a-i**, and **25a-b)** was synthesized according to **schemes 1 – 10** and tested.

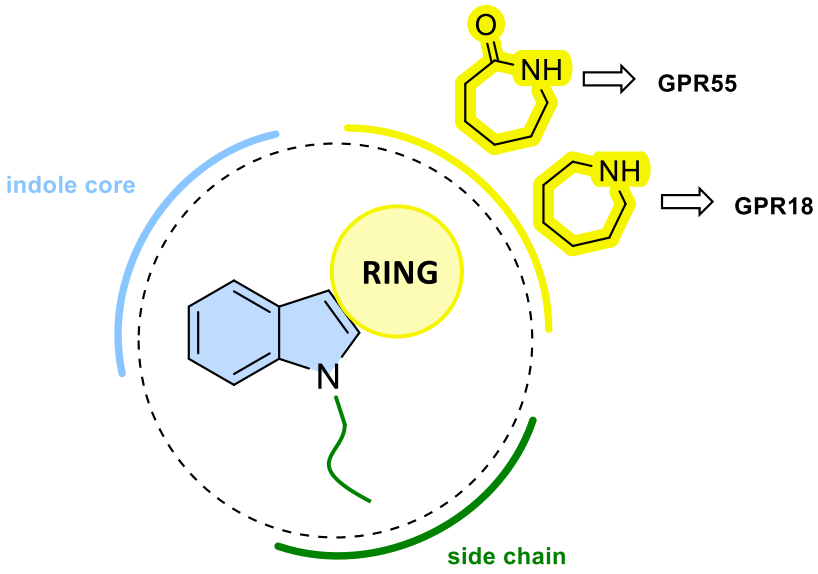

Figure 24. *Schematic representation of the heterotricyclic indole-fused scaffold. THAIs and HHAIs are selective modulators of GPR55 and GPR18, respectively. The generic scaffold is divided into three parts: the indole core, the fused ring, and the side chain, all of which were investigated during this study.*

3.4 Syntheses

The *N*6-substituted derivatives of 3,4,5,6-tetrahydroazepino[4,3-*b*]indol-1(2*H*)-one (compounds **5a**, **5f**, and **5m**) and of 1,2,3,4,5,6-hexahydroazepino[4,3-*b*]indole (compound **6c**) were synthesized as shown in Scheme 1. Phenylhydrazine reacted with 1,3-cyclohexanedione to provide the hydrazone **1,** which, by treatment with refluxing trifluoroacetic acid (TFA) under Fischer conditions, rearranged to the partially saturated carbazolone **2**. Hydroxylamine hydrochloride was used to obtain the respective ketoxime **3** (85% yield), which then underwent a Beckmann rearrangement by treatment with preheated PPA at 110 °C to provide the 3,4,5,6-tetrahydroazepino[4,3-*b*]indol-1(2*H*)-one **4**.

Chemoselective alkylation by suitable alkyl halides at the indole nitrogen was achieved, in the presence of TBAB as phase transfer catalyst in stirred 50% aq. NaOH/DCM *v/v* biphasic mixture (24-72 h at r.t. or 40 °C), affording compounds **5a**, **5f**, and **5m**, as confirmed by the *N*6-H proton singlet (δ 11.40 ppm) disappearance in ^{1}H-NMR spectrum.

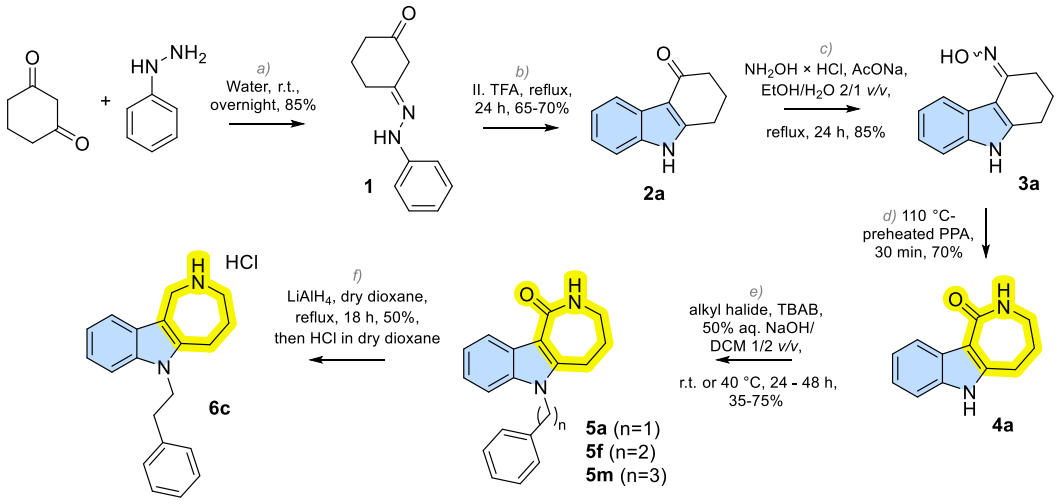

Scheme 1. *General synthesis of THAI and HHAI derivatives (**5a-c** and **6**). Reagents and conditions: a) Water, r.t., overnight, 85%; b) TFA, reflux, 24 h, 65-70%; c) $NH_2OH \times HCl$, AcONa, $EtOH/H_2O$ 2/1 v/v, reflux, 24h, 85%; d) 110 °C-preheated PPA, 30 min, 70%; e) alkyl halide, TBAB, 50% aq. NaOH/DCM 1/2 v/v, r.t. or 40 °C, 48 h, 35-75%; f) $LiAlH_4$, dry dioxane, reflux, 18 h, 50%, then HCl in dioxane.*

Reduction of the lactam was achieved by refluxing compound **5f** with $LiAlH_4$ in dry dioxane to obtain compound **6**. One-step alkylation products of THAI derivatives at *N*6 are reported in Scheme 2. Compounds **5a-n** and **7a-c** were obtained following the same procedure described in Scheme 1, starting from the commercially available phenylhydrazine or 4-fluorophenylhydrazine and 1,3-cyclohexanedione or 5,5-dimethyl-1,3-cyclohexanedione. Methylation of the lactam nitrogen (compound **5n**) was achieved using NaH 60% in m.o., anhydrous DMF and methyl iodide.

Inspired by the computational studies of Shore D.M. and Reggio P.H.,[84], we synthesized a series of derivatives bearing a variety of side chains on the indole nitrogen (compounds **9a-i**, Figure 25). The study indicated that GPR55 antagonists (such as ML191, ML192, and ML193) possess a broad head region that occupies a horizontal binding pocket near the extracellular end of the receptor, and a side chain that can fit vertically in the receptor binding pocket, terminating in a pendant aromatic or heterocyclic ring that juts out from the central portion of the molecule.

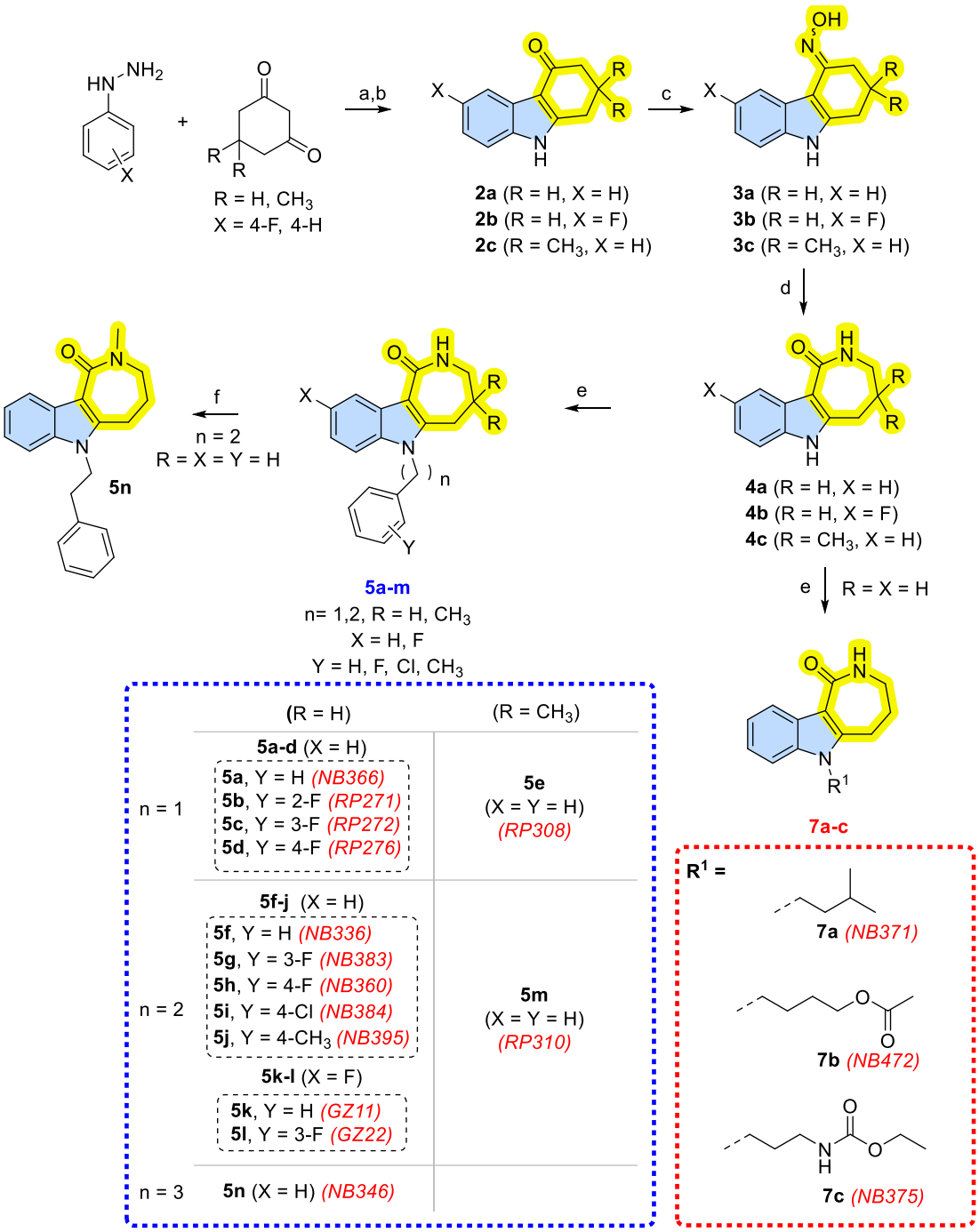

Scheme 2. *Alkylation products of THAI derivatives. Aromatic and aliphatic side chains (indicated by blue and red dashed boxes, respectively) are listed. Reagents and conditions for steps a-e are reported in Scheme 1; f) CH3I, NaH 60% m.o., dry DMF, r.t., overnight, 36%.*

They concluded that both the region that extends extracellularly and the pendant ring were features associated with antagonism. Compounds can be grouped into four major classes: one piperidine, acylpiperazines, 1,4-disubstituted-1,2,3-triazoles, and 4-aminopiperidines.

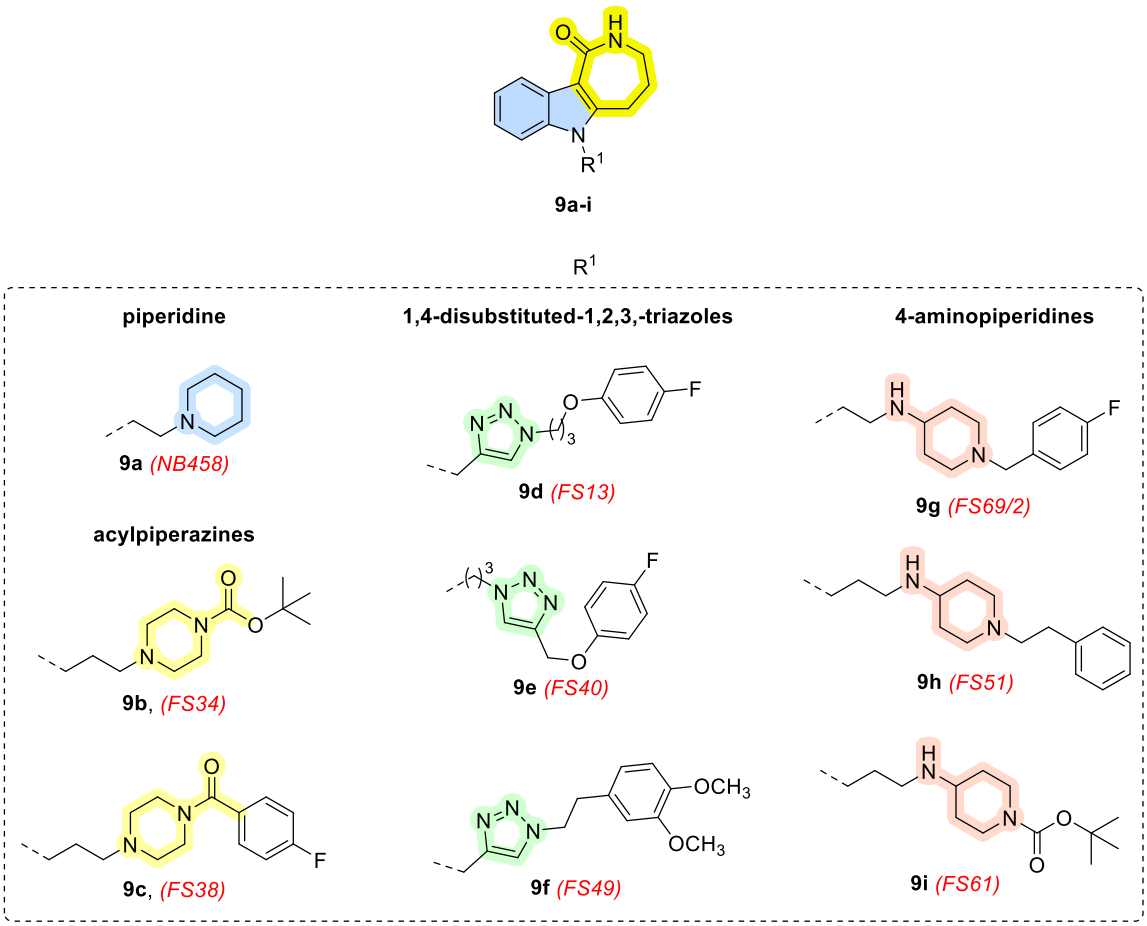

Figure 25. *Series of THAI N6-substituted derivatives bearing different side chains. Compounds can be grouped in 4 major classes: one piperidine (light blue), acylpiperazines (yellow), 1,4-disubstituted-1,2,3-triazoles (green) and 4-aminopiperidines (pink).*

The preparation of compounds **9a-i** proceeded *via* the intermediates presented in Scheme 3 (**8a-h**). For the intermediates **8a-b**, the chemoselective alkylation at the indole nitrogen (*N6*) was achieved by using the suitable α,ω-di-halo-alkanes in the presence of TBAB as phase transfer catalyst in stirred 50% aq. NaOH/DCM *v/v* biphasic mixture (24-72 h at r.t. or 40 °C). Then, compounds **8c** and **9a-c** were obtained by refluxing **8a-b** with piperidine, the suitable acylpiperazines (terz-butyloxycarbonyl or 4-fluorobenzoyl) or sodium azide, and potassium carbonate in acetonitrile or acetone. Where not commercially available, piperazines were synthesized by applying synthesis described elsewhere.

For the intermediates **8d-f**, alkylation was achieved using NaH 60% in mineral oil in dry DMF. Copper-catalyzed azide-alkyne cycloaddition allowed the synthesis of the 1,4-disubstituted 1,4-disubstituted-1,2,3-triazoles (compounds **9d-f**) starting from intermediates **8c-d** and the suitable alkyne (**8i**) or azide (**8j**, **8k**). Reduction of

the nitrile groups of compounds **8e-f** was accomplished using $CoCl_2$, $NaBH_4$ in MeOH at room temperature. From the corresponding amines **8g-h ,** reductive aminations with the suitable 4-piperidones provided the 4-aminopiperidines **(9g-i).**

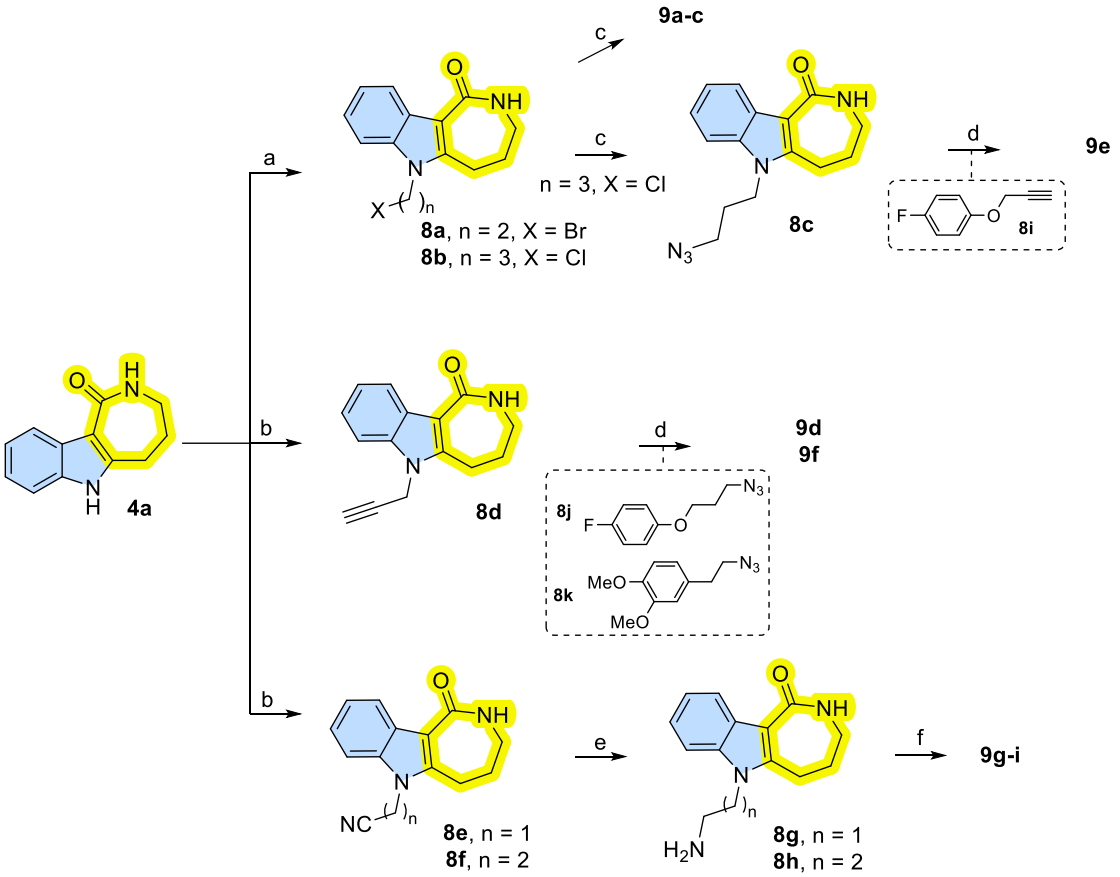

Scheme 3. *Synthesis of N6-substituted-THAI (compounds **9a-i**). Reagents and conditions: a) alkyl halide, TBAB, 50% aq. NaOH/DCM 1/2 v/v, r.t. or 40 °C, 48 h, 35-75%; b) alkyl halide, NaH 60% in m.o., dry DMF, r.t. 24 h, 40-70%; c) piperidine/ suitable acylpiperazine/sodium azide, K_2CO_3, ACN or acetone, r.t. or reflux, 40-60%; d) **8i**,**8j** or **8k**, NaAscorbate, $CuSO_4 \cdot 5H_2O$, dry DMF, overnight, 50 - 70%; e) $CoCl_2$, $NaBH_4$, MeOH, r.t., 60-70%; f) suitable 1-(substituted)piperidin-4-one, acetic acid, NaCNBH3, MeOH, r.t., overnight, 12-40%.*

When phenylhydrazine reacted with 1,2-cyclohexanedione, the same procedure discussed in Scheme 1 provided the [3,4-b] fusion isomer **10** (Scheme 4).

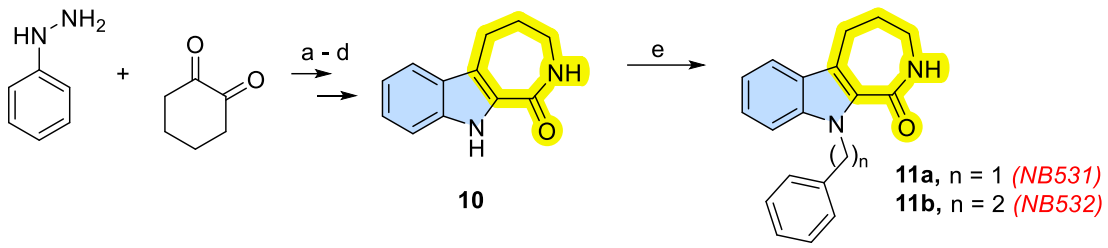

Scheme 4. *Synthesis of 3,4,5,10-tetrahydroazepino[3,4-b]indol-1(2H)-one derivatives. Reagents and conditions are reported in Schme 1.*

Different conditions of the Beckmann rearrangement were explored. As shown in Scheme 5, the 1,2,3,9-tetrahydro-4*H*-carbazol-4-one (**2a**) obtained in Fischer conditions was reacted with hydroxylamine hydrochloride and sodium acetate in a solution of ethanol and water (2/1 *v/v*) to give the ketoxime (**3a**), which was first treated with tosyl chloride, to provide the sulphonyloxime (**12**). It was possible to obtain from sulphonyloxime both the [4,3-*b*] (compound **4a**) and [3,2-*b*] (compound **13**) isomers, by changing the reaction conditions. By refluxing sulphonyloxime in *n*-butanol or in toluene, a mixture 1:1 of the two [3,2-*b*] (GC t_R = 13.98 min) and [4,3-*b*] isomer (GC t_R = 16.68 min), as showed in the GC-MS spectrum. After chromatographic separation on silica gel, the two isomers were isolated and identified by ^{1}H-NMR spectroscopy, where the signal of the lactam NH in [3,2-*b*] isomer appeared as a singlet at δ 7.53 ppm, instead of as a triplet at δ 7.43 ppm in the [4,3-*b*] isomer (in deuterated DMSO). In contrast, by refluxing compound **12** in acetonitrile (ACN) only the [4,3-*b*] isomer was obtained in satisfactory yields. Subsequent alkylations at the indole nitrogen were achieved as in Scheme 1.

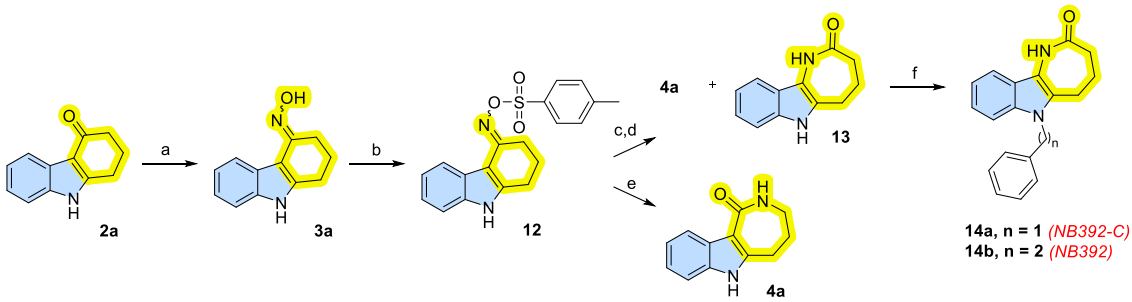

Scheme 5. *Synthesis of [3,2-b] and [4,3-b]-THAI fusion isomers. Reagents and conditions: a) $NH_2OH{\cdot}HCl$, NaOAc, EtOH/H_2O 2/1 v/v, reflux, 24 h, 85%; b) tosyl chloride, DMAP, dry DCM, 4 h, 60%; c) BuOH, reflux, overnight, 63% d) toluene, reflux, 24h, 63%; e) ACN, reflux, 24h, 70%; f) benzyl or alkyl halide, TBAB, 50% aq. NaOH/DCM 1/2 v/v, r.t. or 40 °C, 48 h, 35-75%.*

To explore the effect of ring size on activity, the pyrido-indolone analogs of compounds **5a** and **5f** were synthesized, as reported in Scheme 6. *N*-Boc-β-Ala and Meldrum's acid were dissolved in dry dichloromethane in presence of 4-dimethylaminopyridine to give compound **9**, which in turn gave the tert-butyl-2,4-dioxopiperidine-1-carboxylate (**10**) through an intramolecular reaction in refluxing ACN. Phenylhydrazine reacted with tert-butyl-2,4-dioxopiperidine-1-carboxylate, to provide the hydrazone (**17**) which, by treatment with refluxing trifluoroacetic acid (TFA) under Fischer conditions, afforded the 2,3,4,5-tetrahydro-1*H*-pyrido[4,3-*b*]indol-1-one (**18**). Chemoselective alkylation by suitable alkyl halides at the indole nitrogen was achieved using NaH (60% in m.o.) in dry DMF (24 hours at r.t.), affording compounds **19a** and **19b**.

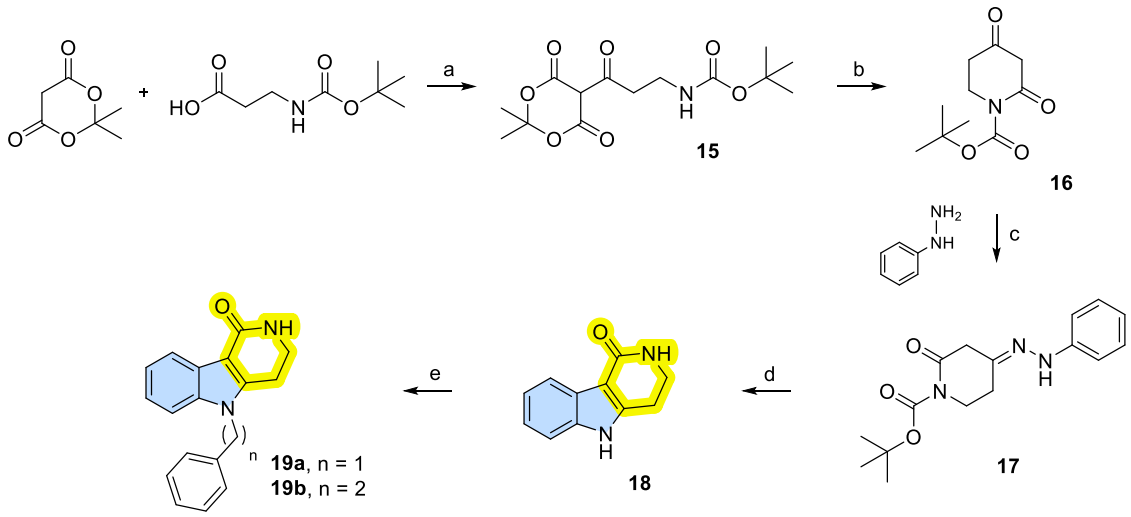

Scheme 6. *Syntheis of 2,3,4,5-tetrahydro-1H-pyrido[4,3-b]indol-1-one derivatives. Reagents and conditions: a) DCM, DCC, DMAP rt, overnight, 76% b) ACN, reflux, 3h, 97% c) ethyl alcohol, phenylhydrazine, rt, 1h, 65% d) TFA, rt, 2 hours, 65% e) dry DMF, NaH, appropriate alkyl or benzyl halide, r.t., 24 hours, 50%.*

The corresponding amines of the already described lactams were synthetized as reported in schemes 7, 8 and 9. Treatment of *N*6-alkylated-3,4,5,6-tetrahydroazepino[4,3-*b*]indol-1(2*H*)-one with lithium aluminum hydride in dry dioxane and vigorous reflux afforded compounds **6a-d**, which were treated with HCl 4M in dioxane to obtain the respective hydrochloride salts (Scheme 7).

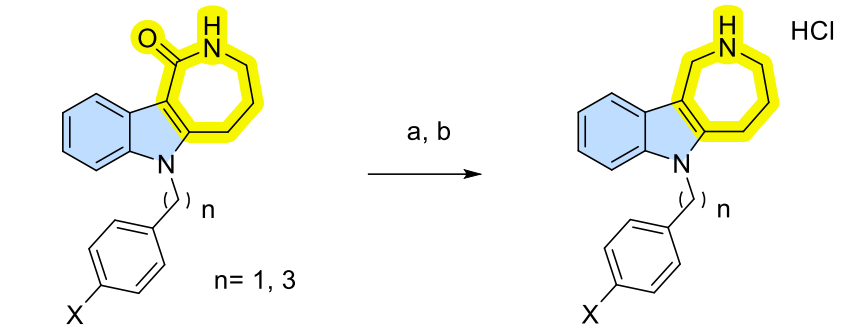

5d, n = 1, X = F *(RP276)*
5a, n = 1, X = H *(NB366)*
5f, n = 2, X = H *(NB336)*
5m, n = 3, X = H *(NB346)*

6a, n = 1, X = F *(NB560)*
6b, n = 1, X = H *(NB553)*
6c, n = 2, X = H *(NB344)*
6d, n = 3, X = H *(NB556)*

***Scheme** 7. Synthesis of N6-substituted-1,2,3,4,5,6-hexahydroazepino[4,3-b]indole (HHAI) derivatives in the form of HCl salts. Reagents and conditions: a) $LiAlH_4$, dry dioxane, reflux, 18 h, 50%; b) 4M HCl dioxane, absolute EtOH, quantitative.*

Alkylations of the azepine nitrogen was achieved as described in Scheme 8. Compound **4a**, reacted with suitable benzoyl- or phenylalkanoyl chlorides. Then a reduction reaction, followed by crystallization of the HHAIs as hydrochloride salts, led to **6e-h** in satisfactory yields.

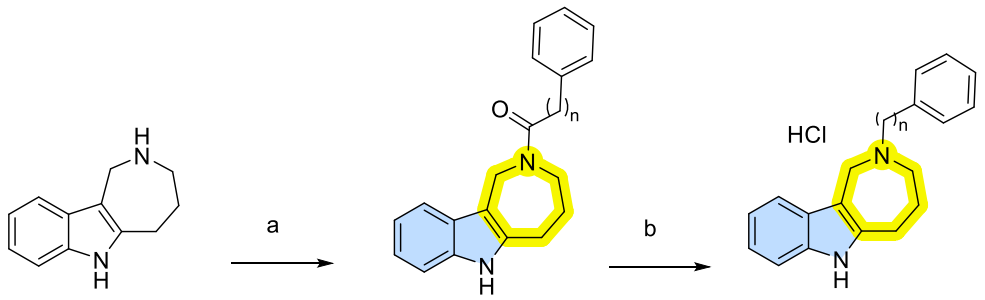

4a

n = 0, 1, 2, 3

6e, n = 1
6f, n = 2
6g, n = 3
6h, n = 4 *(NB339)*

***Scheme 8.** Alkylation of the azepine nitrogen. Reagents and conditions: a) acyl halides, TEA, dry DCM, overnight; b) 1. $LiAlH_4$, dry dioxane, reflux (50-75%); 2. HCl sat. MeOH solution.*

The *N*5-benzyl-2,3,4,5-tetrahydro-1*H*-pyrido[4,3-*b*]indole derivatives were obtained as illustrated in Scheme 9. Differently substituted phenylhydrazine reacted with carbethoxy-piperidone to provide the ethyl 1,3,4,5-tetrahydro-2*H*-pyrido[4,3-*b*]indole-2-carboxylate derivatives (**20a-f**) in Fischer conditions. We used the non-

regiospecificity of the Fischer indole synthesis to synthesize different regioisomers from a single reaction when using an asymmetric phenylhydrazine (for example, compounds **20d** and **20f,** Figure 26). These were subsequently alkylated (**21a-j**) and de-protected with KOH in EtOH to give the compounds **22a-i** as hydrochloride salts (Scheme 9).

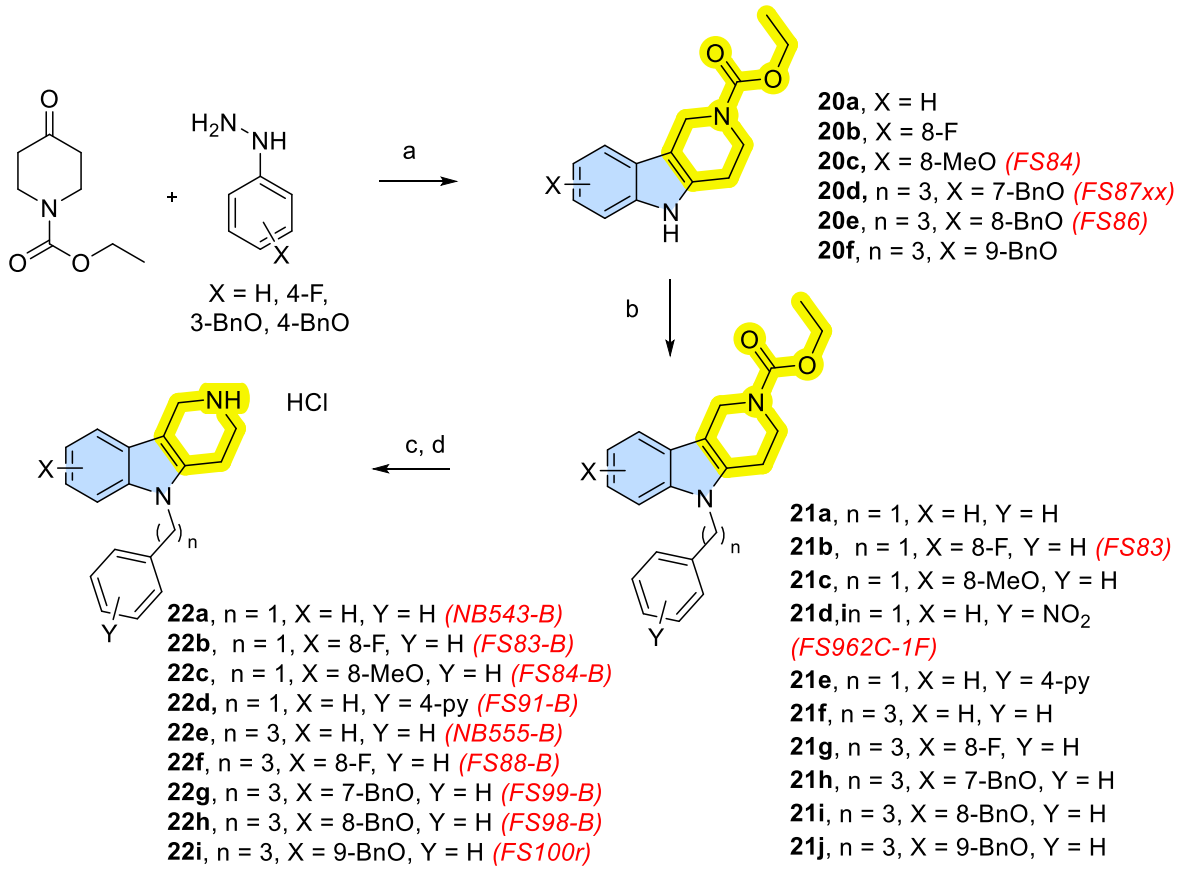

Scheme 9. *Synthesis of N5-benzyl-2,3,4,5-tetrahydro-1H-pyrido[4,3-b]indole derivatives. Reagents and conditions: a) absolute EtOH, 4M HCl in dioxane, reflux 4 hours, 75%; b) NaH (60% m.o.), dry DMF, suitable benzyl or alkyl bromide, r.t., overnight, 35-70%; c) KOH 10 M in EtOH/water (9:1 v/v), reflux, 60-80%; d) 4M HCl dioxane, absolute EtOH, quantitative.*

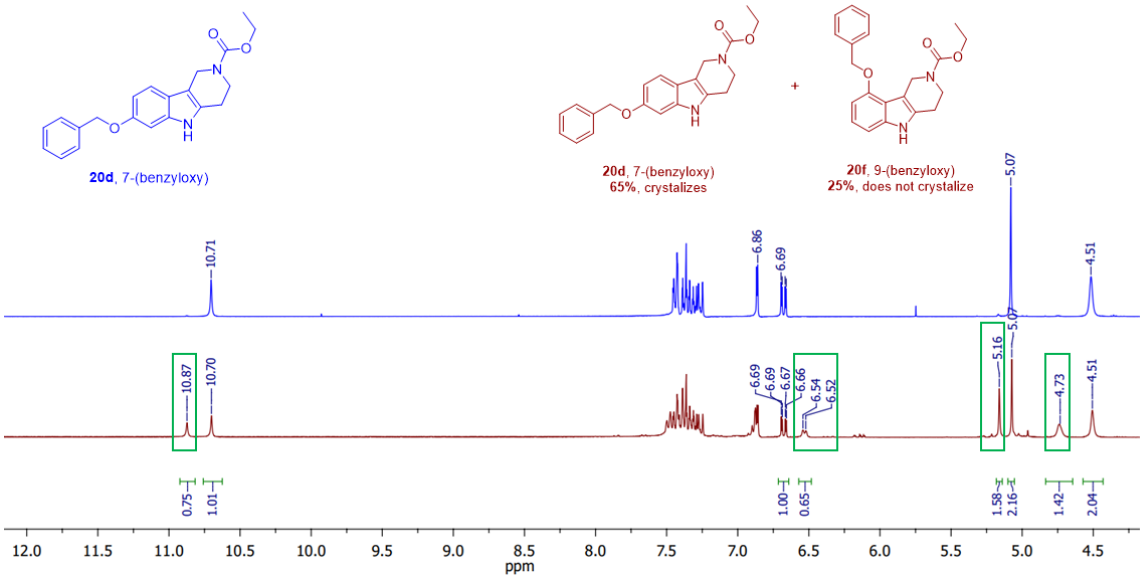

Figure 26. *Overlay of the [1]H-NMR spectra of the 7-benzyloxy regioisomer crystallized from EtOH (in blue) and of the mixture of 7- and 9-benzyloxy tetrahydropyridoindole derivatives present in the crystallizing EtOH (in red). In the green boxes, the signals relating to the 9-benzyloxy regioisomer.*

Finally, a couple of *N*-[(1*H*-indol-3-yl)methyl]propan-2-amine were synthesized *via* reductive amination starting from the commercially available indole-3-carboxaldehyde, in order to evaluate the role of the aliphatic heterocycles fused to the indole. (Scheme 10).

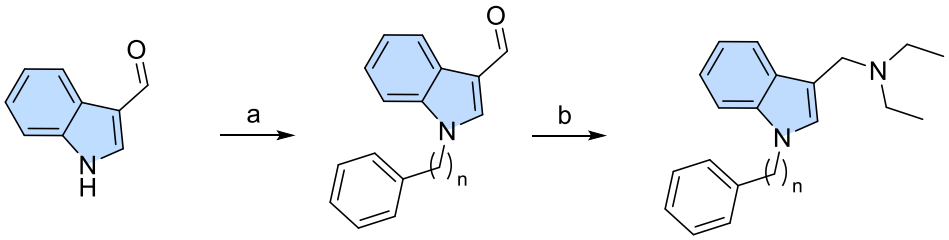

23

24a, n = 1, *(RP297)*
24b, n = 2, *(RP292)*

25a, n = 1, *(RP300)*
25b, n = 2, *(RP301)*

Scheme 10. *Reagents and conditions: a) NaH, benzyl or phenethyl bromide, dry DMF, rt, 24h, 47%. b) CH_3COOH, isopropyl amine, MeOH, $Na(CN)BH_3$, 0 °C to r.t., > 42%.*

4 RESULTS AND DISCUSSION

4.1 Modulation of 7-membered alicyclic indole-fused derivatives at cannabinoid and cannabinoid-related receptors GPR18 and GPR55

4.1.1 GPR55 antagonists

As a first step, we investigated the substitution pattern of the THAI core at the *N6*-position (Table 4) since we assumed, based on results in Table 3, that the heterotricyclic azepino[4,3-*b*]indole scaffold may be important for interaction with GPR55.

Table 4. *Variations of the substitution pattern of the THAI core at the N6-position. Affinities at human cannabinoid receptors (hCB_1R, hCB_2R) and biological activities at cannabinoid-related receptors hGPR18 and hGPR55 are reported.*

cmpd	R¹	K_i (μM) or % inhibition (10 μM)[a]		IC_{50} (μM) or % inhibition (10 μM)[b]	
		*h*CB1	*h*CB2	*h*GPR18	*h*GPR55
7a	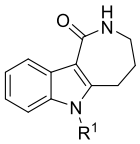 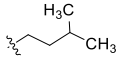	**>10** (29%)	**>10** (34%)	**>10** (13%)	≈ **10** (54%)
7b	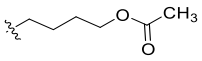	**>10** (29%)	**>10** (34%)	**>10** (8%)	**>10** (22%)
7c	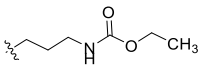	**>10** (16%)	**>10** (1%)	**>10** (-4%)	**>10** (27%)
5b	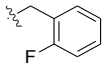			**>10** (-10%)	**>10** (1%)
5c	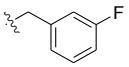			**>10** (-41%)	**>10** (4%)
5d	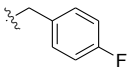			**>10** (-43%)	**>10** (-3%)
5g	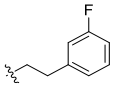	**>10** (23%)	**>10** (23%)	**>10** (11%)	**8.26** ± 2.42
5h	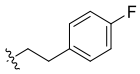	**>10** (22%)	**>10** (23%)	**>10** (9%)	**4.76** ± 0.85
5i	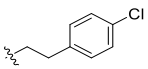	**>10** (35%)	**>10** (31%)	**>10** (6%)	**5.68** ± 0.67
5j	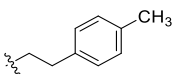	**>10** (33%)	**>10** (35%)	**>10** (22%)	≈ **10** (51%)

[a] determined with radioligand binding assay, % of displacement of [^{3}H]CP55940 binding by test compound at 10 μM; [b] determined with PathHunter β-arrestin assays, data

compared to activation of agonist-induced luminescence signal at its corresponding EC_{80} (GPR18: 0.1 µM PSB-KK-1415; GPR55: 4 µM LPI). Data represent mean values of IC_{50} ± Standard Error Measurement (SEM) or % of inhibition of agonist-induced activation of receptor by test compound at 10 µM.

At GPR55, aliphatic substituents at the *N6*-position resulted in poorly active (**7a,** $IC_{50} \approx 10\mu M$) or inactive compounds (**7b-c**). Among the compounds with arylalkyl side chains, those bearing phenylethyl groups showed moderate antagonistic effects with IC_{50} values of 5-8 µM. Substitution at the phenyl ring led to modulation of GPR55 inhibitory activity: halogen substituents are preferable compared to the methyl group. Compound **5h** (NB360, $IC_{50} = 4.76 \pm 0.85$, Figure 27) was the most potent GPR55 antagonist of this series.

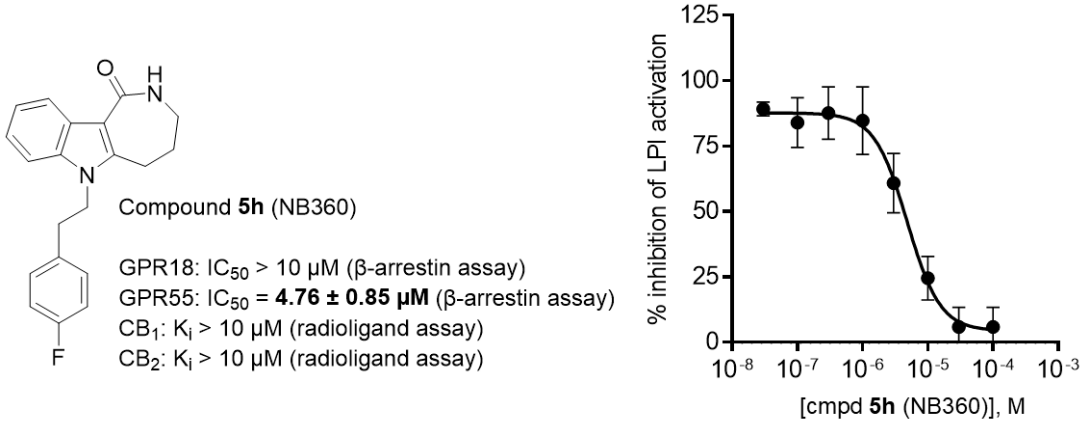

Figure 27. *Chemical structure and concentration-dependent inhibition curve of compound* ***5h*** *(NB360) at human GPR55. Determined with PathHunter β-arrestin assays, data compared to activation of agonist-induced luminescence signal at its corresponding EC_{80} (GPR55: 4 µM LPI). Data represent the mean value of IC_{50} ± Standard Error Measurement (SEM) resulting from 3 independent assays performed in duplicates.*

Extensive efforts to implement various side chains at the *N6*-position (as shown in Table 5), inspired by computational studies in the literature[84,85], were unsuccessful. Only compound **9d** achieved 50% inhibition of LPI-induced response at 10µM. Chains longer than phenylethyl-, whether aliphatic or aromatic, are not tolerated at this position. In contrast, similar approaches were successful in designing selective inhibitors of BChE.[4]

Table 5. *Other variations of the substitution pattern of the THAI core at the N6-position. Affinities at human cannabinoid receptors (hCB_1R, hCB_2R) and biological activities at cannabinoid-related receptors hGPR18 and hGPR55 are reported.*

cmpd	R¹	K_i (μM) or % inhibition (10 μM)[a]		IC_{50} (μM) or % inhibition (10 μM)[b]	
		*h*CB1	*h*CB2	*h*GPR18	*h*GPR55
9a	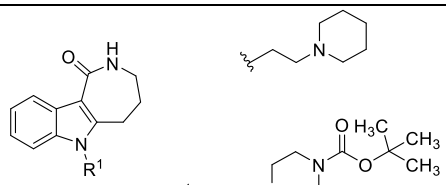	**>10** (26%)	**>10** (6%)	**>10** (18%)	**>10** (4%)
9b		**>10** (9%)	**>10** (10%)	**>10** (29%)	**>10** (12%)
9c	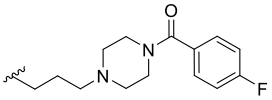	**>10** (7%)	**>10** (6%)	**>10** (43%)	**>10** (32%)
9d	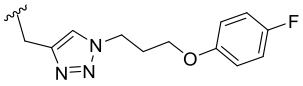	**>10** (24%)	**>10** (38%)	**≈10** (50%)	**>10** (19%)
9e	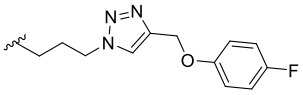	**>10** (20%)	**>10** (13%)	**>10** (0%)	**>10** (17%)
9f	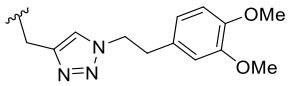	**>10** (12%)	**>10** (8%)	**>10** (43%)	**>10** (17%)
9g	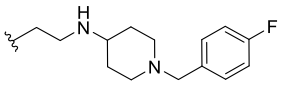	**>10** (4%)	**>10** (9%)	**>10** (39%)	**>10** (20%)
9h	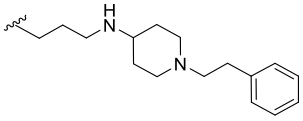	**>10** (3%)	**>10** (8%)	**>10** (39%)	**>10** (7%)
9i	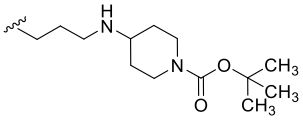	**>10** (27%)	**>10** (11%)	**>10** (45%)	**>10** (33%)

[a] *determined with radioligand binding assay, % of displacement of [³H]CP55940 binding by test compound at 10 μM;* [b] *determined with PathHunter β-arrestin assays, data compared to activation of agonist-induced luminescence signal at its corresponding EC_{80} (GPR18: 0.1 μM PSB-KK-1415; GPR55: 4 μM LPI). Data represent mean valueS of IC_{50} ± Standard Error Measurement (SEM) or % of inhibition of agonist-induced activation of receptor by test compound at 10 μM.*

Data in Table 6 show the modification of the tricyclic head. In particular, we studied the introduction of small substituents (9-F in **5k**, and methyl substituents on the

lactam nitrogen and on the alicyclic chain in **5h**, and **5e**, **5l**, respectively), the fusion isomerism ([3,4-*b*] and [4,3-*b*], in compounds **11a-b**, **14a-b**) and the ring size (**19a-b**). An unsubstituted indole ring was preferred by the receptor, as even the introduction of a fluorine in position 9 decreased the activity. The azepinone ring is essential for activity. Methylation of the lactam nitrogen strongly reduces activity (compound **5h**), suggesting a probable involvement of the lactam moiety in a network of hydrogen bonds with the receptor counterpart hydrogen. Geminal dimethyl substitution on the alicyclic side of the hydrogenated azepinone increases the activity, leading one of the most active compounds of the series (**5e**, RP308, IC_{50} = **4.40** ± 2.06 μM). A reduction in the size of the lactam ring produces inactive 2,3,4,5-tetrahydro-1*H*-pyrido[4,3-*b*]indol-1-one derivatives (**19a-b**).

Table 6. *Tricyclic head modifications. Affinities at human cannabinoid receptors (hCB_1R, hCB_2R) and biological activities at cannabinoid-related receptors hGPR18 and hGPR55 are reported.*

cmpd		R^1	K_i (μM) or % inhibition (10 μM)[a]		IC_{50} (μM) or % inhibition (10 μM)[b]	
			***h*CB1**	***h*CB2**	**GPR18**	**GPR55**
5a	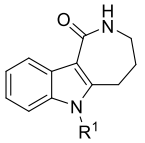	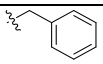	**>10** (24%)	**>10** (28%)	**>10** (11%)	**7.31** ± 0.37
5f		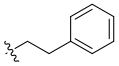	**>10** (8%)	**>10** (6%)	**>10** (1%)	**5.18** ± 1.5
5m		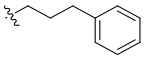	**>10** (1%)	**>10** (19%)	**>10** (11%)	**>10** (22%)
6c	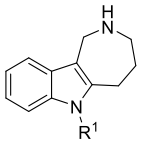	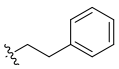	**>10** (7%)	**>10** (28%)	**8.10** ± 0.56	**>10** (-9%)
5n	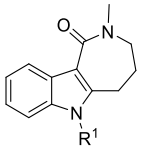	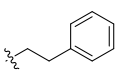	**>10** (7%)	**>10** (14%)	**>10** (1%)	**>10** (37%)

5k	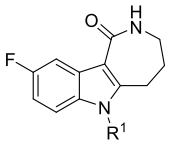	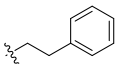	**>10** (11%)	**>10** (15%)	**>10** (12%)	**>10** (45%)
5e	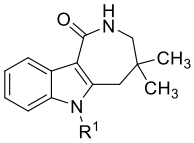	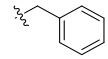			**>10** (-3%)	**4.40** ± 2.06
5l		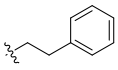			**>10** (36%)	**>10** (26%)
11a	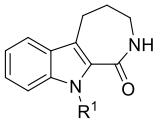	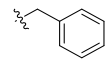			**>10** (-18%)	**>10** (46%)
11b		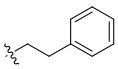			≈**10** (59%)	**>10** (34%)
14a	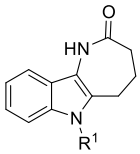	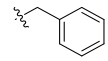			**>10** (20%)	**>10** (29%)
14b		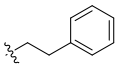			**>10** (-21%)	**>10** (24%)
19a	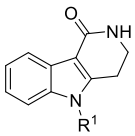	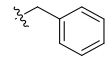			**>10** (-17%)	**>10** (45%)
19b		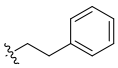			**>10** (-15%)	**>10** (36%)

[a] determined with radioligand binding assay, % of displacement of [^{3}H]CP55940 binding by test compound at 10 μM; [b] determined with PathHunter β-arrestin assays, data compared to activation of agonist-induced luminescence signal at its corresponding EC_{80} (GPR18: 0.1 μM PSB-KK-1415; GPR55: 4 μM LPI). Data represent mean valueS of IC_{50} ± Standard Error Measurement (SEM) or % of inhibition of agonist-induced activation of receptor by test compound at 10 μM.

4.1.2 GPR18 antagonists and inverse agonists

The same investigation at the *N6*-position was adopted for HHAI derivatives. Alkylation at both the indole nitrogen and the basic nitrogen leads to modulators of GPR18 (Tables 7 and 8).

Table 7. *Variations of the substitution pattern of the HHAI core at the N6-position. Affinities at human cannabinoid receptors (hCB_1R, hCB_2R) and biological activities at cannabinoid-related receptors hGPR18 and hGPR55 are reported.*

cmpd	R¹	K_i (μM) or % inhibition (10 μM)		IC_{50} (μM) or % inhibition (10 μM)	
		*h*CB1	*h*CB2	GPR18	GPR55
6a	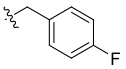			**0.701** ± 0.122	(2)
6b	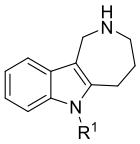 			(2%)	(-9%)
6c	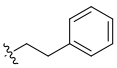	(7%)	(28%)	**8.10** ± 0.56	(-9%)
6d	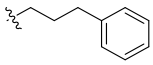			(44%)	(-10%)

Table 8. *Variations of the substitution pattern of the HHAI core at the azepine N-position. Affinities at human cannabinoid receptors (hCB_1R, hCB_2R) and biological activities at cannabinoid-related receptors hGPR18 and hGPR55 are reported.*

cmpd	R¹	K_i (μM) or % inhibition (10 μM)		IC_{50} (μM) or % inhibition (10 μM)	
		*h*CB1	*h*CB2	GPR18	GPR55
6e	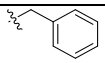	(14%)	(16%)	(45%)	(-11%)
6f	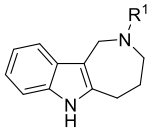 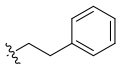	(-1%)	(9%)	≈ **10** (50%)	(-1%)
6g	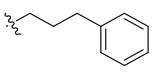	(27%)	(4%)	(27%)	(40%)
6h	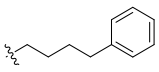	(-8%)	(3%)	**4.72** ± 0.14	(44%)

At GPR18 only two compounds, namely **6c** (NB344, IC_{50} = 8.10 ± 0.56 μM) and **6h** (NB339, IC_{50} = 4.72 ± 0.14 μM) showed moderate activity as antagonists (vs. the agonist PSB-KK-MZ1415 0.1 μM, Figure 28). The concentration dependent inhibition curve was atypical since the signal was inhibited below the signal of the

control. This might be due to basal activity of the receptor and the compounds might act as inverse agonists. However, another possibility is that the compounds may be toxic to the cells at higher concentration.

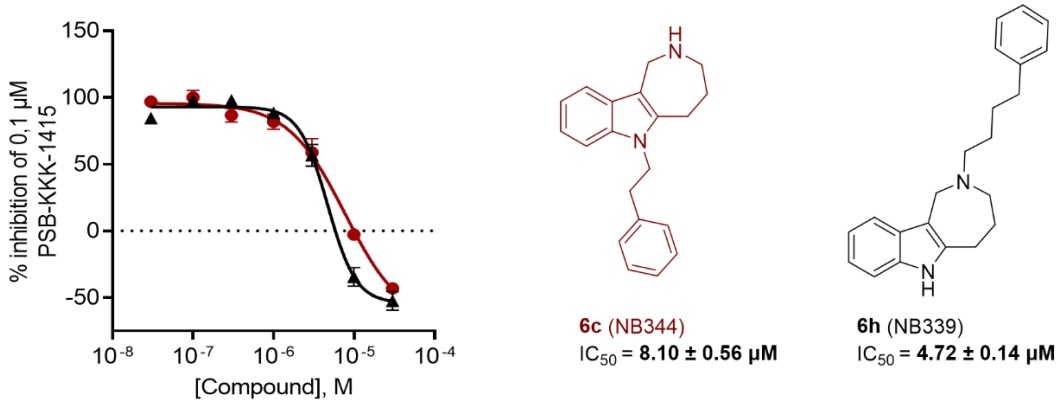

Figure 28. *Concentration-dependent inhibition of compound* ***6c*** *(in red, NB344) and compound* ***6h*** *(in black, NB339) at human GPR18-induced PSB-KK-1415 activation. The chemical structures of the compounds are shown on the right.*

We further tested the compounds versus another, more lipid-like GPR18 agonist, THC (Figure 29 A-C). Both compounds showed similar results with comparable IC_{50} values (compound **6c**, NB344, IC_{50} = **10.6** ± 1.2 µM and **6h**, NB339, IC_{50} = **3.32** ± 0.67 **µM**) versus THC as vs. the other, more peptide-like GPR18 agonist. Also in this case the curve went down well below the baseline.

We investigated possible reasons for this effect. Hence, the compounds were tested in the absence of agonist (PSB-KK-1415 or THC). Even in the absence of THC, we observed a reduction of the signal which might be indicating that these compounds could act as inverse agonists of GPR18.

These two compounds did not show such an effect at GPR55 (Figure 29 B-D). Therefore, the reduction of the signal was neither caused by cell toxicity nor by interference with the assay system (e.g. by inhibition of galactosidase) but might be mediated by an effect on GPR18. Thus, we can conclude that this series of compounds acts as GPR18 inverse agonists. To the best of our knowledge, these are the first GPR18 inverse agonists reported to date.

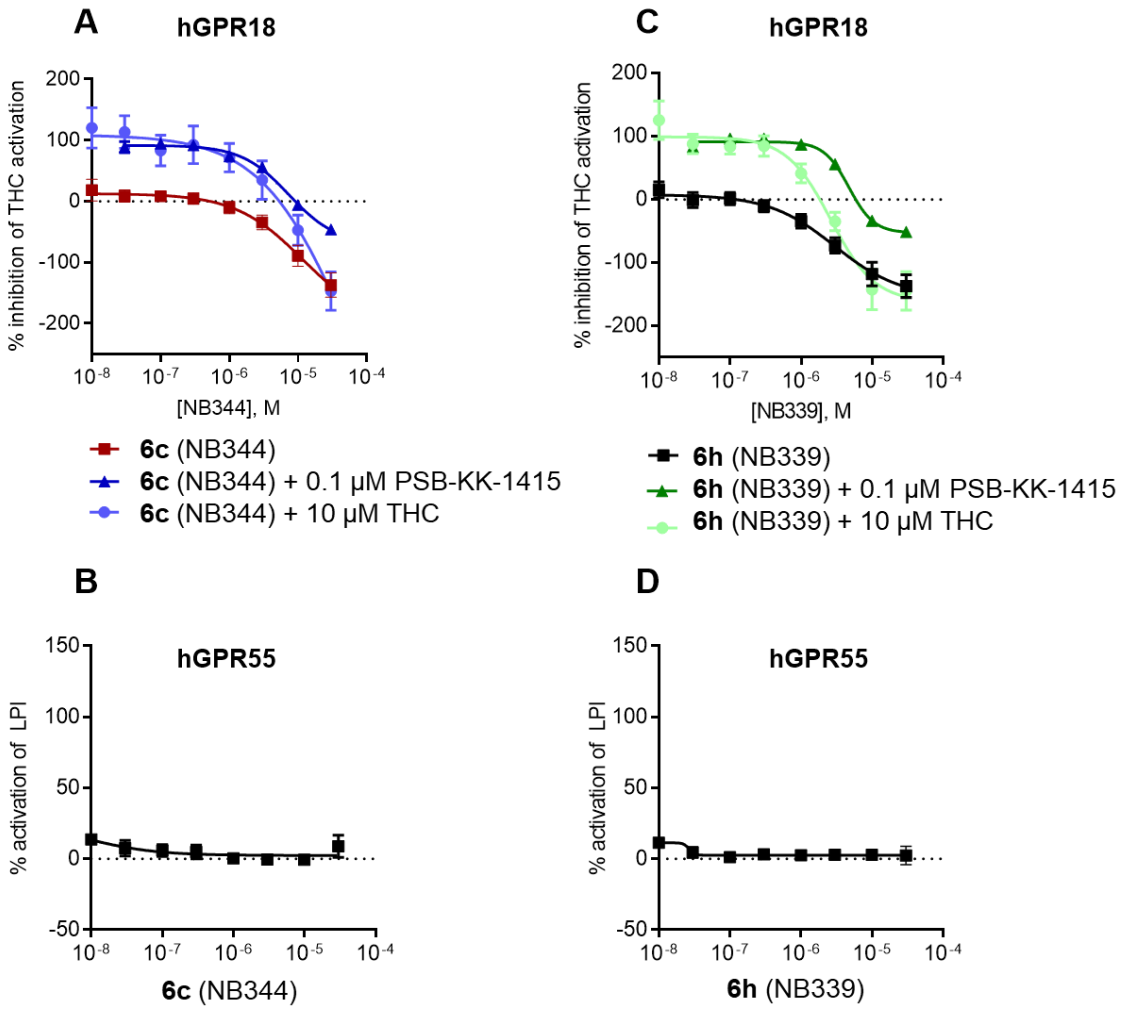

Figure 29. *Modulation effect compound* ***6c*** *(NB344) and compound* ***6h*** *(NB339) at hGPR18 and hGPR55. A) Compound* ***6c*** *(NB344) induced responses at hGPR18 in the absence and presence of known agonists at their corresponding EC_{80} (EC_{80} PSB-KK-1415 = 0.1 µM, EC_{80} THC = 10 µM). B) The effect of compound* ***6c*** *at hGPR55 at various concentrations. C) Compound* ***6h*** *(NB339) induced responses at hGPR18 in the absence and present of known agonists at their corresponding EC_{80} (EC_{80} PSB-KK-1415 = 0.1 µM, EC_{80} THC = 10 µM). D) The effect of compound* ***6h*** *at hGPR55 at various concentrations. None of the compounds showed significant increase or decrease basal levels of GPR55 activation, proving that the trend of the curve is due to an inverse agonism effect and not to cytotoxicity.*

Both compounds, **6c** and **6h**, share the same HHAI scaffold and a basic amine appears to be beneficial for GPR18 activity. On the other hand, non-basic residues are beneficial for GPR55 activity.

Thus, 1,2,3,4,5,6-hexahydroazepino[4,3-*b*]indole derivatives might serve as lead structures for developing novel tool compounds to study GPR18.

Reduction of the ring size to produce 2,3,4,5-tetrahydro-1*H*-pyrido[4,3-*b*]indole derivatives (THPI) in this case proved to be beneficial, leading to the most active compounds of the series compound **22a** (IC_{50} = 0.753 ± 0.116 μM) and compound **22e** (IC_{50} = 0.753 ± 0.223 μM). Acyclic compounds proved to be inactive at GPR18 (compounds **25a-b**, Table 9).

Table 9. *Ring modifications: reduction of ring size and acyclisation. Biological activities at cannabinoid-related receptors hGPR18 and hGPR55 are reported.*

cmpd		R_1	IC_{50} (μM) or % inhibition (10 μM)	
			GPR18	GPR55
22a	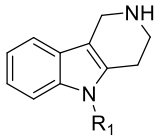	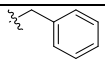	**0.753** ± 0.116	(4%)
22e		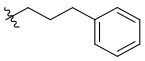	**0.753** ± 0.223	(2%)
25a	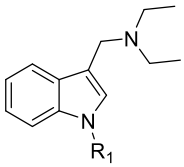	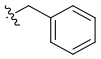	(30%)	(18%)
25b		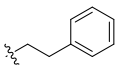	(45%)	(24%)

4.2 Modulation of 6-membered alicyclic indole-fused derivatives at cannabinoid and cannabinoid-related receptors GPR18 and GPR55

Given the promising results obtained on GPR18 upon reduction of the 7-membered hydrogenated azepine ring to a 6-membered piperidine ring, we investigated a larger series of 2,3,4,5-tetrahydro-1*H*-pyrido[4,3-*b*]indole derivatives (THPI). A library consisting of 10 newly synthesized compounds bearing the THPI scaffold was tested on human cannabinoid receptors (*h*CB_1 and *h*CB_2) and cannabinoid-like receptors (GPR18 and GPR55, Table 10).

Table 10. *Affinities at human cannabinoid receptors (hCB$_1$R, hCB$_2$R) and biological activities at cannabinoid-related receptors hGPR18 and hGPR55 of 2,3,4,5-tetrahydro-1H-pyrido[4,3-b]indole derivatives.*

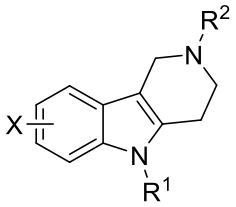

Cmpd	X	R^1	R^2	***h*CB$_1$R** IC_{50} ± SEM (μM)[a]	***h*CB$_2$R** IC_{50} ± SEM (μM)[a]	***h*GPR18** IC_{50} ± SEM (μM)[b]	***h*GPR55** IC_{50} ± SEM (μM)[b]
22i	**9-(BnO)-**	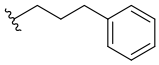	H	**≈10** (52%)*	**2.80 ±** 0.23*	**3.64 ±** 0.96	**>10** (34%)
22h	**8-(BnO)-**			**≈10** (53%)*	**3.83 ±** 1.07*	**3.98 ±** 1.20	**>10** (30%)
22g	**7-(BnO)-**			**3.46 ±** 0.46*	**7.51 ±** 2.80*	**5.56 ±** 0.68	**>10** (33%)
22f	**8-(F)-**			**>10** (29%)**	**>10** (21%)**	**5.11 ±** 0.81	**>10** (28%)
22d		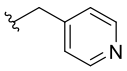		**>10** (18%)**	**>10** (17%)**	**≈10** (54%)	**>10** (27%)
22c	**8-(MeO)-**	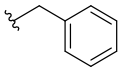		**>10** (43%)**	**>10** (46%)**	**≈10** (56%)	**>10** (8%)
22b	**8-(F)-**			**>10** (30%)**	**>10** (20%)**	**>10** (25%)	**>10** (6%)
21d	**H**	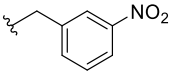	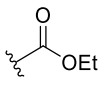	**0.914 ±** 0.112*	**6.05 ±** 2.96*	**>10** (34%)	**8.13 ±** 0.56
20d	**7-(BnO)-**	H		**2.58 ±** 0.69*	**2.86 ±** 0.09*	**≈10** (56%)	**8.49 ±** 1.32
20e	**8-(BnO)-**			**>10** (36%)**	**>10** (47%)**	**≈10** (45%)	**≈10** (50%)

[a)] *determined with PathHunter β-arrestin assays, data compared to activation of agonist-induced luminescence signal at CB$_1$ and CB$_2$ receptors at their corresponding EC$_{80}$s (CB$_1$R : 0.003 μM CP55940; CB$_2$R : 0.001 μM CP55940). Determined with PathHunter β-arrestin assays or % of displacement of [^{3}H]CP55940 binding by test compound at 10 μM; *β-arrestin assays; **radioligand binding assay.* [b)] *determined with PathHunter β-arrestin assays, data compared to activation of agonist-induced luminescence signal at its corresponding EC$_{80}$ (GPR18: 0.1 μM PSB-KK-1415; GPR55: 4 μM LPI). Data represent*

mean values of IC_{50} ± Standard Error Measurement (SEM) or percent of inhibition of agonist-induced activation of receptor by test compound at 10 μM.

4.2.1 GPR55 antagonists

As expected, none of the compounds was able to activate GPR18 and GPR55, a result also found in the previous series of THAI and HHAI derivatives. However, antagonistic activity at GPR55 was registered for compounds **21d** (FS962C1F), **20d** (FS87xx) and **20e** (FS86), all of them having an ethyl 1,3,4,5-tetrahydro-2*H*-pyrido[4,3-*b*]indole-2-carboxylate scaffold (Figure 30) and being the only carbamates of the series, confirming the importance of the carbonyl group in the interaction with GPR55.

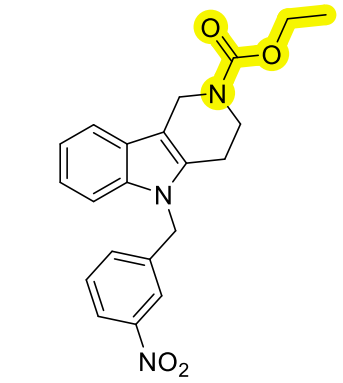

21d

compound 21d (FS96-2C-1F)
GPR18: IC_{50} > 10 μM (β-arrestin assay)
GPR55: IC_{50} = **8.13** ± 0.56 μM (β-arrestin assay)
CB_1: K_i = **2.80** ± 0.56 μM (radioligand assay)
CB_2: K_i = **0.357** ± 0.082 μM (radioligand assay)

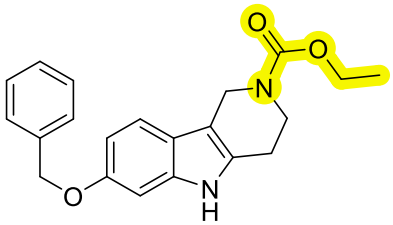

20d

compound 20d (FS87xx)
GPR18: IC_{50} > 10 μM (β-arrestin assay)
GPR55: IC_{50} = **8.49** ± 1.32 μM (β-arrestin assay)
CB_1: K_i = **2.16** ± 0.90 μM (radioligand assay)
CB_2: K_i > 10 μM (radioligand assay)

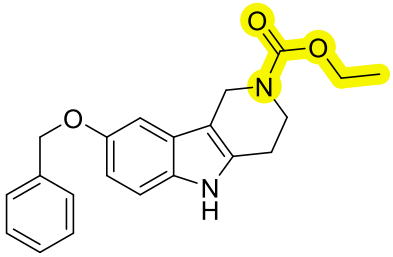

20e

compound 20e (FS86)
GPR18: IC_{50} > 10 μM (β-arrestin assay)
GPR55: IC_{50} **~ 10 μM** (β-arrestin assay)
CB_1: K_i > 10 μM (radioligand assay)
CB_2: K_i > 10 μM (radioligand assay)

Figure 30. *Ethyl 1,3,4,5-tetrahydro-2H-pyrido[4,3-b]indole-2-carboxylates* ***21d, 20d*** *and* ***20e*** *showed weak antagonistic activity at GPR55.*

4.2.2 GPR18 antagonists and inverse agonists

Compounds **22i** (FS100r), **22g** (FS99-B), **22h** (FS98-B), **22f** (FS88-B), **22d** (FS91), **22c** (FS84-B), **20d** (FS87xx) and **20e** (FS86), emerged as potential antagonists or inverse agonist at *h*GPR18 from a screening using *β*-arrestin functional assays and their IC_{50} values have been calculated (Table 11). In almost every case, at the highest concentrations, the signal went significantly below zero, which can indicate either inverse agonistic activity or cytotoxicity. We can now reasonably exclude cytotoxicity, since the same trend was not observed in other assays on transfected CHO cells expressing GPR55 and HEK293 cells expressing CB_1 and CB_2 receptors at the same concentrations of test compounds (see Tables 4 and 11). IC_{50}s for compounds **22i** (FS100r), **22g** (FS99-B), **22h** (FS98-B), **22f** (FS88-B) are respectively equal to **3.64** ± 0.93 μM, **5.56** ± 0.68 μM, **3.98** ± 1.20 μM, and **5.11** ± 0.81 μM, while for **22d** (FS91), **22c** (FS84-B), **20d** (FS87xx) and **20e** (FS86) the IC_{50}s were about equal to 10 μM. Concentration-dependent inhibition curves of **22a** (NB543-B), **22e** (NB555B) and **6a** (NB560) at human GPR18-induced PSB-KK-1415 activation, and of compound **5e** (RP308) at human GPR55-induced LPI activation are reported in Figure 31.

Table 11. *2,3,4,5-tetrahydro-1H-pyrido[4,3-b]indole derivatives showing inverse agonistic activity at hGPR18. Assay performed using PathHunter β-arrestin kit, data compared to activation of agonist-induced luminescence signal at its corresponding EC_{80} (0.1 μM PSB-KK-1415).*

Concentration-dependent inactivation of GPR18	Chemical structure of compounds
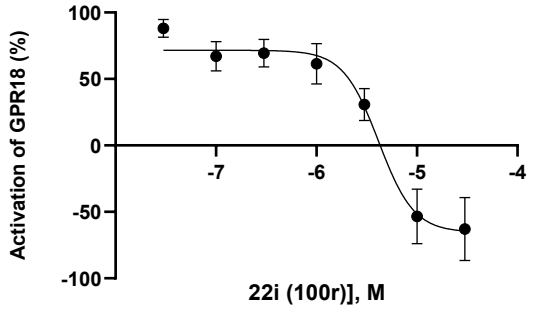	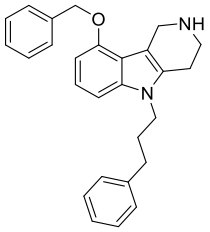 **22i (FS100r)** IC_{50} @ *h*GPR18 3.64 ± 0.93 μM
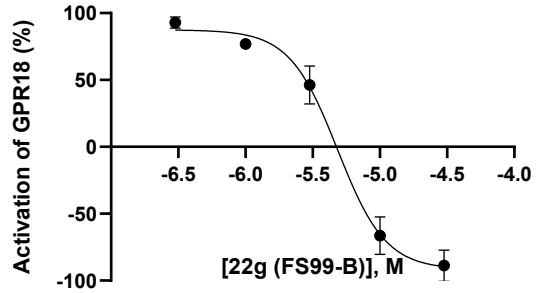	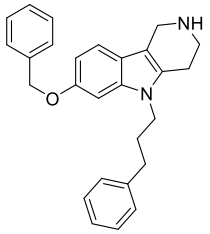 **22g (FS99-B)** IC_{50} @ *h*GPR18 5.56 ± 0.68 μM
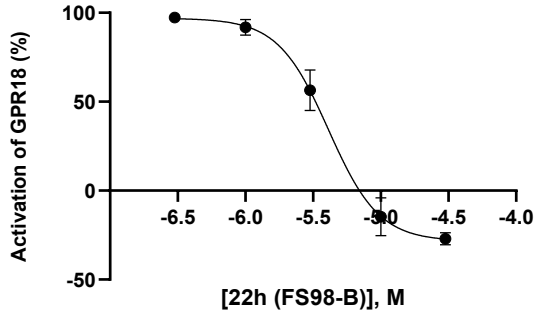	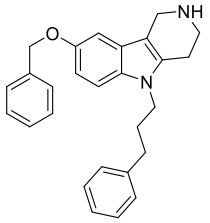 **22h (FS98-B)** IC_{50} @ *h*GPR18 3.98 ± 1.20 μM
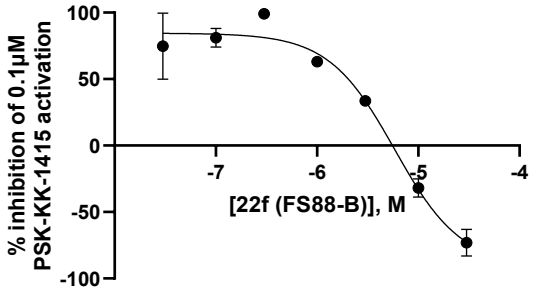	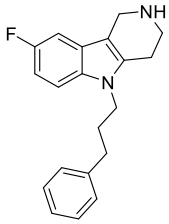 **22f (FS88-B)** IC_{50} @ GPR18 5,11 ± 0,81 μM

Data represent mean values of IC_{50} ± Standard Error Measurement (SEM) of three independent experiments performed in duplicates.

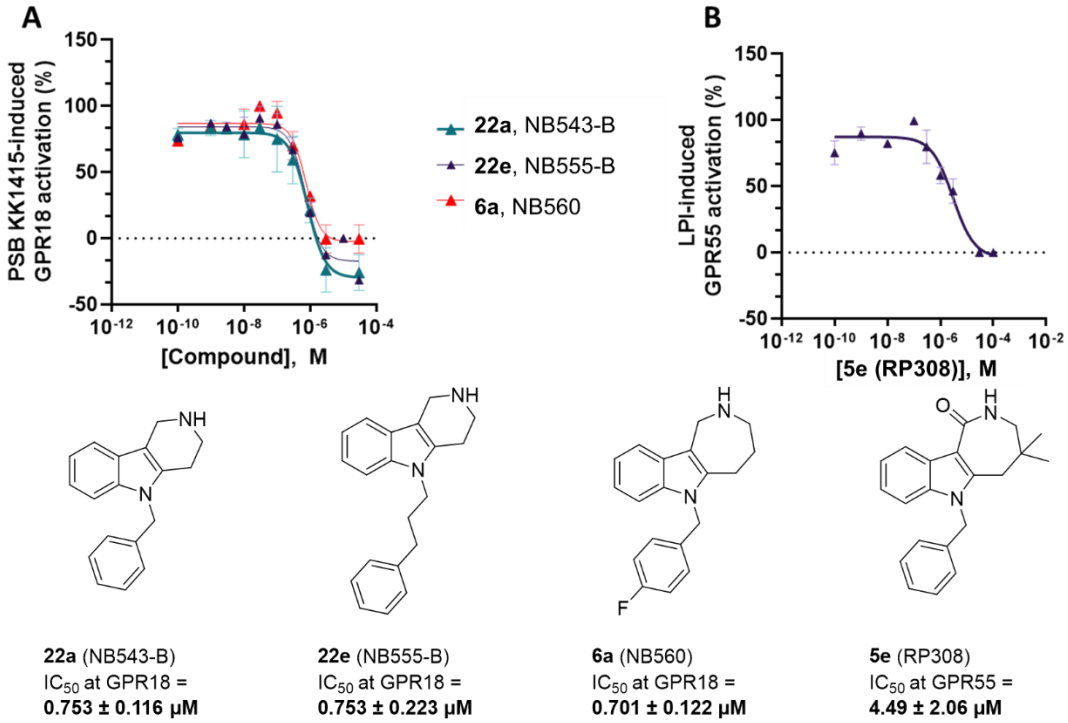

Figure 31. *A) Concentration-dependent inhibition curves of* ***22a*** *(NB543-B),* ***22e*** *(NB555B) and* ***6a*** *(NB560) at human GPR18-induced PSB-KK-1415 activation. The concentration dependent inhibition curves for* ***16*** *and* ***17*** *were atypical since the signals were inhibited below the signal of the control. In the absence of the agonist (tested at 10 µM), compounds* ***22e*** *and* ***6a*** *decreased constitutive activity of GPR18. B) Concentration-dependent inhibition curve of compound* ***5e*** *(RP308) at human GPR55-induced LPI activation. Data was determined using the corresponding agonists at their EC_{80} concentrations with β-arrestin assay (EC_{80} PSB-KK-1415 = 0.1 µM for GPR18 and EC_{80} LPI = 0.1 µM for GPR55). All data are presented from three independent experiments.*

4.2.3 Docking studies of GPR18 ligands

Docking studies carried out on a homology model of the GPR18[86], allowed us to visualize the key interactions of this series of GPR18 ligands (Figure 32): (1) a cation-π interaction between the protonated amino nitrogen of the tetrahydropyridine or hexahydroazepine rings and a residue of tyrosine 264 (Y264); (2) and a π-π interaction between the phenyl ring attached to the indole nitrogen and two phenylalanines (F248 and F252) in the receptor binding site. This interaction appears particularly important because the two phenylalanines are located near the toggle switch, *i.e.* a portion of the receptor made up of 4 amino acids (Y3.35, M7.42, H6.52 and F6.48), whose interactions determine the activation/inactivation state of the GPR18 receptor. The residues of the toggle switch, in fact, are packed and interact via hydrophobic interactions when the receptor is in the inactive state.[87] Antagonists, therefore, must stabilize this inactive

state and strengthen the hydrophobic interactions of the toggle switch. Considering the π-π interaction with the phenylalanine F248 (i.e. 6.51), which is adjacent to the histidine H6.52 present in the toggle switch, it is reasonable to think that the antagonist/inverse agonistic activity of our compounds can be explained through a reinforcement of the hydrophobic interactions of the toggle switch.

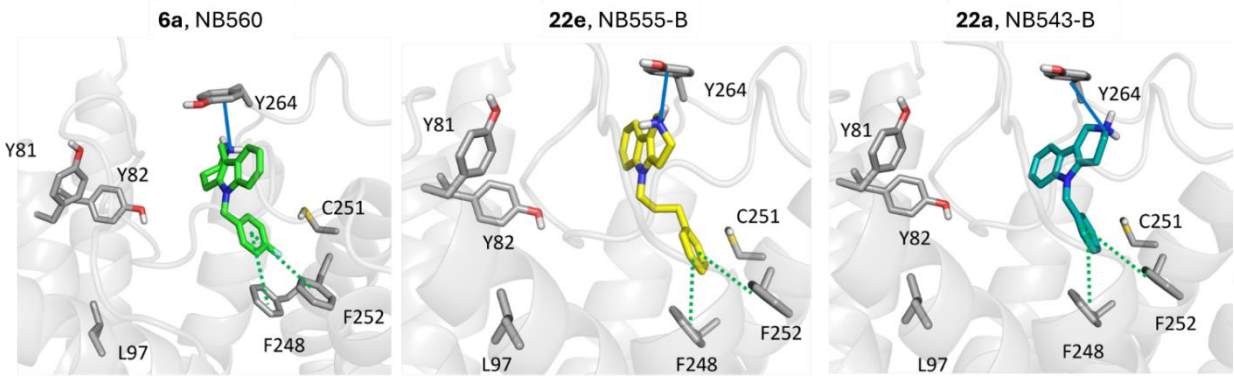

Figure 32. *Proposed binding mode of compounds* ***6a*** *(NB560),* ***22e*** *(NB555-B), and* ***22a*** *(NB543-B, from left to right). Docked pose in complex with the homology model of the human GPR18 shown with some residues forming the binding pocket. The receptor is displayed in cartoon representation, the amino acid residues (grey) and compounds (green, yellow and cyan) are shown as stick models. Oxygen atoms are colored red, nitrogen atoms in blue. Key polar interactions are also highlighted: cation-π interactions are represented as continuous blue lines; π-π stacking interactions are represented as dotted green lines.*

4.2.4 Cannabinoid receptors antagonists

4.2.4.1 Radioligand binding assays

From the screening campaign on *h*CB receptors, some compounds were able to replace the binding of more than 50% of the radioligand [^{3}H]CP55,940 (Table 12). Compounds **22i** (FS100r), **22g** (FS99-B), **22h** (FS98-B), **21d** (FS962C-1F) and **20d** (FS87xx) showed affinity towards *h*CB_1R and *h*CB_2R. Their curves of concentration-dependent displacement of radioligand were elaborated and the respective K_i values were calculated (Table 13).

Table 12. *Affinity of test compounds at hCB$_1$R and hCB$_2$R. Compounds displacing more than 50% of radioligand [^{3}H]CP55930 at 10 μM are highlighted in green and were further characterized through K_i calculation and agonistic/antagonistic activity determination using two different functional assays (β-arrestin and Trupath assay, data reported in Table 14 and 15).*

Compound	***h*CB$_1$R** K_i ± SEM (μM)[a)]	***h*CB$_2$R** K_i ± SEM (μM)[a)]
22i	**3.89** ± 0.63	**3.38 ±** 0.37
22g	**2.82** ± 0.16	**4.00** ± 0.91
22h	**9.60** ± 2.72	**9.86** ± 0.39
22f	>10 (29%)	>10 (21%)
22d	>10 (18%)	>10 (17%)
22c	>10 (43%)	>10 (46%)
22b	>10 (30%)	>10 (20%)
21d	**2.80** ± 0.81	**0.357** ± 0.082
20d	**2.16** ± 0.90	>10 (45%)
20e	>10 (36%)	>10 (47%)

[a)] *determined with radioligand binding assays using membrane preparation (vs [^{3}H]CP55930). Data represent the means value of K_i ± Standard Error Measurement (SEM) or displacement of [^{3}H]CP55930 binding by test compound at 10 μM.*

Table 13. *Curves of concentration-dependent displacement of [^{3}H]CP55930 binding by test compounds at hCB$_1$R (pink) and hCB$_2$R (green). Determined with radioligand binding assays using membrane preparation.*

CB$_1$ receptor	Compounds	CB$_2$ receptor
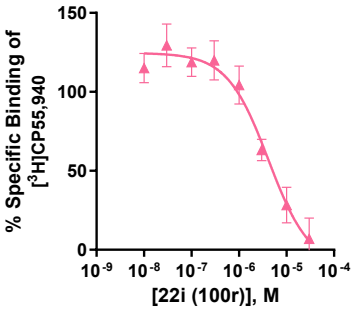	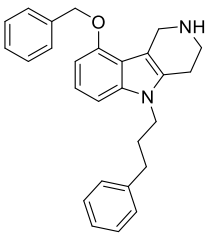 **22i (FS100r)** CB$_1$: K_i = **3.89** ± 0.63 µM CB$_2$: K_i = **3.38** ± 0.37 µM	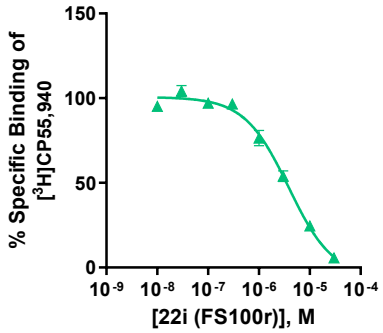
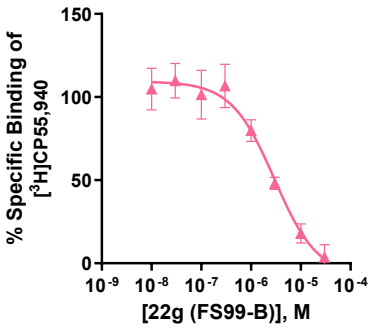	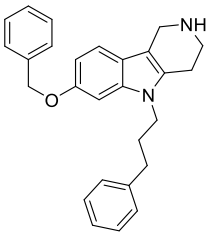 **22g (FS99-B)** CB$_1$: K_i = **2.82** ± 0.16 µM CB$_2$: K_i = **4.00** ± 0.91 µM	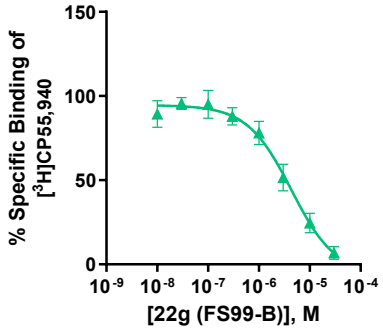
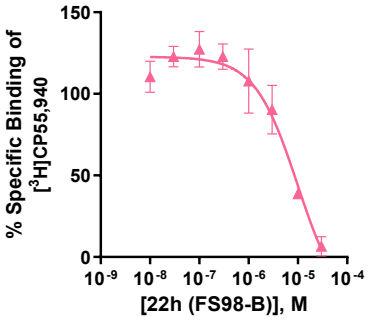	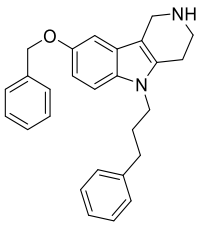 **22h (FS98-B)** CB$_1$: K_i = **9.59** ± 2.72 µM CB$_2$: K_i = **9.86** ± 0.39 µM	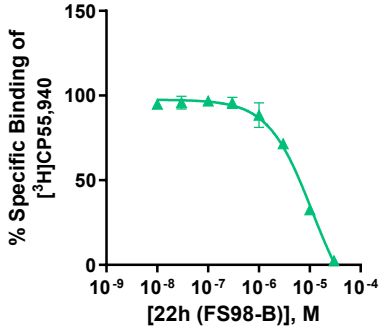
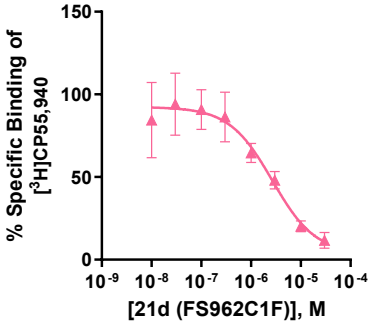	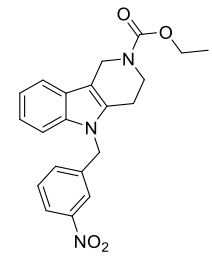 **21d (FS962C-1F)** CB$_1$: K_i = **2.80** ± 0.81 µM CB$_2$: K_i = **0.357** ± 0.082 µM	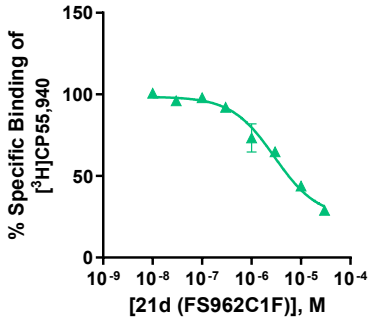

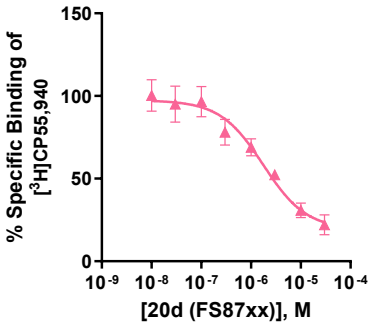

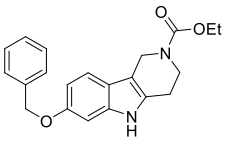

20d (FS87xx)

CB_1: K_i = **2.15** ± 0.90 µM

CB_2: K_i ~ 10 µM

Concentration-dependent curve not available because $K_i \approx 10$ µM from the screening.

4.2.4.2 Functional assays

Trupath and *β*-arrestin functional assays to assess the agonistic activity of these compounds at the cannabinoid receptors were performed. None of them showed agonistic activity. The results of the experiments on compound **22i** (FS100r) are reported as an example in Table 14.

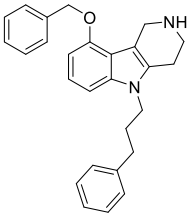

1 (FS100r)

Table 14. *Compound **22i** (FS100r) did not show any agonistic activity on cannabinoid receptor subtypes 1 and 2 (CB_1R and CB_2R) either in the Trupath assay or the β-arrestin assay. No agonistic activity was detected either on the other compounds that emerged from the radioligand binding assays, namely compounds **22g** (FS99-B), **22h** (FS98-B) **21d** (FS962C-1F) and **20d** (FS87xx). Only results from compound **1** (FS100r) are reported.*

	Trupath	***β*-arrestin complementation assay**
CB_1R	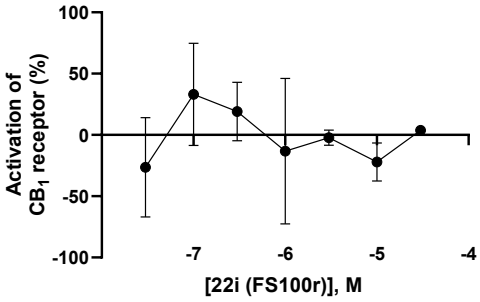	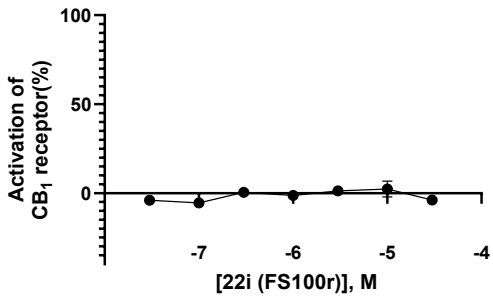
CB_2R	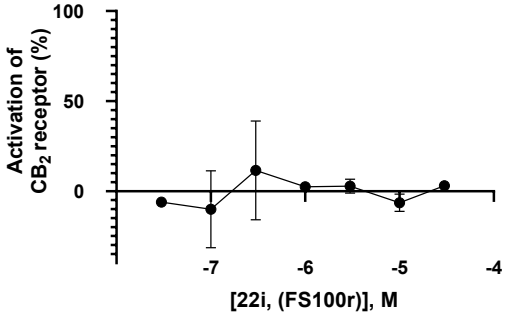	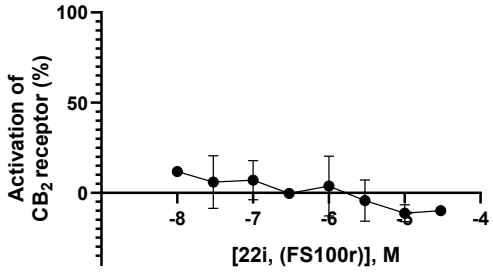

Hence, *β*-arrestin functional assays to assess the antagonistic activity were performed. All the compounds showed a concentration-dependent inhibition of agonist-induced activation, as shown in Table 15.

Table 15. *Concentration-dependent inhibition of agonist-induced activation at CB_1 (red) and CB_2 (blue) receptors at their corresponding EC_{80}s (CB_1R : 0.003 µM CP55940; CB_2R : 0.001 µM CP55940). Determined with PathHunter β-arrestin assays. K_i values for each compound at CB receptors are also reported. N=3 independent experiments, performed in duplicates.*

CB_1 receptor	Compounds	CB_2 receptor
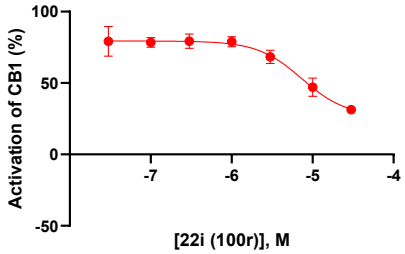	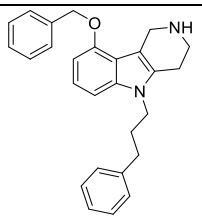 **22i (FS100r)** CB_1: K_i = **3.89** ± 0.63 µM CB_2: K_i = **3.38** ± 0.37 µM CB_1: IC_{50} ~ 10 µM CB_2: IC_{50} = 2.80 ± 0.23 µM	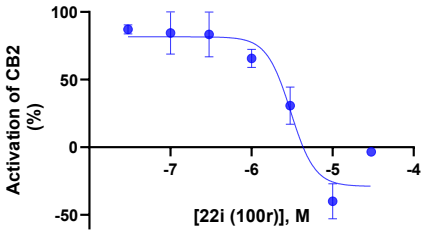
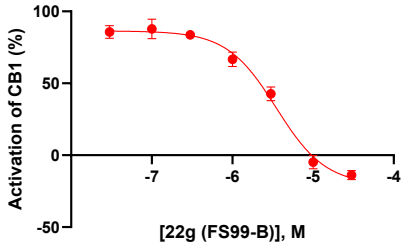	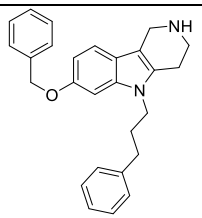 **22g (FS99-B)** CB_1: K_i = **2.82** ± 0.16 µM CB_2: K_i = **4.00** ± 0.91 µM CB_1: IC_{50} = 3.46 ± 0.46 µM CB_2: IC_{50} = 7.51 ± 2.80 µM	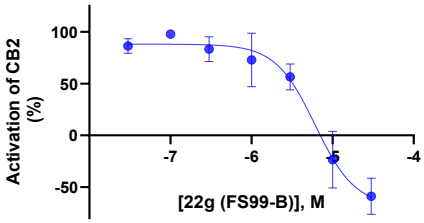
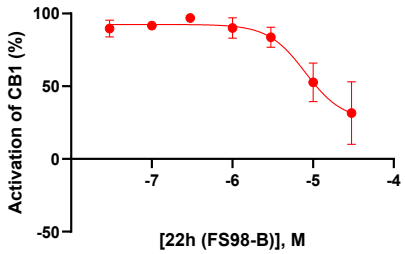	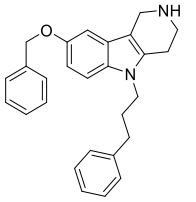 **22h (FS98-B)** CB_1: K_i = **9.59** ± 2.72 µM CB_2: K_i = **9.86** ± 0.39 µM CB_1: IC_{50} ~ 10 µM CB_2: IC_{50} = 3.83 ± 1.07 µM	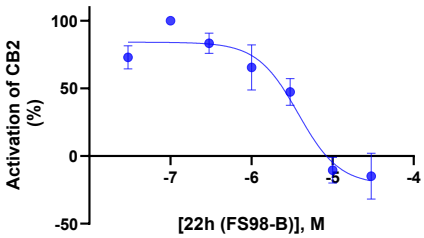
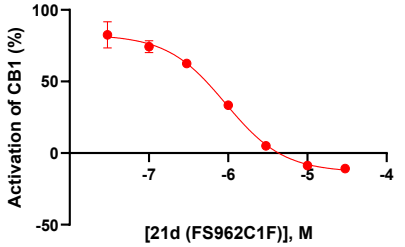	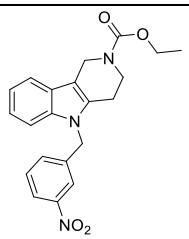 **21d (FS962C-1F)** CB_1: K_i = **2.80** ± 0.81 µM CB_2: K_i = **0.357** ± 0.082 µM CB_1: IC_{50} = 0.914 ± 0.112 µM CB_2: IC_{50} = 6.05 ± 2.96 µM	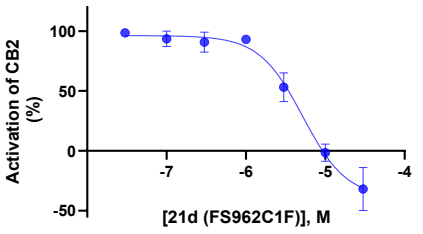

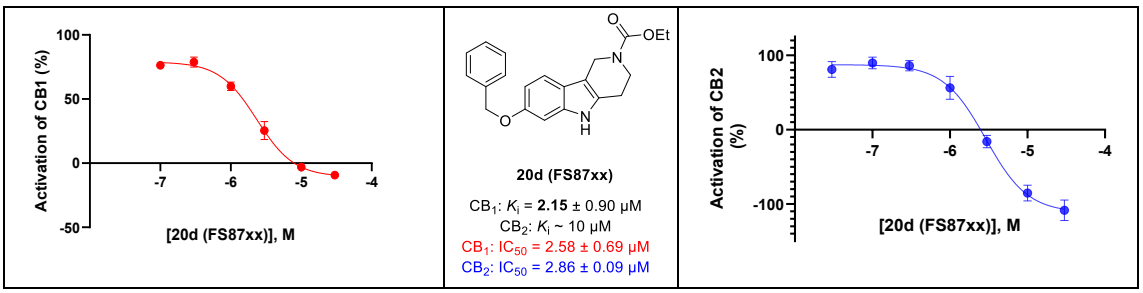

A correlation can be found between K_i values and IC_{50}s on CB_1 receptor, where small K_i values correlate with small IC_{50} values. In the case of CB_2 receptor, this correlation was not as apparent (Figure 33).

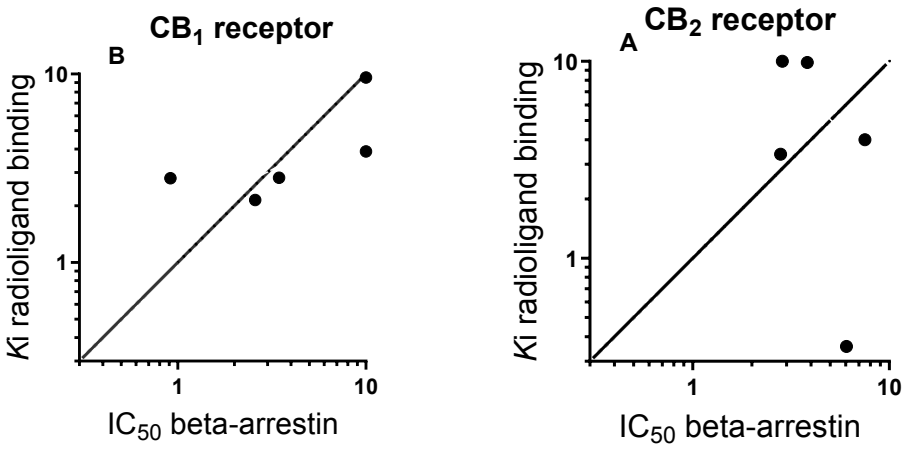

Figure 33. *Correlation of K_i and IC_{50} values of tested compounds at CB_1 and CB_2 receptors.*

4.2.4.3 Docking studies at CB receptors

To better understand this correlations and to validate the hypothesis of the orthosteric binding of the compounds, molecular docking analyses were performed on human CB_1 and CB_2 receptors in complex with the antagonists AM6538 (PDB: 5TGZ) and AM10257 (PDB: 5ZTY), and on the CB_1 receptor structure containing a co-crystallized allosteric modulator (PDB: 6KQI, Figure 34).

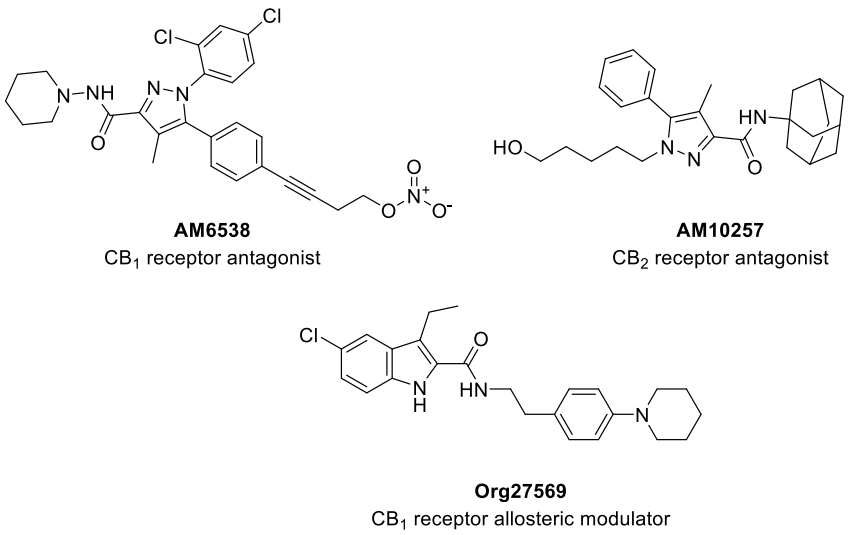

Figure 34. *Chemical structures of human CB_1 and CB_2 receptors ligands.*

In the context of the CB_1 receptor molecular docking analysis, the interactions for each compound are detailed in Figure 35. Across all compounds, binding predominantly involves hydrophobic interactions. Notably, π-π contacts with residues F170, F268, F379, and W356 are highlighted for the docked compounds. Additionally, hydrogen bonding with S383 is observed specifically for compounds **22h** (FS98-B) and **20d** (FS87-xx). Overall, these structures exhibited good docking score values, especially when compared to the co-crystallized compound, a known CB1 antagonist, which recorded a binding energy of -11.99 kcal/mol (Table 16).

Table 16. *Docking scores of compounds within the orthosteric site of CB_1 and CB_2 receptors (CB_1R and CB_2R).*

Compounds	CB_1R (kcal/mol)	CB_2R (kcal/mol)
22i	-9.87	-9.82
22g	-10.22	-10.15
22h	-9.65	-10.49
20d	-9.03	-8.85
21d	-8.52	-8.73

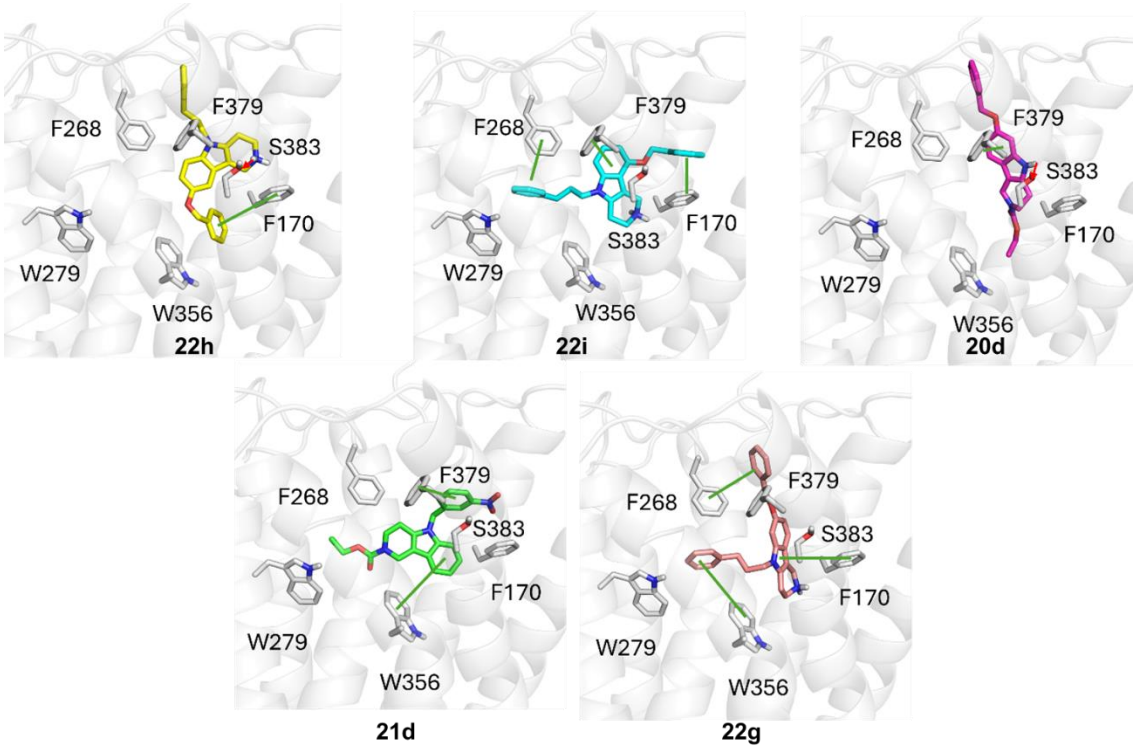

Figure 35. *Zoomed in view at the CB_1 receptor binding site. Compounds **22h** (FS98-B), **22i** (FS100r), **20d** (FS87-xx), **21d** (FS962C-1F) and **22g** (FS99-B) are depicted as yellow, cyan, magenta, green and salmon sticks, respectively. Red arrows and green lines represent hydrogen bond and π-π interactions, respectively.*

As far as the CB_2 receptor docking analysis is concerned, results are summarized in Figure 36. Hydrophobic interactions are the primary driving force behind the binding of all compounds to the CB_2 receptor orthosteric site. Specifically, compounds **22g-i** (FS99-B, FS98-B and FS100r) interact with the toggle switch W258, a well-known feature of CB_2 receptor antagonists. Their aromatic moiety is also sandwiched between W194 and F117, forming T-shaped π-π interactions. Additionally, important π-π interactions with F183, F87, and F94 were observed. Hydrogen bonds were identified for compounds **22i** (FS100r) and **21d** (FS962C-1F), with S285 and H95, respectively. The docking scores for these compounds are comparable to that of the cognate ligand, with a value of -11.81 kcal/mol.

Finally, we also explored their potential binding within an allosteric pocket identified in the CB_1 crystal structure. In this respect, docking scores are summarized in Table 17, and molecular interactions depicted in Figure 37.

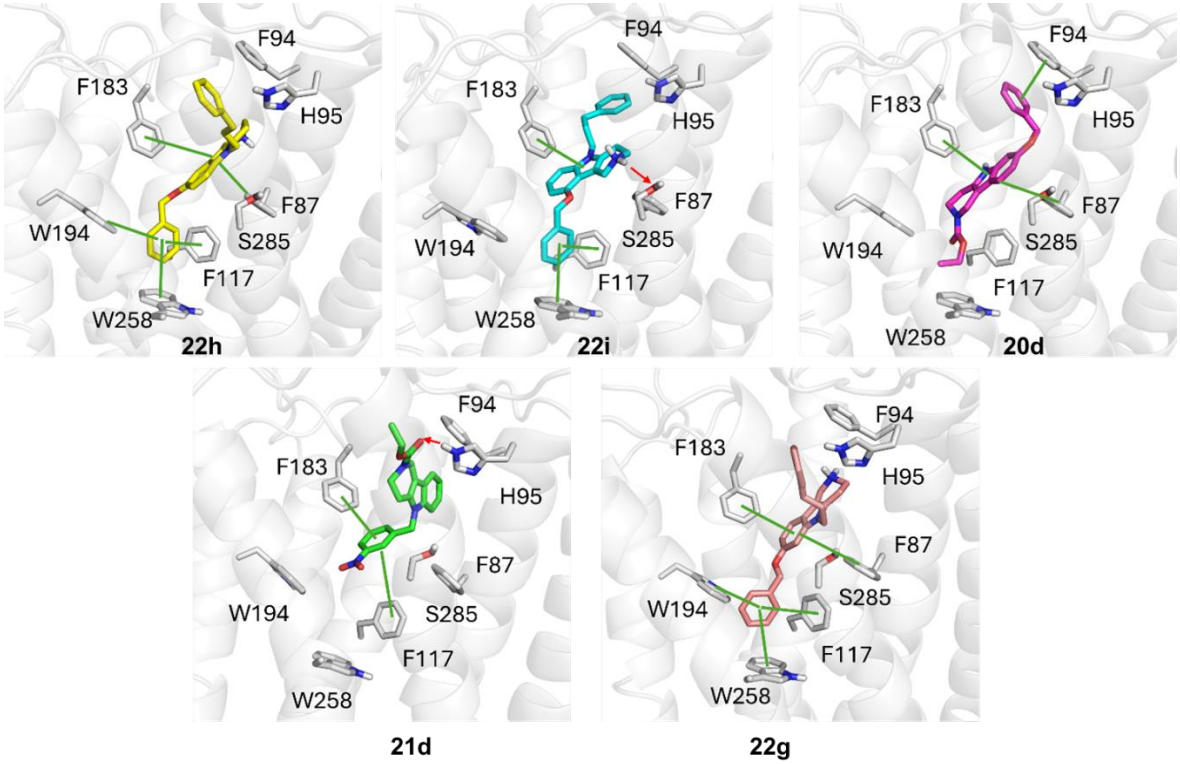

Figure 36. *Close-up of the CB_2 receptor binding site, with compounds* ***22h*** *(FS98-B),* ***22i*** *(FS100r),* ***20d*** *(FS87-xx),* ***21d*** *(FS962C-1F) and* ***22g*** *(FS99-B) shown as yellow, cyan, magenta, green, and salmon-colored sticks, respectively. Red arrows indicate hydrogen bonds, while green lines represent π-π interactions.*

The indole portion of all compounds can interact with the W241, while an additional π-π interaction with H154 is also flagged for compound **22g** (FS98-B). Interestingly, the docking score values of each compound are better than the one returned for the cognate allosteric ligand, equal to -3.63 kcal/mol, thus potentially enhancing the hypothesis that these compounds could also function as allosteric modulators.

Table 17. *Docking scores of compounds within the allosteric binding pocket of CB_1 receptor (CB_1R).*

Compounds	**CB_1R allosteric (kcal/mol)**
22i	-5.99
22g	-6.47
22h	-6.56
20d	-5.70
21d	-5.56

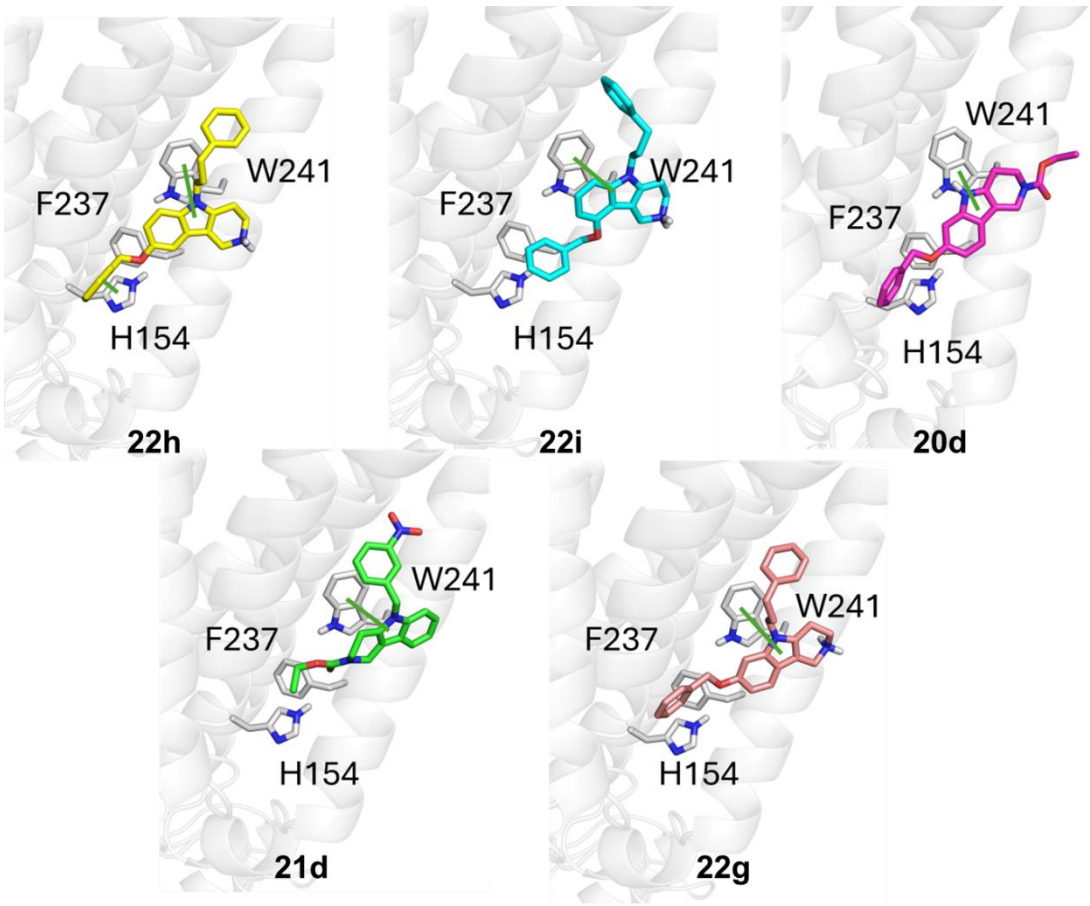

Figure 37. *Allosteric binding site of CB1 receptor, with compounds FS98-B, FS100r, FS97-xx, FS962C-1F, and FS99-B represented as yellow, cyan, magenta, green, and salmon-colored sticks, respectively. Green lines represent π-π interactions.*

4.3 Structure-activity relationships of GPR55 antagonists

The azepinone[4,3-*b*] ring helps maintain the optimal angle and directionality of the lactam function, as confirmed by the inactivity of other fusion isomers (for example [3,2-*b*]), and of smaller pyrido[4,3-*b*]indolone analogs (Compound **14a-b** and **19a-b** in Table 6). However, evidence in toxicology studies present in literature[78,88] show that some *N*-alkylindoles bearing a carbonyl group in position 3 (of a ketone, amide or ester) have been found to be antagonists of GPR55 (Figure 38). This suggests that the azepinone ring might be opened to allow higher flexibility and the possibility to easily introduce a variety of substituents on the lactam nitrogen.

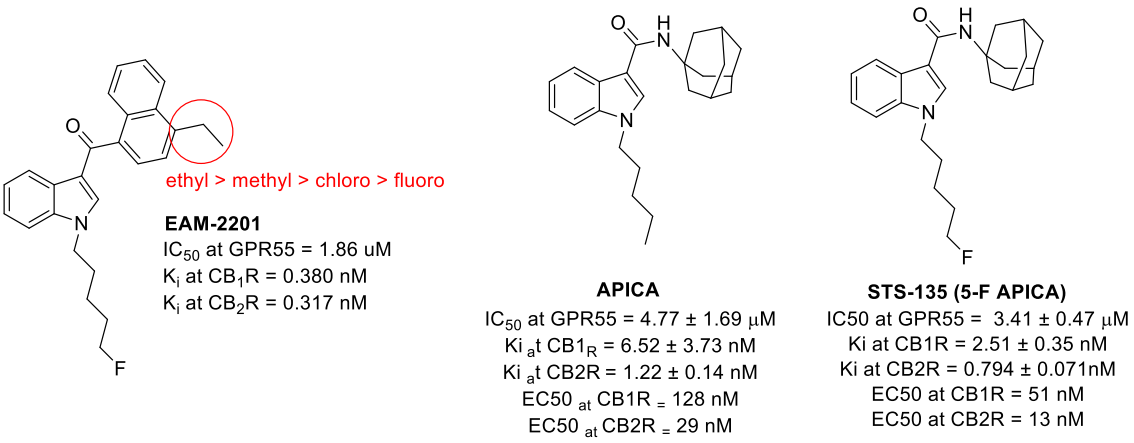

Figure 38. *Synthetic cannabinoids identifed as constituents of "Spice", a preparation sold on the illicit drug market, endowed with antagonistic activity at GPR55.*

Undoubtedly, the azepinone ring has also been an element of potency and selectivity towards GPR55, and this should be considered in the design of new GPR55 antagonists (Figure 39).

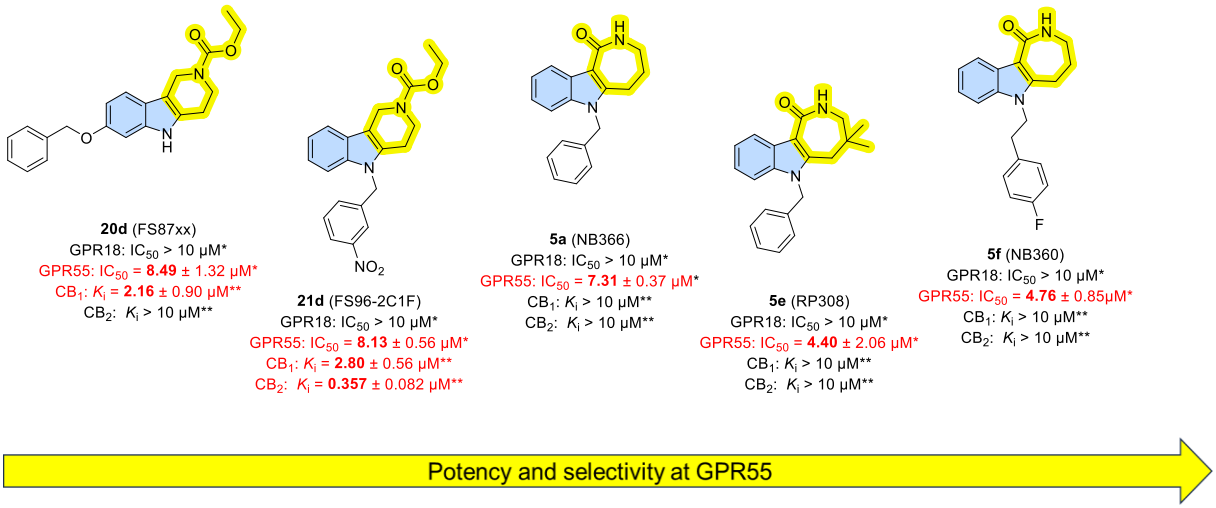

Figure 39. *Potency and selectivity at GPR55 increase passing from ethyl 1,3,4,5-tetrahydro-2H-pyrido[4,3-b]indole-2-carboxylates to 3,4,5,6-tetrahydroazepino[4,3-b]indol-1(2H)-ones. *β-arrestin assys; **radioligand binding assays.*

Aliphatic groups at the *N*6-position resulted in compounds that were either poorly active (**7a**, IC_{50} 10μM) or completely inactive (**7b-c**, Table 4). Among the compounds with aromatic side chains, those that featured phenylethyl substituents exhibited moderate antagonistic effects, with IC_{50} values ranging from 5 to 8 μM. Modifications to the phenyl ring influenced the GPR55 inhibitory activity: halogen substituents were more effective than the methyl substituent. Compound **5h**

(NB360, IC_{50} = 4.76 ± 0.85, Figure 27) emerged as one of the most potent GPR55 antagonists within this series. Compound **21d**, bearing a nitro group on the *N*6-benzyl, indicates that negatively charged functional groups are tolerated at this position. This observation is also supported by the docking scores of preliminary computational studies (data not shown). In contrast, the attempt to introduce a tertiary basic nitrogen as seen in compound **9a** was not successful.

From a comparison between the activities of compounds **5e** (RP308), **5l** (RP310) and **5f** (NB360) it can be deduced that when the azepinone ring is *gem*-dimethyl substituted, only a benzyl substituent at *N*6 is tolerated, while a phenylethyl performs better when the azepinone is unsubstituted, suggesting that limited space is available in this side of the binding pocket, where lipophilic interactions appear to be beneficial.

Even if some substitutions on the indole phenyl appear to be detrimental for activity, as in the case of 9-F in compound **5k** (Table 6), some others might be tolerated (for example 7-benzyloxy in compound **20d**, Table 10) and used to increase affinity at the receptor. A pictorial SAR of indole-fused tricyclic antagonists of GPR55 is reported in Figure 40.

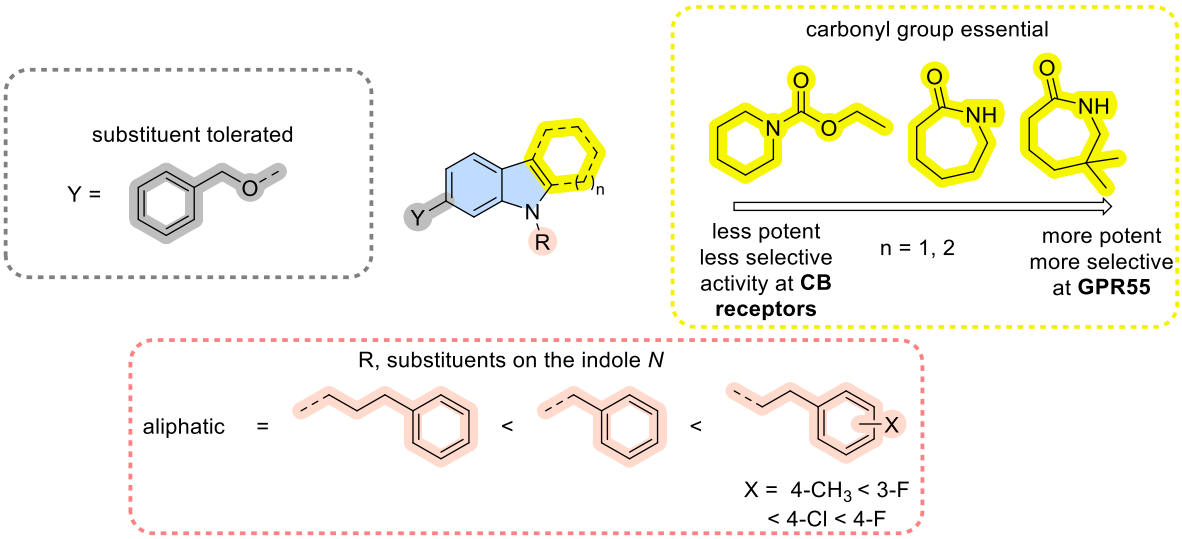

Figure 40. *Structure-activity relationships of indole-fused tricyclic antagonists of GPR55.*

From a functional perspective, the atypical behavior of our GPR55 carbamate-containing ligands can be observed here. Usually, ligands display opposite effects at GPR55 compared to CB receptors: CB antagonists activate GPR55, while CB agonists have antagonistic effect at GPR55. This phenomenon – reverse intrinsic

activity at GPR55 *versus* CB receptors – has been demonstrated for the CB agonist CP55,940 (Figure 15), for the CB_1 inverse agonist AM251 (Figure 16), for compounds in Figure 38, and for other CB receptor ligands[78,88] and led to the designation of GPR55 as an 'anti-cannabinoid receptor'.[49] Peculiarly, compounds **20d-e** and **21d** (*i.e.* the only carbamates of the series showing GPR55/CB dual activity) do not have this behavior and act as antagonist at both receptors (Tables 14,15). This peculiarity might make these compounds eligible as pharmacological tools to investigate unexplored effects of biochemical cross-talks in GPR55/CBR heteromers.[34,89]

4.4 Structure-activity relationships of GPR18 antagonists/inverse agonists

An aliphatic heterocycle containing a basic nitrogen is essential for activity at GPR18. Acyclic analogs proved to be inactive (**25a-b**), as well as non-basic compounds (for example THAIs). The aliphatic heterocycle can be hydrogenated azepine or a piperidine. Quenching the basicity of the nitrogen with a carbonyl group switches the selectivity towards GPR55. This is apparent when comparing both 7-membered alicyclic fused derivatives such as **5a** (NB336, lactam) with its reduced analog **6c** (NB344, azepine), and 6-membered alicyclic fused derivatives such as 2,3,4,5-tetrahydro-1*H*-pyrido[4,3-*b*]indoles and their corresponding carbamate precursors (**20d-e** and **21d**). Phenylbutyl- substitution on the azepine nitrogen resulted in the inverse agonist **6h** (NB339, Figure 28), indicating that larger macrocycles might be tolerated (see Annex 6.1 on annulated azecines[90]). As for the substitutions on the indole nitrogen, when the fused cycle is a hydrogenated azepine the substitutions can be ranked in the following order of potency: 4-F benzyl > phenylethyl > phenylpropyl > benzyl (**6a**, IC_{50} = 0.701 μM > **6c**, IC_{50} = 8.10 μM, > **6d**, IC_{50} ≈ 10 μM > **6b**, 2% inhibition at 10 μM, Table 7).

When the fused cycle is piperidine (compounds **22b-d**, **22f-i**), a phenylpropyl chain is generally better tolerated compared to the benzyl (**22f** *vs* **22b**, Table 10). A fluorine substitution at position 8 appears to be detrimental in this series of compounds. Compound **22e** is almost 7 times more potent than its 8-fluorinated analog **22f**. The substitutions on the indole phenyl of 2,3,4,5-tetrahydro-1*H*-pyrido[4,3-*b*]indoles can be ranked in the following order of potency: unsubstituted > 9-benzyloxy > 8-benzyloxy > 8-fluoro ≈ 7-benzyoxy (**22e**, IC_{50} = 0.753 μM > **22i**, IC_{50} = 3.64 μM > **22h**, IC_{50} = 3.98 μM > **22f**, IC_{50} = 5.11 μM ≈ **22g**, IC_{50} = 5.56

μM). An improvement in potency can be observed when the benzyloxy- is moved from position 7 to position 9 (Figure 42), suggesting that the latter might be the object of further chemical modifications. However, the introduction of the benzyloxy moiety is also responsible for the extension of the activity of compounds **22g-i** towards the cannabinoid receptors CB_1 and/or CB_2, as confirmed by the docking studies presented in section 4.2.4.3. A pictorial SAR with the main findings on this class of compounds is presented in Figure 41.

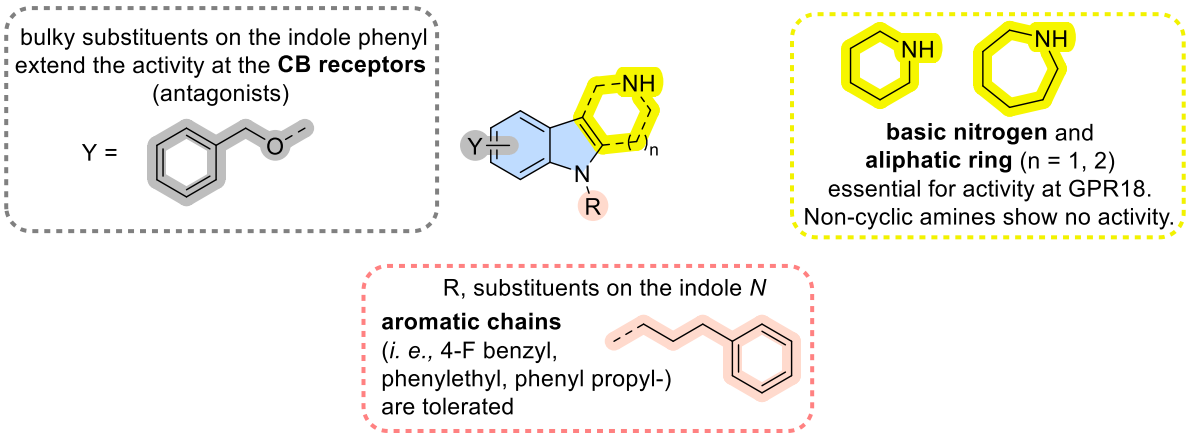

Figure 41. *Structure-activity relationships of indole-fused tricyclic antagonists and inverse agonists of GPR18.*

Some additional considerations are necessary about compounds active as dual ligands of CB receptors and GPR18/55 (**22g-i**, **21d** and **20d**).

The IC_{50} and K_i values, together with the docking scores and the interactions highlighted by the computational studies at the CB_1 and CB_2 receptor, indicate that the compounds most likely behave as orthosteric ligands. However, docking studies on the allosteric site of CB_1 show that they might be also able to interact with the allosteric pocket of the receptor. Studies on the allosteric pocket of CB_2 couldn't be performed due to the lack of a crystal structure of an allosteric modulator bound to this receptor.

As suggested by experimental data, the increase in lipophilicity of the compounds is related to an increase in activity at CB receptors. Docking studies show how the network of hydrophobic interactions extends through the creation of π-π bonds between the benzyloxy- moiety of compounds **22g-i** (FS99-B, FS98-B and FS100r) and some amino acids in the orthosteric binding pockets. This is very apparent in the case of CB_2 receptor, where the aromatic moiety is sandwiched between W194

and F117 and interacts with the toggle switch W258, a well-known feature of CB_2 receptor antagonists.

These compounds could represent useful pharmacological tools to investigate the complex relationships between cannabinoid receptors and the cannabinoid-related receptors GPR55 and GPR18. **20d** (FS87xx**)** and **21d** (FS962C-1F**)** emerge as dual CB_1/CB_2 receptors ligands with IC_{50} values ranging from 0.914 μM to 7.51 μM. They both have a weak antagonistic activity at the cannabinoid-relater receptor GPR55 conferred by the carbamate function ($IC_{50} \approx 8.00$ μM). Specifically, while **21d** (FS962C-1F**)** acts as antagonist at both CB receptors, **20d** (FS87xx**)** acts as an antagonist at CB_1 receptor and as full inverse agonist at CB_2 receptor. Researchers are currently exploring the therapeutic possibilities of CB_2 receptor antagonists and inverse agonists in clinical applications. For example, a newly identified CB_2 receptor antagonist, TT816 (structure undisclosed, IC_{50} at CB_2 receptor = 26.2 nM) developed by Teon Therapeutics, is now in phase 2 clinical trials (NCT05525455) for advanced cancers lung, renal cell, and ovarian cancer. Furthermore, the CB_2 receptor inverse agonist SMM-189[74] has shown promise as a potential treatment, proving effective in managing colitis and inflammatory bowel disease (IBD). Compounds **22h-i** (FS100r and FS98-B**)** are dual CB_2/GPR18 receptors ligands with comparable IC_{50} values at both targets (IC_{50} between 2 and 4 μM). Removal of the benzyloxy- moiety switches off the activity at CB_2 receptors, as the fundamental π-π interactions with the aromatic residues F117, W194 and W28 disappear, while retaining the effect at GPR18 (see compound **22f**, FS88-B, Table 18).

Table 18. *Biological activities of test compounds at human cannabinoid (hCB_1R, hCB_2R) and cannabinoid-related (hGPR18, hGPR55) receptors*

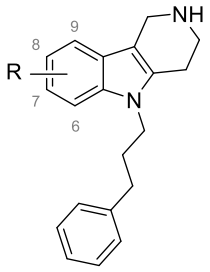

Cmpd	R	***h*CB$_1$R** IC$_{50}$ ± SEM (μM)[a]	***h*CB$_2$R** IC$_{50}$ ± SEM (μM)[a]	***h*GPR18** IC$_{50}$ ± SEM (μM)[b]	***h*GPR55** IC$_{50}$ ± SEM (μM)[b]
22i	**9-(BnO)-**	**≈10** (52%)*	**2.80 ±** 0.23*	**3.64** ± 0.96	**>10** (34%)
22h	**8-(BnO)-**	**≈10** (53%)*	**3.83** ± 1.07*	**3.98** ± 1.20	**>10** (30%)
22g	**7-(BnO)-**	**3.46** ± 0.46*	**7.51** ± 2.80*	**5.56** ± 0.68	**>10** (33%)
22f	**8-(F)-**	**>10** (29%)**	**>10** (21%)**	**5.11** ± 0.81	**>10** (28%)

*[a] determined with PathHunter β-arrestin assays, data compared to activation of agonist-induced luminescence signal at CB_1 and CB_2 receptors at their corresponding EC_{80}s (CB_1R : 0.003 μM CP55940; CB_2R : 0.001 μM CP55940). Determined with PathHunter β-arrestin assays or % of displacement of [^{3}H]CP55940 binding by test compound at 10 μM; *β-arrestin assays; **radioligand binding assay. [b] determined with PathHunter β-arrestin assays, data compared to activation of agonist-induced luminescence signal at its corresponding EC_{80} (GPR18: 0.1 μM PSB-KK-1415; GPR55: 4 μM LPI). Data represent mean values of IC_{50} ± Standard Error Measurement (SEM) or percent of inhibition of agonist-induced activation of receptor by test compound at 10 μM.*

Moreover, a common trend of structure-activity relationship towards GPR18 and CB_2 can be identified. Moving the benzyloxy- moiety from position 7 to position 9 enhances the potency at both receptors (Figure 42). **22g** (FS99-B) is a moderate modulator of CB_1, CB_2 and GPR18 receptors (IC_{50} equal to 3.46, 7.51 and 5.56 μM, respectively).

The dual action of compounds **2h-i** (FS98-B and FS100r) results particularly interesting considering that the two target proteins can dimerize to form heteromers. CB_2-GPR18 heteroreceptor complexes have been identified in primary cultures of microglia by *in situ* proximity ligation assays. These heteromers displayed particular functional properties (heteromer fingerprints) often consisting of

negative cross-talk (activation of one receptor reduces signaling arising from the partner receptor) and cross-antagonism (the response of one of the receptors is blocked by a selective antagonist of the partner receptor), suggesting that GPR18 and its heteromers may play important roles in neurodegenerative processes (Figure 43).[91]

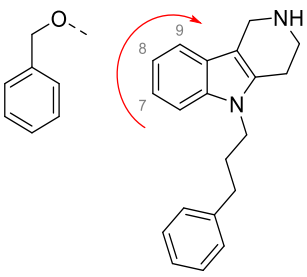

Target	activity
GPR18	↑
CB_2	↑
CB_1	↓

Figure 42. *A common trend of structure-activity relationship towards GPR18 and CB_2 can be identified in 5-(3-phenylpropyl)-2,3,4,5-tetrahydro-1H-pyrido[4,3-b]indole derivatives. Moving the benzyloxy- moiety from position 7 to position 9 enhances the potency at both GPR18 and CB2 receptors.*

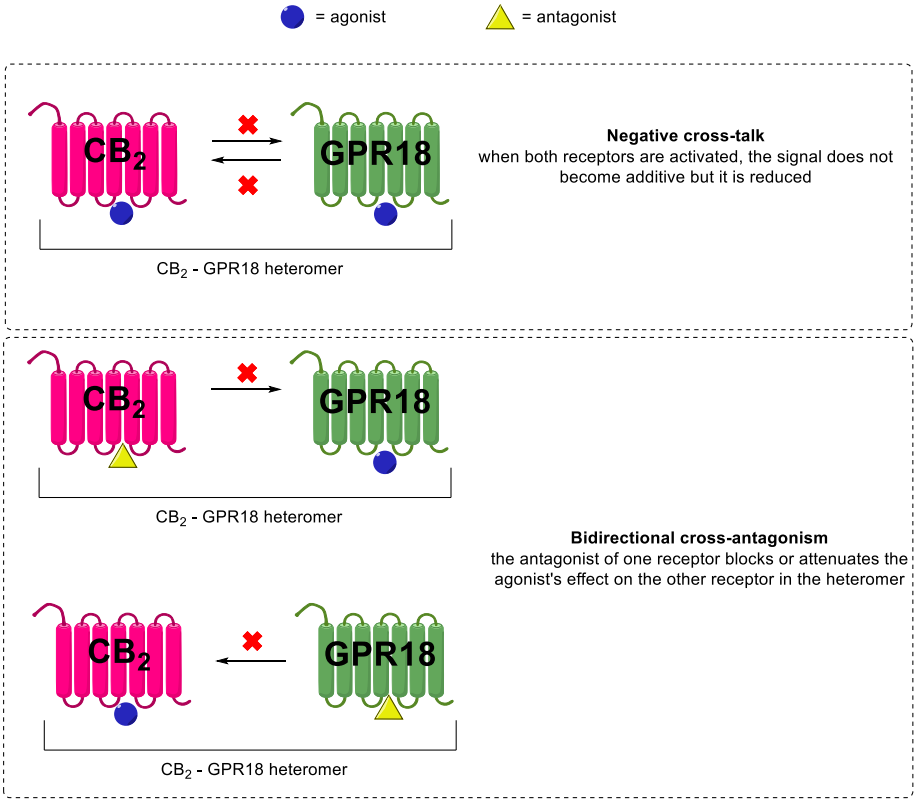

Figure 43. *Representation of CB_2-GPR18 heteroreceptor complexes and their biochemical cross-talk. In a negative crosstalk, when both receptors are activated by an agonist, the signal does not become additive, but is reduced. So, the activation of GPR18 is a break for CB_2 activation, and vice versa. In a bidirectional cross-antagonism, the antagonist of one receptor blocks or attenuates the agonist's effect on the other receptor in the heteromer.*

4.5 Cholinesterases inhibition

Cholinesterases, including acetylcholinesterase (AChE) and butyrylcholinesterase (BChE), play pivotal roles in the nervous system by regulating the levels of acetylcholine, a neurotransmitter essential for cognitive function. In the context of neurodegenerative diseases, such as AD, the dysregulation of these enzymes is a critical factor. Elevated levels of AChE and BChE have been associated with increased amyloid-beta plaque formation, a hallmark of Alzheimer's pathology. Furthermore, the imbalance in cholinesterase activity contributes to the disruption of cholinergic signaling, exacerbating cognitive decline and neuronal damage.

The newly synthesized compounds were characterized as ChEs' inhibitors using the classical Ellman's colorimetric assay. Electric eel acetylcholinesterase (*ee*AChE) and horse serum butyrylcholinesterase (*hs*BChE), which share high structural homology with human isoforms, were used in a first step, as a biological screening to identify the most interesting compounds, which were then further tested on human isoforms. Results comprehensive of all biological activity data collected and elaborated are displayed in Table 19.

Table 19. *Biological activities and/or affinities of test compounds at human cannabinoid (hCB_1R, hCB_2R) and cannabinoid-related (hGPR18, hGPR55) receptors and at heterologous and/or human cholinesterases (electric eel acetylcholinesterase and horse serum butyrylccholinesterase, eeAChE and hsBChE).*

cmpd	K_i (μM) or % inhibition (10 μM)[a]		IC_{50} (μM) or % inhibition (10 μM)[b]		IC_{50} (μM) or % inhibition (10 μM)[c]	
	***h*CB1**	***h*CB2**	***h*GPR18**	***h*GPR55**	***ee*AChE**	***hs*BChE**
5a	(24%)	(28%)	(11%)	**7.31** ± 0.37	(9%)	(24%)
5b			(-10%)	(1%)	(39%)	**0.395 ± 0.086**
5c			(-41%)	(4%)	(16%)	(15)
5d			(-43%)	(-3%)	(34%)	(12%)
5e			(-3%)	**4.40** ± 2.06	**≈10** (50%)	**0.185 ± 0.074**
5f	(8%)	(6%)	(1%)	**5.18** ± 1.5	**≈10** (54%)•	**0.013** ± 0.005•
5g	(23%)	(23%)	(11%)	**8.26** ± 2.42	(6%)•	**0.0018** ± 0.001•

5h	(22%)	(23%)	(9%)	**4.76** ± 0.85	**≈10** (50%)•	**5.00** ± 1.03•
5i	(35%)	(31%)	(6%)	**5.68** ± 0.67	(2%)	**1.90** ± 0.33
5j	(33%)	(35%)	(22%)	≈ **10** (51%)	(10%)	(32%)
5k	(11%)	(15%)	(12%)	(45%)	(5%)	**0.028** ± 0.002
5l			(36%)	(26%)	(28%)	**0.185 ± 0.083**
5m	(1%)	(19%)	(11%)	(22%)	(5%)	(18%)
5n	(7%)	(14%)	(1%)	(37%)	(44.8%)	(10%)
6a			**0.701** ± 0.122	(2%)	(45%)	**3.18** ± 0.23
6b			(2%)	(-9%)	(10%)	**1.90 ± 0.67**
6c	(7%)	(28%)	**8.10** ± 0.56	(-9%)	(33%)	**1.136** ± 0.030
6d			(44%)	(-10%)	**6.32 ± 1.00**	**0.353 ± 0.091**
6e	(14%)	(16%)	(45%)	(-11%)	**8.70** ± 0.40	**2.00** ± 0.30
6f	(-1%)	(9%)	≈ **10** (50%)	(-1%)	**9.00** ± 1.50	**0.700** ± 0.200
6g	(27%)	(4%)	(27%)	(40%)	(41%)	**0.278** ± 0.050
6h	(-8%)	(3%)	**4.72** ± 0.14	(44%)	(43%)	**0.199** ± 0.010•
7a	(29%)	(34%)	(13%)	≈ **10** (54%)	(10%)	(25%)
7b	(29%)	(34%)	(8%)	(22%)	(2%)	≈ **10** (52%)
7c	(16%)	(1%)	(-4%)	(27%)	(5%)	(40%)
9a	(26%)	(6%)	(18%)	(4%)	(28%)	(39%)

9b	(9%)	(10%)	(29%)	(12%)	(41%)	(34%)
9c	(7%)	(6%)	(43%)	(32%)	(28%)	(30%)
9d	(24%)	(38%)	**≈10** (50%)	(19%)	(38%)	(41%)•
9e	(20%)	(13%)	(0%)	(17%)	(30%)	(34%)
9f	(12%)	(8%)	(43%)	(17%)	(45%)	(16%)
9g	(4%)	(9%)	(39%)	(20%)	(45%)	**2,10** ± 0,24•
9h	(3%)	(8%)	(39%)	(7%)	(25%)	**7,45** ± 0,77
9i	(27%)	(11%)	(45%)	(33%)	(33%)	(20%)
11a			(-18%)	(46%)	(30%)	(37%)
11b			≈**10** (59%)	(34%)	(32%)	(18%)
14a			(20%)	(29%)	(31%)	(16%)
14b			(-21%)	(24%)	(13%)	(25%)
19a			(-17%)	(45%)	(31%)	(7%)
19b			(-15%)	(36%)	**1.34 ± 0.67**	**0.830± 0.270**
20d	**2.58** ± 0.69*	**2.86** ± 0.09*	**≈10** (56%)	**8.49** ± 1.32	(25%)	(43%)
20e	(36%)	(47%)	**≈10** (45%)	**≈10** (50%)	(17%)	(19%)
21d	**0.914** ± 0.112*	**6.05** ± 2.96*	(34%)	**8.13** ± 0.56	(28%)	(15%)
22a			**0.753** ± 0.116	(4%)	**5.68 ± 0.44**	**3.62 ± 1.02**
22b	(30%)	(20%)	(25%)	(6%)	(36%)	**5,82** ± 1,17•

22c	(43%)	(46%)	**≈10** (56%)	(8%)	(27%)	28%
22d	(18%)	(17%)	**≈10** (54%)	(27%)	(33%)	**3.89** ± 1.51
22e			**0.753** ± 0.223	(2%)	(34%)	**1.38 ± 0.75**
22f	**>10** (29%)	**>10** (21%)	**5.11** ± 0.81	(28%)	(33%)	**1.55** ± 0.06•
22g	**3.46** ± 0.46*	**7.51** ± 2.80*	**5.56** ± 0.68	(33%)		
22h	**≈10** (53%)*	**3.83** ± 1.07*	**3.98** ± 1.20	(30%)	(27%)•	**6.39** ± 1.20
22i	**≈10** (52%)*	**2.80 ±** 0.23*	**3.64** ± 0.96	(34%)		
25a			(30%)	(18%)	(29%)	**1.81** ± 0.99
25b			(45%)	(24%)	**≈10** (56%)	**1.23** ± 1.14

*[a] data represent percent of displacement of [^{3}H]CP55940 binding by test compound at 10 μM [b] determined with PathHunter β-arrestin assays, data compared to activation of agonist-induced luminescence signal at its corresponding EC_{80} (GPR18: 0.1 μM PSB-KK-1415; GPR55: 4 μM LPI). Data represent means value of IC_{50} ± Standard Error Measurement (SEM) or percent of inhibition of agonist-induced activation of receptor by test compound at 10 μM. [c] determined with Ellman's colorimetric assay; * IC_{50} values determined with PathHunter β-arrestin assays, data compared to activation of agonist-induced luminescence signal at CB_1 and CB_2 receptors at their corresponding EC_{80}s (CB_1R : 0.003 μM CP55940; CB_2R: 0.001 μM CP55940). •data from human cholinesterases isoforms.*

The compounds presented in Table 19 can be categorized, as detailed in Table 20, into two distinct groups based on their biological activities: those that exhibit dual BChE inhibitors/GPR55 antagonists (compounds **5e-i**), and those that act as dual BChE inhibitors and antagonists or inverse agonists of GPR18 (compounds **6a**, **6c**, **6h**, **22a**, **22e-f**, **22h**).

Table 20. *Compounds showing multi-target profiles. Biological activities and/or affinities of test compounds at human cannabinoid (hCB_1R, hCB_2R) and cannabinoid-related (hGPR18, hGPR55) receptors and at heterologous and/or human cholinesterases (electric eel acetylcholinesterase and horse serum butyrylccholinesterase, eeAChE and hsBChE).*

cmpd	K_i (μM) or % inhibition (10 μM)[a]		IC_{50} (μM) or % inhibition (10 μM)[b]		IC_{50} (μM) or % inhibition (10 μM)[c]	
	***h*CB1**	***h*CB2**	***h*GPR18**	***h*GPR55**	***ee*AChE**	***hs*BChE**
5e			(-3%)	**4.40** ± 2.06	**≈10** (50%)	**0.185 ± 0.074**
5f	(8%)	(6%)	(1%)	**5.18** ± 1.5	**≈10** (54%)•	**0.013** ± 0.005•
5g	(23%)	(23%)	(11%)	**8.26** ± 2.42	(6%)•	**0.0018** ± 0.001•
5h	(22%)	(23%)	(9%)	**4.76** ± 0.85	**≈10** (50%)•	**5.00** ± 1.03•
5i	(35%)	(31%)	(6%)	**5.68** ± 0.67	(2%)	**1.90** ± 0.33
6a			**0.701** ± 0.122	(2%)	(45%)	**3.18** ± 0.23
6c	(7%)	(28%)	**8.10** ± 0.56	(-9%)	(33%)	**1.136** ± 0.030
6h	(-8%)	(3%)	**4.72** ± 0.14	(44%)	(43%)	**0.199** ± 0.010•
22a			**0.753** ± 0.116	(4%)	**5.68 ± 0.44**	**3.62 ± 1.02**
22e			**0.753** ± 0.223	(2%)	(34%)	**1.38 ± 0.75**
22f	**>10** (29%)	**>10** (21%)	**5.11** ± 0.81	(28%)	(33%)	**1,55** ± 0,06•
22h	**≈10** (53%)*	**3.83** ± 1.07*	**3.98** ± 1.20	(30%)	(27%)•	**6,39** ± 1,20

[a]data represent percent of displacement of [^{3}H]CP55940 binding by test compound at 10 μM [b] determined with PathHunter β-arrestin assays, data compared to activation of agonist-induced luminescence signal at its corresponding EC_{80} (GPR18: 0.1 μM PSB-KK-1415; GPR55: 4 μM LPI). Data represent means value of IC_{50} ± Standard Error Measurement (SEM) or percent of inhibition of agonist-induced activation of receptor by test compound at 10 μM. [c] determined with Ellman's colorimetric assay; IC_{50} values determined with PathHunter β-arrestin assays, data compared to activation of agonist-induced luminescence signal at CB_1 and CB_2 receptors at their corresponding EC_{80}s (CB_1R : 0.003 μM CP55940; CB_2R : 0.001 μM CP55940). •data from human cholinesterases isoforms.*

The identification of MTDLs that target human BChE and human GPR18/GPR55, demonstrating inhibition potencies that are comparable in magnitude, as illustrated in Figure 56, may hold promise for reversing cognitive impairment associated with neurodegenerative diseases

Moreover, a significant number of compounds act as selective BChE inhibitors. Specifically, the compounds from the 9 series, characterized by long chains on the indole nitrogen, demonstrate efficacy against BChE while exhibiting no activity against GPR55. Concentration-inhibition curves of compound **9g** at heterologous and human BChE isoforms with the corresponding IC_{50} values are reported as example in Table 21.

Table 21. *Inhibitory potencies of compound **9g** (FS69-2) as hsBChE and hBChE inhibitor in Ellman's colorimetric assay. Data are mean ± SEM of three independent experiments performed in duplicates (n = 3).*

COMPOUND	CURVE vs BChE	IC_{50} ± SEM
9g (FS69-2) 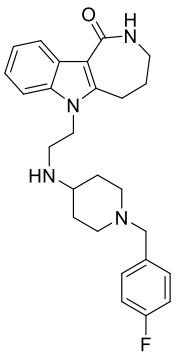	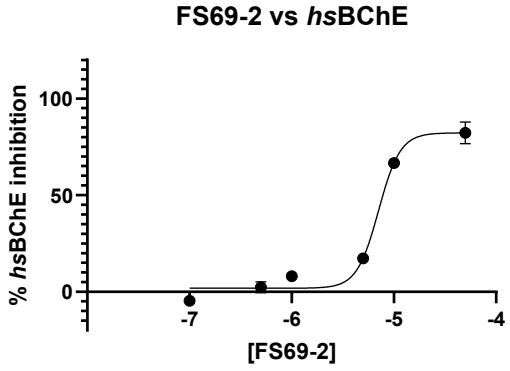	*hs*BChE 6,14 ± 0,88 µM
	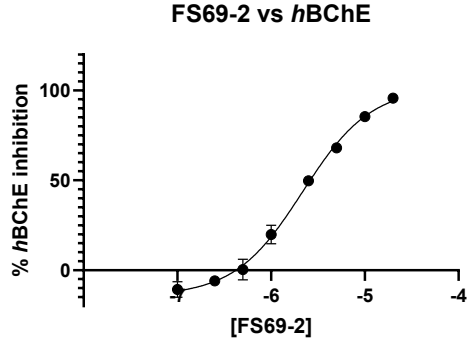	*h*BChE 2,10 ± 0,24 µM

This observation establishes a structural distinction that enhances the activity on BChE but reduces it on GPR55. Although this series did not result in the identification of multi-target compounds, it inspired the development of additional selective BChE inhibitors that also incorporate a long chain on the indole nitrogen.

We synthetized and tested twenty-two new THAI derivatives designed and prepared by introducing alkyl chains bearing differently decorated piperazine fragments (Figure 44).

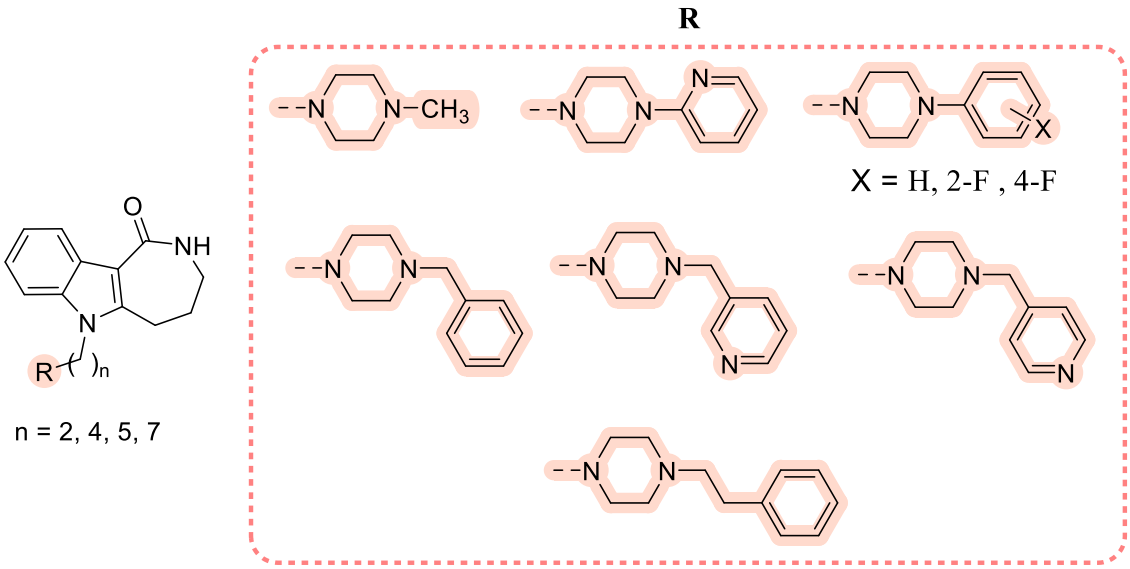

Figure 44. *Piperazines-containing THAI-based multitarget derivatives synthetized and tested.*

Evaluated in vitro as inhibitors of ChEs, the newly synthesized compounds showed selective inhibition of BChE. Molar volume and molar refractivity were the physicochemical parameters mainly correlating with the inhibition potency. The most potent derivatives **26a** (*h*BChE IC_{50} = 190 nM) and **26b** (*h*BChE IC50 = 72 nM, Figure 45 and 46) exhibited *h*BChE-selective inhibition in the nanomolar range of concentration. They showed mixed-type inhibition of BChE, with binding kinetics indicating long residence times (8 seconds for **26a** and 47 seconds for **26b**), and thus suggests a prolonged effect of these inhibitors on the enzyme.

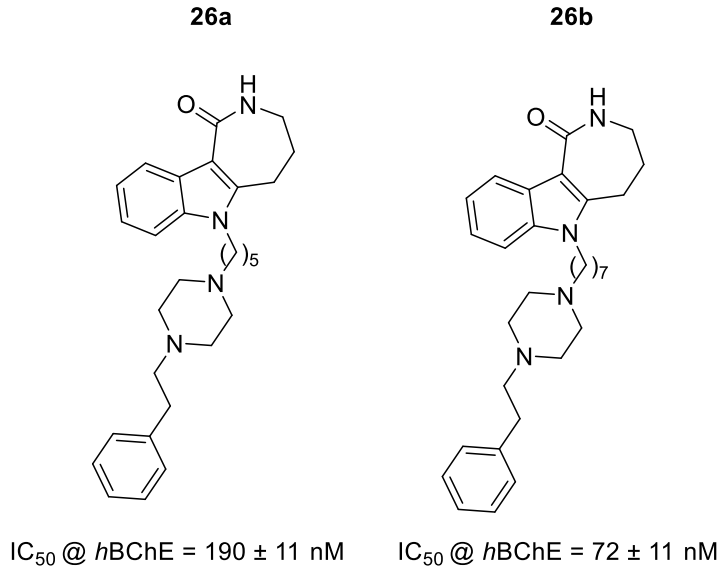

Figure 45. *BChE-selective inhibitors 6-alkyl-bridged 4-arylalkylpiperazin-1-yl derivatives of azepino[4,3-b]indol-1(2H) compounds* ***26a-b****.*

Chemical synthesis, mechanism of action, neuroprotective effect, structure-activity relationships, safety profile, and other results have been discussed and published.[4]

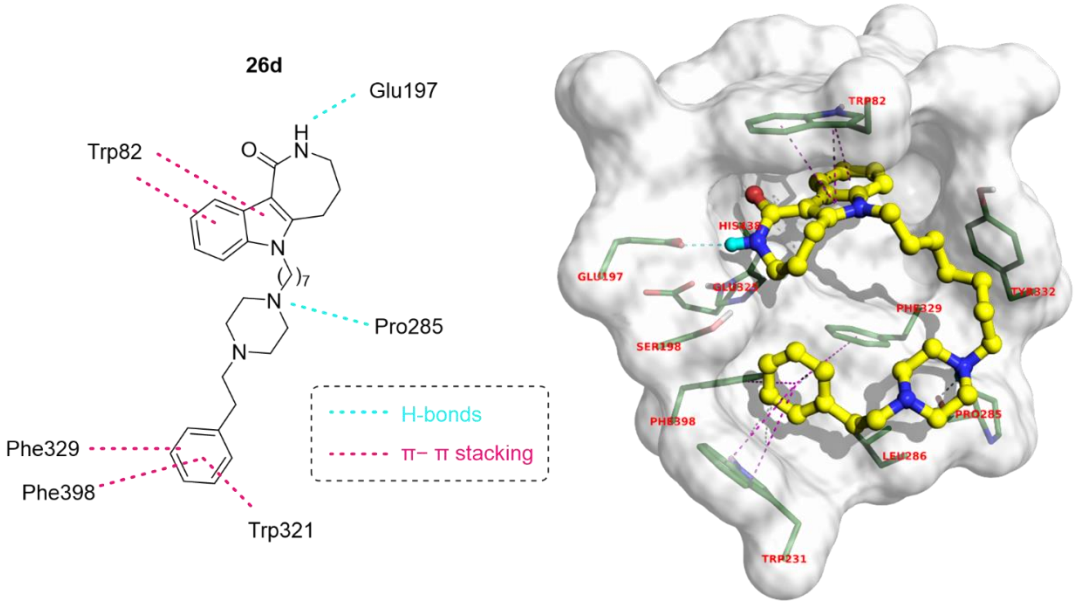

Figure 46*. Binding mode of compound* ***26b*** *into the BChE active site. H-bonds and π-π stackings are depicted in cyan and magenta dashed lines, respectively.*

4.6 Radiosynthesis and whole-body distribution in mice of a ^{18}F-labeled azepino[4,3-*b*]indole-1-one derivative

To progress in featuring the in vivo pharmacological characterization of our compounds, a^{18}F-labeled congener **5k** was synthesized, by applying the aromatic ^{18}F-fluorination method, and its whole-body distribution in healthy mice, including brain penetration, was evaluated through positron emission tomography imaging, and recently published in collaboration with other research groups (Figure 47).[5] [^{18}F]**5k** exhibited a rapid and high brain uptake (3.35 ± 0.26% ID g^{-1} at 0.95 ± 0.15 min after injection), followed by a rapid clearance ($t_{1/2}$ = 6.50 ± 0.93 min), showing good blood–brain barrier crossing. After a transient liver accumulation of [18F]**5k**, the intestinal and urinary excretion was quantified. *Ex vivo* pharmacological experiments in mice showed that the unlabeled **5k** affects the transmitters' neurochemistry, which might be favorable to reverse cognition impairment in neurodegenerative diseases such as AD.

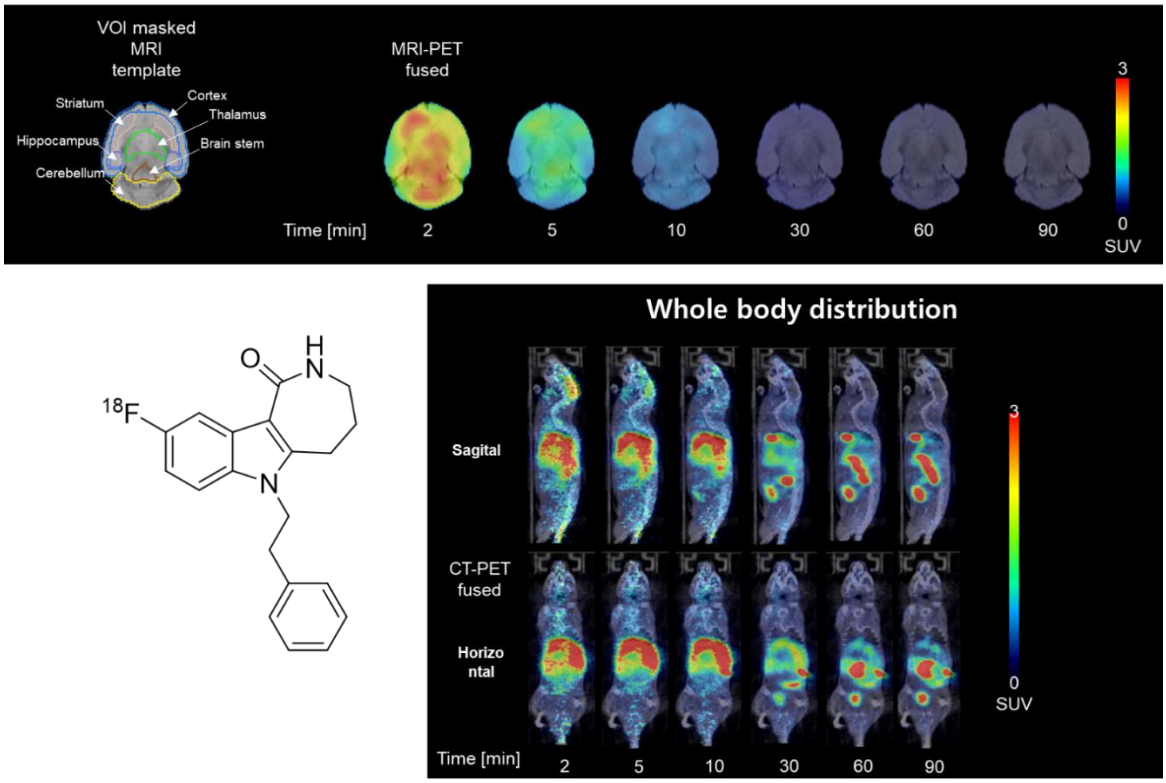

Figure 47. *Representative positron emission tomography images (a and b) and time–activity curves (c) of [18F]2a in the brain, gallbladder, heart, lungs, liver, urinary bladder, kidneys, liver, and intestine in the healthy mice.*

5 OTHER MULTITARGET STRATEGIES FOR NEURODEGENERATIVE DISEASES

The following sections, 5.1, 5.2, 5.3, and 5.4 will focus on projects published in collaboration with other research groups.[92–94] Our contributions in sections 5.1, 5.2 and 5.3 involve mainly, but not only, the biological assessment of newly synthesized molecules on AChE and BChE, with an emphasis on the subsequent analysis of structure-activity relationships. Section 5.4 highlights the key findings - resulting from a machine learning analysis of a clinical database - regarding the pleiotropic effects of direct oral anticoagulants (DOACs) beyond their primary role in anticoagulation. These effects include anti-inflammatory, antioxidant, and anti-fibrotic actions on endothelial cells, which contribute to improved endothelial function and integrity—a condition often associated with enhanced cognitive performance. [95,96]

5.1 Thioether-triazine as dual 5-HT$_6$R and AChE/BChE ligands

Serotonin 5-HT$_6$ receptors (5-HT$_6$R) represent a particularly promising target for therapeutic interventions, given their role in cognitive functions as well as in depression and psychosis. We reported and published the synthesis and extensive biological characterization of a new set of 18 compounds featuring a distinctive 1,3,5-triazine backbone, which act as potent ligands for the 5-HT$_6$ receptor (Figure 48).[92]

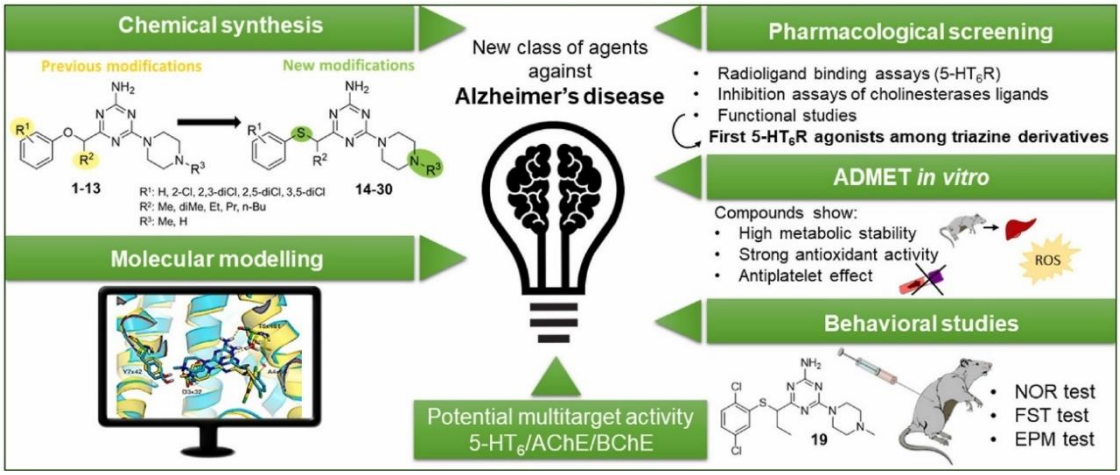

Figure 48. *Graphical abstract of the published article[92] presenting the studies on (thio)ether-1,3,5-triazines as dual 5-HT$_6$R and AChE/BChE ligands. This investigation included chemical synthesis, pharmacological screening, molecular modeling, ADMET in vitro, and behavioral studies.*

The primary objective of this study is to evaluate the biological activity of the newly created sulfur derivatives in comparison with their oxygen analogs and their *N*-demethylated *O*- and *S*-metabolites, which have been reported for the first time. The

majority of the new triazines exhibited a high affinity (K_i < 200 nM) and selectivity for the 5-HT_6R, when evaluated against 5-HT_{2A}R, 5-HT_7R, and D_2R, in radioligand binding assays. For selected active compounds, crystallographic studies, functional bioassays, and in vitro ADME-Tox profiling were conducted. A notable finding is that the sulfur derivatives display an agonistic action, in contrast to the previously reported oxygen analogs. Advanced computational analyses suggest that this interesting functional variation may be attributed to the presence of chalcogen bonds formed exclusively by the sulfur atom. Furthermore, the *N*-demethylated derivatives have proven to be highly effective antioxidants and show a significant enhancement in metabolic stability relative to the parent compounds. The cholinesterase testing revealed micromolar inhibitory effects on AChE and BChE activity for both the 5-HT_6 agonist **27b** and the potent antagonist **27a** (Figure 49). Ultimately, behavioral studies on compound **27b** indicated its antidepressant-like effects and a modest capacity to enhance cognitive deficits, without causing memory impairments by itself. The pharmacological characteristics of both compounds (**27b** and **27a**) provide insights that could guide the creation of multitarget compounds featuring 5-HT6 (both agonist and antagonist) in conjunction with AChE and/or BChE mechanisms from the 1,3,5-triazine derivatives group.

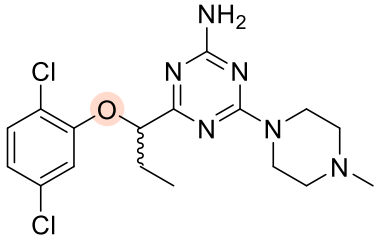

27a

K_i 5HT_6R = 6 ± 2 nM
pK_B10.57 ± 0.065
K_i 5HT_{2a} = 484 ± 58 nM
Ki 5HT_7 = 5706 ± 498 nM
Ki D_2 = 320 ± 49 nM
IC_{50} AChE = 11.2 ± 0.18 μM
IC_{50} BChE = n.a.

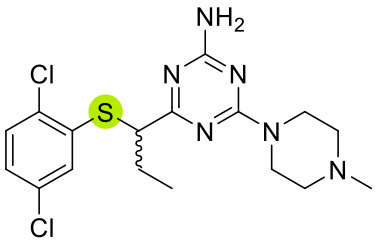

27b

K_i 5HT_6R = 5 ± 2 nM
pEC_{50} = 6.81 ± 0.08
K_i 5HT_{2a} = 551 ± 95 nM
Ki 5HT_7 = 5142 ± 687 nM
Ki D_2 = 1004 ± 182 nM
IC_{50} AChE = n.a.
IC_{50} BChE = 12.10 ± 0.55 μM

Figure 49. *Compounds 27a-b show high affinity for 5HT_6 receptors and different functional effects (antagonist and agonist, respectively). Molecular dynamics simulations suggest that the presence of a chalcogen bond, formed only by the sulfur atom, might be responsible for this functional shift. Cholinesterase inhibition data are also reported (n.a., not active).*

A newly formulated series of 18-membered triazine-based ligands aimed at the 5-HT_6R has been extensively characterized in terms of its biological properties. One

of the most relevant discoveries was the replacement of an oxygen atom with a sulfur atom in the linker, which led to a different intrinsic activity. This represents the first identification of 5-HT_6R agonists within this novel class of non-sulfone and non-indole chemical entities.

It is important to highlight that focusing on the 5-HT_6R is particularly compelling, considering that all 5-HT_6R ligands that have failed in Alzheimer's disease (AD) clinical trials were antagonists, and no agonists have yet progressed to human testing. Among these new compounds, the triazine 5-HT_6R agonist (compound **27b**), chosen for additional evaluation, exhibited less effective procognitive effects than anticipated while still maintaining the antidepressant activity typical of the triazine antagonist (**27a**) in rat models.

Given the diverse potency observed in pharmacological actions on 5-HT_6R during the radioligand binding and functional experiments, compound **27b** is positioned as an important asset for exploring new cellular signaling pathways related to 5-HT_6R. Furthermore, cholinesterase assessments conducted on compounds **27a** and **27b** have yielded design insights for developing multitarget compounds that function through both 5-HT_6 (agonist and antagonist) and acetylcholinesterase (AChE) and/or butyrylcholinesterase (BChE) actions among 1,3,5-triazine derivatives. This could pave the way for effective treatment strategies for multifactorial neurological diseases.

5.2 Chiral pyrrolidines as multipotent agents in Alzheimer and neurodegenerative diseases

The pyrrolidine scaffold is noteworthy for its versatility, particularly in terms of spatial arrangement, synthetic accessibility, and pharmacological profile. However, there is limited evidence supporting the role of pyrrolidine as a scaffold for multipotent agents targeting neurodegenerative diseases. In this study, we assessed the anti-AD potential of ten newly synthetized enantiomeric pairs of compounds, by first studying their activity as AChE inhibitors thanks to a certain degree of similarity with the pharmacophoric elements of the well-known AChE inhibitor donepezil (*i.e.* chargeable nitrogen with a lipophilic pendant, stereocenter, hydrogen bond accepting atom, and aromatic rings, Figure 50), that could endow these ligands with a similar pharmacological profile.

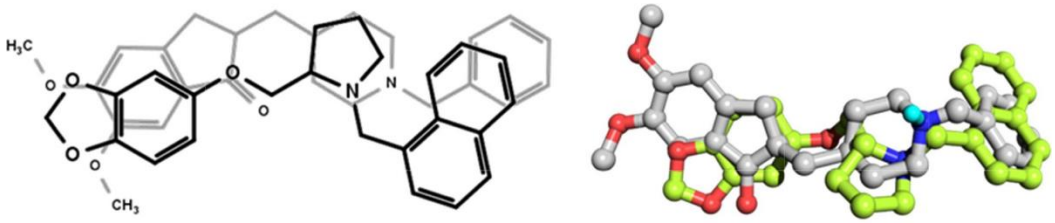

Figure 50. *Graphical abstract of the published article[93] showing the superpositions of the 2D and 3D structures of donepezil vs compound (R)-**30a**.*

The in vitro activity of all presented enantiomer pairs was measured toward electric eel (ee) AChE, and horse serum (hs) BChE, by applying the Ellman colorimetric assay, with slight modifications (see experimental section). All derivatives were first tested at a single point 10 μM concentration, and those showing at least 35% inhibition were further tested to determine their half-maximal inhibitory concentrations (IC_{50} values). Donepezil and tacrine were tested as positive controls against AChE and BChE, respectively. The results (Table 22) suggested that substituent fragments on pyrrolidine ring, as well as stereoisomerism, deeply affected the activity profile.

Table 22. *Biological activity of test compounds towards eeAChE and hsBChE.*

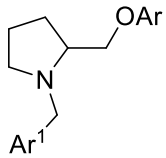

Ar	**Ar[1]**	**compd**	***ee*AChE**[a] IC_{50}, μM[c] (or % inhib)[d]	***eq*BChE**[b] IC_{50}, μM[c] (or % inhib)[d]
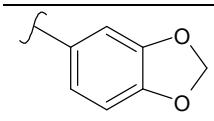	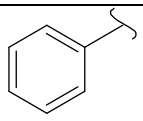	(*R*)-**28a**	3.15 ± 0.27	2.2 ± 0.5
		(*S*)-**28a**	(38 ± 3)	0.656 ± 0.130
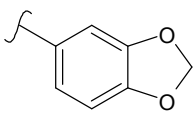	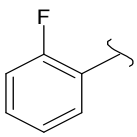	(*R*)-**29a**	0.950 ± 0.110	(25 ± 6)
		(*S*)-**29a**	(32± 2)	9.91 ± 0.15

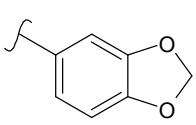	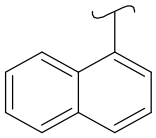	(*R*)-**30a**	0.215 ± 0.005	(27 ± 6)
		(*S*)-**30a**	(32 ± 1)	(7 ± 4)
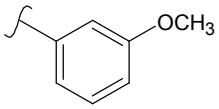	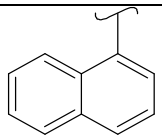	(*R*)-**31b**	10.3± 2.1	2.03± 0.13
		(*S*)-**31b**	15.7± 1.1	1.70 ± 0.11
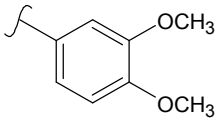	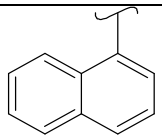	(*R*)-**32c**	10.0 ± 1.2	11.2 ± 0.5
		(*S*)-**32c**	(20 ± 10)	(18 ± 11)
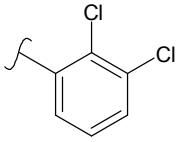	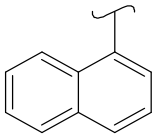	(*R*)-**33d**	(13 ± 4)	10.0 ± 0.24
		(*S*)-**33d**	(17 ± 6)	2.8 ± 0.9
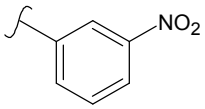	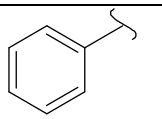	(*R*)-**34e**	1.31 ± 0.42	(18 ± 5)
		(*S*)-**34e**	7.22 ±0.25	(13 ± 2)
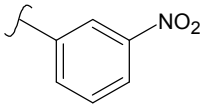	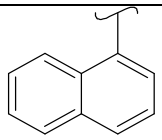	(*R*)-**35e**	16.7 ± 1.5	11.1 ± 0.6
		(*S*)-**35e**	2.66 ± 0.21	(14.5 ± 0.3)
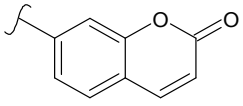	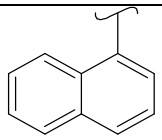	(*R*)-**36f**	3.73 ± 0.20	(35 ± 5)
		(*S*)-**36f**	2.35 ± 0.11	0.950 ± 0.040
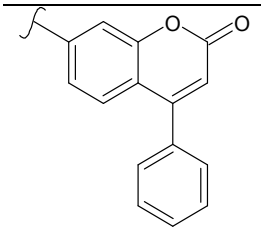	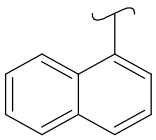	(*R*)-**37g**	19.0 ± 0.8	0.640 ± 0.260
		(*S*)-**37g**	9.90 ± 1.05	0.155 ± 0.018
		Donepezil	0.021 ± 0.011	2.25 ± 0.30
		Tacrine	0.030 ± 0.010	0.020 ± 0.009

[a]Electric eel acetylcholinesterase. [b]Horse serum butyrylcholinesterase. [c]IC_{50} values by regression of the sigmoid dose–response curves through GraphPad Prism software (vers. 5.01). Data are means ± s.e.m. of three independent measurements. At least five-to-seven different concentrations of each compound were used to determine IC_{50} values.

Most of the R-enantiomers achieved a low-to-moderate inhibition over *ee*AChE and a weak activity against *hs*BChE, except for derivative (*R*)-**30a**, which returned as the most interesting *ee*AChE inhibitor, thus showing activity in the submicromolar range of concentrations (IC_{50} = 0.215 μM). A better inhibition of BChE was

achieved by most of the *S*-enantiomers that also reported a weak AChE inhibition. The most active *S*-enantiomer as BChE inhibitor was compound (*S*)-**37g** (IC_{50} = 0.155 μM). Both enantiomers of the 3-nitrophenoxy ethers (compounds **34e** and **35e**) appeared as selective inhibitors of AChE. The *N*-benzyl derivative (*R*)-**34e** (IC_{50} = 1.3 μM) was six times more active than the corresponding *S*-isomer. Whilst the replacement of the phenyl ring by a naphthyl reversed the pattern of stereoselectivity, thus showing derivative (*S*)-**35e** a significant higher activity than (*R*)-**35**, and it was only two times less active than (*R*)-**34e**. By focusing on the sesamol fragment containing ethers **28a**–**30a**, the *R*-stereoisomers were found promising inhibitors of AChE, unlike their *S*-congeners. The activity profile of **28a**–**30a** was deeply affected by the lipophilicity of substituents on the pyrrolidine nitrogen, expressed as Log *D* values at the pH of assay conditions, by following the ranking Bn < 2-F-Bn < naphthylmethyl. The 2-F-benzyl derivative (*R*)-**29a** was three times more active than the unsubstituted congener (*R*)-**28a**. Most of all, the introduction of a naphthalene moiety achieved a significant increase of anti-AChE activity, being (*R*)-**30a** the most active AChE inhibitor of the series. Only both *R*- and *S*-isomers of the *N*-benzyl derivative **28a** also showed a moderate BChE inhibition, thus identifying them as dual acting inhibitors of cholinesterases. Compound (*S*)-**28a** showed a BChE inhibition two times higher than (*R*)-**28a**.

The methoxy derivatives **31b** and **32c**, designed as open analogues of the sesamol-containing derivatives, were found to be significantly less active than (*R*)-**30a** in the inhibition of AChE. Both enantiomers of compound **31b** showed a moderate BChE inhibition, without any significant difference between (*R*)-**31b** (IC_{50} = 2.03 μM) and (*S*)-**31b** (IC_{50} = 1.70 μM). The introduction of a second methoxy substituent in **32c** made a relevant lower BChE inhibition. Surprisingly, compounds (*R*)-**36f** and (*S*)-**36f** obtained by maintaining the naphthylmethyl substituent on pyrrolidine and substituting sesamol by a coumarin fragment, proved both a quite similar moderate anti-AChE potency. The enantiomer (*S*)-**36f** also showed BChE inhibition in the submicromolar range of concentration.

AChE and BChE share about 70% of sequence homology. The active site of both enzymes is a deep and narrow gorge, containing the high conserved catalytic triad, the so-called oxyanion hole stabilizing the transient tetrahedral enzyme-substrate complex, the acyl binding pocket (ABP), and the choline binding site at the bottom of the gorge. Finally, the peripheral active site (PAS) is located on the rim of the

active site gorge. Two aromatic residues in the ABP, and six of the aromatic residues lining the AChE gorge rim and PAS of AChE are replaced by aliphatic residues in BChE, thus resulting the BChE cavity larger than AChE gorge, and able to recognize hindered groups (Figure 51). On this basis, it can be explained that employing a 4-phenyl substituted coumarin group in compounds **37g** the most interesting inhibitors of BChE in the series were obtained. Furthermore, the stereochemistry significantly affected the activity profile, by showing the enantiomer (*S*)-**37g** (IC_{50} = 0.155 μM) a BChE inhibition four times higher than the corresponding (*R*)-**37g** (IC_{50} = 0.64 μM) isomer.

The inhibition mechanism of the most interesting compound (*R*)-**30a** against AChE, and (*R*)-**37g** against BChE, respectively, was further studied. The Lineweaver-Burk curves were derived by varying the substrates concentrations (ranging from 25 to 300 μM for AChE, and from 25 to 500 μM for BChE), in the absence or presence of inhibitor at different concentrations. The binding study revealed a change in both V_{max} and K_m values, as a trend that is generally ascribed to mixed-type inhibition.

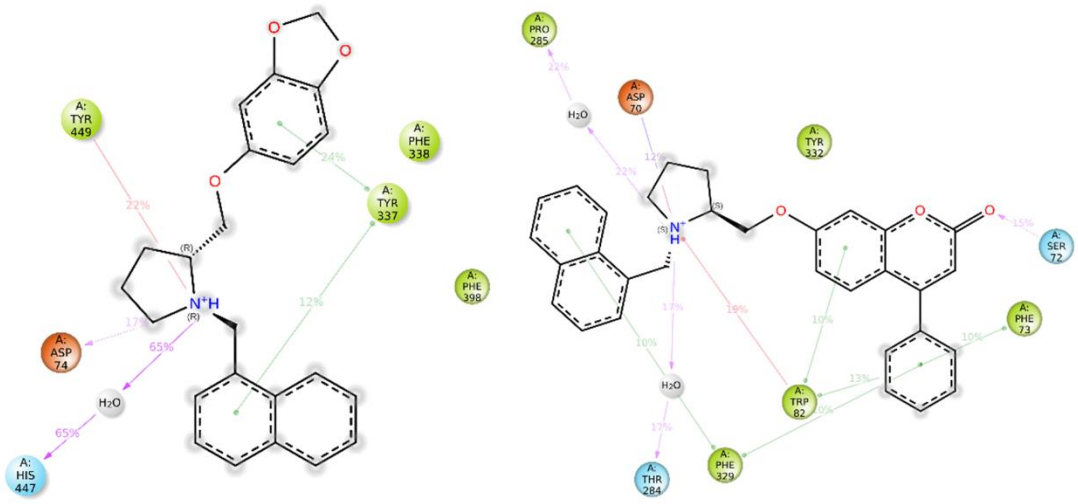

Figure 51. *Simulation interactions diagrams for (R)-30**a** (left) and (S)-**37g** (right) with AChE and BChE binding sites, respectively. The minimum contact strengths shown are at least 10% of trajectories length from 200 to 2200 ns.*

Additional research on the activities of human FAAH enzymes and their antioxidant effects in the DCFH-DA assay on HepG2 and SHSY-5Y cell lines was conducted by other research groups and reported in the article. Overall, twenty novel pyrrolidine containing derivatives resulted as innovative molecular entities with a promising framework for targeting and inhibiting cholinesterases, in conjunction with other critical molecular targets implicated in neurodegenerative diseases.

5.3 Assessing the role of a malonamide linker in the design of potent dual inhibitors of blood coagulation factor Xa and cholinesterases

In this study, we focused on identifying new selective inhibitors of factor Xa (fXa), with the potential to also target other serine proteases involved in neurodegenerative diseases, specifically cholinesterases (ChEs). Due to fXa's role in the coagulation cascade, selective inhibitors of fXa are viewed as effective treatments for venous thromboembolism and as a preventive measure for strokes in patients with atrial fibrillation. Inhibitors of fXa prevent the generation of new thrombin without affecting the baseline levels of thrombin, thereby ensuring primary hemostasis..[97,98] Compared to the classical antithrombotic drugs (heparins and warfarin), and direct thrombin inhibitors, fXa selective inhibitors should be characterized by lower bleeding risks.

Malonamide derivatives (MAMDs) are privileged chemical structures in drug design, widely employed to obtain peptidomimetic and chelating compounds.[99] MAMDs occur in many natural products and pharmaceuticals[100], and have been exploited to identify antidiabetics, k-opioid receptor agonists, and anticancer agents. The malonamide bridge can be considered similar to the glycine residue in which one of the peptide bonds has been inverted.[101] Such a reversed amide link contributes toward maintaining chemical properties, stereochemical features, and binding modes similar to those of the parent peptide; these isomeric forms can however explore diverse conformational spaces.[102] Moreover, the amide retro-inversion can affect both pharmacodynamic and pharmacokinetic profiles, leading (in most cases) to an increase in target selectivity, a reduction in off-target undesired activities, and enhanced proteolytic resistance to proteases and CYP (cytochrome P)-mediated metabolism. The crossing of BBB, due to the change in the polar surface area, has also been reported. MAMDs can be considered as retro-inverted analogues of the tripeptide sequence Phe-Gly-Arg recognized by fXa. Herein, we focused on the synthesis and activity of new compounds built on the malonamide bridge as the molecular core, linking a benzamidine as an arginine-mimetic moiety (P1 moiety) and varying the aromatic/lipophilic P4 fragments. The newly

synthesized compounds were firstly assayed as fXa/thr inhibitors and compared with the corresponding glycinamide analogues (Figure 52).

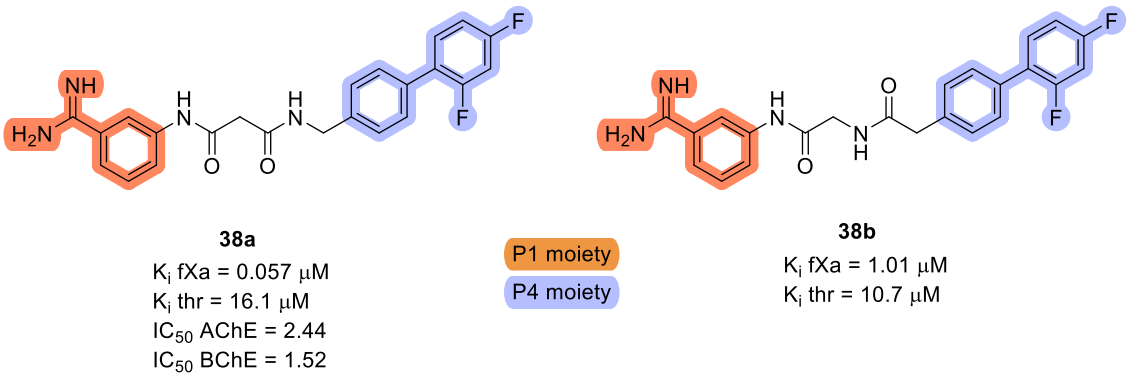

Figure 52. *Chemical structures of representative malonamide and glycinamide derivatives* ***38a-b****. The benzamidine moiety P1 and the aromatic/lipophilic moiety P4 are highlighted in orange and violet respectively.* K_i *were values determined by applying the Cheng–Prousoff equation to* IC_{50} *values, by regression (GraphPad Prism software ver. 5.01). Electric eel acetylcholinesterase and horse serum butyrylcholinesterase were tested as the target enzymes. Data are means of three independent measurements, performed in triplicate (SEM < 5%).*

The malonamide linker resulted in significantly increase in the potency and selectivity of the inhibitors compared to the glycinamide linker. Data on the inhibition constants (K_i) for various compounds are presented in the article, some of them achieving low nanomolar inhibition against fXa and single-digit micromolar activity against ChEs. In our SAR study, we indicate that the malonamide linker contributes positively to the overall inhibitory activity compared to the glycinamide linker. The experimental data resulting from the inhibition assays were supported by molecular docking studies, which were performed to visualize the binding interactions between the malonamide derivatives and their target enzymes. The docking results provide insights into the binding modes and interactions, such as hydrogen bonds and hydrophobic contacts, that contribute to the observed inhibitory activities (Figure 53).

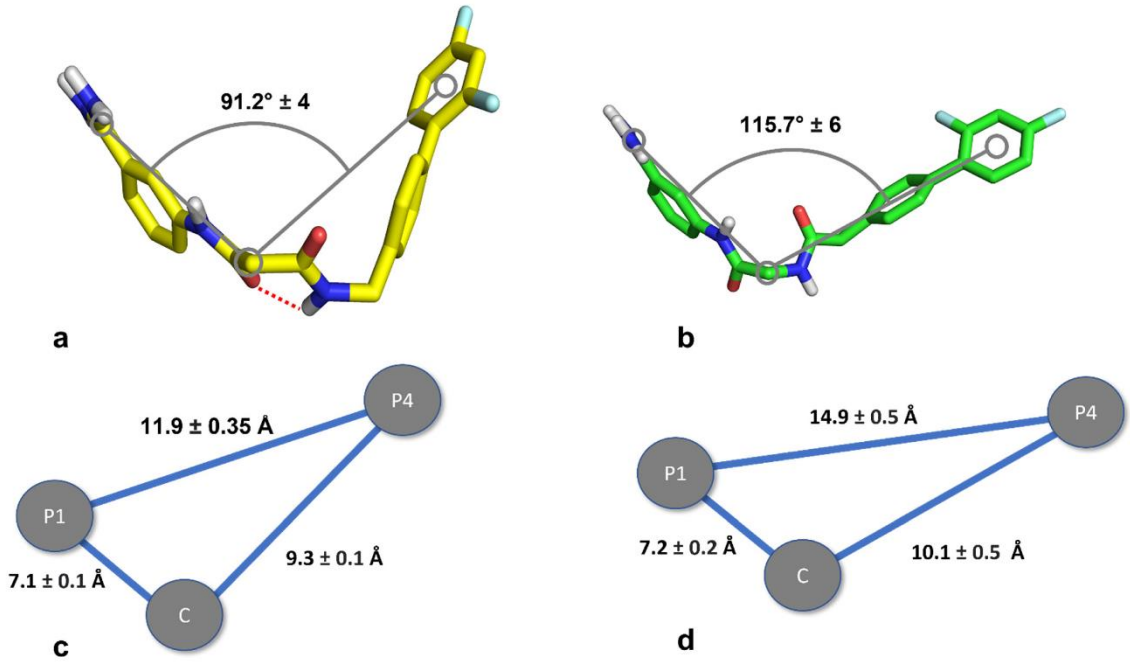

Figure 53. *Panels (a,b) show the best conformer of compound* ***38a*** *and* ***38b*** *depicted as yellow and green sticks, respectively. The intramolecular hydrogen bond is shown as dashed red lines. Joined by gray lines, the three gray circles indicate the anchoring point of the amidine group (P1), the center of malonamide/glycinamide bridge (C), and the centroid of the terminal phenyl of the P4 group. Panels (c,d) report the distances and the standard deviation among P1-C-P4 for both compounds.*

Overall, the structural characteristics of the malonamide derivatives allowed for better conformational flexibility and binding interactions with the target enzymes. The malonamide linker may facilitate a more favorable orientation of the active moieties within the binding sites of fXa and ChEs, leading to increased inhibitory activity.

5.4 Pleiotropic Effects of Direct Oral Anticoagulants

In this study we outlined several important findings regarding the effects of direct oral anticoagulants (DOACs) in patients with chronic heart failure (HF) and atrial fibrillation (AF), and in particular the pleiotropic effect of DOACs, which proved to be beneficial beyond their primary role in anticoagulation. They exhibit anti-inflammatory, antioxidant, and anti-fibrotic effects on endothelial cells, which improve endothelial function and integrity. We demonstrated, through the implementation of machine learning analysis, the positive impact of DOACs on cardiac remodeling and inflammatory biomarkers. Switching from vitamin K antagonists (VKAs) to DOACs (Figure 54) was associated with better clinical outcomes in patients with AF and HF. Specifically, DOACs were linked to reduced mortality rates and improved overall health status in these patients. We also found that transitioning to DOACs resulted in enhanced endothelial function and a

decrease in inflammatory markers, such as C-Reactive Protein levels, particularly in patients with heart failure with reduced ejection fraction (HFrEF). Compared to warfarin, DOACs demonstrated a superior safety and efficacy profile, characterized by fewer drug interactions, no need for routine monitoring, and a lower risk of bleeding. Overall, the findings suggest that DOACs not only serve their anticoagulant purpose but also significantly contribute to the management of chronic heart failure in patients with atrial fibrillation.

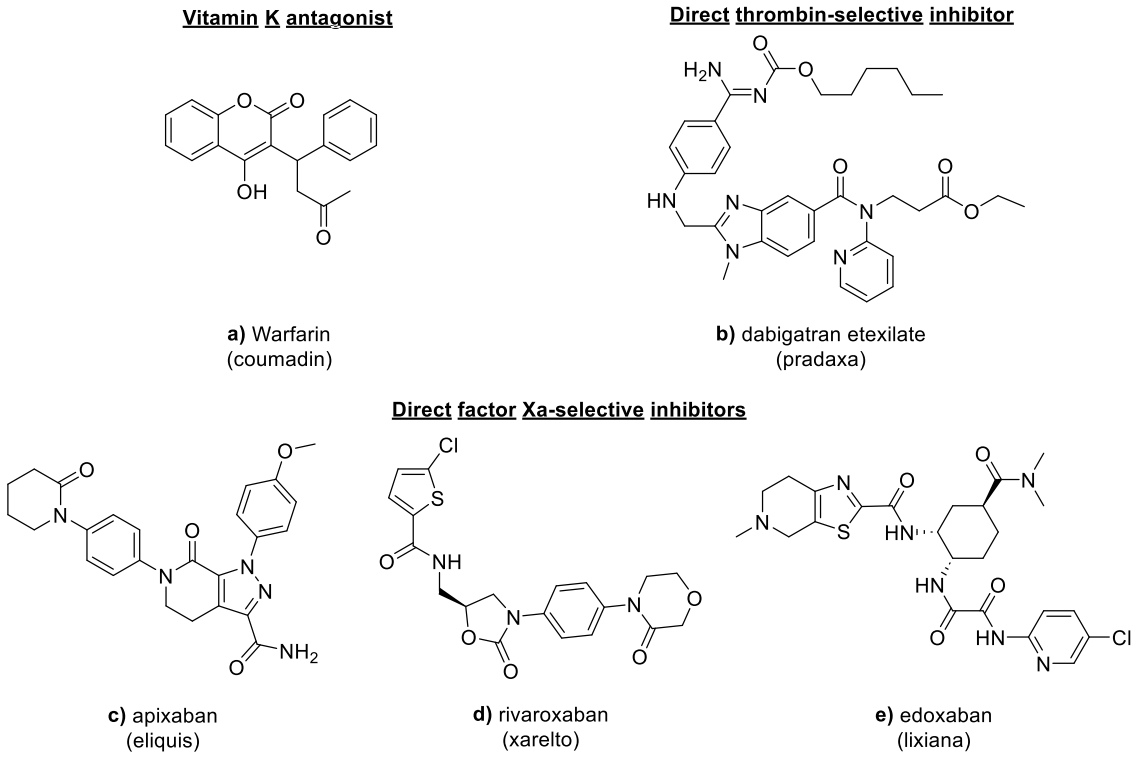

Figure 54. *The structures of the oral anticoagulants investigated in this study. Warfarin (a) is a vitamin K antagonist used as a racemic mixture of S- and R-enantiomers. Among the new oral anticoagulants (b, c, d, e), dabigatran etexilate (b) is a prodrug converted by esterase-catalyzed hydrolysis to dabigatran, a direct thrombin inhibitor; apixaban (c), rivaroxaban (d) and edoxaban (e), are direct factor Xa inhibitors.*

6 CONCLUSIONS

We have identified novel chemotypes derived from the THAI, HHAI and THPI scaffolds, as selective modulators for GPR55 and GPR18 with additional inhibitory activity on BChE.

In particular, THAI derivatives exhibited antagonistic activity in the micromolar range at GPR55, with the most potent compounds being **5h** (NB360, IC_{50} = 4.76 μM) and **5e** (RP308, IC_{50} = 4.40 μM); *N*2-ethyl carboxylate THPIs also showed weak antagonistic activity at GPR55 (**21d**, FS962C-1F, IC_{50} = 8.13 μM) confirming the importance of the carbonyl function for the recognition by the receptor. HHAI and THPI derivatives exhibited antagonistic or inverse agonistic activity in the micromolar range at GPR18, with the most potent compounds being **6a** (NB560, IC_{50} = 0.701 μM), **22a** (NB543-B, IC_{50} = 0.753 μM) and **22e** (NB555-B. IC_{50} = 0.753 μM, see Figure 55).

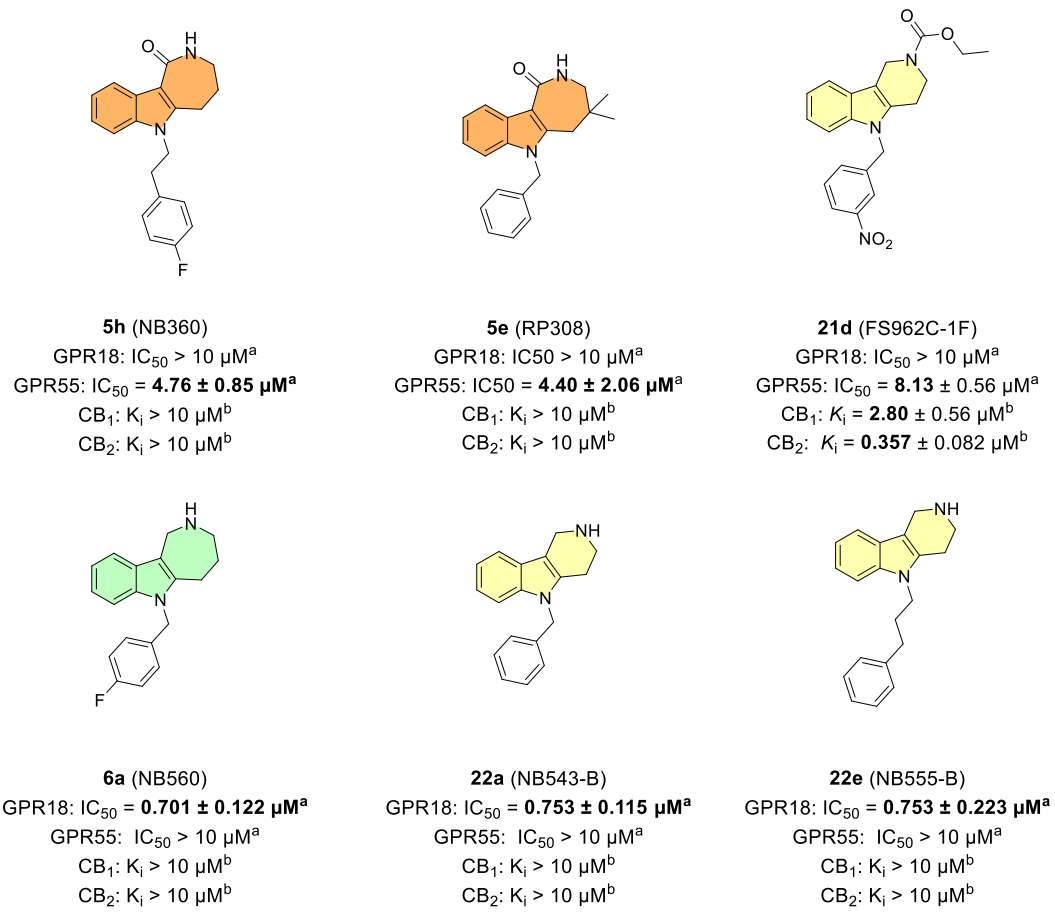

Figure 55. *Chemical structures and activities of heterotricyclic indole-fused modulators of GPR55 and GPR18. The different heterotricyclic heads have been highlighted in orange (THAI), green (HHAI) and yellow (THPI).* [a]*β- arrestin assay;* [b]*radioligand binding assay.*

Design, synthesis, radioligand binding and functional assays, kinetics of enzyme inhibition, and molecular modeling studies, allowed us to trace the structure-

activity relationships of these classes of compounds, assess their selectivity for cannabinoid (CB) and CB-like receptors, and choose one candidate for *in vivo* pharmacological testing.

We successfully identified MTDLs that target BChE and human GPR18/GPR55, demonstrating comparable inhibition potencies, as illustrated in Figure 56. This may hold promise for reversing cognitive impairment associated with neurodegenerative diseases.

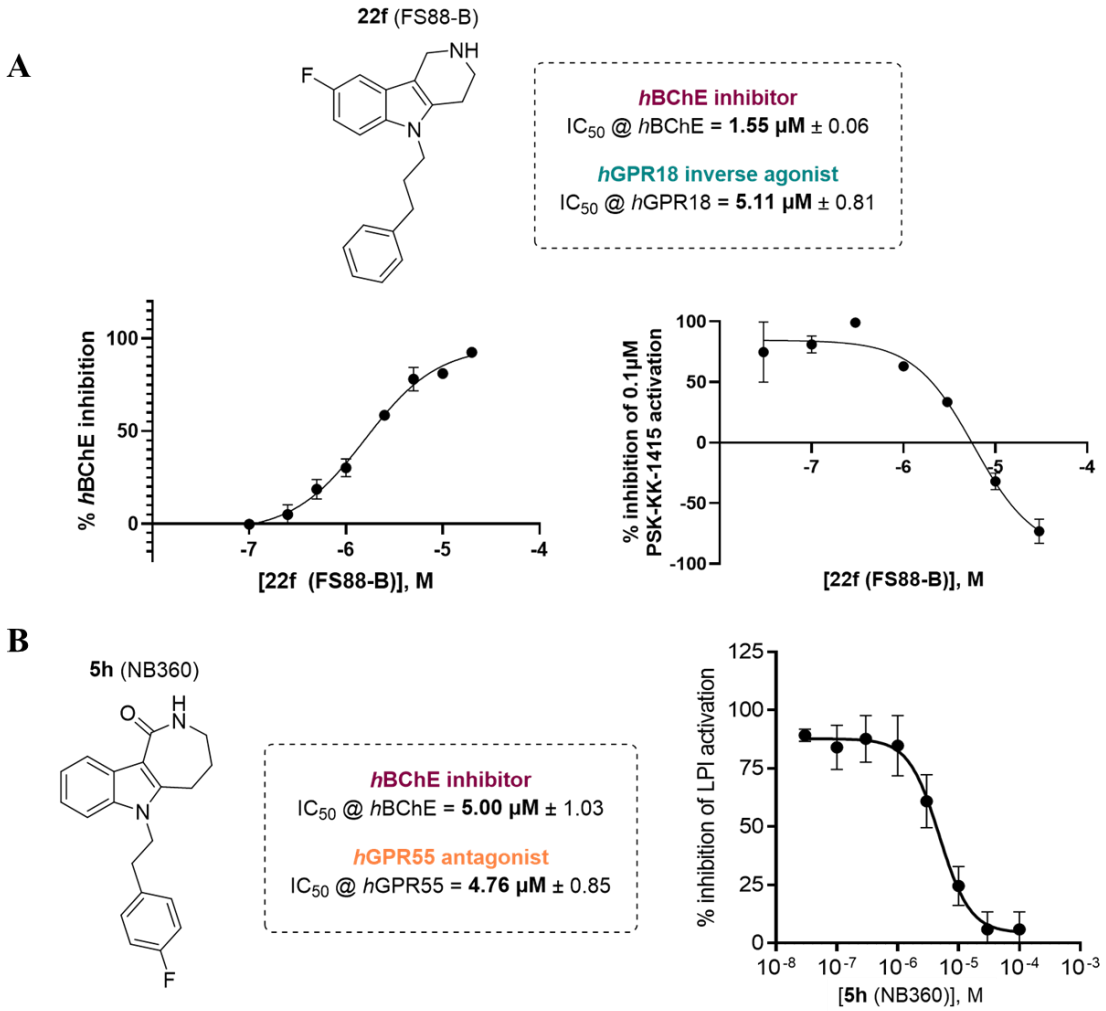

Figure 56. *MTDL candidates acting on BChE and GPR18/55 with comparable potencies at both targets. A) Compound* ***22f*** *acts as dual BChE inhibitor/GPR18 inverse agonists. B) Compound* ***5h*** *acts as dual BChE inhibitor/GPR55 antagonist. Chemical structures, concentration-response curves, and* IC_{50} *values for each compound are reported.*

Among the compounds examined, we have discerned certain structural features that enhance their activity towards cannabinoid (CB) receptors, such as the presence of bulky lipophilic substituents on the tricyclic head (compounds **20d**, **21d** and **22g-i**), as well as towards butyrylcholinesterase (BChE), such as long side chains on the indole nitrogen. Our findings motivated us to synthesize a series of 6-alkyl-bridged

4-arylalkylpiperazin-1-yl derivatives of THAI. Among them, compounds **26a** and **26b** exhibited *h*BChE-selective inhibition in the nanomolar range of concentration (*h*BChE IC_{50} = 190 nM and 72 nM, respectively, Figure 45).

Our research has clarified some pharmacological aspects related to the modulation of GPR18 and GPR55 relatively to their *β*-arrestin recruitment signaling pathways. While functional characterization can be considered completed for GPR18, being the *β*-arrestin recruitment signaling pathway the only scientifically accepted and approved transduction pathway for this receptor, despite some discordant data probably originated from the lack of selective ligands, the functional profile of GPR55 should be further investigated, being instead capable of coupling to different transducing proteins, including G_{13}, G_q and *β*-arrestins.

Although the compounds examined exhibit micromolar potent modulation of the two GPCRs under investigation, their activity and efficacy constitute a peculiarity of this work. Notably, to the best of our knowledge, we have discovered the first full inverse agonists of GPR18 documented to date (see **22f**, **22g**, Table 11), which might allow pharmacologists to gain some valuable insight into the physiological role of this receptor and the effects of its constitutive activity. Moreover, the dual GPR/CBR activity of THPI derivatives (**20d**, **21d, 22g-i**) described in sections 4.3 and 4.4 could position these compounds as pharmacological tools for exploring biochemical cross-talks in GPR/CBR heteromers.

In vivo studies to assess the whole-body distribution in healthy mice and brain penetration through positron emission tomography imaging, validated our compounds as CNS-directed agents due to their ability to cross BBB.

We expect that the results of this work, along with findings from other collaborative projects presented here, will help clarify the complex dynamics involved in neurodegeneration. This could pave the way for studies aimed at validating GPR18 and GPR55 as potential drug targets, as well as establishing multi-target drug design as a reliable strategy to address the multifaceted nature of most neurological disorders.

7 ANNEX

7.1 Advances in synthesis of novel benzazecines and their unique pharmacological properties

Benzazecines, mostly as partially saturated benzo[*d*]azecine and dibenzo[*c*,*g*]azecine fusion isomers, constitute a unique class of alkaloids and nature-inspired azaheterocyclic compounds, with interesting reactivity, physicochemical and biological properties. Due to difficulties associated with the construction of the scaffold they are often not the focus of organic and medicinal chemists' attention. At the same time, it is worth noting the range of their pharmacological activities and their practical application. We reviewed[90] the synthetic methodologies of benzazecine derivatives known up to date and reported about the progress in disclosing their potential in drug discovery. Indeed, their conformational restriction or liberation drives their selectivity towards diverse biological targets, making them versatile scaffolds or building blocks for developing drugs, including antipsychotic and anticancer drugs, but also potential agents for anti-neurodegenerative treatments, as the recent literature shows (Figure 57).

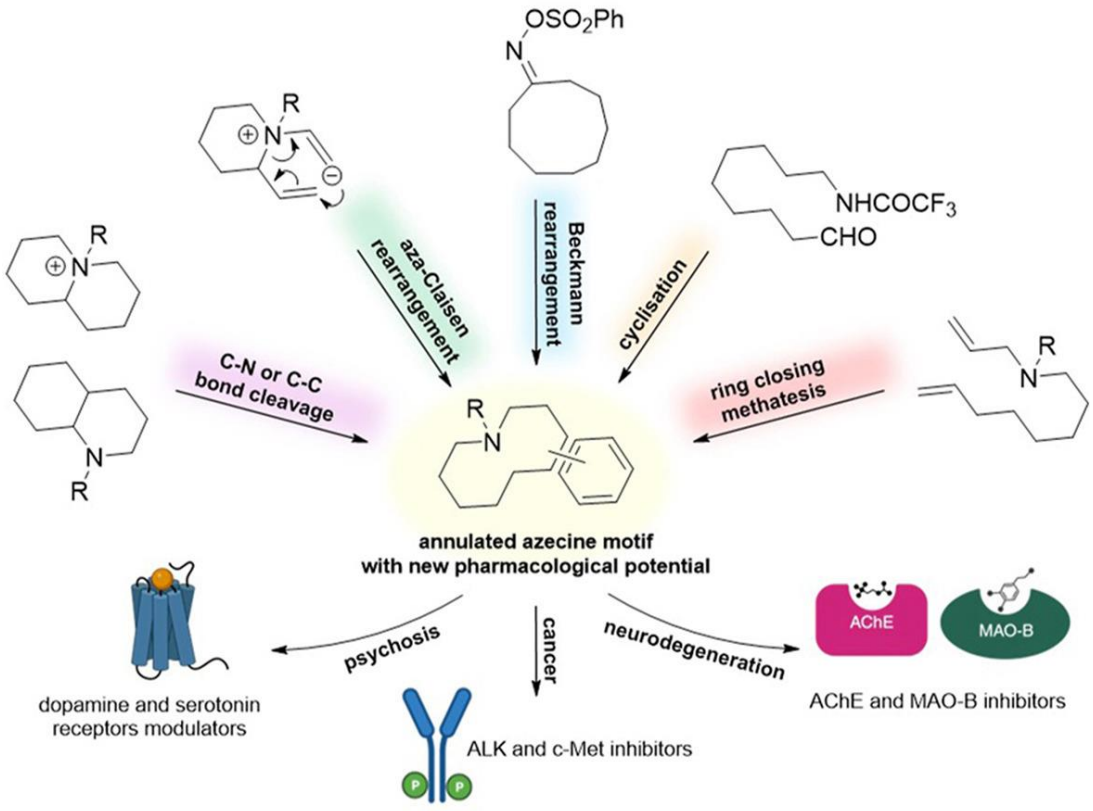

Figure 57. *Graphical abstract of the published review[90] illustrating the different synthetic strategies to obtain the azecine motif and its pharmacologic potential at different biological targets such as dopamine, serotonine and tyrosin kinase receptors, and acetylcholinesterase (AChE) and mono-amino oxidase B (MAO-B) enzymes.*

The benzo[*d*]azecine scaffold is notable for its involvement in compounds that engage with multiple biological targets, including dopamine and serotonin receptors, acetylcholinesterase (AChE), monoamine oxidase B (MAO-B), tyrosine kinase receptors, and P-glycoproteins (P-gp). This interaction suggests their pharmacological potential is linked to antipsychotic effects, anticancer properties, and applications in neurodegenerative diseases. The article also explores various synthetic methods for producing azecine derivatives, ranging from ring-closing metathesis to aza-Claisen rearrangements.

A very interesting example is represented by compound LE300 in Figure 58, a molecule designed and synthesized by Lehman *et al.*[103] to incorporate the structures of 5-hydroxytryptamine (5-HT) and β-phenylethylamine (DA) in order to target with a single molecule both 5-HT and DA receptors. In fact, mixed D_2/5-HT_{2A} receptor antagonists (like risperidone and clozapine) lead to the so-called 'atypical neuroleptics', more effective than the traditional neuroleptics in treating the symptoms of psychoses and causing less extra-pyramidal side effects.

As a result of the merge strategy, LE300 proved to be a potent D_1 antagonist and a moderate D_2 and 5-HT_{2A} antagonist whereas, the more conformationally restricted quinolizidine was devoid of any activity. Surprisingly, the conformational liberation, that derives from the cleavage of the carbon-nitrogen bond, disclosed the potential of the resulting 7-methyl-6,7,8,9,14,15-hexahydro-5*H*-benzo[7,8]azecino[5,4-*b*]indole to act as dopaminergic and serotoninergic receptor ligands (K_i = 0.08 nM *vs* D_1 receptor, 6.0 nM *vs* D_2 receptor, 20.0 nM *vs* 5-HT_{2A} receptor). It is noteworthy that, unlike the many cases in which conformation restriction increases the potency of a ligand by stabilizing a favorable binding conformation and reducing the entropic penalty on binding to the target[104–106], in this case a conformational liberation proved to be beneficial.

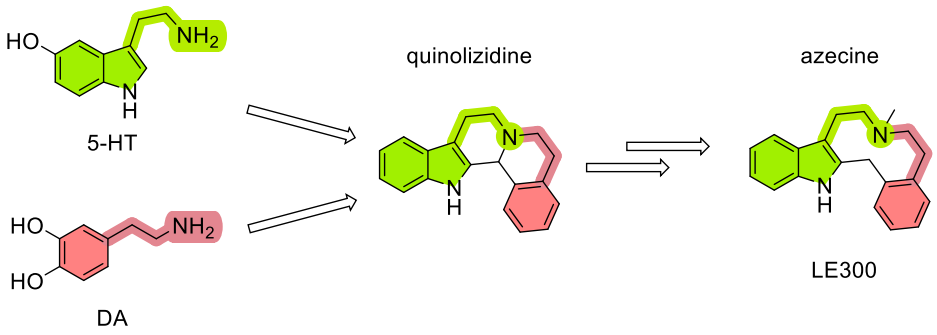

Figure 58. *The conformational liberation that derives from the C-N bond cleavage of quinolizidines is responsible for the pharmacological activity of the azecine LE300 compound as dopaminergic and serotoninergic antagonist.*

7.2 Small Molecules for the Treatment of Long- COVID-Related Vascular Damage and Abnormal Blood Clotting: A Patent-Based Appraisal

Individuals affected by COVID-19 are at risk for abnormal clotting and endothelial dysfunction, which can lead to complications such as deep vein thrombosis, cerebrovascular disorders, and both ischemic and non-ischemic heart diseases. Treatments for COVID-19 include antiplatelet agents (such as aspirin and clopidogrel) and anticoagulants; however, their effects on morbidity and mortality have not been conclusively established. Furthermore, due to the interconnected prothrombotic and proinflammatory events associated with viremia, the use of anti-inflammatory drugs has also been explored to alleviate immune dysregulation caused by the cytokine storm. By reviewing patent literature, small molecules that have been patented for addressing long-COVID-related blood clotting and hematological complications have been evaluated, along with supporting evidence from both preclinical and clinical studies.

In the context of COVID-related cardiovascular issues, we identified recently patented compounds used for the treatment of cardiovascular complications associated with long-term COVID, namely natural or nature-inspired polyphenolic compounds, ramatroban, a dual antagonist of prostaglandin D2 (PGD2/DPr2) and thromboxane A2/TPr receptors[107,108], procyanidins[109,110], NHE-1 inhibitors[111], and caspase inhibitors.[112] Table 23 summarizes the aforementioned compounds, with their target(s)/mechanism(s) of action, the phase of clinical trials or preclinical investigation.

Table 23. *Summary of small molecules studied as potential treatments of long-COVID-associated vasculopathies and blood clotting abnormalities, along with information on the mechanisms of action and the state of clinical investigation.*

Molecules	Target(s)/Mechanism(s) of Action[a]	Phase of Clinical or Preclinical Investigation
Ramatroban	DPr2 and TPr receptor antagonist	Phase 2/3
Emricasan	Pan-caspase inhibitor	Phase 1 (terminated)
Pycnogenol®	Antioxidant, eNOS	Phase 3
Rimeporide	NHE-1 inhibitors	Preclinical investigation

[a] DPr2: Prostaglandin D2 receptor; TPr: Thromboxane receptor; eNOS: Endothelial nitric oxide synthase; NHE-1: Sodium–Hydrogen Exchanger 1.

During SARS-CoV-2 infection, cyclooxygenase enzymes (COXs), particularly COX-2, are upregulated, leading to increased expression and release of lipid mediators. A lipidomic analysis of bronchoalveolar lavages (BALs) from healthy controls and COVID-19 patients revealed a "lipid mediator storm" in infected patients, characterized by elevated levels of prostaglandins and thromboxane. Among the most increased COX metabolite there were thromboxane B (2TXB2, the stable metabolite of TXA2), and prostaglandin D2 (PGD2).[113,114]

PGD2 interacts with the DP2 receptor, causing bronchoconstriction and inflammation, while TXA2 has prothrombotic properties, affecting platelets and endothelial cells. Ramatroban, a dual DP2/TrP antagonist, emerged as the most interesting agent, as it blocks the harmful effects of both PGD2 and TXA2. It has shown promise in treating COVID-19 by providing rapid symptom relief and is currently being evaluated in a phase-2/phase-3 clinical trial for its efficacy and safety in hospitalized COVID-19 patients (Figure 59).

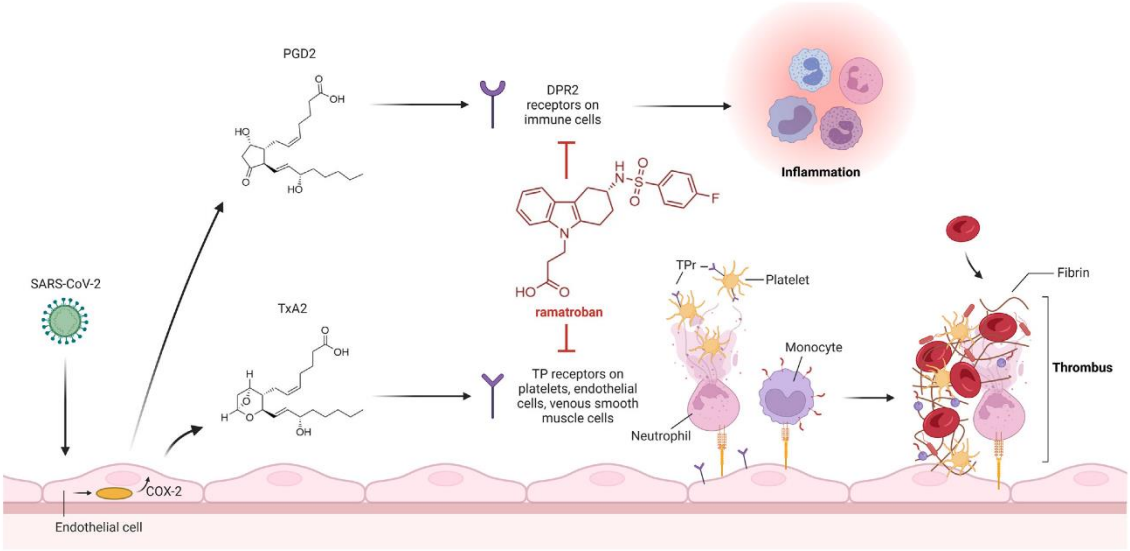

Figure 59. *Schematic representation of the mechanism of action of ramatroban, a dual prostaglandin D2 receptor (DPr2) and thromboxane A2 receptor (TPr) antagonist in clinical trials for thromboinflammatory dysregulation in acute and long COVID-19.*

8 LIST OF ABBREVIATIONS

2-AG	2-arachidonoylglycerol
2-AG-PI	2-arachidonoylphoyphatidylinositol
5-HT	5-hydroxy-tryptamine, serotonine
AA-5-HT	arachidonoylserotonine
AAIs	aminoalkylindoles
Abn-CBD	abnormal cannabidiol
ACh	acetylcholine
AChE	acetylcholinesterase
AD	Alzheimer's disease
AEA	anandamide, arachidonoylethanolamine
BSA	bovine serum albumin
BChE	butyrylcholinesterase
cAMP	cyclic adenosine monophosphate
CAS	catalytic anionic site
CB	cannabinoid
CB_1 receptor	cannabinoid receptor type 1
CB_2 receptor	cannabinoid receptor type 2
CBD	cannabidiol
CB receptor	cannabinoid receptor
CHO	cells chinese hamster ovary cells
CNS	central nervous system
Compd.	compound
DAG	diacylglycerol
DAGL	diacylglycerol lipase
DCM	dichloromethane

DMEM	Dulbecco's Modified Eagle's Medium
DMSO	dimethylsulfoxide
EC_{50}	half maximal activatory concentration
ECL	extracellular loop
EMCDDA	European Monitoring Centre for Drugs and Drug Addiction
ERK	extracellular singal-regulated kinase
ESI	electronspray ionization
EUDA	European Union Drugs Agency
FAAH	fatty acid amide hydrolase
FBS	fetal bovine serum
FRET	Förster-resonance energy transfer
GABA	γ-aminobutyric acid
GPCR	G protein-coupled receptor
GDP	guanosine diphosphate
GTP	guanosine triphosphate
GTPγS	guanosine 5'-O-[γ-thio]triphosphate
HHAI	1,2,3,4,5,6-hexahydroazepino[4,3-*b*]indole
HB	hydrogen bond
HD	Huntington's disease
HepG2	human hepatocellular carcinoma cell line
HEK293	human embryonic kidney cell line
HEPES	(4-(2-Hydroxyethyl)-1-piperazineethanesulfonic acid
HPLC	high performance liquid chromatography
HTS	high throughput screening

IBD	inflammatory bowel disease
IC_{50}	half-maximal inhibitory concentration
ICL	intracellular loop
IP3	inositoltriphosphate
IUPHAR	International Union of Basic and Clinical Pharmacology
$LiAlH_4$	Lithium Aluminum Hydride
LPI	lysophosphatidylinositol
LPS	lipopolysaccharide
MAGL	monoacylglycerol lipase
MS	multiple sclerosis
MTDL	multi target-directed ligand
NAGly	N-arachidonoylglycine
NAPE	N-acyl phosphatidylethanolamine
NFAT	nuclear factor of activated T-cells
NFκB	nuclear factor kappa-light-chain-enhancer of activated B-cells
NMDA-receptor	N-methyl-D-aspartate receptor, a glutamate receptor
NMR	nuclear magnetic resonance spectroscopy
NOS	nitric oxide synthase
PAS	peripheral anionic site
PB	phosphate Buffer
PBS	phosphate Buffered Saline
PDB	protein data bank
PPARγ	receptor peroxisome proliferator-activated receptor gamma

QSAR	quantitative structure-activity relationships
RLU	relative luminescence units
RMSD	root mean square deviation
SAR	structure-activity relationships
TAE	buffer Tris-acetate-EDTA buffer
TBAB	tetrabutyl ammonium bromide
TFA	trifluoro acetic acid
THAI	3,4,5,6-tetrahydroazepino[4,3-*b*]indol-1(2*H*)-one
THC or Δ^9-THC	Δ^9-tetrahydrocannabinol
THPI	2,3,4,5-tetrahydro-1*H*-pyrido[4,3-*b*]indole
TM	transmembrane
tPSA	total polar surface area
Tris	tris(hydroxymethyl)-aminomethane
TRPA	transient receptor potential cation channels
TRPV subfamily V (“Vanilloid”)	transient receptor potential cation channels

9 EXPERIMENTAL SECTION

9.1 Chemistry

Starting materials, reagents, and solvents were used as purchased from Alfa Aesar, Sigma-Aldrich, or Fluorochem. The progress of the reactions was monitored by thin layer chromatography (TLC, Merck, 0,2 mm silica gel 60 F254). Column chromatography was performed on silica gel, 0.060−0.200 mm, pore diameter ca. 6 nm. ^{1} H and ^{13}C NMR data were collected either on a Varian-Mercury-VX 300 MHz, Bruker Avance 400 or 500 MHz NMR spectrometer or JEOL FT-NMR 500 at 500 MHz (^{1}H) or 126 MHz (^{13}C) or on a Bruker Ascend 600 MHz NMR spectrometer at 600 MHz (^{1}H) or 151 MHz (^{13}C). Chemical shifts are reported in parts per million in relation to the deuterated solvent: DMSO, δ (^{1}H) 2.50 ppm; δ (^{13}C) 39.52 ppm; CDCl3, δ (^{1}H) 7.26 ppm; δ (^{13}C) 77.16 ppm. Coupling constants *J* are given in Hertz (Hz), and spin multiplicities are given as singlet (s), doublet (d), doublet of doublet (dd), triplet (t), quartet (q), multiplet (m), and broad signal (br). The purities of isolated final products were determined by HPLC coupled to a diode array detector (DAD) measuring UV absorption from 200 to 950 nm, and electrospray ionization (ESI) mass spectrometer (Applied Biosystems API 2000 LC-MS/MS, HPLC Agilent 1100) using a Phenomenex Luna 3 μ C18 column (50 × 2.00 mm) (HPLC UV/ESI-MS) or were assessed by elemental analyses (C, H, N), performed on Euro EA3000 analyzer (Eurovector, Milan, Italy) by the Analytical Laboratory Service of the Department of Pharmacy-Drug Sciences of the University of Bari (Italy), and the results agreed to within ±0.40% of theoretical values. The compounds were dissolved at a concentration of 1.0 mg/mL in acetonitrile containing 2 mM ammonium acetate. Then, 10 μL of the sample was injected into an HPLC column, and elution was performed with a gradient of water/acetonitrile (containing 2 mM ammonium acetate) from 90:10 to 0:100 for 20 min at a flow rate of 300 μL/min, starting the gradient after 10 min. The purity of the compounds was in almost all cases >95%, unless otherwise noted. The high-resolution molecular masses of test compounds were assessed by Agilent 6530 Accurate Mass Q-TOF (Agilent Technologies Italia S.p.A., Cernusco sul Naviglio, Milan, Italy). IR spectra were recorded via KBr disks on a Perkin-Elmer Spectrum One Fourier transform infrared spectrophotometer (Perkin-Elmer Ltd., Buckinghamshire, U.K.), and the most significant absorption bands are listed. Compounds **2a-b**, **3a-b**, **4a-b**, **5a**, **5f-k**, **5m-n**, **7a-c**, **26a-b** have been described and published elsewhere.[4,76]

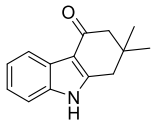

Compound **2c**. *Synthesis of 2,2-dimethyl-1,2,3,9-tetrahydro-4H-carbazol-4-one. (NB534)*

1.43 mL of phenylhydrazine (14.5 mmol) and 2 g of 3,3-dimethylcyclohexan-1-one were added (14 mmol) in 10 mL of H_2O and 20mL of MeOH. This mixture was left stiirring for 4 hours at room temperature until the formation of precipitate. After, the precipitate was filtered and washed with hot water. The hydrazone formed was used without further purification. 2 mmol of the hydrazone were treated with 3ml TFA at reflux for one day. The excess of TFA was removed with argon and the mixture was washed with water. The water was decanted, and the precipitate was washed with saturated solution of sodium carbonate to obtain brown-green precipitate that was filtered off (317 mg = 1.49 mmol). Yield: 74% crude. ^{1}H NMR (300 MHz, $CDCl_3$) δ 9.00 (s, 1H, NH), 8.17 (dd, J = 6.1, 2.8 Hz, 1H), 7.37 (dd, J = 6.3, 2.8 Hz, 1H), 7.25 – 7.17 (m, 2H), 2.82 (s, 2H), 2.47 (s, 2H), 1.14 (s, 6H, $(CH_3)_2$).

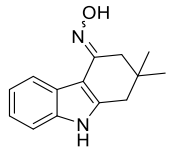

Compound **3c**. *Synthesis of 2,2-dimethyl-1,2,3,9-tetrahydro-4H-carbazol-4-one oxime. (NB535)*

A mixture of NB534 (0.5 mmol), $NH_2OH{\cdot}HCl$ (1.5 mmol), NaOAc (1.5 mmol), in 7.5 mL of a solution of EtOH/H_2O (2:1, v/v), was refluxed in argon atmosphere for 1 day. After TLC control the reaction was cooled at room temperature and the solvent evaporated under vacuum. The residue was taken up with water, sonicated, filtered and dried (79 mg = 0.35 mmol). The product was purified by chromatography on silica gel (Hex/EtOAc, 7:3) to obtain 50 mg of pure product. YIELD : 44% ^{1}H NMR (500 MHz, DMSO) δ 11.15 (s, 1H, NOH), 10.23 (s, 1H, NH), 7.83 (d, J = 7.7 Hz, 1H), 7.28 (d, J = 7.7 Hz, 1H), 7.04 (t, J = 7.5 Hz, 1H), 6.99 (t, J = 7.4 Hz, 1H), 2.64 (s, 2H), 2.52 (s, 2H), 1.02 (s, 6H, $(CH_3)_2$).

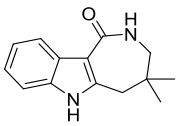

Compound **4c**. Synthesis of *4,4-dimethyl-3,4,5,6-tetrahydroazepino[4,3-b]indol-1(2H)-one. (NB536).*

50 mg (0.22 mmol) of oxime **3c** was added at PPA (1.5 g) and warmed at 150°C (oil bath at 165°C) for 30min. After cooling, the mixture was puored into ice and the solid formed was filtered off. The solid was treated with 2 ml of NaOH (2N) and 3mL of EtOH with stirring for 2 h. The organic layer was extracted with $CHCl_2$, dried and filtered. Solvent was removed under vacuum to obtain a brown product (50 mg). The product was purified with chromatographic column (EtOAc 100%) to obtain 20 mg (0.088 mmol) Yield : 40%. 1H NMR (500 MHz, cdcl3) δ 9.14 (s, 1H, NH ind), 8.18 (dd, J = 6.2, 2.9 Hz, 1H, H-7), 7.34 (dd, J = 6.1, 2.8 Hz, 1H), 7.20 (dd, J = 6.0, 3.2 Hz, 2H), 6.63 (s, 1H, CONH), 3.04 (d, J = 5.4 Hz, 2H, 3-CH_2), 2.79 (s, 2H,5-CH_2), 1.05 (s, 6H, 4-$(CH_3)_2$).

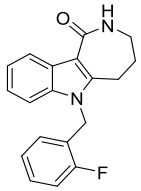

Compound **5b**. *Synthesis of 6-(2-fluorobenzyl)-3,4,5,6-tetrahydroazepino[4,3-b]indol-1(2H)-one. (RP271)*

^{1}H NMR (300 MHz, cdcl$_3$) δ 8.46 – 8.37 (m, 1H), 7.34 (m, 5H), 7.15 – 7.08 (t, 1H), 6.97 (t, *J* = 8.0 Hz, 1H), 6.49 (t, *J* = 7.7 Hz, 1H), 5.40 (s, 2H), 3.45 – 3.42 (t, 2H), 3.05 (t, *J* = 6.7 Hz, 2H), 2.23 – 2.15 (m, 2H).

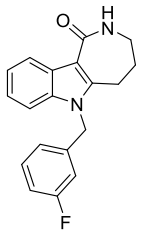

Compound **5c**. *Synthesis of 6-(3-fluorobenzyl)-3,4,5,6-tetrahydroazepino[4,3-b]indol-1(2H)-one. (RP272)*

^{1}H NMR (300 MHz, cdcl$_3$) δ 8.44–8.37 (m, 1H), 7.66 (s, 1H), 7.27 (m, 5H), 6.96 (m, 1H), 6.74–6.66 (m, 2H), 5.35 (s, 2H), 3.49–3.46 (m, 2H), 3.03 (t, *J* = 6.7 Hz, 2H), 2.23–2.15 (m, 2H).

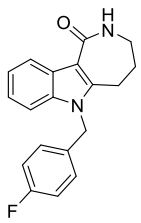

Compound **5d**. *Synthesis of 6-(4-fluorobenzyl)-3,4,5,6-tetrahydroazepino[4,3-b]indol-1(2H)-one. (RP276)*

^{1}H NMR (300 MHz, cdcl$_3$) δ 8.29 (s, *J* = 4.1 Hz, 1H), 7.35-7.33 (m, *J* = 9.1, 3.2 Hz, 3H), 7.03 – 6.95 (m, 5H), 5.37 (s, 2H), 3.60 (t, 2H), 3.08 (m, *J* = 14.4, 6.8 Hz, 2H), 2.26 (m, 2H).

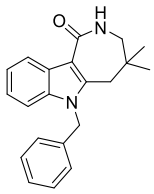

Compound **5e.** *Synthesis of 6-benzyl-4,4-dimethyl-3,4,5,6-tetrahydroazepino[4,3-b]indol-1(2H)-one. (RP308)*

50 mg (0.219mmol) of compound **4c** was added at solution of CH_2Cl_2 (4ml), H_2O/50% NaOH (4ml), TBAB (77,36mg). Then 65,02ml of benzyl bromide was added to the mixture of reaction and the reaction was stirred at r.t. for one day. After TLC control, the product was extracted with CH_2Cl_2 and the organic layer was evaporated under vacuum to obtain 56 mg (yield crude product = 78%). The crude product was purified by chromatographic column (CH_2Cl_2 9.4 / MeOH 0.6) to obtain. Yield: 59%. ESI-MS: $[M+H]^+$ calcd: 319.1805, found: 319.1802; $[M+Na]^+$ calcd: 341.1624, found: 341.1625. IR (KBr, cm^{-1}): 3176, 3032, 1634, 1463,1450 cm^{-1}. ^{1}H NMR (500 MHz, cdcl$_3$) δ 8.31 (dd, J = 7.5, 2.0 Hz, 1H, H7), 7.39 – 7.10 (m, 6H), 7.02 – 6.87 (m, 2H, H9-H10), 5.89 (t, J = 5.2 Hz, 1H, CONH), 5.36 (s, 2H, CH_2 Bn), 3.01 (d, J = 5.7 Hz, 2H, 3CH_2), 2.75 (s, 2H,5CH_2), 1.02 (s, 6H, 4-$(CH_3)_2$).

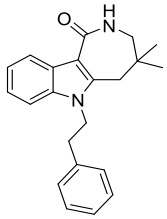

Compound **5l.** *Synthesis of 4,4-dimethyl-6-phenethyl-3,4,5,6-tetrahydroazepino[4,3-b]indol-1(2H)-one. (RP310)*

50 mg (0.219 mmol) of 4a was added at solution of CH_2Cl_2 (4 ml), H_2O/50% NaOH (4 ml), TBAB(77,36 mg, 0.240 mmol). Then 74,70ml (0.547 mmol) of 2-bromoethylbenzene was added to the reaction mixture and the reaction stirred at r.t. for two day. After TLC control, the product was extracted with CH_2Cl_2 and water and the organic layer was evaporated under vacuum. The product was treated with hexane and isolated to give the product as powder 33 mg (Yield crude product:

41%). The crude product was purified in the chromatographic column (CH_2Cl_2 9.4 / MeOH 0.6) to obtain 15 mg (yield column:50%). ESI-MS: $[M+H]^+$ calc.: 333.1961, found: 333.1961; $[M+Na]^+$ calc.: 355.1781, found: 355.1783. IR: 3409. 2925. 1637, 1462, 1386 cm^{-1}. ^1H NMR (500 MHz, cdcl$_3$) δ 8.38 – 8.23 (m, 1H, H7), 7.37 – 7.15 (m, 6H), 6.98 (dd, J = 7.1, 1.9 Hz, 2H, H9 - H10), 5.94 (s, 1H, CONH), 4.31 (t, J = 7.0 Hz, 2H, CH_2-Ph), 3.06 (t, J = 7.0 Hz, 2H, CH_2-Ph), 2.90 (d, J = 5.7 Hz, 2H, 3CH_2), 2.33 (s, 2H,5CH_2), 0.97 (s, 6H, 4-(CH_3)$_2$).

General procedure for the preparation of compounds **6a-d**. The preparation of 6-(4-bromobutyl)-2,3,4,5-tetrahydroazepino[4,3- b]indol-1(6*H*)-one (**6c**) has been reported as a representative example.

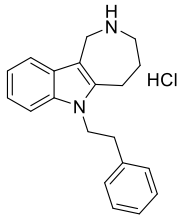

Compound **6c**. Synthesis of *6-(2-Phenylethyl)-1,2,3,4,5,6-hexahydroazepino[4,3-b]indole hydrochloride. (NB344)*.

LiAlH4 (0.127 g, 3.33 mmol) was added to a solution of 5f (0.145 g, 0.48 mmol) in 20 mL of dry dioxane, and the mixture was refluxed until disappearance of the starting material (TLC). After cooling, the reaction was quenched by adding 10 mL of a saturated solution of potassium bisulfate ($KHSO_4$) and stirred at rt for 30 min. The mixture was then filtered, and the precipitate was washed with 20 mL of dioxane. The collected filtrates were concentrated and the residue, suspended in 50 mL of distilled water, was extracted with 3 × 50 mL of $CHCl_3$. The organic fractions were dried over sodium sulfate (Na_2SO_4), filtered and concentrated under reduced pressure, and stored under vacuum. The residue was dissolved in a solution of 4M HCl in dry dioxane . After solvent removal, the solid residue was recrystallyzed from ethyl acetate and few drops of ethanol, to afford compound 14$HCl salt as dark brown solid (0.070 g, Yield 50%). m.p. 241-242 °C. IR (KBr, cm^{-1}): 3230, 1520, 1460, 810, 742, 700. 1 H NMR (300 MHz, DMSO-d6) d ppm 9.17 (s, 2H), 7.56 (d, *J* = 7.0 Hz, 1H), 7.44 (d, *J* = 8.0 Hz, 1H), 7.39-7.08 (m, 6H), 7.07 (t, *J* = 8.5 Hz, 2H), 4.45- 4.25 (m, 4H), 3.40 - 3.25 (m, 2H), 2.95 - 2.75 (m, 4H), 1.95 - 1.75 (m, 2H). ^{13}C NMR (CDCl3): 25.4, 26.5, 31.6, 42.2, 42.8, 46.0, 110.1, 120.9, 121.9, 122.5, 122.7, 126.7, 128.0, 128.3 (2 C), 128.5 (2 C), 135.0, 137.3, 139.2 HRMS (ESI) *m/z* $[M+H]^+$ calcd for $C_{20}H_{23}N_2^+$, 291.1856; found, 291.1852. Anal.

Calcd for C20H23ClN2 × H2O: C, 69.63; H, 7.31; N, 8.12. Found: C, 69.85; H, 7.54; N, 8.09.

Obtained 30 mg of the final compound, which was converted in HCl salt (4M HCl in dioxane). ^{1}H NMR (300 MHz, dmso) δ 8.98 (s, 2H), 7.61 (dd, *J* = 6.2, 2.7 Hz, 1H), 7.46 (dd, *J* = 6.8, 1.7 Hz, 1H), 7.34 – 7.18 (m, 3H), 7.10 – 7.06 (m, 12), 7.01 (d, *J* = 6.9 Hz, 1H), 5.48 (s, 2H), 4.42 (s, 2H), 3.43 – 3.35 (m, 2H), 3.07 – 2.91 (m, 2H), 1.95 (s, 2H).

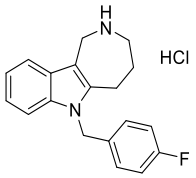

Compound **6a**. *Synthesis of 6-benzyl-1,2,3,4,5,6-hexahydroazepino[4,3-b]indole hydrochloride.* (NB560)

^{1}H NMR (500 MHz, dmso) δ 9.09 (s, 2H), 7.60 (d, *J* = 7.4 Hz, 1H), 7.47 (d, *J* = 8.0 Hz, 1H), 7.16 – 6.99 (m, 6H), 5.46 (s, 2H), 4.40 (s, 2H), 3.39 (s, 2H), 3.10 – 2.88 (m, 2H), 1.94 (s, 2H). IR KBr (cm^{-1}) 3414, 2956, 2849, 2736, 1509, 1469, 1355, 1223, 847, 812, 742.

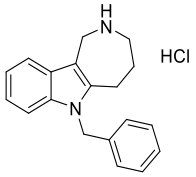

Compound **6b**. *Synthesis of 6-(4-fluorobenzyl)-1,2,3,4,5,6-hexahydroazepino[4,3-b]indole hydrochloride*. (*NB553)*

^{1}H NMR (300 MHz, dmso) δ 8.98 (s, 2H), 7.61 (dd, *J* = 6.2, 2.7 Hz, 1H), 7.46 (dd, *J* = 6.8, 1.7 Hz, 1H), 7.34 – 7.18 (m, 3H), 7.10 – 7.06 (m, 12), 7.01 (d, *J* = 6.9 Hz, 1H), 5.48 (s, 2H), 4.42 (s, 2H), 3.43 – 3.35 (m, 2H), 3.07 – 2.91 (m, 2H), 1.95 (s, 2H).

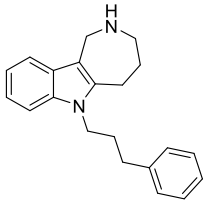

Compound **6d**. *Synthesis of 6-(3-phenylpropyl)-1,2,3,4,5,6-hexahydroazepino[4,3-b]indole. (NB556)*

^{1}H NMR (500 MHz, dmso) δ 8.98 (s, 2H), 7.38 (t, J = 8.0 Hz, 1H), 7.27 (t, *J* = 7.5 Hz, 3H), 7.18 (d, *J* = 6.6 Hz, 3H), 7.15 – 7.08 (m, 1H), 7.06 – 7.04 (m, 1H), 4.37

(s, 2H), 4.20 (t, *J* = 7.3 Hz, 2H), 3.41 (s, 2H), 3.08 – 2.98 (m, 2H), 2.68 – 2.53 (m, 2H), 2.01 (s, 2H), 1.90 (m, 2H).

General procedure for the preparation of compounds **8a-b**. The preparation of 6-(2-bromoethyl)-3,4,5,6-tetrahydroazepino[4,3-*b*]indol-1(2*H*)-one (**8a**) has been reported as a representative example.

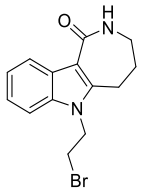

Compound **8a**. *Synthesis of 6-(2-bromoethyl)-3,4,5,6-tetrahydroazepino[4,3-b]indol-1(2H)-one. (NB569)*

A mixture of compound 4a (200 mg, 1mmol), TBAB(322 mg, 1 mmol) and a solution of CH_2Cl_2 (5 ml) and aq. NaOH 50% *(w/v)* (5 ml) is stirred at r.t. for 10 minutes. Then 5 eq. of 1,ω-dihaloalkane (1,2-dibromoethane or 1-bromo-3-chloropropane) were added to the reaction mixture and the reaction stirred at r.t. for two days. The reaction should not be stirred for more than two days to avoid the formation of the beta-elimination product (*N*-vinyl). After TLC control, the product was extracted with CH_2Cl_2 and water and the organic layer was evaporated under vacuum. The crude product was purified through chromatographic column (CH_2Cl_2 9.8 / MeOH 0.2) to obtain 100 mg (yield: 35%) of a brown solid. **^{1}H NMR** (300 MHz, cdcl$_3$) δ 8.49 – 8.39 (m, 1H), 7.29 – 7.20 (m, 3H), 6.33 (s, 1H), 4.48 (t, *J* = 7.4 Hz, 2H), 3.58 (t, *J* = 7.4 Hz, 2H), 3.38 (dd, *J* = 9.9, 5.3 Hz, 2H), 3.13 (t, *J* = 6.8 Hz, 2H), 2.23 (m, 2H).

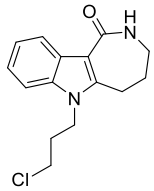

Compound **8b**. *6-(3-chloropropyl)-3,4,5,6-tetrahydroazepino[4,3-b]indol-1(2H)-one. (FS2)*

^{1}H NMR (300 MHz, dmso) δ 8.23 (d, *J* = 7.8 Hz, 1H), 7.45 (m, 7.50 - 7.43 , 2H), 7.15 (t, *J* = 7.2 Hz, 1H), 7.06 (t, *J* = 7.4 Hz, 1H), 4.30 – 4.18 (m, 2H), 3.71 (t, *J* = 6.2 Hz, 2H), 3.23 – 3.13 (m, 2H), 3.10 (t, *J* = 6.6 Hz, 2H), 2.12 (m, 2H), 2.06 – 1.95 (m, 2H).

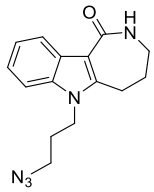

Compound **8c**. Synthesis of *6-(3-azidopropyl)-3,4,5,6-tetrahydroazepino[4,3-b]indol-1(2H)-one. (FS22)*

A mixture of compound 8b (150 mg, 0.18 mmol), sodium azide (18 mg, 0.27 mmol), KI (cat. amount) in acetone was stirred at r.t. overnight. A TLC (100% EA) shows a product with the same rf of the starting compound 8b. The solvent is evaporated under reduced pressure and the residue is suspended in water and extracted with EA. The collected organic phase is dried over magnesium sulphate, filtered and evaporated under reduced pressure. An IR analysis reveals the presence an organic azide. The product was used without further purification.

IR (KBr, cm^{-1}): 2096 (azide).

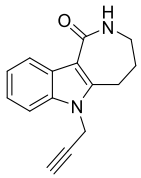

Compound **8d**. *Synthesis of 6-(prop-2-yn-1-yl)-3,4,5,6-tetrahydroazepino[4,3-b]indol-1(2H)-one. (NB516)*

Compound 4a (1.25 mmol) is suspended in 10 mL of dichloromethane. Then TBAB (1.56 mmol) and 10 mL of an aqueous solution of NaOH 25% are added. The mixture is stirred for 20 minutes and then propargyl bromide (1.56 mmol) is added. The reaction was stirred at room temperature for 48 hours. A TLC (eluent 100 % EtOAc) showed the formation of a new compound. Then, the product was suspended in water and extracted with DCM 3 times. The organic phase is then washed (1 × 50 ml) with distilled water to remove the excess of TBAB. The organic phase is dried over sodium sulfate, filtered, and evaporated under vacuum. The residue is washed with hexane many times and is used without further purification. Aspect: yellow solid. Yield 60% (178 mg). ^{1}H NMR (300 MHz, cdcl3) δ 8.54 – 8.31 (m, 1H), 7.54 - 7.58 (m, 1H), 7.38 – 7.13 (m, 1H), 6.94 (t, J = 6.4 Hz, 1H), 5.97 (s, 1H), 5.55 (d, J = 6.4 Hz, 2H), 3.38 (dd, J = 10.0, 5.4 Hz, 2H), 3.16 (t, J = 6.7 Hz, 2H), 2.22 (m, 2H). IR (KBr) cm^{-1} : 3271, 3179, 3035, 2977, 2122, 1630, 1462, 1195, 748, 684.

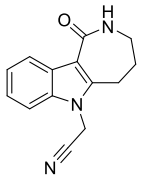

Compound **8e**. Synthesis of 2-(1-oxo-2,3,4,5-tetrahydroazepino[4,3-b]indol-6(1H)-yl)acetonitrile. *(FS56)*

A mixture of compound 4a (0.5 mmol), 2 ml of N,N-dimethylformamide, sodium hydride (0.7 mmol, 60% in mineral oil) and chloroacetonitrile (1.5 mmol) is stirred at room temperature overnight. A TLC (95:05, DCM:MeOH) reveals the presence of a new spot slightly higher than that of the starting compound 4a. Ethyl acetate is added to the mixture, and the mixture is washed with water and a brine. The organic phase is dried over sodium sulphate and concentrated under vacuum. The prodduct was purified on silica gel, eluent 98:02 DCM:MeOH. Yield: 37%. Aspect: Brown solid. GC-MS r.t. 16.859 min *m/z* calcd for C14H13N3O $[M]^{+\bullet}$ = 239, found 239. ^{1}H NMR (300 MHz, cdcl$_3$) δ 8.48 – 8.37 (m, 1H), 7.38 – 7.27 (m, 3H), 6.17 (t, *J* = 5.2 Hz, 1H), 4.95 (s, 2H), 3.39 (td, *J* = 5.5, 1.2 Hz, 2H), 3.11 (t, *J* = 6.7 Hz, 2H), 2.25 (ddd, *J* = 15.2, 6.7, 1.2 Hz, 1H). IR (KBr) cm^{-1}**:** 3048, 2927, 2195, 1928, 1635, 1464, 747.

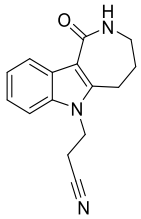

Compound **8f**. *Synthesis of 3-(1-oxo-2,3,4,5-tetrahydroazepino[4,3-b]indol-6(1H)-yl)propanenitrile. (NB347)*

Compound 4a (0.50 mmol) is suspended in 4 mL of dichloromethane. Then TBAB (0.55 mmol) and 4 mL of an aqueous solution of NaOH 25% are added. The mixture is stirred for 20 minutes and then 3-bromopropionitrile (1.35 mmol) is added. The reaction was stirred at room temperature for 48 hours. A TLC (eluent 100 % EtOAc) showed the formation of a new compound. Then, the product was suspended in water and extracted with DCM 3 times. The organic phase is then washed (1 × 50 ml) with distilled water to remove the excess of TBAB. The organic phase is dried over sodium sulfate, filtered, and evaporated under vacuum. The product crystalizes in EA. Aspect: pale brown solid. GC-MS: rt = 18.87, *m/z* calcd for C15H15N30 $[M]^{+\cdot}$ = 253, found $[M]^{+\cdot}$ = 253, fragrments 213, 170, 157, 129, 115. IR (KBr) cm^{-1}**:** 3263, 3182, 2254, 1628, 1529, 1465, 1371, 1189, 753. ^{1}H-NMR (d6-DMSO) δ:

8.22 (d, *J* = 7 Hz, 1H), 7.55 – 7.52 (m, 2H), 7.20 – 7.00 (m, 2H), 4.49 (t, *J* = 6.5 Hz, 2H), 3.20 – 3.10 (m, 4H), 2.98 (t, *J* = 7 Hz, 2H), 2.05 – 1.95 (m, 2H).

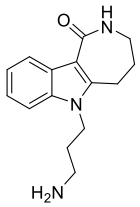

Compounds **8g** and **8h**. *Synthesis of 6-(3-aminopropyl)-3,4,5,6-tetrahydroazepino[4,3-b]indol-1(2H)-one. (FS66/2 and NB350)*

$NaBH_4$ (5.50 mmol) is slowly added to a solution of compound 8f (0,55 mmol) and $CoCl_2$ (1.10 mmol) hexahydrate in 17 mL of MeOH at 0°C and stirred at r.t. overnight. A check on TLC (eluent 100 % EtOAc) treated with an ethanolic solution of 2% ninhydrin reveals the presence of the desired compound. The reaction is quenched with 3N HCl until the existing precipitate is dissolved, and then filtered through Celite. The reaction mixture is concentrated and the aqueous solution is brought to pH = 9 and extracted with DCM (3x40 mL). Aspect: yellow solid. Yield: 105 mg (87% yield). HRMS (ESI-MS) calcd for C15H20N3O *m/z*: $[M+H]^+$ = 258.34, found $[M+H]^+$ = 258.17. IR (KBr) cm^{-1} : 3343, 3261, 1627, 1523, 1465, 783, 754. ^{1}H-NMR (d6-DMSO) δ: 8.21 (d, *J* = 8 Hz, 1H), 8.11 (s, 2H, exchange with D_2O), 7.60 (br s, 1H, exchange with D_2O) 7.53 (d, *J* = 8 Hz, 1H), 7.15 (t, *J* = 7 Hz, 1H), 4.26 (t, *J* = 7.5 Hz, 2H), 3.21 – 3.16 (m, 2H), 3.07 (t, *J* = 6.5 Hz, 2H), 2.89 – 2.80 (m, 2H), 2.05 – 1.90 (m, 4H). Compound 8g was used without further purification.

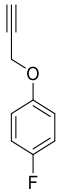

Compound **8i**. *Synthesis of 1-fluoro-4-(prop-2-yn-1-yloxy)benzene. (NB571)*

To the 4-fluorophenol and potassium carbonate in DMF was added 3-bromopropyne and stirred at reflux (56°C) overnight. Then the mixture was quenched with NaOH 1N, and extracted with DCM (20 mL x 3) and the combined organic layer was washed by saturated sodium chloride solution, then dried by anhydrous Na2SO4 and concentrated under reduced pressure to give an oil. ^{1}H-NMR (300 MHz, $CDCl_3$) δ: 7.04 – 6.86 (m, 4H), 4.66 (d, *J* = 2.3 Hz, 2H), 2.52 (t, *J* = 2.3 Hz, 1H).

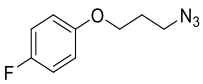

Compound **8j**. *Synthesis of 1-(3-azidopropoxy)-4-fluorobenzene. (FS11)*

Step a: synhesis of 1-(3-chloropropoxy)-4-fluorobenzene. 4-fluorophenol (1.78mmol) is dissolved in 10 mL of DMF and K_2CO_3 (2.67 mmol) is added. The mixture is stirred for 30 min and then 1-bromo-3-chloropropane (3.56 mmol) in 2 ml of DMF is added dropwise. The mixture is stirred at r.t. overnight. TLC control (1 EA : 1 Hex, r.f. = 0.9, higher than the starting 4-fluorophenol). The mixture is extracted with EA and a saturated solution of Na_2CO_3. The organic phases collected are dried over sodium sulfate, filtered and concentrated under vacuum. The product is used without further purification for step b. Aspect: yellow oil, yield 60% (200mg). IR (KBr) cm^{-1} : 2966, 2933, 2879, 1601, 1505, 1471, 1247, 1210, 828.

Step b: synthesis of 1-(3-azidopropoxy)-4-fluorobenzene. 1-(3-chloropropoxy)-4-fluorobenzene (1.06 mmol) from step a, is solubilized in DMF (5 mL) and KI (6.36 mmol) is added. The suspension is stirred for 30 min and then NaN_3 (2.12mmol) is added. The reaction mixture is stirred for 3 days at 40 °C. The reaction mixture is taken up with EA and filtered on gooch. The solution is concentrated under vacuum. 5 ml of Et_2O are added, then mix and keep in the refrigerator for an hour and a half. The supernatant is removed and this operation is repeated 3 or 4 times. Wash the supernatant wash with distilled water (2 ×50 mL) and brine (1×30 mL). The organic phase is dried over magnesium sulfate, filtered and evaporated under nitrogen gas. Compound 8j obtained is used without further purification. ^1H NMR (500 MHz, cdcl3) δ : 7.00 – 6.94 (m, 2H), 6.83 (dd, J = 9.1, 4.3 Hz, 2H), 4.01 (t, J = 5.9 Hz, 2H) 3.51 (t, J = 6.6 Hz, 2H), 2.04 (quintet, J = 6.5 Hz, 2H). IR (KBr) cm^{-1} : 2099, 1602, 1506, 1248, 1209, 828.

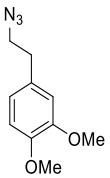

Compound **8k**. *Synthesis of 4-(2-azidoethyl)-1,2-dimethoxybenzene. (FS48)*

To a DMF solution (3 mL) of 4-(2-bromoethyl)-1,2-dimethoxybenzene (0.4 mmol), were added sodium iodide (0.05 eq) and sodium azide (1.2 eq). The reaction mixture was stirred at 40 °C overnight. Et_2O (20 mL) was added to the mixture then the organic layer was washed with water (3 × 20 mL), dried over $MgSO_4$ and concentrated under reduced pressure to give the azide derivative. Yield 93%. IR KBr (cm^{-1}): 3000, 2936, 2873, 2835, 2099, 1607, 1591, 1516, 1464, 1263, 1236,

1157, 1141, 1028, 806, 764. ^{1}H NMR (300 MHz, cdcl$_3$) δ 6.89 – 6.69 (m, 3H), 3.88 (s, 3H), 3.87 (s, 3H), 3.48 (t, J = 7.2 Hz, 2H), 2.84 (t, J = 7.2 Hz, 2H).

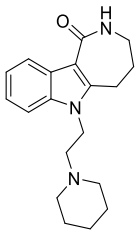

Compound **9a**. *Synthesis of 6-[2-(piperidin-1-yl)ethyl]-3,4,5,6-tetrahydroazepino[4,3-b]indol-1(2H)-one. (NB458)*

To a suspension of compound 6-(2-bromoethyl)-3,4,5,6-tetrahydroazepino[4,3-*b*]indol-1(2*H*)-one (0.6 mmol) in 6 mL of acetonitrile (ACN) were added K_2CO_3 (1.8 mmol), and piperidine (0.9 mmol). The mixture was refluxed 6 hours, until the disappearance of the starting material. **Work-up.** After cooling, the solvent was removed under reduced pressure and the obtained oil was suspended in 25 mL of water and extracted twice with 20 mL of methylene chloride. The collected organic phases were dried over anhydrous Na_2SO_4, and concentrated under reduced pressure. The obtained residue was purified by chromatography on silica gel, by eluting with a methylene chloride/ methanol (95/5, *v/v*) mixture as a mobile phase. Aspect: white solid. Yield: 55% (100 mg). **^{1}H NMR** (300 MHz, CDCl3) δ 8.56 – 8.34 (m, 1H), 7.37 – 7.10 (m, 3H), 5.96 (t, *J* = 4.9 Hz, 1H), 4.32 – 4.15 (m, 2H), 3.37 (td, *J* = 5.4, 1.4 Hz, 2H), 3.15 (t, *J* = 6.8 Hz, 2H), 2.66 – 2.55 (m, 2H), 2.52 – 2.39 (m, 4H), 2.31 – 2.12 (m, 2H), 1.63 – 1.54 (m, 4H), 1.45 (dd, *J* = 10.9, 5.6 Hz, 2H). **LC/MS** (ESI): RT [min]: 4.771, m/z calcd for [M+H]+ = 312.2, found 312.1.

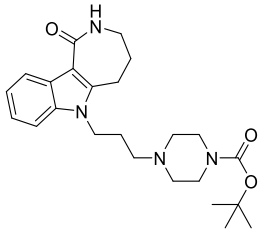

Compound **9b**. *Synthesis of tert-butyl 4-[3-(1-oxo-2,3,4,5-tetrahydroazepino[4,3-b]indol-6(1H)-yl]propyl)piperazine-1-carboxylate. (FS34)*

A mixture of tert-butyl piperazine-1-carboxylate (0.30 mmol), K_2CO_3 (0.90 mmol) in ACN (8 mL) is stirred for 5 minutes before adding 6-(3-chloropropyl)-3,4,5,6-tetrahydroazepino[4,3-*b*]indol-1(2*H*)-one (0.30 mmol). The mixture is stirred and refluxed for 48h. A TLC control reveals the formation of the product (95:5, DCM:MeOH, rf = 0.3). **Work-up.** After cooling to r.t., the solvent is evaporated and the solid re-suspended in EA and washed with water (3 x 30 mL). The organic

phase is dried over sodium sulfate, filtered and evaporated under vacuum. The crude product is purified on chromatography column (95:5, DCM:MeOH). Yield: 39% (40 mg) Aspect: white solid. **^{1}H NMR** (300 MHz, cdcl$_3$) δ 8.47 – 8.40 (m, 1H), 7.32 (dd, *J* = 6.3, 3.0 Hz, 1H), 7.24 – 7.18 (m, 2H), 5.89 (t, *J* = 5.5 Hz, 1H), 4.19 (t, *J* = 7.1 Hz, 2H), 3.45 (br s, 4H), 3.37 (ddd, *J* = 8.3, 5.5, 1.5 Hz, 2H), 3.14 (t, *J* = 6.8 Hz, 2H), 2.41 – 2.29 (m, 6H), 2.21 (ddd, *J* = 15.2, 6.6, 1.5 Hz, 2H), 2.01 – 1.88 (m, 2H), 1.46 (s, 9H). **LC/MS** (ESI): RT [min]: 6.276, calcd. for [M+H]$^{+}$ = 427.56, found 427.200.

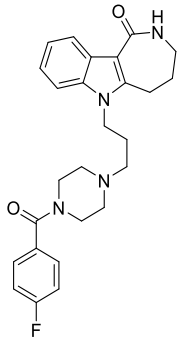

Compound **9c**. *Synthesis of 6-{3-[4-(4-fluorobenzoyl)piperazin-1-yl]propyl}-3,4,5,6-tetrahydroazepino[4,3-b]indol-1(2H)-one. (FS38)*

A mixture of 4-fluorobenzoylpiperazine (TFA salt, 0.28 mmol), K_2CO_3 (0.84 mmol) in ACN (8 mL) is stirred for 5 minutes before adding 6-(3-chloropropyl)-3,4,5,6-tetrahydroazepino[4,3-*b*]indol-1(2*H*)-one (0.28 mmol). The mixture is stirred and refluxed for 48h. A TLC control reveals the formation of the product (95:5, DCM:MeOH, rf = 0.3). **Work-up.** After cooling to r.t., the solvent is evaporated and the solid re-suspended in EA and washed with water (3 x 30 mL). The organic phase is dried over sodium sulfate, filtered and evaporated under vacuum. The crude product is purified on chromatography column (95:5, DCM:MeOH). Yield: 53% (67 mg) Aspect: white solid. **^{1}H NMR** (300 MHz, cd$_3$od) δ 8.22 (d, *J* = 7.7 Hz, 1H), 7.51 – 7.38 (m, 3H), 7.25 – 7.07 (m, 4H), 4.28 (t, *J* = 6.9 Hz, 2H), 3.72 (s, 2H), 3.45 (s, 2H), 3.38 – 3.32 (m, 2H), 3.22 (t, *J* = 6.7 Hz, 2H), 2.45 (s, 2H), 2.40 (t, *J* = 6.8 Hz, 4H), 2.19 (dd, *J* = 15.4, 7.1 Hz, 2H), 1.99 (p, *J* = 6.7 Hz, 2H). **LC/MS** (ESI): RT [min]: 5.496, calcd. for [M+H]$^{+}$ = 449.227, found 449.200. **IR (KBr) cm^{-1} :** 3406, 3266, 3180, 2929, 2809, 1627, 1462, 1436, 1298, 1018, 755.

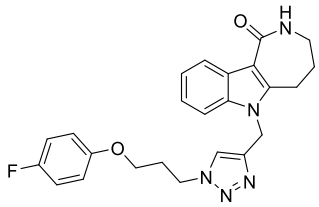

Compound **9d**. *Synthesis of 6-{[1-(3-(4-fluorophenoxy)propyl)-1H-1,2,3-triazol-4-yl]methyl}-3,4,5,6-tetrahydroazepino[4,3-b]indol-1(2H)-one. (FS13)*

6-(prop-2-yn-1-yl)-3,4,5,6-tetrahydroazepino[4,3-*b*]indol-1(2*H*)-one (0.13 mmol), 4-(2-azidoethyl)-1,2-dimethoxybenzene and Na Ascorbate (0.13 mmol) are solubilized in 2 ml of DMF. Then $CuSO_4 \cdot 2H_2O$ (0.05 mmol) is added and the and the reaction is stirred at r.t. for 1.30 hours. A TLC control (100% EA) showed the formation of the product (rf = 0.1). **Work-up.** The reaction mixture is extracted with EA and distilled water and then the organic phases washed with distilled water (2×40 ml) and brine (1×40 ml). The collected organic phases are dried over Na_2SO_4, filtered and concentrated under vacuum. The solid was purified on silica gel 40-63 μm (99 $CHCl_3$: 01 MeOH). Yield 53 %. **^{1}H NMR** (300 MHz, cdcl3) δ 8.46 (dd, *J* = 5.9, 2.1 Hz, 1H), 7.34 – 7.17 (m, 4H), 7.13 (s, 1H), 7.02 – 6.87 (m, 2H), 6.70 (dd, *J* = 9.1, 4.3 Hz, 2H), 6.01 (t, *J* = 5.4 Hz, 1H), 5.41 (s, 2H), 4.46 (t, *J* = 6.9 Hz, 2H), 3.83 (t, *J* = 5.7 Hz, 2H), 3.33 (dd, *J* = 9.8, 5.4 Hz, 2H), 3.18 (t, *J* = 6.7 Hz, 2H), 2.29 (quintet, *J* = 6.0 Hz, 2H), 2.16 (dd, *J* = 16.3, 6.7 Hz, 2H). **LC/MS** (ESI): RT [min]: 5.971, $[M+H]^+$ calc. 434.5, found 434.2.

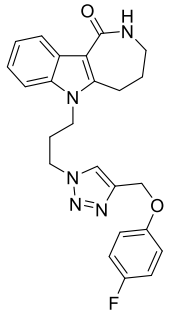

Compound **9e**. *Synthesis of 6-{3-[4-((4-fluorophenoxy)methyl)-1H-1,2,3-triazol-1-yl]propyl}-3,4,5,6-tetrahydroazepino[4,3-b]indol-1(2H)-one. (FS40p)*

6-(3-azidopropyl)-3,4,5,6-tetrahydroazepino[4,3-*b*]indol-1(2*H*)-one (0.18 mmol), Na Ascorbate (0.18 mmol) are added to 1-fluoro-4-(prop-2-yn-1-yloxy)benzene solubilized in 2 ml of DMF. Then $CuSO_4 \cdot 2H_2O$ (0.09 mmol) is added and the reaction is stirred at r.t. for 3 hours. A TLC control (95 $CHCl_3$: 05 MeoH, r.f. = 0.25) showed the formation of the product. **Work-up.** The reaction mixture is extracted with EA and distilled water and brine. The collected organic phases are dried over Na_2SO_4, filtered and concentrated under vacuum. The yellow oil obtained was purified on silica gel (98:02 $CHCl_3$:MeOH) and monitored with TLC (95 $CHCl_3$: 05 MeoH). The product was crystallized in a solution of EtOAc and Hex (2:1). Aspect: white powder. Yield: 43,6 % (34 mg). **^{1}H NMR** (500 MHz, $cdcl_3$) δ 9.12 (s, 1H), 8.21 (d, *J* = 8.4 Hz, 1H), 7.63 (s, 1H), 7.32 - 7.28 (m, 2H), 7.25 - 7.22 (m,

1H), 6.97 (t, *J* = 8.6 Hz, 2H), 6.92 (dd, *J* = 9.2, 4.3 Hz, 2H), 5.15 (s, 2H), 4.46 (t, *J* = 5.8 Hz, 2H), 4.26 (t, *J* = 7.3 Hz, 2H), 3.48 (s, 2H), 3.02 (dd, *J* = 10.4, 6.2 Hz, 2H), 2.47 (m, 2H), 2.16 (s, 2H). **^{1}H NMR** (600 MHz, DMSO) δ 8.26 (s, 1H), 8.24 (d, *J* = 7.9 Hz, 1H), 7.45 (t, *J* = 5.3 Hz, 1H), 7.35 (d, *J* = 8.1 Hz, 1H), 7.16 – 6.97 (m, 6H), 5.12 (s, 2H), 4.49 (t, *J* = 7.0 Hz, 2H), 4.21 – 4.12 (m, 2H), 3.17 (dd, *J* = 8.9, 5.0 Hz, 2H), 3.00 (t, *J* = 6.6 Hz, 2H), 2.30 – 2.18 (m, 2H). **^{13}C NMR** (151 MHz, DMSO) δ 167.3, 156.8 (d, *J* = 236.4 Hz), 154.5, 142.9, 142.1, 135.9, 128.1, 124.7, 122.1, 121.9, 120.6, 116.2 (d, *J* = 7.9 Hz), 116.0 (d, *J* = 23.1 Hz), 109.2, 107.2, 61.8, 47.2, 40.5, 29.7, 26.9, 26.6. **LC/MS** (ESI) rt: 5.88, m/z calcd. for C24H24FN5O2 $[M+H]^+$ = 434.1914, found $[M+H]^+$ = 424.100. **HRMS** (ESI-MS) calcd for C24H24FN5O2 *m/z*: $[M+H]^+$ = 434.1914, found $[M+Na]^+$ = 456.1808.

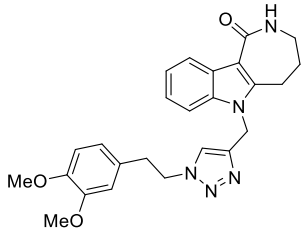

Compound **9f**. *Synthesis of 6-{[1-(3,4-dimethoxyphenethyl)-1H-1,2,3-triazol-4-yl]methyl}-3,4,5,6-tetrahydroazepino[4,3-b]indol-1(2H)-one. (FS49)*

6-(prop-2-yn-1-yl)-3,4,5,6-tetrahydroazepino[4,3-*b*]indol-1(2*H*)-one (0.13 mmol), 4-(2-azidoethyl)-1,2-dimethoxybenzene and Na Ascorbate (0.13 mmol) are solubilized in 2 ml of DMF. Then $CuSO_4 \cdot 2H_2O$ (0.05 mmol) is added and the and the reaction is stirred at r.t. for 1.30 hours. A TLC control (100% EA) showed the formation of the product (rf = 0.1). **Work-up.**The reaction mixture is extracted with EA and distilled water and then the organic phases washed with distilled water (2×40 ml) and brine (1×40 ml). The collected organic phases are dried over Na_2SO_4, filtered and concentrated under vacuum. The solid was purified on silica gel 40-63 μm (97:3 DCM:MeOH). Yield 51 %. **^{1}H NMR** (300 MHz, $cdcl_3$) δ 8.46 – 8.40 (m, 1H), 7.28 – 7.19 (m, 3H), 6.81 (s, 1H), 6.66 (d, *J* = 8.0 Hz, 1H), 6.53 – 6.46 (m, 2H), 6.25 (t, *J* = 5.2 Hz, 1H), 5.38 (s, 2H), 4.43 (t, *J* = 7.2 Hz, 2H), 3.83 (s, 3H), 3.76 (s, 3H), 3.36 (dd, *J* = 9.2, 4.9 Hz, 2H), 3.14 (t, *J* = 6.7 Hz, 2H), 3.05 (t, *J* = 7.2 Hz, 2H), 2.22 – 2.13 (m, 2H). **LC/MS** (ESI): RT [min]: 5.023, $[M+H]^+$ calc. 446.218, found 446.200. **IR** (KBr, cm^{-1}): 2960, 2933, 1633, 1464, 1263, 1141, 754.

HRMS (ESI-MS) calcd for C25H27N5O3 $[M+H]^+$ = 446.2187, found $[M+Na]^+$ = 468.2013, fragments 247.0840, 223.0839, 165.0908.

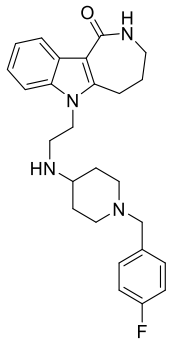

Compound **9g**. *Synthesis of 6-{2-[(1-(4-fluorobenzyl)piperidin-4-yl)amino]ethyl}-3,4,5,6-tetrahydroazepino[4,3-b]indol-1(2H)-one. (FS69-2)*

A mixture of 6-(2-aminoethyl)-3,4,5,6-tetrahydroazepino[4,3-*b*]indol-1(2*H*)-one (FS66, 0.16 mmol), 1-(4-fluorobenzyl)lpiperidin-4-one (0.18 mmol), $NaCNBH_3$ (0.32 mmol) in 5 mL of methanol is stirred for 30 minutes. Then acetic acid (100 µL) is added and the mixture is stirred at r.t. overnight. TLC (9 DCM : 1 MeOH, 2 drops of TEA) shows the formation of a new product (r.f. = 0.28). **Work-up.** The reaction mixture is concentrated under vacuum, the residue suspended in EtOAc and washed with a saturated bicarbonate solution. The organic phase is dried over sodium sulfate, filtered and evaporated under vacuum. The product is purified on chromatography column (DCM:MeOH, gradient from 98:2 to 9:1). 8 mg obtained as a white solid (yield 12%). **^{1}H NMR** (300 MHz, cd_3od) δ 8.23 (d, *J* = 7.6 Hz, 1H), 7.42 (d, *J* = 8.0 Hz, 1H), 7.31 (dd, *J* = 8.6, 5.5 Hz, 2H), 7.24 – 7.17 (m, 1H), 7.17 – 7.10 (m, 1H), 7.08 – 6.98 (m, 2H), 4.26 (t, *J* = 7.3 Hz, 2H), 3.47 (s, 2H), 3.37 – 3.32 (m, 2H), 3.19 (t, *J* = 6.8 Hz, 2H), 2.92 (t, *J* = 7.3 Hz, 2H), 2.80 (d, *J* = 12.1 Hz, 2H), 2.47 (m, 1H), 2.18 (dtd, *J* = 7.9, 6.6, 0.9 Hz, 2H), 2.04 (td, *J* = 11.6, 1.8 Hz, 2H), 1.83 (d, *J* = 11.8 Hz, 2H), 1.47 – 1.30 (m, 2H), 1.28 (s, 1H). **LC/MS (ESI)** rt: 5.22, m/z calcd for C26H31FN4O $[M+H]^+$ = 435.2532, found $[M+H]^+$ = 435.300. **HRMS** (ESI-MS) calcd for *m/z*: C26H31FN4O $[M+H]^+$ = 435.2532, found $[M+Na]^+$ = 457.2378.

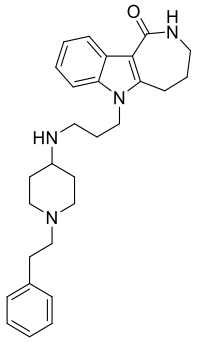

Compound **9h**. *Synthesis of 6-{3-[(1-phenethylpiperidin-4-yl)amino]propyl}-3,4,5,6-tetrahydroazepino[4,3-b]indol-1(2H)-one. (FS51)*

A mixture of 6-(3-aminopropyl)-3,4,5,6-tetrahydroazepino[4,3-*b*]indol-1(2*H*)-one (NB350, 0.16mmol) and phenylethylpiperidone in 2 mL of methanol is stirred for 20 minutes. Then acetic acid is added and, after 30 minutes, $NaCNBH_3$ stirred at r.t. overnight. A TLC (9 DCM : 1 MeOH, 0,5% TEA) shows the formation of a new product (r.f. = 0.1, with a tail). The solventi s evaporated under vacuum, suspended in EtOAc and washed twice with a saturated solution of $NaHCO_3$. The product crystalizes in EtOAc. **^{1}H NMR (300 MHz, cdcl$_3$)** δ 8.48 – 8.38 (m, 1H), 7.36 – 7.27 (m, 3H), 7.24 – 7.15 (m, 5H), 6.16 (t, *J* = 5.4 Hz, 1H), 4.20 (t, *J* = 7.1 Hz, 2H), 3.36 (ddd, *J* = 8.4, 5.4, 1.5 Hz, 2H), 3.13 (t, *J* = 6.7 Hz, 2H), 2.98 (t, *J* = 3.1 Hz, 2H), 2.80 (dd, *J* = 10.3, 6.1 Hz, 2H), 2.64 (t, *J* = 6.6 Hz, 2H), 2.61 – 2.53 (m, 2H), 2.42 (tt, *J* = 10.4, 3.9 Hz, 1H), 2.19 (ddd, *J* = 15.2, 6.7, 1.5 Hz, 2H), 2.10 – 2.00 (m, 2H), 1.97 - 1.82 (m, *J* = 13.8, 7.0 Hz, 4H), 1.40 (ddd, *J* = 15.2, 12.2, 3.8 Hz, 2H). **LC/MS (ESI)** rt: 5.34, *m/z* calcd for C28H37N4O $[M+H]^+$ = 455.62, found $[M+H]^+$ = 445.300.

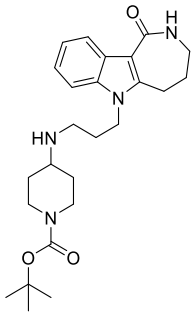

Compound **9i**. *Synthesis of tert-butyl 4-{[3-(1-oxo-2,3,4,5-tetrahydroazepino[4,3-b]indol-6(1H)-yl)propyl]amino}piperidine-1-carboxylate. (FS61)*

The compound was synthetized as compound 9h. The crude product was purified on silica column (gradient from 97 DCM:03 MeOH + 0,01% TEA to 92 DCM :08 MeOH + 0,01% TEA. **^{1}H NMR** (300 MHz, cdcl$_3$) δ 8.45 – 8.35 (m, 1H), 7.34 – 7.27 (m, 1H), 7.24 – 7.15 (m, 2H), 6.34 (t, *J* = 5.3 Hz, 1H), 4.19 (t, *J* = 7.2 Hz, 2H), 4.03 (d, *J* = 11.8 Hz, 2H), 3.34 (td, *J* = 5.3, 1.3 Hz, 2H), 3.09 (t, *J* = 6.7 Hz, 2H), 2.77 (d, *J* = 11.8 Hz, 2H), 2.68 (t, *J* = 6.7 Hz, 2H), 2.63 – 2.52 (m, 1H), 2.16 (ddd, *J* = 15.0, 6.7, 1.2 Hz, 2H), 1.95 (quint, *J* = 6.9 Hz, 1H), 1.82 (d, *J* = 11.1 Hz, 2H), 1.44 (s, 9H), 1.37 – 1.18 (m, 2H). **LC/MS** (ESI) rt: 5.14, *m/z* calcd for C25H37N4O $[M+H]^+$ = 441.28, found $[M+H]^+$ = 441.300. **HRMS** (ESI-MS) calcd for *m/z*: C25H37N4O $[M+H]^+$ = 441.28, found $[M+Na]^+$ = 463.2680.

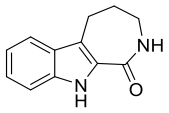

Compound **10**. *2,3,4,5-tetrahydroazepino[3,4-b]indol-1(10H)-one. (NB529)*

^{1}H NMR (300 MHz, $CDCl_3$) δ ppm: 11.1 (s, 1H), 7.94 (t, *J* = 7.5, 1H), 7.54 (d, *J* = 8.0 Hz, 1H), 7.37 (d, *J* = 8.0 Hz, 1H), 7.18 (t, *J* = 7.5, 1H), 7.00 (t, *J* = 7.5, 1H), 3.28 (dd, *J* = 9.0 Hz, *J* = 4.8 Hz, 2H), 3.01 (t, *J* = 6.4, 2H), 2.01 (dt, *J* = 9.0 Hz, *J* = 6.0 Hz, 2H).

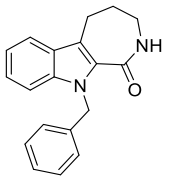

Compound **11a**. *10-benzyl-2,3,4,5-tetrahydroazepino[3,4-b]indol-1(10H)-one (NB531)*

^{1}H NMR (300 MHz, $CDCl_3$) δ ppm: 7.67 (d, *J* = 8.0 Hz, 1H), 7.40 – 7.34 (m, 2H), 7.36 – 7.20 (m, 5H), 7.02 (d, *J* = 6.0 Hz, 2H), 5.74 (s, 2H), 3.42 – 3.35 (m, 2H), 3.20 (t, *J* = 7.0, 2H), 2.26 – 2.13 (m, 2H).

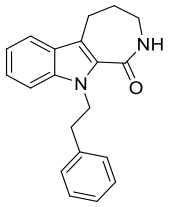

Compound **11b**. *10-(2-phenyl ethyl)-2,3,4,5-tetrahydroazepino[3,4-b]indol-1(10H)-one (NB532)*

^{1}H NMR (300 MHz, $CDCl_3$) δ ppm: 7.63 (d, J = 8.6 Hz, 1H), 7.37 (t, *J* = 8.4 Hz, 2H), 7.29 – 7.12 (m, 6H), 6.46 (s, br, 1H), 4.76 (t, *J* = 7.6 Hz, 2H), 3.20 – 3.15 (m, 2H), 3.08 (t, *J* = 7.3, 2H), 2.17 – 2.05 (m, 2H)

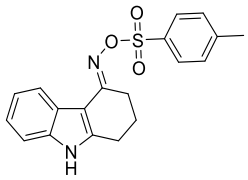

Compound **12**. *Synthesis of N-{[(4-Methylphenyl)sulfonyl]oxy}-1,2,3,9-tetrahydro-4H-carbazol-4-imine.*

DMAP (1.83 g, 15.0 mmol) and, dropwise, a solution of tosyl chloride (1.05 g, 15.0 mmol) in 10 mL of dry DCM were added to a solution of 3a (1.00 g, 5 mmol) in 15 mL of dry DCM cooled at 0 °C. The mixture was stirred at r.t. under N_2 atmosphere for 48 h. The reaction mixture was then washed with 1 N HCl (3 x 20 mL) and brine (3 x 20 mL), dried over Na_2SO_4, filtered and concentrated under reduced pressure, to afford the desired product (0.625 g, Yield 70%), whose analytical data were in good agreement with those of literature (*J.B. Hester, Azepinoindoles. II. 1,2,3,4,5,6-*

Hexahydroazepino[3,2-b]indole and 1,2,3,4,5,6-Hexahydroazepino[4,3-b]indole, J. Org. Chem 31 (1967), 3804 – 3808). **M.p.** 138 °C (lit. 135e138 °C). **IR** (KBr, cm^{-1}): 3383,3061, 2925, 1915, 1885, 1799, 1774, 1639, 1621, 1591, 1567, 1177, 742, 716. **^{1}H NMR** (300 MHz, DMSO-d6) δ ppm 10.16 (s, 1H), 7.92 (d, *J* = 8.0 Hz, 1H), 7.82 (d, *J* = 8.5 Hz, 2H), 7.34 (d, *J* = 8.0 Hz, 1H), 7.28 (d, *J* = 8.5 Hz, 2H), 7.08 (t, *J* = 8.0 Hz, 1H), 7.02 (t, *J* = 8.0 Hz, 1H), 2.82 (t, *J* = 6.5 Hz, 1H), 2.70 (t, *J* = 6.5 Hz, 1H), 2.33 (s, 3H), 1.94 (quintet, *J* = 6.5 Hz, 2H). **HRMS** (ESI-MS) calcd for $C_{19}H_{19}N_2O_3S^+$ *m/z*: $[M+H]^+$ = 355.4240, found $[M+H]^+$ = 355.1838.

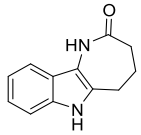

Compound **13**. *Synthesis of 3,4,5,6-Tetrahydroazepino[3,2-b]indol-2(1H)-one.*

A solution of compound 12 (0.100 g, 0.28 mmol) in toluene (5mL) is refluxed overnight. The reaction mixture was concentrated under reduced pressure. The residue was treated with 30 mL of EtOAC and washed with a saturated solution of Na_2CO_3 (3 x 30 mL). The collected organic phase was dried (Na_2SO_4), filtered and concentrated under reduced pressure to afford the mixture of isomers (55 mg, 63%) as shown by GC-MS (two peaks with the same *m/z*, but different retention times and different fragmentations). The same result was achieved by using BuOH instead of Toluene. **GC-MS:** retention time (peak 1, [3,2-b] isomer) 14.214 min; $M^{+\bullet}$ = 200, mm 171, 156, 145, 129, 117, 103, 89, 76; retention time (peak 2, [4,3-b] isomer) 15.719 min; $M^{+\bullet}$ = 200, mm 183, 170, 157, 143, 130, 115, 102, 91, 86, 71.

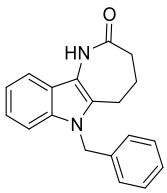

Compound **14a**. *Synthesis of 6-benzyl-3,4,5,6-tetrahydroazepino[3,2-b]indol-2(1H)-one. (NB392-C)*

^{1}H-NMR(500 MHz,cdcl3) δ 7.53 (s, 1H), 7.50 (d, *J* = 7.8 Hz, 1H), 7.32 – 7.23 (m, 3H), 7.20 (dt, *J* = 6.5 Hz, *J* = 1.0 Hz, 1H), 7.17 – 7.12 (m, 1H), 6.95 (d, *J* = 6.9 Hz, 2H), 5.29 (s, 2H), 2.90 (t, *J* = 6.8 Hz, 2H), 2.72 – 2.61 (m, 2H), 2.17 (dt, *J* = 11.5, 6.7 Hz, 2H).

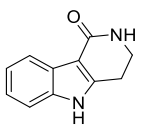

Compound **18**. *Synthesis of 3,4-dihydro-2H-pyrido[4,3-b]indol-1(5H)-one*

250 mg of crude hydrazone were added to 6 mL of cooled (0 °C) TFA, and solution was stirred 2 hours a t room temperature. After removal of TFA by using N_2 stream, the residue was dissolve in EA, and the organic phase washed with saturated carbonate solution, dried, filtered. After removal of the solvent 170 mg of the desired product were obtained (yield 78%). **^{1}H NMR** (300 MHz, DMSO-d6) δ ppm 11.89 (s, 1H), 8.02 (s, 1H), 7.30 (d, *J* = 7.6 Hz, 1H), 7.30 (d, *J* = 8.0 Hz, 1H), 7.04 (dt, *J* = 9.0, 2.0 Hz, 1H), 6.96 (dt, *J* = 9.0, 2.0 Hz, 1H), 5.50 (d, *J* = 7.5 Hz, 1H), 4.48-4.40 (m, 2H), 3,52 (t, *J* = 3.5 Hz, 2H).

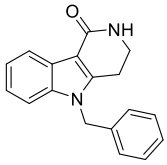

Compound **19a**. *Synthesis of 5-benzyl-2,3,4,5-tetrahydro-1H-pyrido[4,3-b]indol-1-one. (NB537)*

^{1}H NMR (300 MHz, cdcl$_3$) δ 8.22 (d, *J* = 8.5 Hz, 1H), 7.36 – 7.19 (m, 6H), 7.02 (dd, *J* = 7.3, 1.7 Hz, 2H), 5.34 (s, 2H), 3.65 (td, *J* = 7.0, 2.4 Hz, 2H), 2.94 (t, *J* = 6.9 Hz, 2H).

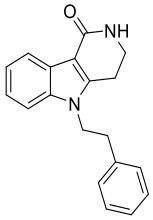

Compound **19b**. *Synthesis of 5-phenethyl-2,3,4,5-tetrahydro-1H-pyrido[4,3-b]indol-1-one. (NB539)*

^{1}H NMR (500 MHz, cdcl$_3$) δ 8.22 – 8.17 (m, 1H), 7.41 – 7.37 (m, 1H), 7.33 – 7.27 (m, 2H), 7.24 – 7.20 (m, 3H), 6.89 – 6.83 (m, 2H), 5.24 (s, 1H), 4.31 (t, *J* = 6.5 Hz, 2H), 3.32 (td, *J* = 6.9, 2.5 Hz, 2H), 3.08 (t, *J* = 6.4 Hz, 2H), 2.27 (t, *J* = 6.4 Hz, 2H).

General procedure for the preparation of compounds **20a-f**. The preparation of ethyl 8-(benzyloxy)-1,3,4,5-tetrahydro-2*H*-pyrido[4,3-*b*]indole-2-carboxylate (**20e**) has been reported as a representative example.

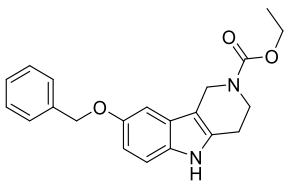

Compound **20e**. *Synthesis of ethyl 8-(benzyloxy)-1,3,4,5-tetrahydro-2H-pyrido[4,3-b]indole-2-carboxylate. (FS86)*

The 4-benzyloxy phenylhydrazine HCl (o.67 mmol) is solubilized in EtOH abs (12 mL) and the carbetoxypiperidone (0.67 mmol) is added. The mixture is stirred under reflux. The reaction reaches completion after 1 hour and 45 minutes. A TLC (7 Hex: 3 EA) shows the disappearance of the starting phenylhydrazine and the formation of a product (r.f. = 0.6). **Work-up.** The reaction solvent is evaporated under reduced pressure. 260 mg of a spotted brown solid is be obtained (quantitative yield). The product was used without further purification. ^{1}H NMR (300 MHz, cdcl$_3$) δ 7.77 (s, 1H), 7.48 (d, *J* = 6.7 Hz, 2H), 7.39 (t, *J* = 7.2 Hz, 2H), 7.33 (d, *J* = 7.1 Hz, 1H), 7.20 (d, *J* = 8.8 Hz, 1H), 7.00 (d, *J* = 2.4 Hz, 1H), 6.89 (dd, *J* = 8.7, 2.4 Hz, 1H), 5.10 (s, 2H), 4.65 (s, 2H), 4.21 (q, *J* = 7.1 Hz, 2H), 3.85 (s, 2H), 2.82 (t, *J* = 5.3 Hz, 2H), 1.31 (t, *J* = 7.1 Hz, 3H). LC/MS (ESI) rt: 7.78 min, *m/z* calcd for $C_{21}H_{23}N_2O_3^+$ $[M+H]^+$: 351.163, found: 351. 100.

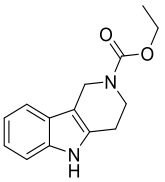

Compoud **20a**. *Ethyl 1,3,4,5-tetrahydro-2H-pyrido[4,3-b]indole-2-carboxylate. (NB542-B)*

^{1}H NMR (300 MHz, cdcl$_3$) δ 7.88 (s, 1H), 7.46 (d, *J* = 7.0 Hz, 1H), 7.32 (d, *J* = 7.6 Hz, 1H), 7.16 (td, *J* = 7.2, 1.2 Hz, 1H), 7.10 (td, *J* = 7.2, 1.2 Hz, 1H), 4.70 (s, 1H), 4.20 (qd, *J* = 7.1, 2.6 Hz, 2H), 3.87 (s, 1H), 3.77 (t, *J* = 6.2 Hz, 1H), 2.85 (t, *J* = 5.5 Hz, 1H), 2.46 (t, *J* = 6.2 Hz, 1H), 1.30 (td, *J* = 7.1, 2.3 Hz, 3H).

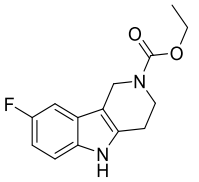

Compoud **20b**. *Ethyl 8-fluoro-1,3,4,5-tetrahydro-2H-pyrido[4,3-b]indole-2-carboxylate. (FS81)*

Data in accordance with J. Med. Chem., 1980, Vol. 23, n.6.

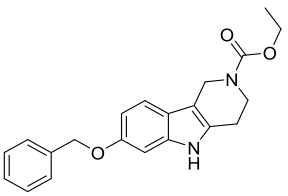

Compounds **20d** and **20f**. *Synthesis of ethyl 7-(benzyloxy)-1,3,4,5-tetrahydro-2H-pyrido[4,3-b]indole-2-carboxylate (FS87xx) and ethyl 9-(benzyloxy)-1,3,4,5-tetrahydro-2H-pyrido[4,3-b]indole-2-carboxylate.*

3-benzyloxyphenylhydrazine hydrochloride (0.67 mmol) is solubilized in EtOH abs (10 mL) and the 1-carbethoxy-4-piperidone (0.67 mmol) is added. The mixture is kept under reflux for 1 hour and 45 minutes. A TLC (7 Hex: 3 EA) shows the disappearance of the reagents and the formation of a product (a single spot, rf= 0.35, same as that of 1-carbethoxy-4-piperidone). **Work-up.** The reaction mixture is concentrated under vacuum. 281 mg of a dark brown solid is obtained (quantitative yield). ^{1}H-NMR of the crude product shows the possible formation of the two regioisomers, *i.e.* 7-(benzyloxy) and 9-(benzyloxy)-1,3,4,5-tetrahydro-2*H*-pyrido[4,3-*b*]indole-2-carboxylate). The mixture is purified on a gravitational silica column (eluent 99.5% chloroform, 0.5% methanol). The purified product is crystallized in ethanol as reported in *J. Med. Chem.*, 1980, vol. 23, n.6. ^{1}H-NMR of the crystals reveals the formation of 7-(benzyloxy)-1,3,4,5-tetrahydro-2*H*-pyrido[4,3-*b*]indole-2-carboxylate regioisomer. Yield: 140 mg (60% yield). Aspect: yellow crystalline solid.

There is no trace of the 9-benzyloxy regioisomer in the crystallized precipitate. However, an ^{1}H-NMR analysis of properly the crystallization ethanol clearly shows the presence of two regioisomers 7-benzyloxy (still the most abundant) and 9-benzyloxy in a ratio of 3 to 2. Crystallization could be performed several times to definitively separate the two regioisomers. We continued with the subsequent alkylation and then deprotection reactions without further purifying the mixture. The compounds were therefore purified only in the final carbamate deprotection. **^{1}H NMR** (300 MHz, cdcl$_3$) δ 7.77 (s, 1H), 7.48 (d, *J* = 6.7 Hz, 2H), 7.39 (t, *J* = 7.2 Hz, 2H), 7.33 (d, *J* = 7.1 Hz, 1H), 7.20 (d, *J* = 8.8 Hz, 1H), 7.00 (d, *J* = 2.4 Hz, 1H), 6.89 (dd, *J* = 8.7, 2.4 Hz, 1H), 5.10 (s, 2H), 4.65 (s, 2H), 4.21 (q, *J* = 7.1 Hz, 2H), 3.85 (s, 2H), 2.82 (t, *J* = 5.3 Hz, 2H), 1.31 (t, *J* = 7.1 Hz, 3H). **GC/MS:** rt 25.616 min, *m/z* calcd for [M$^{\bullet+}$]= 350, found 350, fragmentation 321, 259, 213, 158, 130, 91. **LC/MS** (ESI) rt: 7.78 min, m/z calcd for [M+H]$^{+}$: 351.163, found: 351. 100.

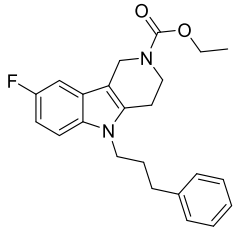

Compound **21f**. *Synthesis of ethyl 8-fluoro-5-(3-phenylpropyl)-1,3,4,5-tetrahydro-2H-pyrido[4,3-b]indole-2-carboxylate. (FS88)*

NaH (1.5 mmol) is suspended in 2 mL of DMF and ethyl 8-fluoro-1,3,4,5-tetrahydro-2*H*-pyrido[4,3-*b*]indole-2-carboxylate (0.30 mmol) is added. The mixture is stirred at r.t. for 15 minutes, then cooled at 0 °C and 1-bromo-3-phenylpropane (0.75 mmol) solubilized in 0.5 mL DMF is added dropwise. The reaction mixture is stirred at r.t. overnight. **Work-up**. A TLC control 7 *n*-Hex: 3EA shows the formation of the product (r.f. = 0.35). The reaction mixture is extracted with EA and distilled water. 160 mg of a brown oil are obtained, purified on chromatography column (7 *n*-Hex: 3EA, rf = 0.35). Yield: 44% (50 mg) Aspect: yellow oil. **^{1}H NMR** (300 MHz, cdcl$_3$) δ 7.34 – 7.26 (m, 2H), 7.22 (dt, *J* = 5.2, 2.1 Hz, 1H), 7.15 (d, *J* = 6.7 Hz, 2H), 7.12 – 7.09 (m, 1H), 7.08 (d, *J* = 3.0 Hz, 1H), 6.89 (td, *J* = 9.1, 2.4 Hz, 1H), 4.64 (s, 2H), 4.20 (q, *J* = 7.1 Hz, 2H), 4.02 (t, *J* = 7.5 Hz, 2H), 3.85 (s, 2H), 2.73 (t, *J* = 4.9 Hz, 2H), 2.65 (t, *J* = 7.6 Hz, 1H), 2.06 (quint, *J* = 7.2 Hz, 2H), 1.30 (t, *J* = 7.1 Hz, 3H). **LC/MS** (ESI) rt: 9.38 min, *m/z* calcd for [M+H$^+$]: 381.5 , found: 381.1.

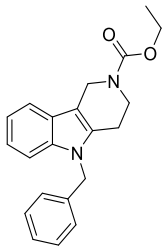

Compound **21a**. *Ethyl 5-benzyl-1,3,4,5-tetrahydro-2H-pyrido[4,3-b]indole-2-carboxylate. (NB543-A)*

A mixture of compound 20a (0.33 mmol), NaH (60% in m.o., 1.85 mmol) in 1 mL of dry DMF is stirred at r.t. for 15 min. Benzylbromide (0.85 mmol) is added dropwise and the reaction is stirred overnight. A TLC reveals the formation of the desired product (eluent: 7 EA/3 n-Hex or 1 EA/1 n-Hex). Work-up. The reaction mixture is diluted with water and extracted with 3x25 mL of EtOAc.

The crude is purified by chromatography (gradient eluent starting from 2 EA/8 n-Hex). 160 mg of a yellow oil are obtained (yield 48%).

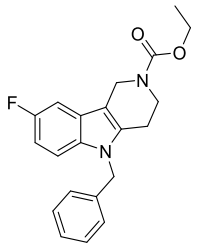

Compound **21b**. *Synthesis of ethyl 5-benzyl-8-fluoro-1,3,4,5-tetrahydro-2H-pyrido[4,3-b]indole-2-carboxylate. (FS83)*

The procedure followed was the same as the one for 5-benzyl-8-methoxy-1,3,4,5-tetrahydro-2*H*-pyrido[4,3-*b*]indole-2-carboxylate (**FS84**). Aspect: yellow oil. Yield: 54%. **^{1}H NMR** (300 MHz, cdcl3) δ 7.33 - 7.28 (m, 2H), 7.26 – 7.23 (m, 1H), 7.17 – 7.10 (m, 2H), 7.01 – 6.93 (m, 2H), 6.87 (td, *J* = 9.1, 2.5 Hz, 1H), 5.23 (s, 2H), 4.68 (s, 2H), 4.20 (q, *J* = 7.1 Hz, 2H), 3.85 (s, 2H), 2.74 (s, 2H), 1.30 (t, *J* = 7.2 Hz, 3H). **LC/MS** (ESI): RT [min] 8.465, *m/z* $[M+H]^+$ = 353.158, found 353.100. **IR (cm^{-1}) :** 2980, 2928, 1698, 1626, 1587, 1231, 1146, 1109, 901, 763.

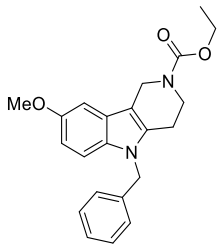

Compound **21c**. *Synthesis of ethyl 5-benzyl-8-methoxy-1,3,4,5-tetrahydro-2H-pyrido[4,3-b]indole-2-carboxylate. (FS84)*

NaH (1.8 mmol) is suspended in 4 mL of DMF and ethyl 8-methoxy-1,3,4,5-tetrahydro-2*H*-pyrido[4,3-*b*]indole-2-carboxylate (0.36 mmol) is added. The mixture is stirred at r.t. for 15 minutes, then cooled at 0 °C and benzylbromide (0.91 mmol) is added dropwise. The reaction mixture is stirred at r.t. overnight. **Work-up**. A TLC control 7 *n*-Hex: 3EA shows the formation of the product (r.f. = 0.35). The reaction mixture is extracted with EA and distilled water. 70 mg of a yellow oil are obtained, purified on chromatography column (gradient from 85:15 to 7:3, *n*-Hex/EA, rf = 0.35). Yield: 53% (70 mg) Aspect: yellow oil. **^{1}H NMR (300 MHz, cdcl$_3$) δ** 7.37 (d, *J* = 4.4 Hz, 1H), 7.25 – 7.21 (m, 2H), 7.12 (d, *J* = 8.8 Hz, 1H), 7.02 – 6.93 (m, 3H), 6.79 (dd, *J* = 8.8, 2.4 Hz, 1H), 5.22 (s, 2H), 4.70 (s, 2H), 4.20 (q, *J* = 7.1 Hz, 2H), 3.86 (s, 5H), 2.72 (s, 2H), 1.30 (t, *J* = 7.0 Hz, 3H).

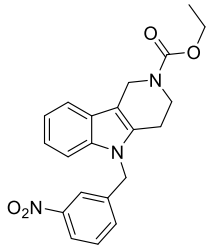

Compound **21d**. *Synthesis of ethyl 5-(3-nitrobenzyl)-1,3,4,5-tetrahydro-2H-pyrido[4,3-b]indole-2-carboxylate. (FS962C1F)*

A mixture of ethyl 1,3,4,5-tetrahydro-2*H*-pyrido[4,3-*b*]indole-2-carboxylate (0.8 mmol) and NaH 60% in m.o. (0.96 mmol) in 1 mL of dry DMF is stirred for 15

minuti under nitrogen. The misture is cooled to 0 °C and a solution of 3-nitrobenzylchloride in 2 mL of dry DMF is added. The reaction mixture is stirred overnight at 50 °C. A TLC control 7 (*n*-Hex: 3EA) shows the formation of the product (r.f. = 0.3). **Work-up.** The reaction mixture is extracted with EA and distilled water. The organic phase is dried over sodium sulfate, filtered and evaporated under vacuum. The crude product is purified on flash chromatography column (gradient from 9 *n*-Hex: 1EA to 7 *n*-Hex: 3EA). Yield: 30% (90 mg) Aspect: yellow wax. **^{1}H NMR** (300 MHz, cdcl$_3$) δ 8.10 (d, *J* = 7.0 Hz, 1H), 7.99 (s, 1H), 7.57 – 7.48 (m, 1H), 7.43 (t, *J* = 7.9 Hz, 1H), 7.22 – 7.08 (m, 4H), 5.34 (s, 2H), 4.75 (s, 2H), 4.20 (q, *J* = 7.1 Hz, 2H), 3.88 (s, 2H), 2.73 (s, 2H), 1.31 (t, *J* = 7.0 Hz, 3H). **^{13}C NMR** (126 MHz, cdcl$_3$) δ 148.60, 139.88, 136.56, 132.06, 130.01, 125.49, 122.65, 121.92, 121.17, 119.93, 118.04, 108.96, 61.58, 60.37, 45.79, 41.21, 14.73, 14.18. **LC/MS** (ESI) rt: 8.24 min, m/z calcd for [M+H+]: 380.2 , found: 380.1. **GC-MS:** r.t. 25.3 min, *m/z* calcd for [M$^{\bullet+}$]= 379, found 379. **IR** (KBr) cm^{-1}: 1697 (C=O st carbamate), 1531 (NO_2 st as), 1348 (NO_2 st sy), 1111 (indole).

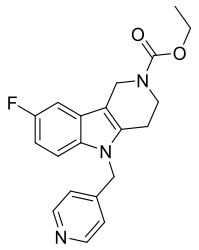

Compound **21e**. *Ethyl 8-fluoro-5-(pyridin-4-ylmethyl)-1,3,4,5-tetrahydro-2H-pyrido[4,3-b]indole-2-carboxylate. (FS91)* **^{1}H NMR (300 MHz, cdcl$_3$) δ** 8.51 (dd, *J* = 4.4, 1.6 Hz, 2H), 7.16 (dd, *J* = 9.2, 2.4 Hz, 1H), 7.05 (dd, *J* = 8.9, 4.2 Hz, 1H), 6.90 (dd, *J* = 9.1, 2.5 Hz, 1H), 6.85 (d, *J* = 5.9 Hz, 2H), 5.23 (s, 2H), 4.69 (s, 2H), 4.20 (q, *J* = 7.1 Hz, 2H), 3.86 (t, *J* = 5.1 Hz, 2H), 2.70 (t, *J* = 5.3 Hz, 2H), 1.30 (t, *J* = 7.1 Hz, 3H).

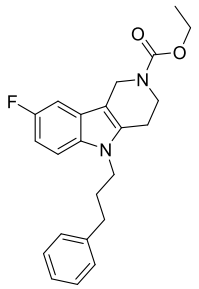

Compound **21g**. *Synthesis of ethyl 8-fluoro-5-(3-phenylpropyl)-1,3,4,5-tetrahydro-2H-pyrido[4,3-b]indole-2-carboxylate. (FS88)*

NaH (1.5 mmol) is suspended in 2 mL of DMF and ethyl 8-fluoro-1,3,4,5-tetrahydro-2*H*-pyrido[4,3-*b*]indole-2-carboxylate (FS81, 0.30 mmol) is added. The

mixture is stirred at r.t. for 15 minutes, then cooled at 0 °C and 1-bromo-3-phenylpropane (0.75 mmol) solubilized in 0.5 mL DMF is added dropwise. The reaction mixture is stirred at r.t. overnight. **Work-up**. A TLC control 7 *n*-Hex: 3EA shows the formation of the product (r.f. = 0.35). The reaction mixture is extracted with EA and distilled water. 160 mg of a brown oil are obtained, purified on chromatography column (7 *n*-Hex: 3EA, rf = 0.35). Yield: 44% (50 mg) Aspect: yellow oil. **^{1}H NMR (300 MHz, cdcl$_3$) δ** 7.34 – 7.26 (m, 2H), 7.22 (dt, *J* = 5.2, 2.1 Hz, 1H), 7.15 (d, *J* = 6.7 Hz, 2H), 7.12 – 7.09 (m, 1H), 7.08 (d, *J* = 3.0 Hz, 1H), 6.89 (td, *J* = 9.1, 2.4 Hz, 1H), 4.64 (s, 2H), 4.20 (q, *J* = 7.1 Hz, 2H), 4.02 (t, *J* = 7.5 Hz, 2H), 3.85 (s, 2H), 2.73 (t, *J* = 4.9 Hz, 2H), 2.65 (t, *J* = 7.6 Hz, 1H), 2.06 (quint, *J* = 7.2 Hz, 2H), 1.30 (t, *J* = 7.1 Hz, 3H). **LC/MS** (ESI) rt: 9.38 min, *m/z* calcd for [M+H$^+$]: 381.5 , found: 381.1.

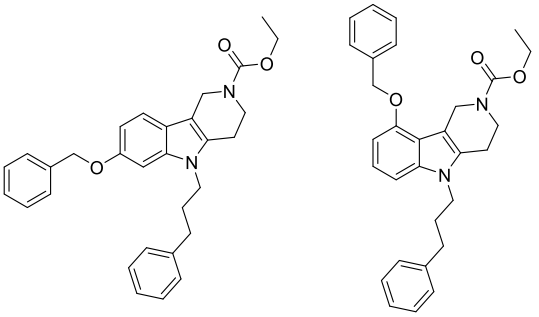

Compounds **21h** and **21j**. *Ethyl 7-(benzyloxy)-5-(3-phenylpropyl)-1,3,4,5-tetrahydro-2H-pyrido[4,3-b]indole-2-carboxylate and ethyl 9-(benzyloxy)-5-(3-phenylpropyl)-1,3,4,5-tetrahydro-2H-pyrido[4,3-b]indole-2-carboxylate. (FS99 mix)* The mixture of regioisomers was used without further purification.

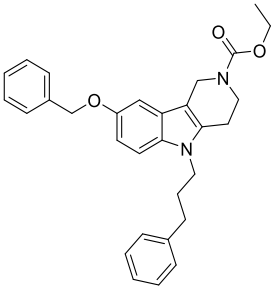

Compound **21i**. *Synthesis of ethyl 8-(benzyloxy)-5-(3-phenylpropyl)-1,3,4,5-tetrahydro-2H-pyrido[4,3-b]indole-2-carboxylate. (FS98)*

The procedure followed was the same as the one for 5-benzyl-8-methoxy-1,3,4,5-tetrahydro-2*H*-pyrido[4,3-*b*]indole-2-carboxylate (**FS84**). The crude product is purified on chromatography column (*n*-Hex/EA, rf = 0.5). Yield: 50% (70 mg) Aspect: yellow dense oil. **^{1}H NMR** (300 MHz, cdcl$_3$) δ 7.53 – 7.45 (m, 2H), 7.44 – 7.25 (m, 5H), 7.24 – 7.08

(m, 4H), 7.01 (d, *J* = 2.4 Hz, 1H), 6.90 (dd, *J* = 8.8, 2.4 Hz, 1H), 5.11 (s, 2H), 4.65 (s, 2H), 4.20 (q, *J* = 7.1 Hz, 2H), 4.00 (t, *J* = 6.9 Hz, 2H), 3.85 (br s, 2H), 2.73 (br s, 2H), 2.65 (t, *J* = 6.9 Hz, 2H), 2.06 (quint, *J* = 7.5 Hz, 2H), 1.61 (s, 1H), 1.31 (t, *J* = 7.1 Hz, 3H). **GC/MS:** RT [min] 71 *m/z* calcd for $[M^{\bullet+}]$ = 468, found 469, fragmentation 439, 377, 276, 91.

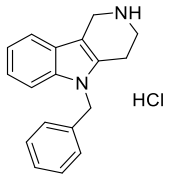

Compound **22a**. *5-benzyl-2,3,4,5-tetrahydro-1H-pyrido[4,3-b]indole hydrochloride. (NB543-B)* **^{1}H NMR** (300 MHz, dmso) δ 9.42 (s, 2H), 7.58 – 7.39 (m, 2H), 7.31 – 7.16 (m, 3H), 7.08 (m, 4H), 5.39 (s, 2H), 4.31 (s, 2H), 3.47 (t, *J* = 5.8 Hz, 1H), 3.00 (t, *J* = 5.3 Hz, 1H). **GC-MS**: retention time 15.067 min *m/z* calcd for $[C_{18}H_{18}N_2]^{+\bullet}$ = 262, found 262, fragments = 232, 218, 169, 142, 115, 91. **HRMS** (ESI-MS) calcd for $C_{18}H_{19}N_2^+$ *m/z*: $[M+H]^+$ = 263.3560, found $[M+H]^+$ = 263.1808.

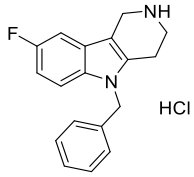

Compound **22b**. *Synthesis of 5-benzyl-8-fluoro-2,3,4,5-tetrahydro-1H-pyrido[4,3-b]indole. (FS83-B)*

The procedure followed was the same as the one for 5-benzyl-8-methoxy-2,3,4,5-tetrahydro-1*H*-pyrido[4,3-*b*]indole hydrochloride (**FS84-B**). Aspect: white solid. Yield: quantitative. **^{1}H NMR** (300 MHz, dmso) δ 9.46 (s, 2H), 7.47 (dd, *J* = 8.9, 4.4 Hz, 1H), 7.34 (dd, *J* = 9.8, 2.5 Hz, 1H), 7.31 – 7.21 (m, 3H), 7.06 (d, *J* = 6.8 Hz, 2H), 6.96 (td, *J* = 9.3, 2.5 Hz, 1H), 5.39 (s, 2H), 4.28 (s, 2H), 3.46 (t, *J* = 5.9 Hz, 2H), 3.00 (t, *J* = 5.6 Hz, 2H). **^{13}C NMR** (126 MHz, DMSO) δ 157.2 (d, *J* = 232.4 Hz, C-F), 137.8, 134.0, 133.1, 128.7, 127.4, 126.7, 125.0 (d, *J* = 10.3 Hz, **C**-C-CF), 111.1 (d, *J* = 9.7 Hz, **C**-C-CF), 109.5 (d, *J* = 25.8 Hz, **C**-CF), 103.2 (d, *J* = 23.9 Hz, **C**-CF), 102.6 (d, *J* = 4.4 Hz, **C**-C-C-CF), 46.0, 40.7, 19.5. **LC/MS** (ESI): RT [min] 6.322, *m/z* $[M+H]^+$ = 281.145, found 281.100.

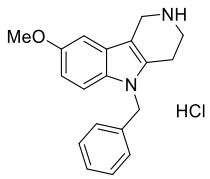

Compound **22c**. *Synthesis of 5-benzyl-8-methoxy-2,3,4,5-tetrahydro-1H-pyrido[4,3-b]indole hydrochloride (FS84-B).*

Deprotection of the corresponding ethyl carbamate is carried out in basic conditions. ethyl 5-benzyl-8-methoxy-1,3,4,5-tetrahydro-2*H*-pyrido[4,3-*b*]indole-2-carboxylate (0.3 mmol) is suspended is a 5 mL solution of EtOH/H_20 (9:1 *v/v*) and stirred under reflux for 1 hour and 30 minutes. A TLC (99 DCM:01 MeOH) reveals the disappearance of the starting material and the formation of the product. **Work-up.** The reaction mixture is cooled to room temperature, concentrated under vacuum and extracted with DCM and distilled water. The organic phase is dried over sodium sulfate and evaporated under vacuum. The product is precipitated as the corresponding hydrochloride salt using a solution of HCl 4M in dioxane (2.5 eq.). Yield: quantitative (90 mg). Aspect: white crystals. ^{1}H NMR (500 MHz, DMSO) δ 9.59 (s, 2H), 7.33 (d, *J* = 8.8 Hz, 1H), 7.28 (t, *J* = 7.3 Hz, 2H), 7.22 (t, *J* = 7.1 Hz, 1H), 7.07 (s, 1H), 7.05 (s, 2H), 6.74 (dd, *J* = 8.8, 2.0 Hz, 1H), 5.33 (s, 2H), 4.27 (s, 2H),3.75 (s, 3H), 3.45 (d, *J* = 3.6 Hz, 2H), 2.99 (t, *J* = 5.1 Hz, 2H). **^{13}C NMR** (126 MHz, DMSO) δ 153.8, 138.2, 132.3, 131.5, 128.7, 127.3, 126.6, 125.2, 111.2, 110.8, 102.0, 100.4, 55.5, 45.9, 40.8, 19.4. **LC/MS** (ESI): RT [min] 6.079, *m/z* $[M+H]^+$ calc. 293.158, found 293.100.

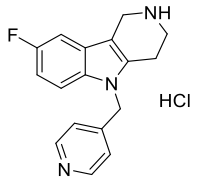

Compound **22d**. *8-fluoro-5-(pyridin-4-ylmethyl)-2,3,4,5-tetrahydro-1H-pyrido[4,3-b]indole. (FS91-B)*

^{1}H NMR (400 MHz, CD3OD) δ 8.79 (s, 2H), 7.64 (s, 2H), 7.31 (s, 2H), 6.98 (s, 1H), 5.82 (s, 2H), 4.52 (s, 2H), 3.69 (s, 2H), 3.17 (s, 2H). **^{1}H NMR (300 MHz, dmso) δ** 9.67 (s, 2H, disappears in exchange with D_2O), 8.73 (s, 2H), 7.42 (dd, *J* = 8.6, 4.2 Hz, 2H), 7.37 (dd, *J* = 6.5, 3.7 Hz, 2H), 6.98 (td, *J* = 9.2, 1.8 Hz, 1H), 5.70 (s, 2H), 4.29 (s, 2H), 3.45 (s, 2H), 2.97 (s, 2H). **HRMS** (ESI-MS) calcd for $C_{17}H_{17}FN_3^+$ $[M+H]^+$ *m/z* = 282,1401, found $[M+H]^+$ = 282.1411, fragmentation 253.1138, 237.0834, 189.0806, 161.0635, 93.0575, 65.0390.

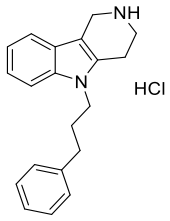

Compound **22e**. *5-(3-phenylpropyl)-2,3,4,5-tetrahydro-1H-pyrido[4,3-b]indole hydrochloride. (NB555-B)* **^{1}H NMR** (500 MHz, dmso) δ 9.39 (s, 2H), 7.47 (d, *J* = 7.8 Hz, 1H), 7.40 (d, *J* = 8.2 Hz, 1H), 7.26 (t, *J* = 7.5 Hz, 2H), 7.17 (d, *J* = 7.4 Hz, 3H), 7.13 (t, *J* = 7.6 Hz, 1H), 7.03 (t, *J* = 7.4 Hz, 1H), 4.29 (s, 2H), 4.13 (t, *J* = 7.2 Hz, 2H), 3.47 (t, *J* = 5.4 Hz, 2H), 3.03 (t, *J* = 4.7 Hz, 2H), 2.64 – 2.53 (m, 1H), 1.94 (quint, *J* = 7.4 Hz, 2H). **HRMS** (ESI-MS) calcd for $C_{20}H_{23}N_2^+$ *m/z*: $[M+H]^+$ = 291.4100, found $[M+H]^+$ = 291.1796.

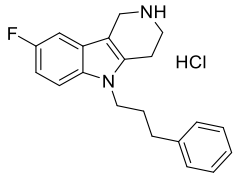

Compound **22f**. *Synthesis of 8-fluoro-5-(3-phenylpropyl)-2,3,4,5-tetrahydro-1H-pyrido[4,3-b]indole hydrochloride. (**FS88-B**)*

Deprotection of the corresponding ethyl carbamate is carried out in basic conditions. Ethyl 8-fluoro-5-(3-phenylpropyl)-1,3,4,5-tetrahydro-2*H*-pyrido[4,3-*b*]indole-2-carboxylate (0.13 mmol) is suspended is a 5 mL solution of EtOH/H_20 (9:1 *v/v*) and stirred under reflux for one hour. A TLC (99 DCM:01 MeOH) reveals the disappearance of the starting material and the formation of the product. **Work-up.** The reaction mixture is cooled to room temperature, concentrated under vacuum and extracted with DCM and distilled water. The organic phase is dried over sodium sulfate and evaporated under vacuum. The product is precipitated as the corresponding hydrochloride salt using a solution of HCl 4M in dioxane (2.5 eq.). Yield: quantitative (37 mg). Aspect: white crystals. **^{1}H NMR (300 MHz, dmso) δ** 9.56 (s, 2H), 7.43 (dd, *J* = 8.9, 4.4 Hz, 1H), 7.30 (dd, *J* = 9.5, 2.0 Hz, 1H), 7.27 – 7.22 (m, 2H), 7.17 (d, *J* = 7.0 Hz, 3H), 4.24 (s, 2H), 4.13 (t, *J* = 7.1 Hz, 2H), 3.45 (s, 2H), 3.02 (t, *J* = 5.7 Hz, 2H), 2.63 – 2.52 (m, 2H), 1.93 (quint, *J* = 7.5 Hz, 2H). **LC/MS** (ESI) rt: 6.83 min, *m/z* calcd for [M+H$^+$]: 309.176 , found: 309.200.

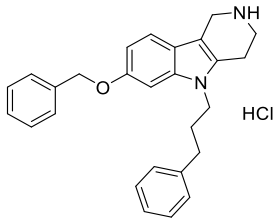

Compound **22g**. *7-(benzyloxy)-5-(3-phenylpropyl)-2,3,4,5-tetrahydro-1H-pyrido[4,3-b]indole hydrochloride. (FS99-B)*

^{1}H NMR (400 MHz, $CDCl_3$) δ 7.48 (d, *J* = 7.3 Hz, 2H), 7.40 (t, *J* = 7.4 Hz, 2H), 7.36 – 7.26 (m, 4H), 7.26 – 7.20 (m, 1H), 7.18 (d, *J* = 7.3 Hz, 2H), 6.85 (dd, *J* =

8.6, 1.9 Hz, 1H), 6.74 (d, *J* = 1.7 Hz, 1H), 5.08 (s, 2H), 4.19 (s, 2H), 4.01 – 3.91 (m, 2H), 3.36 (t, *J* = 5.6 Hz, 2H), 2.82 (t, *J* = 4.6 Hz, 2H), 2.66 (t, *J* = 7.5 Hz, 2H), 2.14 – 2.00 (m, 2H). **LC/MS** (ESI)**:** RT [min] 8.421, calcd for $C_{27}H_{29}N_2O^+$ *m/z* $[M+H]^+$ = 397.227, found 397.200.

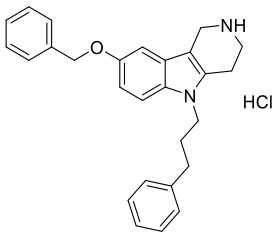

Compound **22h**. *Synthesis of 8-(benzyloxy)-5-(3-phenylpropyl)-2,3,4,5-tetrahydro-1H-pyrido[4,3-b]indole hydrochloride. (FS98-B)*

The procedure followed was the same as the one for 5-benzyl-8-methoxy-2,3,4,5-tetrahydro-1*H*-pyrido[4,3-*b*]indole hydrochloride (**FS84-B**). Aspect: white solid. Yield: quantitative. **^{1}H NMR (400 MHz, DMSO) δ** 9.30 (s, 2H), 7.47 (d, *J* = 7.0 Hz, 2H), 7.40 (t, *J* = 7.3 Hz, 2H), 7.36 – 7.32 (m, 2H), 7.29 (dd, *J* = 10.4, 4.4 Hz, 2H), 7.22 – 7.17 (m, 3H), 7.15 (d, *J* = 2.4 Hz, 1H), 6.87 (dd, *J* = 8.9, 2.4 Hz, 1H), 5.10 (s, 2H), 4.27 (s, 2H), 4.11 (t, *J* = 7.3 Hz, 2H), 3.49 (d, *J* = 5.8 Hz, 2H), 3.02 (t, *J* = 5.7 Hz, 2H), 2.65 – 2.53 (m, 2H), 2.01 – 1.86 (quint, *J* = 7.3 Hz, 2H). **LC/MS** (ESI)**:** RT [min] 9.141, calcd for $C_{27}H_{29}N_2O^+$ *m/z* $[M+H]^+$ = 397.227, found 397.200.

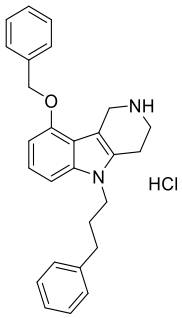

Compound **22i**. *9-(benzyloxy)-5-(3-phenylpropyl)-2,3,4,5-tetrahydro-1H-pyrido[4,3-b]indole hydrochloride. (FS100r)*

^{1}H NMR (400 MHz, $CDCl_3$) δ 7.47 (t, *J* = 9.2 Hz, 2H), 7.40 (dd, *J* = 10.1, 4.7 Hz, 2H), 7.32 (dd, *J* = 13.1, 6.2 Hz, 2H), 7.22 (t, *J* = 4.8 Hz, 1H), 7.18 (d, *J* = 6.9 Hz, 2H), 7.04 (t, *J* = 8.0 Hz, 1H), 7.04 (t, *J* = 8.0 Hz, 2H), 6.85 (d, *J* = 8.1 Hz, 1H), 6.54 (d, *J* = 7.8 Hz, 1H), 5.17 (s, 2H), 4.38 (s, 2H), 4.05 – 3.97 (m, 2H), 3.29 (t, *J* = 5.7 Hz, 2H), 2.75 (t, *J* = 5.5 Hz, 2H), 2.71 – 2.65 (m, 2H), 2.09 (quint, *J* = 7.6 Hz, 2H). **LC/MS** (ESI)**:** RT [min] 8.700, calcd for $C_{27}H_{29}N_2O^+$ *m/z* $[M+H]^+$ = 397.227, found 397.200.

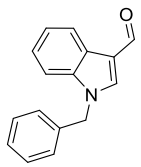

Compound **24a**. *Synthesis of 1-benzyl-1H-indole-3-carbaldehyde*. *(RP297)*

To a suspension of NaH 60% in oil (2.25 mmol) in dry DMF (1.8 mL) was added at 0° and under organ atmosphere, a solution of indole carboxaldhehyde (1 mmol) in dry DMF (1 ml)) [color changed from yellow to peach]. After stirring for 30 min at rt, benzyl bromide (1 ml, 2.25 mmol) was slowly added. After stirring overnight, the mixture was poured into a water-ice mixture, and a white-pink solid precipitated. The crude product was treated with Hexane and decanted. The precipitate obtained was the desired product. (167 mg =0.71 mmol). Yield :71%. ^{1}H NMR (300 MHz, cdcl3) δ 9.98 (s, 2H), 8.38 – 8.27 (m, 2H), 7.73 (s, 2H), 7.42 – 7.26 (m, 6H), 7.19 (dd, J = 4.9, 2.8 Hz, 1H), 5.36 (s, 2H). (known compound, Meguellati A, et al. Eur J Med Chem. 2014 Jun 10;80:579-92. doi: 10.1016/j.ejmech.2014.04.005).

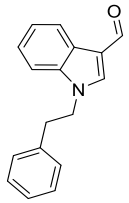

Compound **24b**. *Synthesis of 1-phenethyl-1H-indole-3-carbaldehyde. (RP292)*

To a suspension of NaH 60% (4 mmol) in oil in dry DMF (1.8ml) was added, at 0° and under nitrogen atmosphere, a solution of indole carboxaldehyde (1 mmol) in dry DMF (1ml) [color changed from yellow to peach]. After stirring for 30 min at rt, alkyl halide (456 µL, 2.25 mmol) was slowly added. [The mixture became orange and then the color changed to yellow]. After stirring for 5hs, the reaction was quenched by addition of water, and the product was extracted with diethyl ether. The organic layer was dried over NaSO4, filtered, and concentrated under vacuum obtaining a yellow-orange oil. The crude product was taken up with hexane and decanted obtaining 168 mg (0.67 mmol) of powder. Then the precipitate was purified by column chromatography (Hex/EtOAc 7:3) to obtain 136 mg (0.55 mmol). Yield: 55% ^{1}H NMR (500 MHz, cdcl3) δ 9.87 (s, 1H, CHO), 8.31 (dd, J = 6.4, 2.4 Hz, 1H), 7.45 – 7.16 (m, 6H), 7.11 – 6.92 (m, 2H), 4.41 (t, J = 7.1 Hz, 2H), 3.15 (t, J = 7.0 Hz, 2H). (known compound, Meguellati A, et al. Eur

J Med Chem. 2014 Jun 10;80:579-92. doi: 10.1016/j.ejmech.2014.04.005).

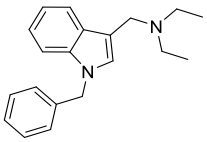

Compound **25a.** *Synthesis of N-[(1-benzyl-1H-indol-3-yl)methyl]-N-ethylethanamine. (RP300)*

To a solution of amine (0.28 mmol) and pTsOH (0.28 mmol) in (2.8 ml) MeOH was added a solution of RP297 (0.25 mmol) in MeOH (2.5 ml) and after 30 min $Na(CN)BH_3$ (0.55 mmol) was added. The reaction was stirred at reflux for 2 days. Then, the reaction was cooled to room temperature and the solvent (MeOH) was evaporated under vacuum. Then the residue was taken up with Na_2CO_3 s.s. and extracted with EtOAc. The organic layer was then dried with Na_2SO_4, filtered, and evaporated to obtain 40 mg=0.14 mmol=Yield:55%. The HCl salt of the compound was made using 1 mL of a solution of HCl (4M) in dry dioxane in a solution of 20 mg of compound in 2 mL od DCM. Afrter 1 hour stirring, the solvent was evaporated under vacuum, and the residue taken up with hexane. The hexane was decanted and the precipitate was the desired salt (19 mg, 0,052 mmol, yield 74%). ESI-MS: $[M+H]^+$ calculated 293.2012, found 293.2017; IR: 3424, 2940, 2649, 1631, 1546, 1468, 1454 cm^{-1}. ^1H NMR (300 MHz, cdcl3) δ 11.86 (s, 1H), 7.90 (s, 1H), 7.57 (s, 1H), 7.36 – 7.09 (m, 7H), 5.35 (s, 2H), 4.39 (s, 2H), 3.18 (s, 2H), 3.05 (s, 2H), 1.47 (s, 6H).

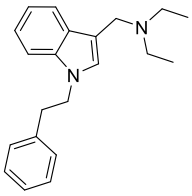

Compound **25b.** *Synthesis of N-ethyl-N-[(1-phenethyl-1H-indol-3-yl)methyl]ethanamine. (RP301)*

To a solution of amine (0.28 mmol) and pTsOH (0.28 mmol) in (2.8 ml) MeOH was added a solution of RP297 (0.25 mmol) in MeOH (2.5 ml) and after 30 min $Na(CN)BH_3$ (0.55 mmol) was added. The reaction was stirred at reflux for 2 days. Then, the reaction was cooled to room temperature and the solvent (MeOH) was evaporated under vacuum. Then the residue was taken up with Na_2CO_3 s.s. and extracted with EtOAc. The organic layer was then dried with Na_2SO_4, filtered, and evaporated to obtain 40 mg=0.14 mmol=Yield:42%. ESI-MS: $[M+H]^+$ calculated 307.2169, found 307.2169, $[M+Na]^+$ calculated 329.1988, found 329.1992; IR:

2967, 2931,1467, 1332 cm^{-1}. ^1H NMR (300 MHz, cdcl3) δ 7.70 (d, *J* = 7.9 Hz, 1H), 7.38 – 7.02 (m, 7H), 6.89 (s, 1H), 4.33 (t, *J* = 7.3 Hz, 2H), 3.80 (s, 2H), 3.10 (t, *J* = 7.3 Hz, 2H), 2.56 (q, *J* = 7.2 Hz, 4H), 1.11 (t, *J* = 7.1 Hz, 6H).

9.2 Radioligand binding assay (CB_1 and CB_2)

The investigation of the compounds was performed using competition radioligand binding assay at *h*CB_1 and *h*CB_2 receptors. Competition binding assays were performed using the unselective CB agonist radioligand [^3H](-)-*cis*-3-[2-hydroxy-4-(1,1-dimethyl-heptyl)phenyl]-*trans*-4-(3-hydroxypropyl)cyclohexanol (CP55,940, at final concentration 0.1 nM). As a source for human CB_1 and CB_2 receptors, membrane preparations of the CHO cells stably expressing the human CB_1 or human CB_2 subtype were used (36 µg of protein/well for CB_1 and 16 µg of protein/well for CB_2 receptor preparations). Stock solutions of the test compounds were prepared in DMSO. After addition of 465µL assay buffer [50 mM Tris, 3 mM $MgCl_2$, 0.1 % bovine serum albumin (BSA), pH 7.4], 15 µL of the test compound in DMSO were added into the reaction plate, followed by 60 µL of [^3H]CP55,940 solutions in assay buffer, and 60 µL of membrane preparation. The suspension was incubated for 2 hours at room temperature. Total binding was determined by adding DMSO without test compound. Nonspecific binding was determined in the presence of 10 µM of unlabeled CP55,940. Incubation was terminated by rapid filtration through a GF/C glass fiber filter that presoaked for 0.5 h with 0.3 % aq. Polyethyleneimine (PEI) solution, using a Brandel 96-channel cell harvester. The filter was washed three times with ice-cold washing buffer (50 mM Tris, 0.1 % BSA, pH 7.4) and dried for 1.5 at 50°C. Radioactivity on the filter was determined in a liquid scintillation counter after 10 h of preincubation with 50 µl of scintillation cocktail. Data were obtained in three independent experiments, performed in duplicates.

9.3 *β*-arrestin enzyme recruitment assay (GPR18 and GPR55)

Recruitment of β-arrestin to the respective receptor was detected by using the β-galactosidase enzyme fragment complementation technology (β-arrestin PathHunter™ assay, DiscoverX, Fremont, CA, USA). CHO cells stably expressing the respective receptor were seeded in a volume of 90 µL into a 96-well plate and were incubated at a density of 40,000 cells/well for GPR18 and 35,000 cells/well for GPR55 in assay medium (Opti-MEM, 2 % FCS, 100 U/mL penicillin, 100 µg/mL Streptomycin, 800 µg/mL geneticin und 300 µg/mL hygromycin) for 24 h

at 37°C. After the given incubation, test compounds were diluted in PBS buffer containing 10 % DMSO and 0.1 % BSA and added to the cells in a volume of 5 µL (for antagonist) or 10 µL (for agonist), followed by incubation for 90 min at 37°C. For determination of baseline luminescence, PBS buffer (containing 10 % DMSO, 0.1 % BSA) in the absence of test compound was used. During the incubation period, the detection reagent was prepared. For determination of β -arrestin recruitment to GPR18 the provided detection reagent was used, according to the supplier's protocol. The detection reagent for GPR55 was varied and obtained by mixing the chemiluminescent substrate Galacton-Star® (2 mM), with the luminescence enhancer Emerald-II™ and a lysis buffer (10 mM TRIS, 1 mM EDTA, 100 mM NaCl, 5 mM $MgCl_2$, 1 % Triton-X; pH 8) in a ratio of 1:4:17 for GPR18 and 1:20:80 for GPR55. After the addition of 50 µL/well of detection reagent to the cells, the plate was incubated for further 60 min at room temperature. Finally, luminescence was determined in a luminometer (TopCount NXT, Packard / Perkin-Elmer).

9.4 Cholinesterases inhibition assays

The test compounds were tested for their inhibitory activity towards electric eel and horse serum AChE and BChE (Sigma-Aldrich), following Ellman's method (DOI: 10.1016/0006-2952(61)90145-9). Enzyme activity was determined in a mixture containing 20 µL of a solution of AChE (1U/mL in 0.1 M phosphate buffer, PB, pH 8.0) or BChE (2U/mL in 0.1 M, PB, pH 8.0), 20 µL of a solution of 5,5-dithio-bis-(2-nitrobenzoic) acid (DTNB 3.3 mM in 0.1 M PB pH 7.0, containing 0.1 mM NaHCO3), 20 µL of a solution of the test compound (100 µM, pH 8.0 PB, 1% DMSO), and 120 µL of PB, pH 8.0. After incubation for 20 min at 25 °C, the substrate (acetylthiocholine iodide or butyrylthiocholine iodide 20 µL, 0.5 mM in PB, pH 8.0) was added and its hydrolysis rates were monitored at 412 nm for 10.0 min at 25 °C. Data were elaborated using Prisma GraphPad software vers. 10.2.3.

9.5 Docking studies

The 3D structures of CB1 and CB2 receptors were collected from the Protein Data Bank database by retrieving the entries 5TGZ and 5ZTY, respectively. The protein preparation wizard tool implemented in the Schrödinger suite was employed to carry out energy minimization on the protein structures, to remove nonstructural water molecules and ions, and assign protonation and tautomeric states of Asp, Arg, Glu, His and Lys residues at physiological pH. 6,7. Next, the ligands were treated

with the LigPrep module implemented in Maestro, using the OPLS4 force field and by employing Epik for the evaluation of ligands protonation states and tautomers at physiological pH. The grid boxes were centered on the centers of mass of CB1 and CB2 receptors cognate ligands.

To validate the protocol, redocking simulations of each co-crystalized ligand were performed. Satisfactorily, the poses obtained from this analysis returned an RMSD (Root Mean Square Deviation) accounted for all heavy atoms equal to 0.25 Å, 0.43 Å, for CB1 and CB2 receptors, respectively. Furthermore, molecular docking analyses were also performed on the CB1 receptor structure containing a co-crystallized allosteric modulator, whose PDB code is 6KQI.

10 PUBLICATIONS

- Purgatorio, R. et al. *Assessing the Role of a Malonamide Linker in the Design of Potent Dual Inhibitors of Factor Xa and Cholinesterases*. Molecules 27, 4269 (**2022**).

- Czarnota-Łydka, K. et al. *Synthesis, computational and experimental pharmacological studies for (thio)ether-triazine 5-HT$_6$R ligands with noticeable action on AChE/BChE and chalcogen-dependent intrinsic activity in search for new class of drugs against Alzheimer's disease.* European Journal of Medicinal Chemistry 259, 115695 (**2023**).

- Lee, SH et al. *Radiosynthesis and whole-body distribution in mice of a ^{18}F-labeled azepino[4,3-b]indole-1-one derivative with multimodal activity for the treatment of Alzheimer's disease*. Archiv der Pharmazie *e2300491* (**2023**)

- Samarelli, F. et al. *Small Molecules for the Treatment of Long-COVID-Related Vascular Damage and Abnormal Blood Clotting: A Patent-Based Appraisal*. Viruses 16, 450 (**2024**).

- Mele, M. et al. *Pleiotropic Effects of Direct Oral Anticoagulants in Chronic Heart Failure and Atrial Fibrillation: Machine Learning Analysis*. Molecules 29, 2651 (**2024**).

- Samarelli, F. et al. *Novel 6-alkyl-bridged 4-arylalkylpiperazin-1-yl derivatives of azepino[4,3-b]indol-1(2H)-one as potent BChE-selective inhibitors showing protective effects against neurodegenerative insults.* European Journal of Medicinal Chemistry 270, 116353 (**2024**).

- Carrieri, A. et al. *Chiral pyrrolidines as multipotent agents in Alzheimer and neurodegenerative diseases.* Bioorganic & Medicinal Chemistry 110, 117829 (**2024**).

- Samarelli, F. et al. *Advances in synthesis of novel annulated azecines and their unique pharmacological properties.* European Journal of Medicinal Chemistry 280, 116947 (**2024**).

11 CONGRESSES AND SEMINARS

- Member of the organizing staff and presenter of a poster entitled "*New peptidomimetic inhibitors of blood coagulation factors with potential against SARS-CoV-2 infection*" at the National Meeting of Medicinal Chemistry, Bari, **September 2022**.

- Parma Summer School 2022 entitled *"Risk Assessment of Regulated Products"* organized by the European Food Safety Agency (EFSA), **September 2022**.

- Oral presentation entitled "*New peptidomimetic inhibitors of blood coagulation factors with potential against SARS-CoV-2 infection"* at the national conference Chimica Sotto L'Albero, Polytechnic University of Bari, **December 2022**.

- "*Training course Promoting research and innovation in an evolving regulatory framework*" organized by the Gianni Benzi Foundation for Pharmacological Research Onlus in collaboration with the University of Bari, Bari, **December 2022**.

- Oral presentation entitled "*Tetrahydroazepino[4,3-b]indole(1H)-2-one derivatives as novel multifunctional agents with potential neuroprotective activities against neurodegenerative diseases*" at the IX edition of the European Workshop in Drug Synthesis, held at the Certosa di Pontignano (SI), from 21st to 24th **May 2023**.

- Participation at the 42nd edition of the European School of Medicinal Chemistry (ESMEC) - Advanced Course of Medicinal Chemistry and Seminar for PhD students, held in Urbino from 2nd to 6th **July 2023**.

- Oral presentation entitled "*Novel azepino [4,3-b]indole derivatives as ligands of the cannabinoid activated orphan receptors GPR18 nad GPR55 with potential against neurodegenerative diseases*" at the XXVIIIth edition of the National Meeting of Medicinal Chemistry 2023 held in Chieti from 17th to 20th **September 2023**.

- Oral presentation entitled "*Tetrahydroazepino[4,3-b]indole(1H)-2-one as scaffold of novel multifunctional agents for neurodegenerative diseases*" at the national conference "Chimica Sotto L'Albero", at the Department of Biosciences, Biotechnology and Environment of the University of Bari**, December 2023**.

- Oral presentation entitled " *Multitarget Neuroprotective Potential of Novel BChE-Selective Inhibitors 6-Alkyl-Bridged 4-Arylalkylpiperazin-1-yl Azepino[4,3-b]indol-1(2H)-ones*" at the 28th national conference of the Italian Chemical Society "XXVIII CONGRESSO NAZIONALE SCI", at the Centro Congressi Allianz MiCo, Milan, **August 2024**.

12 REFERENCES

(1) Cristino, L.; Bisogno, T.; Di Marzo, V. Cannabinoids and the Expanded Endocannabinoid System in Neurological Disorders. *Nat Rev Neurol* **2020**, *16* (1), 9–29. https://doi.org/10.1038/s41582-019-0284-z.

(2) Pathak, C.; Kabra, U. D. A Comprehensive Review of Multi-Target Directed Ligands in the Treatment of Alzheimer's Disease. *Bioorganic Chemistry* **2024**, *144*, 107152. https://doi.org/10.1016/j.bioorg.2024.107152.

(3) Petrosino, S.; Di Marzo, V. The Pharmacology of Palmitoylethanolamide and First Data on the Therapeutic Efficacy of Some of Its New Formulations. *British J Pharmacology* **2017**, *174* (11), 1349–1365. https://doi.org/10.1111/bph.13580.

(4) Samarelli, F.; Purgatorio, R.; Lopopolo, G.; Deruvo, C.; Catto, M.; Andresini, M.; Carrieri, A.; Nicolotti, O.; De Palma, A.; Miniero, D. V.; De Candia, M.; Altomare, C. D. Novel 6-Alkyl-Bridged 4-Arylalkylpiperazin-1-Yl Derivatives of Azepino[4,3-b]Indol-1(2H)-One as Potent BChE-Selective Inhibitors Showing Protective Effects against Neurodegenerative Insults. *European Journal of Medicinal Chemistry* **2024**, *270*, 116353. https://doi.org/10.1016/j.ejmech.2024.116353.

(5) Lee, S. H.; Purgatorio, R.; Samarelli, F.; Catto, M.; Denora, N.; Morgese, M. G.; Tucci, P.; Trabace, L.; Kim, H. W.; Park, H. S.; Kim, S. E.; Lee, B. C.; De Candia, M.; Altomare, C. D. Radiosynthesis and Whole-body Distribution in Mice of a ^{18}F-labeled Azepino[4,3- *b*]Indole-1-one Derivative with Multimodal Activity for the Treatment of Alzheimer's Disease. *Archiv der Pharmazie* **2023**, e2300491. https://doi.org/10.1002/ardp.202300491.

(6) Imming, P. Medicinal Chemistry. In *The Practice of Medicinal Chemistry*; Elsevier, 2015; pp 3–13. https://doi.org/10.1016/B978-0-12-417205-0.00001-8.

(7) Zhang, M.; Chen, T.; Lu, X.; Lan, X.; Chen, Z.; Lu, S. G Protein-Coupled Receptors (GPCRs): Advances in Structures, Mechanisms and Drug Discovery. *Sig Transduct Target Ther* **2024**, *9* (1), 88. https://doi.org/10.1038/s41392-024-01803-6.

(8) Casadó, V.; Casadó-Anguera, V. What Are the Current Trends in G Protein-Coupled Receptor Targeted Drug Discovery? *Expert Opinion on Drug Discovery* **2023**, *18* (8), 815–820. https://doi.org/10.1080/17460441.2023.2216014.

(9) Mao, C.; Xiao, P.; Tao, X.-N.; Qin, J.; He, Q.-T.; Zhang, C.; Guo, S.-C.; Du, Y.-Q.; Chen, L.-N.; Shen, D.-D.; Yang, Z.-S.; Zhang, H.-Q.; Huang, S.-M.; He, Y.-H.; Cheng, J.; Zhong, Y.-N.; Shang, P.; Chen, J.; Zhang, D.-L.; Wang, Q.-L.; Liu, M.-X.; Li, G.-Y.; Guo, Y.; Xu, H. E.; Wang, C.; Zhang, C.; Feng, S.; Yu, X.; Zhang, Y.; Sun, J.-P. Unsaturated Bond Recognition Leads to Biased Signal in a Fatty Acid Receptor. *Science* **2023**, *380* (6640), eadd6220. https://doi.org/10.1126/science.add6220.

(10) Wang, P.; Raja, A.; Luscombe, V. B.; Bataille, C. J. R.; Lucy, D.; Rogga, V. V.; Greaves, D. R.; Russell, A. J. Development of Highly Potent, G-Protein Pathway Biased, Selective, and Orally Bioavailable GPR84 Agonists. *J. Med. Chem.* **2024**, *67* (1), 110–137. https://doi.org/10.1021/acs.jmedchem.3c00951.

(11) Townsend, C. Ion Channels. In *Comprehensive Pharmacology*; Elsevier, 2022; pp 118–150. https://doi.org/10.1016/B978-0-12-820472-6.00003-7.

(12) Khilnani, G.; Khilnani, A. Inverse Agonism and Its Therapeutic Significance. *Indian J Pharmacol* **2011**, *43* (5), 492. https://doi.org/10.4103/0253-7613.84947.

(13) Zhang, J.; Feng, H.; Xu, S.; Feng, P. Hijacking GPCRs by Viral Pathogens and Tumor. *Biochemical Pharmacology* **2016**, *114*, 69–81. https://doi.org/10.1016/j.bcp.2016.03.021.

(14) Jacobson, K. A. New Paradigms in GPCR Drug Discovery. *Biochemical Pharmacology* **2015**, *98* (4), 541–555. https://doi.org/10.1016/j.bcp.2015.08.085.
(15) Devane, W. A.; Dysarz, F. A.; Johnson, M. R.; Melvin, L. S.; Howlett, A. C. Determination and Characterization of a Cannabinoid Receptor in Rat Brain. *Mol Pharmacol* **1988**, *34* (5), 605–613.
(16) Matsuda, L. A.; Lolait, S. J.; Brownstein, M. J.; Young, A. C.; Bonner, T. I. Structure of a Cannabinoid Receptor and Functional Expression of the Cloned cDNA. *Nature* **1990**, *346* (6284), 561–564. https://doi.org/10.1038/346561a0.
(17) Munro, S.; Thomas, K. L.; Abu-Shaar, M. Molecular Characterization of a Peripheral Receptor for Cannabinoids. *Nature* **1993**, *365* (6441), 61–65. https://doi.org/10.1038/365061a0.
(18) Devane, W. A.; Hanuš, L.; Breuer, A.; Pertwee, R. G.; Stevenson, L. A.; Griffin, G.; Gibson, D.; Mandelbaum, A.; Etinger, A.; Mechoulam, R. Isolation and Structure of a Brain Constituent That Binds to the Cannabinoid Receptor. *Science* **1992**, *258* (5090), 1946–1949. https://doi.org/10.1126/science.1470919.
(19) Jung, K.-M.; Astarita, G.; Yasar, S.; Vasilevko, V.; Cribbs, D. H.; Head, E.; Cotman, C. W.; Piomelli, D. An Amyloid B42-Dependent Deficit in Anandamide Mobilization Is Associated with Cognitive Dysfunction in Alzheimer's Disease. *Neurobiology of Aging* **2012**, *33* (8), 1522–1532. https://doi.org/10.1016/j.neurobiolaging.2011.03.012.
(20) Altamura, C.; Ventriglia, M.; Martini, M. G.; Montesano, D.; Errante, Y.; Piscitelli, F.; Scrascia, F.; Quattrocchi, C.; Palazzo, P.; Seccia, S.; Vernieri, F.; Di Marzo, V. Elevation of Plasma 2-Arachidonoylglycerol Levels in Alzheimer's Disease Patients as a Potential Protective Mechanism against Neurodegenerative Decline. *JAD* **2015**, *46* (2), 497–506. https://doi.org/10.3233/JAD-142349.
(21) Di Iorio, G.; Lupi, M.; Sarchione, F.; Matarazzo, I.; Santacroce, R.; Petruccelli, F.; Martinotti, G.; Di Giannantonio, M. The Endocannabinoid System: A Putative Role in Neurodegenerative Diseases. *Int J High Risk Behav Addict* **2013**, *2* (3), 100–106. https://doi.org/10.5812/ijhrba.9222.
(22) Mulder, J.; Zilberter, M.; Pasquaré, S. J.; Alpár, A.; Schulte, G.; Ferreira, S. G.; Köfalvi, A.; Martín-Moreno, A. M.; Keimpema, E.; Tanila, H.; Watanabe, M.; Mackie, K.; Hortobágyi, T.; De Ceballos, M. L.; Harkany, T. Molecular Reorganization of Endocannabinoid Signalling in Alzheimer's Disease. *Brain* **2011**, *134* (4), 1041–1060. https://doi.org/10.1093/brain/awr046.
(23) Bilsland, L. G.; Dick, J. R. T.; Pryce, G.; Petrosino, S.; Di Marzo, V.; Baker, D.; Greensmith, L.; Bilsland, L. G.; Dick, J. R. T.; Pryce, G.; Petrosino, S.; Di Marzo, V.; Baker, D.; Greensmith, L. Increasing Cannabinoid Levels by Pharmacological and Genetic Manipulation Delays Disease Progression in SOD1 Mice. *FASEB j.* **2006**, *20* (7), 1003–1005. https://doi.org/10.1096/fj.05-4743fje.
(24) Novotna, A.; Mares, J.; Ratcliffe, S.; Novakova, I.; Vachova, M.; Zapletalova, O.; Gasperini, C.; Pozzilli, C.; Cefaro, L.; Comi, G.; Rossi, P.; Ambler, Z.; Stelmasiak, Z.; Erdmann, A.; Montalban, X.; Klimek, A.; Davies, P.; the Sativex Spasticity Study Group. A Randomized, Double-Blind, Placebo-Controlled, Parallel-Group, Enriched-Design Study of Nabiximols* (Sativex®), as Add-on Therapy, in Subjects with Refractory Spasticity Caused by Multiple Sclerosis: Sativex for Refractory Spasticity in MS. *European Journal of Neurology* **2011**, *18* (9), 1122–1131. https://doi.org/10.1111/j.1468-1331.2010.03328.x.
(25) Katona, I.; Freund, T. F. Endocannabinoid Signaling as a Synaptic Circuit Breaker in Neurological Disease. *Nat Med* **2008**, *14* (9), 923–930. https://doi.org/10.1038/nm.f.1869.

(26) Mátyás, F.; Urbán, G. M.; Watanabe, M.; Mackie, K.; Zimmer, A.; Freund, T. F.; Katona, I. Identification of the Sites of 2-Arachidonoylglycerol Synthesis and Action Imply Retrograde Endocannabinoid Signaling at Both GABAergic and Glutamatergic Synapses in the Ventral Tegmental Area. *Neuropharmacology* **2008**, *54* (1), 95–107. https://doi.org/10.1016/j.neuropharm.2007.05.028.
(27) Wilson, R. I.; Nicoll, R. A. Endogenous Cannabinoids Mediate Retrograde Signalling at Hippocampal Synapses. *Nature* **2001**, *410* (6828), 588–592. https://doi.org/10.1038/35069076.
(28) Aymerich, M. S.; Aso, E.; Abellanas, M. A.; Tolon, R. M.; Ramos, J. A.; Ferrer, I.; Romero, J.; Fernández-Ruiz, J. Cannabinoid Pharmacology/Therapeutics in Chronic Degenerative Disorders Affecting the Central Nervous System. *Biochemical Pharmacology* **2018**, *157*, 67–84. https://doi.org/10.1016/j.bcp.2018.08.016.
(29) Cassano, T.; Calcagnini, S.; Pace, L.; De Marco, F.; Romano, A.; Gaetani, S. Cannabinoid Receptor 2 Signaling in Neurodegenerative Disorders: From Pathogenesis to a Promising Therapeutic Target. *Front. Neurosci.* **2017**, *11*. https://doi.org/10.3389/fnins.2017.00030.
(30) Russo, M.; Naro, A.; Leo, A.; Sessa, E.; D'Aleo, G.; Bramanti, P.; Calabrò, R. S. Evaluating Sativex® in Neuropathic Pain Management: A Clinical and Neurophysiological Assessment in Multiple Sclerosis. *Pain Med* **2016**, pnv080. https://doi.org/10.1093/pm/pnv080.
(31) Ward, A.; Holmes, B. Nabilone: A Preliminary Review of Its Pharmacological Properties and Therapeutic Use. *Drugs* **1985**, *30* (2), 127–144. https://doi.org/10.2165/00003495-198530020-00002.
(32) Curioni, C.; André, C. Rimonabant for Overweight or Obesity. *Cochrane Database of Systematic Reviews* **2006**, *2010* (1). https://doi.org/10.1002/14651858.CD006162.pub2.
(33) Sam, A. H.; Salem, V.; Ghatei, M. A. Rimonabant: From RIO to Ban. *Journal of Obesity* **2011**, *2011*, 1–4. https://doi.org/10.1155/2011/432607.
(34) Martínez-Pinilla, E.; Reyes-Resina, I.; Oñatibia-Astibia, A.; Zamarbide, M.; Ricobaraza, A.; Navarro, G.; Moreno, E.; Dopeso-Reyes, I. G.; Sierra, S.; Rico, A. J.; Roda, E.; Lanciego, J. L.; Franco, R. CB1 and GPR55 Receptors Are Co-Expressed and Form Heteromers in Rat and Monkey Striatum. *Experimental Neurology* **2014**, *261*, 44–52. https://doi.org/10.1016/j.expneurol.2014.06.017.
(35) Pertwee, R. G.; Howlett, A. C.; Abood, M. E.; Alexander, S. P. H.; Di Marzo, V.; Elphick, M. R.; Greasley, P. J.; Hansen, H. S.; Kunos, G.; Mackie, K.; Mechoulam, R.; Ross, R. A. International Union of Basic and Clinical Pharmacology. LXXIX. Cannabinoid Receptors and Their Ligands: Beyond CB_1 and CB_2. *Pharmacol Rev* **2010**, *62* (4), 588–631. https://doi.org/10.1124/pr.110.003004.
(36) Racz, I.; Nadal, X.; Alferink, J.; Baños, J. E.; Rehnelt, J.; Martín, M.; Pintado, B.; Gutierrez-Adan, A.; Sanguino, E.; Manzanares, J.; Zimmer, A.; Maldonado, R. Crucial Role of CB(2) Cannabinoid Receptor in the Regulation of Central Immune Responses during Neuropathic Pain. *J Neurosci* **2008**, *28* (46), 12125–12135. https://doi.org/10.1523/JNEUROSCI.3400-08.2008.
(37) Di Marzo, V.; Stella, N.; Zimmer, A. Endocannabinoid Signalling and the Deteriorating Brain. *Nat Rev Neurosci* **2015**, *16* (1), 30–42. https://doi.org/10.1038/nrn3876.
(38) Presley, C.; Abidi, A.; Suryawanshi, S.; Mustafa, S.; Meibohm, B.; Moore, B. M. Preclinical Evaluation of SMM -189, a Cannabinoid Receptor 2-specific Inverse Agonist. *Pharmacology Res & Perspec* **2015**, *3* (4), e00159. https://doi.org/10.1002/prp2.159.
(39) Schiöth, H. B.; Fredriksson, R. The GRAFS Classification System of G-Protein Coupled Receptors in Comparative Perspective. *General and Comparative*

Endocrinology **2005**, *142* (1–2), 94–101. https://doi.org/10.1016/j.ygcen.2004.12.018.
(40) Alexander, S. P. H.; Irving, A. J. GPR18, GPR55 and GPR119 in GtoPdb v.2023.1. *GtoPdb CITE* **2023**, *2023* (1). https://doi.org/10.2218/gtopdb/F114/2023.1.
(41) McHugh, D.; Page, J.; Dunn, E.; Bradshaw, H. B. Δ(9) -Tetrahydrocannabinol and N-Arachidonyl Glycine Are Full Agonists at GPR18 Receptors and Induce Migration in Human Endometrial HEC-1B Cells. *Br J Pharmacol* **2012**, *165* (8), 2414–2424. https://doi.org/10.1111/j.1476-5381.2011.01497.x.
(42) Kohno, M.; Hasegawa, H.; Inoue, A.; Muraoka, M.; Miyazaki, T.; Oka, K.; Yasukawa, M. Identification of N-Arachidonylglycine as the Endogenous Ligand for Orphan G-Protein-Coupled Receptor GPR18. *Biochemical and Biophysical Research Communications* **2006**, *347* (3), 827–832. https://doi.org/10.1016/j.bbrc.2006.06.175.
(43) Huang, S. M.; Bisogno, T.; Petros, T. J.; Chang, S. Y.; Zavitsanos, P. A.; Zipkin, R. E.; Sivakumar, R.; Coop, A.; Maeda, D. Y.; De Petrocellis, L.; Burstein, S.; Di Marzo, V.; Walker, J. M. Identification of a New Class of Molecules, the Arachidonyl Amino Acids, and Characterization of One Member That Inhibits Pain. *Journal of Biological Chemistry* **2001**, *276* (46), 42639–42644. https://doi.org/10.1074/jbc.M107351200.
(44) Sheskin, T.; Hanuš, L.; Slager, J.; Vogel, Z.; Mechoulam, R. Structural Requirements for Binding of Anandamide-Type Compounds to the Brain Cannabinoid Receptor. *J. Med. Chem.* **1997**, *40* (5), 659–667. https://doi.org/10.1021/jm960752x.
(45) Console-Bram, L.; Brailoiu, E.; Brailoiu, G. C.; Sharir, H.; Abood, M. E. Activation of GPR 18 by Cannabinoid Compounds: A Tale of Biased Agonism. *British J Pharmacology* **2014**, *171* (16), 3908–3917. https://doi.org/10.1111/bph.12746.
(46) Yin, H.; Chu, A.; Li, W.; Wang, B.; Shelton, F.; Otero, F.; Nguyen, D. G.; Caldwell, J. S.; Chen, Y. A. Lipid G Protein-Coupled Receptor Ligand Identification Using β-Arrestin PathHunter™ Assay. *Journal of Biological Chemistry* **2009**, *284* (18), 12328–12338. https://doi.org/10.1074/jbc.M806516200.
(47) Finlay, D. B.; Joseph, W. R.; Grimsey, N. L.; Glass, M. GPR18 Undergoes a High Degree of Constitutive Trafficking but Is Unresponsive to N-Arachidonoyl Glycine. *PeerJ* **2016**, *4*, e1835. https://doi.org/10.7717/peerj.1835.
(48) Schoeder, C. T.; Kaleta, M.; Mahardhika, A. B.; Olejarz-Maciej, A.; Łażewska, D.; Kieć-Kononowicz, K.; Müller, C. E. Structure-Activity Relationships of Imidazothiazinones and Analogs as Antagonists of the Cannabinoid-Activated Orphan G Protein-Coupled Receptor GPR18. *European Journal of Medicinal Chemistry* **2018**, *155*, 381–397. https://doi.org/10.1016/j.ejmech.2018.05.050.
(49) Rempel, V.; Atzler, K.; Behrenswerth, A.; Karcz, T.; Schoeder, C.; Hinz, S.; Kaleta, M.; Thimm, D.; Kiec-Kononowicz, K.; Müller, C. E. Bicyclic Imidazole-4-One Derivatives: A New Class of Antagonists for the Orphan G Protein-Coupled Receptors GPR18 and GPR55. *Med. Chem. Commun.* **2014**, *5* (5), 632–649. https://doi.org/10.1039/C3MD00394A.
(50) Nazir, M.; Harms, H.; Loef, I.; Kehraus, S.; El Maddah, F.; Arslan, I.; Rempel, V.; Müller, C.; König, G. GPR18 Inhibiting Amauromine and the Novel Triterpene Glycoside Auxarthonoside from the Sponge-Derived Fungus Auxarthron Reticulatum. *Planta Med* **2015**, *81* (12/13), 1141–1145. https://doi.org/10.1055/s-0035-1545979.
(51) Schoeder, C. T.; Mahardhika, A. B.; Drabczyńska, A.; Kieć-Kononowicz, K.; Müller, C. E. Discovery of Tricyclic Xanthines as Agonists of the Cannabinoid-Activated Orphan G-Protein-Coupled Receptor GPR18. *ACS Med. Chem. Lett.* **2020**, *11* (10), 2024–2031. https://doi.org/10.1021/acsmedchemlett.0c00208.

(52) Mahardhika, A. B.; Załuski, M.; Schoeder, C. T.; Boshta, N. M.; Schabikowski, J.; Perri, F.; Łażewska, D.; Neumann, A.; Kremers, S.; Oneto, A.; Ressemann, A.; Latacz, G.; Namasivayam, V.; Kieć-Kononowicz, K.; Müller, C. E. Potent, Selective Agonists for the Cannabinoid-like Orphan G Protein-Coupled Receptor GPR18: A Promising Drug Target for Cancer and Immunity. *J. Med. Chem.* **2024**, *67* (12), 9896–9926. https://doi.org/10.1021/acs.jmedchem.3c02423.

(53) Qin, Y.; Verdegaal, E. M. E.; Siderius, M.; Bebelman, J. P.; Smit, M. J.; Leurs, R.; Willemze, R.; Tensen, C. P.; Osanto, S. Quantitative Expression Profiling of G-Protein-Coupled Receptors (GPCRs) in Metastatic Melanoma: The Constitutively Active Orphan GPCR GPR18 as Novel Drug Target. *Pigment Cell Melanoma Res* **2011**, *24* (1), 207–218. https://doi.org/10.1111/j.1755-148X.2010.00781.x.

(54) McHugh, D.; Tanner, C.; Mechoulam, R.; Pertwee, R. G.; Ross, R. A. Inhibition of Human Neutrophil Chemotaxis by Endogenous Cannabinoids and Phytocannabinoids: Evidence for a Site Distinct from CB_1 and CB_2. *Mol Pharmacol* **2008**, *73* (2), 441–450. https://doi.org/10.1124/mol.107.041863.

(55) Zhang, L.; Fang, Y.; Hang, S.; Wu, W.; Sheng, R.; Guo, R. GPR18 and GPR55-Related Ligands Serving as Antagonists or Agonists: Current Situation, Challenges and Perspectives. *MC* **2023**, *19*. https://doi.org/10.2174/1573406419666230406095220.

(56) Oka, S.; Nakajima, K.; Yamashita, A.; Kishimoto, S.; Sugiura, T. Identification of GPR55 as a Lysophosphatidylinositol Receptor. *Biochemical and Biophysical Research Communications* **2007**, *362* (4), 928–934. https://doi.org/10.1016/j.bbrc.2007.08.078.

(57) Kapur, A.; Zhao, P.; Sharir, H.; Bai, Y.; Caron, M. G.; Barak, L. S.; Abood, M. E. Atypical Responsiveness of the Orphan Receptor GPR55 to Cannabinoid Ligands. *Journal of Biological Chemistry* **2009**, *284* (43), 29817–29827. https://doi.org/10.1074/jbc.M109.050187.

(58) Rempel, V.; Volz, N.; Gläser, F.; Nieger, M.; Bräse, S.; Müller, C. E. Antagonists for the Orphan G-Protein-Coupled Receptor GPR55 Based on a Coumarin Scaffold. *J. Med. Chem.* **2013**, *56* (11), 4798–4810. https://doi.org/10.1021/jm4005175.

(59) Heynen-Genel, S.; Dahl, R.; Shi, S.; Milan, L.; Hariharan, S.; Sergienko, E.; Hedrick, M.; Dad, S.; Stonich, D.; Su, Y.; Vicchiarelli, M.; Mangravita-Novo, A.; Smith, L. H.; Chung, T. D.; Sharir, H.; Caron, M. G.; Barak, L. S.; Abood, M. E. Screening for Selective Ligands for GPR55 - Antagonists. In *Probe Reports from the NIH Molecular Libraries Program*; National Center for Biotechnology Information (US): Bethesda (MD), 2010.

(60) Kargl, J.; Brown, A. J.; Andersen, L.; Dorn, G.; Schicho, R.; Waldhoer, M.; Heinemann, A. A Selective Antagonist Reveals a Potential Role of G Protein–Coupled Receptor 55 in Platelet and Endothelial Cell Function. *J Pharmacol Exp Ther* **2013**, *346* (1), 54–66. https://doi.org/10.1124/jpet.113.204180.

(61) Henstridge, C. M.; Balenga, N. A.; Schröder, R.; Kargl, J. K.; Platzer, W.; Martini, L.; Arthur, S.; Penman, J.; Whistler, J. L.; Kostenis, E.; Waldhoer, M.; Irving, A. J. GPR55 Ligands Promote Receptor Coupling to Multiple Signalling Pathways. *British J Pharmacology* **2010**, *160* (3), 604–614. https://doi.org/10.1111/j.1476-5381.2009.00625.x.

(62) Xia, R.; Yuan, Q.; Wang, N.; Hou, L.; Abe, J.; Song, J.; Ito, Y.; Xu, H. E.; He, Y. Structural Insight into GPR55 Ligand Recognition and G-Protein Coupling. *Cell Res* **2024**. https://doi.org/10.1038/s41422-024-01044-w.

(63) Giacobini, E. Cholinesterase Inhibitors Stabilize Alzheimer's Disease. *Annals of the New York Academy of Sciences* **2000**, *920* (1), 321–327. https://doi.org/10.1111/j.1749-6632.2000.tb06942.x.

(64) Zhan, C.-G.; Zheng, F.; Landry, D. W. Fundamental Reaction Mechanism for Cocaine Hydrolysis in Human Butyrylcholinesterase. *J. Am. Chem. Soc.* **2003**, *125* (9), 2462–2474. https://doi.org/10.1021/ja020850+.
(65) Masson, P.; Carletti, E.; Nachon, F. Structure, Activities and Biomedical Applications of Human Butyrylcholinesterase. *PPL* **2009**, *16* (10), 1215–1224. https://doi.org/10.2174/092986609789071207.
(66) Greig, N. H.; Utsuki, T.; Ingram, D. K.; Wang, Y.; Pepeu, G.; Scali, C.; Yu, Q.-S.; Mamczarz, J.; Holloway, H. W.; Giordano, T.; Chen, D.; Furukawa, K.; Sambamurti, K.; Brossi, A.; Lahiri, D. K. Selective Butyrylcholinesterase Inhibition Elevates Brain Acetylcholine, Augments Learning and Lowers Alzheimer β-Amyloid Peptide in Rodent. *Proc. Natl. Acad. Sci. U.S.A.* **2005**, *102* (47), 17213–17218. https://doi.org/10.1073/pnas.0508575102.
(67) Geula, C.; Darvesh, S. Butyrylcholinesterase, Cholinergic Neurotransmission and Thepathology of Alzheimer's Disease. *Drugs of Today* **2004**, *40* (8), 711. https://doi.org/10.1358/dot.2004.40.8.850473.
(68) Darvesh, S. Butyrylcholinesterase Radioligands to Image Alzheimer's Disease Brain. *Chemico-Biological Interactions* **2013**, *203* (1), 354–357. https://doi.org/10.1016/j.cbi.2012.08.009.
(69) Galdeano, C.; Viayna, E.; Arroyo, P.; Bidon-Chanal, A.; Ramon Blas, J.; Munoz-Torrero, D.; Javier Luque, F. Structural Determinants of the Multifunctional Profile of Dual Binding Site Acetylcholinesterase Inhibitors as Anti-Alzheimer Agents. *CPD* **2010**, *16* (25), 2818–2836. https://doi.org/10.2174/138161210793176536.
(70) Furukawa-Hibi, Y.; Alkam, T.; Nitta, A.; Matsuyama, A.; Mizoguchi, H.; Suzuki, K.; Moussaoui, S.; Yu, Q.-S.; Greig, N. H.; Nagai, T.; Yamada, K. Butyrylcholinesterase Inhibitors Ameliorate Cognitive Dysfunction Induced by Amyloid-β Peptide in Mice. *Behavioural Brain Research* **2011**, *225* (1), 222–229. https://doi.org/10.1016/j.bbr.2011.07.035.
(71) Masson, P.; Froment, M.; Bartels, C. F.; Lockridge, O. Asp70 in the Peripheral Anionic Site of Human Butyrylcholinesterase. *European Journal of Biochemistry* **1996**, *235* (1–2), 36–48. https://doi.org/10.1111/j.1432-1033.1996.00036.x.
(72) Nicolet, Y.; Lockridge, O.; Masson, P.; Fontecilla-Camps, J. C.; Nachon, F. Crystal Structure of Human Butyrylcholinesterase and of Its Complexes with Substrate and Products. *Journal of Biological Chemistry* **2003**, *278* (42), 41141–41147. https://doi.org/10.1074/jbc.M210241200.
(73) Guida, F.; Luongo, L.; Boccella, S.; Giordano, M. E.; Romano, R.; Bellini, G.; Manzo, I.; Furiano, A.; Rizzo, A.; Imperatore, R.; Iannotti, F. A.; D'Aniello, E.; Piscitelli, F.; Sca Rossi, F.; Cristino, L.; Di Marzo, V.; De Novellis, V.; Maione, S. Palmitoylethanolamide Induces Microglia Changes Associated with Increased Migration and Phagocytic Activity: Involvement of the CB2 Receptor. *Sci Rep* **2017**, *7* (1), 375. https://doi.org/10.1038/s41598-017-00342-1.
(74) Naikoo, R. A.; Painuli, R.; Akhter, Z.; Singh, P. P. Cannabinoid Receptor 2 (CB2) Modulators: A Patent Review (2016–2024). *Bioorganic Chemistry* **2024**, *153*, 107775. https://doi.org/10.1016/j.bioorg.2024.107775.
(75) Shohami, E.; Mechoulam, R. Dexanabinol (HU-211): A Nonpsychotropic Cannabinoid with Neuroprotective Properties. *Drug Dev. Res.* **2000**, *50* (3–4), 211–215. https://doi.org/10.1002/1098-2299(200007/08)50:3/4<211::AID-DDR3>3.0.CO;2-G.
(76) de Candia, M.; Zaetta, G.; Denora, N.; Tricarico, D.; Majellaro, M.; Cellamare, S.; Altomare, C. D. New Azepino[4,3-b]Indole Derivatives as Nanomolar Selective Inhibitors of Human Butyrylcholinesterase Showing Protective Effects against NMDA-Induced Neurotoxicity. *European Journal of Medicinal Chemistry* **2017**, *125*, 288–298. https://doi.org/10.1016/j.ejmech.2016.09.037.

(77) European Monitoring Centre for Drugs and Drug Addiction. *Understanding the 'Spice' Phenomenon.*; Publications Office: LU, 2009.
(78) Schoeder, C. T.; Hess, C.; Madea, B.; Meiler, J.; Müller, C. E. Pharmacological Evaluation of New Constituents of "Spice": Synthetic Cannabinoids Based on Indole, Indazole, Benzimidazole and Carbazole Scaffolds. *Forensic Toxicol* **2018**, *36* (2), 385–403. https://doi.org/10.1007/s11419-018-0415-z.
(79) Ward, S. J.; Baizman, E.; Bell, M.; Childers, S.; D'Ambra, T.; Eissenstat, M.; Estep, K.; Haycock, D.; Howlett, A.; Luttinger, D. Aminoalkylindoles (AAIs): A New Route to the Cannabinoid Receptor? *NIDA Res Monogr* **1990**, *105*, 425–426.
(80) Huffman, J.; Padgett, L. Recent Developments in the Medicinal Chemistry of Cannabimimetic Indoles, Pyrroles and Indenes. *CMC* **2005**, *12* (12), 1395–1411. https://doi.org/10.2174/0929867054020864.
(81) Seltzman, H. H.; Shiner, C.; Hirt, E. E.; Gilliam, A. F.; Thomas, B. F.; Maitra, R.; Snyder, R.; Black, S. L.; Patel, P. R.; Mulpuri, Y.; Spigelman, I. Peripherally Selective Cannabinoid 1 Receptor (CB1R) Agonists for the Treatment of Neuropathic Pain. *J. Med. Chem.* **2016**, *59* (16), 7525–7543. https://doi.org/10.1021/acs.jmedchem.6b00516.
(82) Huffman, J. W.; Zengin, G.; Wu, M.-J.; Lu, J.; Hynd, G.; Bushell, K.; Thompson, A. L. S.; Bushell, S.; Tartal, C.; Hurst, D. P.; Reggio, P. H.; Selley, D. E.; Cassidy, M. P.; Wiley, J. L.; Martin, B. R. Structure–Activity Relationships for 1-Alkyl-3-(1-Naphthoyl)Indoles at the Cannabinoid CB1 and CB2 Receptors: Steric and Electronic Effects of Naphthoyl Substituents. New Highly Selective CB2 Receptor Agonists. *Bioorganic & Medicinal Chemistry* **2005**, *13* (1), 89–112. https://doi.org/10.1016/j.bmc.2004.09.050.
(83) Bassoni, D. L.; Raab, W. J.; Achacoso, P. L.; Loh, C. Y.; Wehrman, T. S. Measurements of β-Arrestin Recruitment to Activated Seven Transmembrane Receptors Using Enzyme Complementation. In *Receptor Binding Techniques*; Davenport, A. P., Ed.; Methods in Molecular Biology; Humana Press: Totowa, NJ, 2012; Vol. 897, pp 181–203. https://doi.org/10.1007/978-1-61779-909-9_9.
(84) Shore, D. M.; Reggio, P. H. The Therapeutic Potential of Orphan GPCRs, GPR35 and GPR55. *Front. Pharmacol.* **2015**, *6*. https://doi.org/10.3389/fphar.2015.00069.
(85) Kotsikorou, E.; Sharir, H.; Shore, D. M.; Hurst, D. P.; Lynch, D. L.; Madrigal, K. E.; Heynen-Genel, S.; Milan, L. B.; Chung, T. D. Y.; Seltzman, H. H.; Bai, Y.; Caron, M. G.; Barak, L. S.; Croatt, M. P.; Abood, M. E.; Reggio, P. H. Identification of the GPR55 Antagonist Binding Site Using a Novel Set of High-Potency GPR55 Selective Ligands. *Biochemistry* **2013**, *52* (52), 9456–9469. https://doi.org/10.1021/bi4008885.
(86) Neumann, A.; Engel, V.; Mahardhika, A. B.; Schoeder, C. T.; Namasivayam, V.; Kieć-Kononowicz, K.; Müller, C. E. Computational Investigations on the Binding Mode of Ligands for the Cannabinoid-Activated G Protein-Coupled Receptor GPR18. *Biomolecules* **2020**, *10* (5), 686. https://doi.org/10.3390/biom10050686.
(87) Morales, P.; Lago-Fernandez, A.; Hurst, D. P.; Sotudeh, N.; Brailoiu, E.; Reggio, P. H.; Abood, M. E.; Jagerovic, N. Therapeutic Exploitation of GPR18: Beyond the Cannabinoids?: Miniperspective. *J. Med. Chem.* **2020**, *63* (23), 14216–14227. https://doi.org/10.1021/acs.jmedchem.0c00926.
(88) Hess, C.; Schoeder, C. T.; Pillaiyar, T.; Madea, B.; Müller, C. E. Pharmacological Evaluation of Synthetic Cannabinoids Identified as Constituents of Spice. *Forensic Toxicol* **2016**, *34* (2), 329–343. https://doi.org/10.1007/s11419-016-0320-2.
(89) Balenga, N. A.; Martínez-Pinilla, E.; Kargl, J.; Schröder, R.; Peinhaupt, M.; Platzer, W.; Bálint, Z.; Zamarbide, M.; Dopeso-Reyes, I. G.; Ricobaraza, A.;

Pérez-Ortiz, J. M.; Kostenis, E.; Waldhoer, M.; Heinemann, A.; Franco, R. Heteromerization of GPR 55 and Cannabinoid CB_2 Receptors Modulates Signalling. *British J Pharmacology* **2014**, *171* (23), 5387–5406. https://doi.org/10.1111/bph.12850.

(90) Listratova, A. V.; Samarelli, F.; Titov, A. A.; Purgatorio, R.; De Candia, M.; Catto, M.; Varlamov, A. V.; Voskressensky, L. G.; Altomare, C. D. Advances in Synthesis of Novel Annulated Azecines and Their Unique Pharmacological Properties. *European Journal of Medicinal Chemistry* **2024**, *280*, 116947. https://doi.org/10.1016/j.ejmech.2024.116947.

(91) Reyes-Resina, I.; Navarro, G.; Aguinaga, D.; Canela, E. I.; Schoeder, C. T.; Załuski, M.; Kieć-Kononowicz, K.; Saura, C. A.; Müller, C. E.; Franco, R. Molecular and Functional Interaction between GPR18 and Cannabinoid CB2 G-Protein-Coupled Receptors. Relevance in Neurodegenerative Diseases. *Biochemical Pharmacology* **2018**, *157*, 169–179. https://doi.org/10.1016/j.bcp.2018.06.001.

(92) Czarnota-Łydka, K.; Sudoł-Tałaj, S.; Kucwaj-Brysz, K.; Kurczab, R.; Satała, G.; De Candia, M.; Samarelli, F.; Altomare, C. D.; Carocci, A.; Barbarossa, A.; Żesławska, E.; Głuch-Lutwin, M.; Mordyl, B.; Kubacka, M.; Wilczyńska-Zawal, N.; Jastrzębska-Więsek, M.; Partyka, A.; Khan, N.; Więcek, M.; Nitek, W.; Honkisz-Orzechowska, E.; Latacz, G.; Wesołowska, A.; Carrieri, A.; Handzlik, J. Synthesis, Computational and Experimental Pharmacological Studies for (Thio)Ether-Triazine 5-HT6R Ligands with Noticeable Action on AChE/BChE and Chalcogen-Dependent Intrinsic Activity in Search for New Class of Drugs against Alzheimer's Disease. *European Journal of Medicinal Chemistry* **2023**, *259*, 115695. https://doi.org/10.1016/j.ejmech.2023.115695.

(93) Carrieri, A.; Barbarossa, A.; De Candia, M.; Samarelli, F.; Damiano Altomare, C.; Czarnota-Łydka, K.; Sudoł-Tałaj, S.; Latacz, G.; Handzlik, J.; Brunetti, L.; Piemontese, L.; Limongelli, F.; Lentini, G.; Carocci, A. Chiral Pyrrolidines as Multipotent Agents in Alzheimer and Neurodegenerative Diseases. *Bioorganic & Medicinal Chemistry* **2024**, *110*, 117829. https://doi.org/10.1016/j.bmc.2024.117829.

(94) Mele, M.; Mele, A.; Imbrici, P.; Samarelli, F.; Purgatorio, R.; Dinoi, G.; Correale, M.; Nicolotti, O.; De Luca, A.; Brunetti, N. D.; Liantonio, A.; Amoroso, N. Pleiotropic Effects of Direct Oral Anticoagulants in Chronic Heart Failure and Atrial Fibrillation: Machine Learning Analysis. *Molecules* **2024**, *29* (11), 2651. https://doi.org/10.3390/molecules29112651.

(95) Saleem, M.; Herrmann, N.; Dinoff, A.; Mazereeuw, G.; Oh, P. I.; Goldstein, B. I.; Kiss, A.; Shammi, P.; Lanctôt, K. L. Association Between Endothelial Function and Cognitive Performance in Patients With Coronary Artery Disease During Cardiac Rehabilitation. *Psychosom Med* **2019**, *81* (2), 184–191. https://doi.org/10.1097/PSY.0000000000000651.

(96) Leys, D.; Hénon, H.; Mackowiak-Cordoliani, M.-A.; Pasquier, F. Poststroke Dementia. *The Lancet Neurology* **2005**, *4* (11), 752–759. https://doi.org/10.1016/S1474-4422(05)70221-0.

(97) De Candia, M.; Lopopolo, G.; Altomare, C. Novel Factor Xa Inhibitors: A Patent Review. *Expert Opinion on Therapeutic Patents* **2009**, *19* (11), 1535–1580. https://doi.org/10.1517/13543770903270532.

(98) Lopopolo, G.; de Candia, M.; Panza, L.; Romano, M. R.; Lograno, M. D.; Campagna, F.; Altomare, C. B- D -Glucosyl Conjugates of Highly Potent Inhibitors of Blood Coagulation Factor Xa Bearing 2-Chorothiophene as a P1 Motif. *ChemMedChem* **2012**, *7* (9), 1669–1677. https://doi.org/10.1002/cmdc.201200224.

(99) Aderibigbe, A. D.; Day, D. P. Syntheses and Applications of Malonamide Derivatives – A Minireview. *ChemistrySelect* **2020**, *5* (48), 15222–15232. https://doi.org/10.1002/slct.202004340.
(100) Islam, M. S.; Barakat, A.; Al-Majid, A. M.; Ghabbour, H. A.; Rahman, A. F. M. M.; Javaid, K.; Imad, R.; Yousuf, S.; Choudhary, M. I. A Concise Synthesis and Evaluation of New Malonamide Derivatives as Potential α-Glucosidase Inhibitors. *Bioorganic & Medicinal Chemistry* **2016**, *24* (8), 1675–1682. https://doi.org/10.1016/j.bmc.2016.02.037.
(101) Barakat, A.; Islam, M. S.; Al-Majid, A. M.; Soliman, S. M.; Ghabbour, H. A.; Yousuf, S.; Choudhary, M. I.; Ul-Haq, Z. Synthesis, Molecular Structure, Spectral Analysis, and Biological Activity of New Malonamide Derivatives as α-Glucosidase Inhibitors. *Journal of Molecular Structure* **2017**, *1134*, 253–264. https://doi.org/10.1016/j.molstruc.2016.12.093.
(102) Chorev, M. The Partial Retro–Inverso Modification: A Road Traveled Together. *Biopolymers* **2005**, *80* (2–3), 67–84. https://doi.org/10.1002/bip.20219.
(103) Witt, T.; Hock, F. J.; Lehmann, J. 7-Methyl-6,7,8,9,14,15-Hexahydro-5 *H* -Benz[*d*]Indolo[2,3- *g*]Azecine: A New Heterocyclic System and a New Lead Compound for Dopamine Receptor Antagonists. *J. Med. Chem.* **2000**, *43* (10), 2079–2081. https://doi.org/10.1021/jm9911478.
(104) Fang, Z.; Song, Y.; Zhan, P.; Zhang, Q.; Liu, X. Conformational Restriction: An Effective Tactic in 'Follow-on'-Based Drug Discovery. *Future Medicinal Chemistry* **2014**, *6* (8), 885–901. https://doi.org/10.4155/fmc.14.50.
(105) Lawson, A. D. G.; MacCoss, M.; Heer, J. P. Importance of Rigidity in Designing Small Molecule Drugs To Tackle Protein–Protein Interactions (PPIs) through Stabilization of Desired Conformers: Miniperspective. *J. Med. Chem.* **2018**, *61* (10), 4283–4289. https://doi.org/10.1021/acs.jmedchem.7b01120.
(106) Ferenczy, G. G.; Keserű, G. M. The Impact of Binding Thermodynamics on Medicinal Chemistry Optimizations. *Future Medicinal Chemistry* **2015**, *7* (10), 1285–1303. https://doi.org/10.4155/fmc.15.63.
(107) Chiang, K. C.; Rizk, J. G.; Nelson, D. J.; Krishnamurti, L.; Subbian, S.; Imig, J. D.; Khan, I.; Reddy, S. T.; Gupta, A. Ramatroban for Chemoprophylaxis and Treatment of COVID-19: David Takes on Goliath. *Expert Opinion on Therapeutic Targets* **2022**, *26* (1), 13–28. https://doi.org/10.1080/14728222.2022.2031975.
(108) Gupta, A.; K, K.-Z.; Tr, S. Ramatroban as a Novel Immunotherapy for COVID-19. *jmgm* **2020**, *14* (3). https://doi.org/10.37421/jmgm.2020.14.457.
(109) Maroli, N.; Bhasuran, B.; Natarajan, J.; Kolandaivel, P. The Potential Role of Procyanidin as a Therapeutic Agent against SARS-CoV-2: A Text Mining, Molecular Docking and Molecular Dynamics Simulation Approach. *Journal of Biomolecular Structure and Dynamics* **2022**, *40* (3), 1230–1245. https://doi.org/10.1080/07391102.2020.1823887.
(110) Bardelčíková, A.; Miroššay, A.; Šoltýs, J.; Mojžiš, J. Therapeutic and Prophylactic Effect of Flavonoids in *Post* -COVID-19 Therapy. *Phytotherapy Research* **2022**, *36* (5), 2042–2060. https://doi.org/10.1002/ptr.7436.
(111) Conrad, K. P. Might Proton Pump or Sodium-hydrogen Exchanger Inhibitors Be of Value to Ameliorate SARs-CoV-2 Pathophysiology? *Physiol Rep* **2021**, *8* (24). https://doi.org/10.14814/phy2.14649.
(112) Plassmeyer, M.; Alpan, O.; Corley, M. J.; Premeaux, T. A.; Lillard, K.; Coatney, P.; Vaziri, T.; Michalsky, S.; Pang, A. P. S.; Bukhari, Z.; Yeung, S. T.; Evering, T. H.; Naughton, G.; Latterich, M.; Mudd, P.; Spada, A.; Rindone, N.; Loizou, D.; Ulrik Sønder, S.; Ndhlovu, L. C.; Gupta, R. Caspases and Therapeutic Potential of Caspase Inhibitors in Moderate–Severe SARS-CoV-2 Infection and Long COVID. *Allergy* **2022**, *77* (1), 118–129. https://doi.org/10.1111/all.14907.
(113) Huang, C.; Wang, Y.; Li, X.; Ren, L.; Zhao, J.; Hu, Y.; Zhang, L.; Fan, G.; Xu, J.; Gu, X.; Cheng, Z.; Yu, T.; Xia, J.; Wei, Y.; Wu, W.; Xie, X.; Yin, W.; Li, H.; Liu, M.; Xiao,

Y.; Gao, H.; Guo, L.; Xie, J.; Wang, G.; Jiang, R.; Gao, Z.; Jin, Q.; Wang, J.; Cao, B. Clinical Features of Patients Infected with 2019 Novel Coronavirus in Wuhan, China. *The Lancet* **2020**, *395* (10223), 497–506. https://doi.org/10.1016/S0140-6736(20)30183-5.

(114) Archambault, A.; Zaid, Y.; Rakotoarivelo, V.; Turcotte, C.; Doré, É.; Dubuc, I.; Martin, C.; Flamand, O.; Amar, Y.; Cheikh, A.; Fares, H.; El Hassani, A.; Tijani, Y.; Côté, A.; Laviolette, M.; Boilard, É.; Flamand, L.; Flamand, N. High Levels of Eicosanoids and Docosanoids in the Lungs of Intubated COVID-19 Patients. *The FASEB Journal* **2021**, *35* (6). https://doi.org/10.1096/fj.202100540R.